Catalytic Activity and Mechanochemical Response of Cu(I) NHC Complexes

Dissertation

zur Erlangung des

Doktorgrades der Naturwissenschaften (Dr. rer. nat.)

der

Naturwissenschaftlichen Fakultät II

Chemie, Physik und Mathematik

der Martin-Luther-Universität

Halle-Wittenberg

vorgelegt

von Herrn Kshitij Sanjay Shinde

Gutachter

1.   Prof. Dr. Wolfgang H. Binder
2.   Prof. Dr. André Laschewsky

Verteidigung: 12.11.2024

I. Acknowledgments

This is the last part that I am writing for this thesis. I have reached this part of my PhD journey with a lot of support, and I am only grateful for everyone who has been a part of this journey. The first thanks undoubtedly go to Prof. Dr. Wolfgang H. Binder for providing me with this opportunity, guidance, and supervision. I am sincerely thankful for this invaluable chance to learn and work as part of his working group.

An extension of this gratefulness is also to be extended to Dr. Philipp Michael, Dr. Anja Marinow and Dr. Diana Döhler. Each of them has been a source of unwavering support through different phases of this journey, with each contributing uniquely but significantly to both the professional and personal challenges of life. Their constructive feedback, motivation and most importantly, time, has been valuable and I truly appreciate everything they have done for me.

Furthermore, I would like to express my gratitude to Ms. Anke Hassi. For 5 years, she answered my stupidest of questions, helped me understand German letters, bureaucracy and in some cases, even the German laws. She is truly a remarkable person who goes beyond herself to make you feel welcome and supported. I am also thankful to Ms. Susanne Tanner and Ms. Julia Grossert for not only providing all necessary chemicals and equipment to keep the experiments running smoothly, but also for performing innumerable analytical measurements needed to make these experiments make sense.

I am also thankful for the group members of A.G. Binder, from the past and present. I have met and worked with some wonderful people here throughout my five years and the relationships that were built will last me a lifetime. I thank each one of you personally and wish you luck for your own successes and endeavours.

I extend my thanks to all employees of the analytical department of the Institute of Organic Chemistry for conducting NMR analysis, Prof. Dr. Harald Krautscheid and Dr. Daniel Fuhrmann from Institute of Inorganic Chemistry, Universität Leipzig, for their help and knowledge in the field of metal-organic frameworks (MOFs), Dr. Thomas Heymann (Institute of Chemistry-Lebensmittelchemie, Martin Luther University, Halle-Wittenberg) for FAAS measurements and Mr. Frank Syrowatka (Interdisziplinäres Zentrum für Materialwissenschaften (IZM)—Martin Luther University, Halle-Wittenberg) for SEM measurements.

My sincere gratitude to all my friends, especially the ones here in Europe and pursuing their own PhDs, Sagar Bhagwat, Anand Ayyar and Shreyas Wagle, as well as others who have constantly been at my side.

Finally, there are not enough words to express my love and gratitude to my family and the immovable support of my mother (Aai), Mrs. Vrishali Shinde and my younger brother Aakash Sanjay Shinde. They are my everything, the reason for what I do and the reason that I can continue to keep moving forwards. Without them, all this is meaningless and frankly, not worth it. The love and sacrifices that we have made have been enormous and hopefully I can give them back everything they have given to me.

To my father (Baba), I wish you were around today to see what has been achieved and hopefully I make you proud every single day.

II.   Abstract

N-heterocyclic carbenes (NHC) are important ligands and represent significant catalytic centres due to the minimal ligand dissociation related to the strong interactions between NHC ligands and metal centres. Catalytic systems based on those NHC-ligand-metal complexes are of major interest. Therefore, the basis of this thesis is founded upon the catalytic activity of Cu(I) NHC complexes in incorporating functional groups into unsaturated polymers, as well as their response to mechanochemical activation.

The widespread use of metal-catalysed cyclopropanation for double bonds with diazoesters has been limited to low molecular weight compounds. Within the scope of this thesis, an approach to modify the polymer backbone of poly(diene)s with esters as well as carboxylic groups *via* cyclopropanation in the presence of Cu(I) NHC complexes was explored. Therefore, predominantly *cis*-1,4-poly(isoprene) was converted with ethyl or *tert*-butyl diazoacetate using Cu(I) NHCs catalysts, while maintaining focus on the technically relevant cyclohexane as solvent. Commercially available Cu(I) NHC catalysts yielded modification degrees of 4-5 %, which increased to 17 % in a more polar solvent like dichloromethane. The resulting esters were further converted to the corresponding free carboxylic acid groups by deprotection using trifluoroacetic acid. Thus, an introduction of functional groups along the polymer backbone with a wide variety of application, like ionic interaction or hydrogen bonding motifs, was demonstrated. Its potential for up-scaling makes this approach feasible for an application in large-scale production processes such as for manufacturing of modified synthetic rubbers.

In a second part, this thesis focuses on the mechanochemical activation of a Cu(I) NHC-complex based metal-organic frameworks (MOFs). MOFs, or porous coordination polymers, consist of metal ions and organic linkers, forming robust network-like structures similar to dense polymeric networks. A mechanochemically triggered copper-catalysed azide-alkyne cycloaddition (CuAAC) was achieved first in solution using a Cu(I) NHC-MOF, constructed from 1,3-bis(4-carboxyphenyl)imidazolium chloride as NHC-source and organic linker. A largely amorphous MOF with a Cu(I) bis(NHC)-complex embedded into it was synthesized. Ultrasound activation showed mechanochemical activation of the Cu(I) NHC-MOF to obtain Cu(I) as active catalytic species, subsequently triggering a CuAAC with conversions up to 25 % as monitored by the reaction of benzylazide and phenylacetylene to yield 1-benzyl-4-phenyl-1*H*-1,2,3-triazole over a period of 20 sonication cycles.

Expanding on the results in solution, the NHC-MOF system was transferred to a thermoplastic polyurethane (TPU) polymer matrix, which displays shape-memory effect, to study the mechanochemical activity in bulk. Using oscillating tensile rheology on TPU dumbbell-shaped samples, the NHC-MOF catalysed fluorogenic CuAAC between non-fluorescent precursor dyes, 8-azidonaphthalen-2-ol and 3-hydroxyphenylacetylene, to form the fluorescent dye 8-(4-(3-hydroxyphenyl)-1,2,3-triazol-1-yl)naphthalen-2-ol. Monitoring *via* solid state fluorescence spectroscopy revealed increased fluorescence intensities of up to 12 % in dependence of the measuring point along the sample, exhibiting that a dumbbell-shaped TPU displays higher fluorescence intensities in areas with higher mechanical stress than the surrounding other areas, thus effectively functioning as a three-in-one stress-sensor system.

Overall, the results of this thesis exploit the reactivity of NHC-metal bonds in polymeric systems, highlighting the catalytic role of Cu-NHC complexes after chemical and mechanical activation.

III.   Kurzzusammenfassung

N-heterocyclische Carbene (NHC) sind wichtige Liganden und stellen aufgrund der minimalen Ligandendissoziation in Verbindung mit den starken Wechselwirkungen zwischen NHC-Liganden und Metallzentren bedeutende katalytische Zentren dar. Katalytische Systeme, die auf diesen NHC-Liganden-Metall-Komplexen basieren, sind von großem Interesse. Daher bilden die Untersuchung der katalytischen Aktivität von Cu(I) NHC-Komplexen zur Implementierung funktioneller Gruppen in ungesättigten Polymeren sowie die mechanochemische Aktivierungen der Katalysatoren die Grundlage dieser Arbeit.

Die weit verbreitete Anwendung der metallkatalysierten Cyclopropanierung von Doppelbindungen mit Diazoestern war bisher auf niedermolekulare Verbindungen beschränkt. Im Rahmen dieser Arbeit wurde die Modifizierung von Poly(dien)en mit Ester- und Carboxylgruppen durch Cyclopropanierung in Gegenwart von Cu(I) NHC-Komplexen untersucht. Dazu wurde vorwiegend *cis*-1,4-Poly(isopren) mit Ethyl- oder *tert*-Butyldiazoacetat unter Verwendung von Cu(I) NHC-Katalysatoren umgesetzt, wobei der Fokus auf dem technisch relevanten Cyclohexan als Lösungsmittel lag. Mit handelsüblichen Cu(I)-NHC-Katalysatoren wurden Modifizierungsgrade von 4-5 % erreicht, die in einem polareren Lösungsmittel wie Dichlormethan auf 17 % anstiegen. Die resultierenden Ester wurden durch Entschützen mit Trifluoressigsäure weiter in die entsprechenden freien Carbonsäuregruppen umgewandelt. Auf diese Weise wurde die Einführung funktioneller Gruppen entlang des Polymerrückgrats mit einer Vielzahl von Anwendungsmöglichkeiten demonstriert, wie z. B. ionische Wechselwirkungen oder Wasserstoffbrückenbindungen. Aufgrund des Potenzials zum Upscaling ist dieser Ansatz für eine Anwendung in großtechnischen Produktionsprozessen geeignet, z. B. für die Herstellung modifizierter synthetischer Kunststoffe.

In einem zweiten Teil konzentriert sich diese Arbeit auf die mechanochemische Aktivierung von auf Cu(I) NHC-Komplexen basierenden metallorganischen Gerüsten (metal organic framework, MOF). MOFs, oder poröse Koordinationspolymere, bestehen aus Metallionen und organischen Linkern, die robuste netzwerkartige Strukturen bilden, die dichten polymeren Netzwerken ähneln. Es wurde ein weitgehend amorpher MOF mit einem darin eingebetteten Cu(I) bis(NHC) synthetisiert mit 1,3-Bis(4-carboxyphenyl)imidazoliumchlorid als organischen Linker. Eine mechanochemisch ausgelöste kupferkatalysierte Azid-Alkin-Cycloaddition (CuAAC) wurde zunächst in Lösung getestet. Die Aktivierung des katalytischen Cu(I)-Zentrums *via* Ultraschall erreichte Umsätze von 25 % für eine anschließende CuAAC, wie durch die Reaktion von Benzylazid und Phenylacetylen zu 1-Benzyl-4-phenyl-1H-1,2,3-triazol über einen Zeitraum von 20 Beschallungszyklen beobachtet wurde.

Als Erweiterung der Ergebnisse in Lösung wurde das Cu(I) NHC-MOF-System in eine thermoplastische Polyurethanmatrix übertragen, die einen Formgedächtniseffekt aufweist, um auch hier eine mechanochemische Aktivität zu untersuchen. Unter Verwendung von oszillierender Zugrheologie an hantelförmigen TPU-Proben katalysierte das Cu(I)-NHC-MOF eine fluorogene CuAAC zwischen nicht fluoreszierenden Vorläuferfarbstoffen, 8-Azidonaphthalin-2-ol und 3-Hydroxyphenylacetylen, um den fluoreszierenden Farbstoff 8-(4-(3-Hydroxyphenyl)-1,2,3-triazol-1-yl)naphthalin-2-ol zu bilden. Messungen von Festkörperfluoreszenzspektroskopen ergab einen Anstieg der Fluoreszenzintensität um bis zu 12 %, in Abhängigkeit des Messpunktes entlang der Probe, was darauf hindeutet, dass ein hantelförmiges TPU bei höherer Belastung eine höhere Fluoreszenzintensität als die umgebenden anderen Bereiche aufweist und somit effektiv als ein Drei-in-Eins-Belastungssensor-System funktioniert.

Insgesamt nutzen die Ergebnisse dieser Arbeit die Reaktivität von NHC-Metallbindungen in polymeren Systemen und unterstreichen die katalytische Rolle von Cu-NHC-Komplexen nach chemischer und mechanischer Aktivierung.

Table of Contents

IV.   List of Abbreviations

t-Bu	*tert*-Butyl
%RSD	Relative Standard Deviation
%V_{bur}	Percentage Buried Volume
1,2-DCE	1,2-Dichloroethane
1ce cool	Cooled Once
2ce cool	Cooled Twice
2-pymo	2-Hydroxypyrimidinolate
a.u.	Arbitrary Units
ACN	Acetonitrile
Ad	Adamantly
AFM	Atomic Force Microscopy
atm	Atmospheric Pressure
ATR	Attenuated Total Reflection
BDC	Benzene Dicarboxylate
BDO	1,4-Butane Diol
BET	Brunauer–Emmett–Teller Theory
bIm	2-Benzimidazolate
bs	Broad Singlet
BS	Back-Side
BTC	Benzene Tricarboxylate
CCD	Charge-Coupled Device
CEL	Chan−Evans−Lam
CM	Cross-Metathesis
CuAAC	Copper(I)-Alkyne/Azide Cycloaddition
Cy	Cyclohexyl
d	Doublet
DA	Diazoacetate
DABBF	Diarylbibenzofuranone
DBU	1,8-Diazabicyclo[5.4.0]undec-7-ene
DCM	Dichloromethane
dd	Double Doublet
DFT	Density Functional Theory
dhbdc	2,5-Dihydroxy-1,4-Benzenedicarboxylate

DIPP	2,6-Diisopropylphenyl
DMF	Dimethylformamide
DMSO	Dimethyl Sulfoxide
DP	Degree Of Polymerization
DS	Development Stage
DSC	Differential Scanning Calorimetry
E	E-Modulus (Young´s Modulus)
EDA	Ethyl Diazoacetate
ELP	Elastin-Like Peptide
eq.	Equivalent
ESI	Electron-Spray-Ionization
EtAc	Ethyl Acetate
EXAFS	Extended X-Ray Absorption Fine Structure
FAAS	Flame Atomic Absorption Spectroscopy
FS	Front-Side
FTIR	Fourier-Transform Infrared Spectroscopy
gDBC	Gem-Dibromoclopropane
gDCC	Gem-Dichlorocyclopropane
gDFC	Gem-Difluorocyclopropane
gDHC	Gem-Dihalocyclopropane
GPC	Gel Permeation Chromatography
HDI	Hexamethylene Diisocyanate
HEP	Huynh Electronic Parameter
HOMO	Highest Occupied Molecule Orbital
HS	Hard Segment
IAd	1,3-Bis(1-Adamantyl)Imidazol-2-Ylidene
IBA	4-Iodobenzoic Acid
ICA	Imidazolate-2-Carboxyaldehyde
ICy	1,3-Bis(1-Cyclohexyl)Imidazol-2-Ylidene
Ime	1,3-Di(Methyl)Imidazol-2-Ylidene
IMes	1,3-Bis(2,4,6-Trimethylphenyl)Imidazol-2-Ylidene
IPDI	Isophorone Diisocyanate
IPr	1,3-Bis(2,6-Diisopropylphenyl)Imidazol-2-Ylidene
IR	Infrared
IRMOF	Isoreticular Metal-Organic Framework

LUMO	Lowest Unoccupied Molecule Orbital
m	Middle
m	Multiplet
MALDI	Matrix-Assisted-Laser-Desorption-Ionization
MC	Merocyanine
MCO	5-Methoxycyclooctene
MDI	Methylene Diphenyl Diisocyanate
Me	Methyl Group
MeOH	Methanol
Mes	Mesityl
mIm	2-Methylimidazolate
M_{lim}	Limiting Molecular Weight
M_n	Number Average Molar Mass
MOF	Metal-Organic Framework
MON	Metal-Organic Nanosheets/Network
MS	Mass Spectrometry
M_w	Weight Average Molar Mass
N	Nucleophilicity Parameter
N,N-ligands	Ethylenediamine-Based Ligands
NaAsc	Sodium Ascorbate
NEM	N-Ethylmaleimide
NHC	N-Heterocyclic Carbene
NMR	Nuclear Magnetic Resonance Spectroscopy
OMe	Methyl Ester (Protection Group)
oQDM	Ortho-Quinodimethide Diene
PCP	Porous Coordination Polymer
PDI	Polydispersity Index (PDI = Mw/Mn)
PI	Poly(Isoprene)
PIB	Poly(Isobutylene)
pKA	Negative Common Logarithm Of Acid Dissociation Constant, Ka
pKB	Negative Common Logarithm Of Base Dissociation Constant, Kb
PMA	Poly(Methylacrylate)
PMMA	Poly(Metylmethacrylate)
PNB	Poly(Norbornene)
ppm	Parts Per Million

PS	Poly(Styrene)
PSM	Post-Synthetic Modification
pTHF	Poly(Tetrahydrofuran)
PU	Poly(Urethane)
PXRD	Powder X-Ray Diffraction
q	Quartet
R^2	Correlation Coefficient
RCM	Ring-Closing Metathesis
R_f	Retention Factor
RI	Refractive Index
ROMP	Ring Opening Metathesis Polymerization
rpm	Rounds Per Minute
RT	Room Temperature
s	Strong
s	Singlet
SBU	Secondary Building Units
SE	Stretching Experiment
SEM	Scanning Electron Microscopy
SIPr	*N,N*-Bis(2,6-Diisopropylphenyl)Imidazolidin-2-Ylidene)
SME	Shape Memory Effect
SMFS	Single-Molecule Force Spectroscopy
SMPU	Shape-Memory Polyurethane
SMTPU	Shape-Memory Thermoplastic Polyurethane
SP	Spiropyran
SS	Soft Segment
STP	Spirothiopyran
t	Triplet
TABS	Thermally Activated Barrier To Scission
t-BDA	Tert-Butyl Diazocetate
$T_{deco,end}$	Temperature At The End Of Decomposition
$T_{deco,str}$	Temperature At The Start Of Decomposition
TDI	Toluene Diisocyanate
TEP	Tolman Electronic Parameter
TFA	Trifluoroacetic Acid
T_g	Glass Transition Temperature

TGA	Thermogravimetric Analysis
THF	Tetrahydrofuran
TIF	Tripodal Imidazolate Framework
TLC	Thin-Layer-Chromatography
T_m	Melting Temperature
TMC	Thiomerocyanine
TMP	Trimethylolpropane
TMSCl	Trimethylsilyl Chloride
TNT	2,4,6-Trinitrotoluene
TOF	Time-Of-Flight
Tp^{Br3}	Hydrotris(3,4,5-Tribromo-1-Pyrazolyl)Borate
TPU	Thermoplastic Poly(Urethane)
T_{trans}	Transition Temperature
UPy	2-Ureido-4-Pyromidone
US	Ultrasound/Ultrasonication
UV	Ultraviolet
UXF	Universal Extensional Fixture
VA	4-Vinyl Aniline
vis	Visible
w	Weak
WAXD	Wide-Angle X-Ray Diffraction
WAXS	Wide-Angle X-Ray Scattering
WVTR	Water Vapor Transmission Rate
XRD	X-Ray Diffraction
ZIF	Zeolitic Imidazolate Framework
λ_{em}	Emission Wavelength
λ_{ex}	Excitation Wavelength

Parts of the Introduction, Results and Discussion and the Experimental Part were already published in:

1. "*Cyclopropanation of poly(isoprene) using NHC-Cu(I) catalysts: Introducing carboxylates*"

Shinde, K. S., Michael, P., Rössle, M., Thiele, S., Binder*, W. H.

J Polym Sci. 2020; 58: 2864–2874.

DOI: https://doi.org/10.1002/pol.20200404

(Published under a Creative Commons license, CC BY 4.0)

2. "*A Mechanochemically Active Metal-Organic Framework (MOF) Based on Cu-Bis-NHC-Linkers: Synthesis and Mechano-Catalytic Activation*"

Shinde, K. S., Michael, P., Fuhrmann, D., Binder*, W. H.

Macromol. Chem. Phys. 2023, 224, 2200207

DOI: https://doi.org/10.1002/macp.202200207

(Published under a Creative Commons license, CC BY-NC-ND 4.0)

3. "*Mechanochemical Activation of a Metal–Organic Framework Embedded within a Thermoplastic Polyurethane Matrix: Probing Fluorogenic Stress-Sensing*"

Shinde, K. S., Michael, P., Binder*, W. H.

Macromol. Chem. Phys. 2023, 2300297

DOI: https://doi.org/10.1002/macp.202300297

(Published under a Creative Commons license, CC BY-NC 4.0)

1 INTRODUCTION

1.1 *N*-Heterocyclic Carbenes (NHC)

Nitrogen-heterocyclic carbenes (NHCs) are a fascinating class of organic chemical compounds, thus resulting in widespread investigations over the past 20 years. The first metal-bound NHC complexes were reported independently by Wanzlick and Öfele in the 1960's.[1-4] This was followed by Bertrand and co-workers reporting the first isolable carbene in the presence of heteroatoms such as phosphorus or silicones on adjacent positions to the carbenic carbon in 1988.[5]
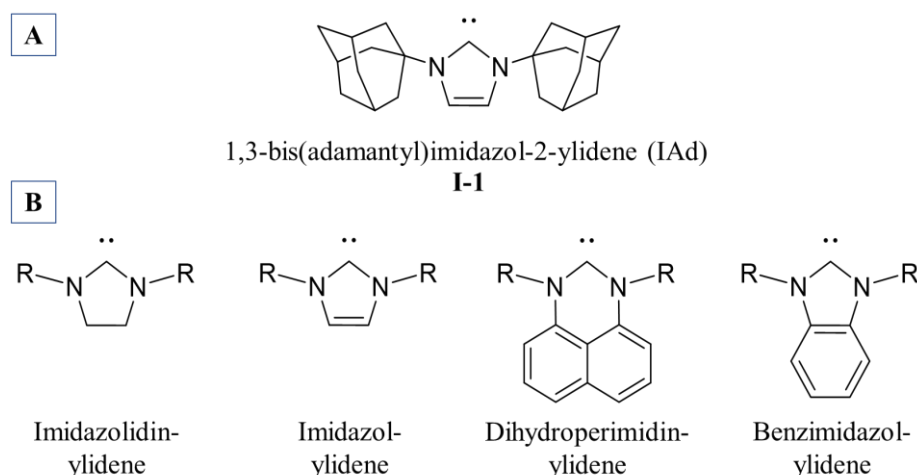
Figure 1. A) The first isolated NHC named 1,3-bis(adamantyl)imidazol-2-ylidene (IAd, (**I-1**)) by A. J. Arduengo.[6] **B**) General structures of some of the commonly used NHC scaffolds.

A. J. Arduengo built on this to demonstrate an extremely stable and therefore isolable carbenic carbon within a nitrogen heterocycle.[6] This first NHC, named 1,3-bis(adamantyl)imidazol-2-ylidene (IAd, **I-1**) (**Figure 1A**), has since led to innumerable theoretical and experimental studies,[7] resulting into a great variety of NHCs with different scaffolds being synthesized (**Figure 1B**). The reactivity of NHC's have neem subject to many considerations, as discussed below in the next chapters.

1.1.1 General Structure and Bonding Properties

The structure and bonding of NHCs are crucial aspects to understanding their properties. Characterized by a divalent carbon atom containing a lone pair of electrons and at least one nitrogen atom within a heterocyclic ring structure,[8, 9] NHCs have been defined by key structural features such as electronic stabilization by heteroatoms, steric-shielding substituents, varying ring sizes and differing backbones (**Figure 2A**),[10] and they all influence the reactivity and the carbene stability.

It is a challenge to describe the shape and steric demands of an NHC in a general way since they strongly depend upon the substituents. The substituents attached to the nitrogen are extremely influential by providing a significant steric environment to the reactive carbenic carbon centre. One of the examples of such an influence of bulky substituents of an NHC is a kinetic stabilization of the carbene to hinder a potential dimerization, as predicted by the Wanzlick equilibrium.[11] The steric properties of the substituents also need to be considered in relation to organocatalysis, as the steric accessibility to the carbenic carbon influences the reactivity of the nucleophilic NHC with other organic electrophilic

materials such as aldehydes, the elimination of the NHC after the cycle, as well as any intermediate steps.[12-15]
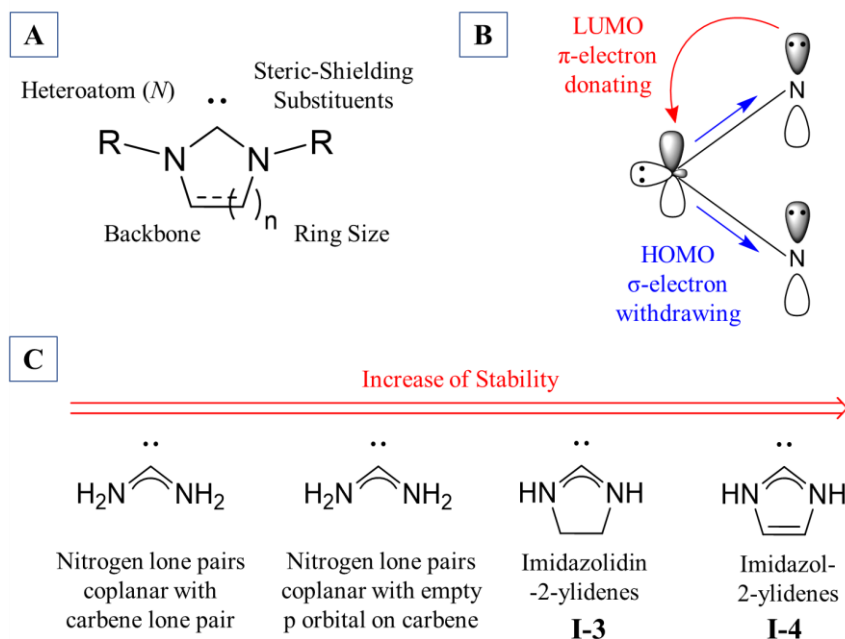
Figure 2. A) The key structural features of any NHC. **B)** Electronic bonding within NHCs. **C)** Stability of some carbenes, determined by isodesmic calculations for the reaction of the carbene with methane.[16]

The electronic stabilization by the adjacent heteroatoms, which in this case is the highly electronegative nitrogen, results in a singlet ground-state electronic configuration with the lowest unoccupied molecular orbital (LUMO) and the highest occupied molecular orbit (HOMO) denoted as an unoccupied p-orbital and a formally sp2-hybridized lone pair at the carbonic carbon, respectively (**Figure 2B**).[7] The presence of the nitrogen results in an inductive σ-electron withdrawing, reducing the electron density at the carbenic carbon. Additionally, the present lone pair of electrons on the heteroatom are donated mesomerically to the empty p-orbital (π- electron donating) (**Figure 2B**).[17]

Conjugation in the cyclic backbone further increases electronic stability of NHCs. Initially when the aromatic nature of the imidazolium ring was considered critical for NHC stability, a saturated NHC with a bulky mesityl *N*-substituent (SIMes, **I-2**) was obtained and characterized in 1995.[18] However, the presence of unsaturation results in an enhanced thermodynamic stability in the NHCs, calculated to be ~25 kcal mol^{-1} higher for the unsaturated imidazol-2-ylidenes (Im, **I-4**) compared to the corresponding saturated imidazolidin-2-ylidenes (SIm, **I-3**), allowing the possibility to obtain NHCs without proximal steric substituents such as methyl-substituted 1,3-di(methyl)imidazol-2-ylidene (IMe).[19, 20] Additionally, isodesmic calculations conducted on a set of samples (**Figure 2C**) show that carbenic carbons surrounded by amino groups were still stabilized without conjugation due to the σ electron-withdrawing properties of the nitrogen. However, the conjugation definitely increased stability, in which imidazolidin-2-ylidenes (**I-3**) were stable, while imidazol-2-ylidenes (**I-4**) were the most stable (**Figure 2C**).[16]

The ring size is an important factor as it leads to changes in orbital overlap, thus affecting the electronic properties. The geometry of the NHC structures also affect the steric properties by effectively pushing the nitrogen in the heterocycle as well as the attached substituents either closer or further from the carbenic carbon.[15] In terms of the electronic properties, the NHC ring size influences the Tolman

electronic parameter (TEP, discussed in detail in **Chapter 1.1.2.1**). As demonstrated in **Figure 3** in a series of substituted five- (**I-2**), six- (**I-5**), and seven-membered NHCs (**I-6**), the TEP of a series of saturated *N*-mesityl-substituted NHCs showed a decrease from 2050.8 cm^{-1} to 2041.9 cm^{-1} with increasing ring size (**Figure 3A**). The size of an NHC ring inherently influences the hybridization of the ground-state orbitals, consequently impacting the stabilization of the carbene centre and, by extension, its electron-donating ability.[15] The percentage buried volume (%V_{bur}, discussed in detail in **Chapter 1.1.2.2**) of different saturated 2,6-diisopropylphenyl *N*-substituted NHCs showed an increase from 47.0 % to 52.7 % with increasing ring size (**I-7**, **I-8** and **I-9**) as the bulky substituents have higher proximity to the carbenic carbon in larger rings (**Figure 3B**).[15]
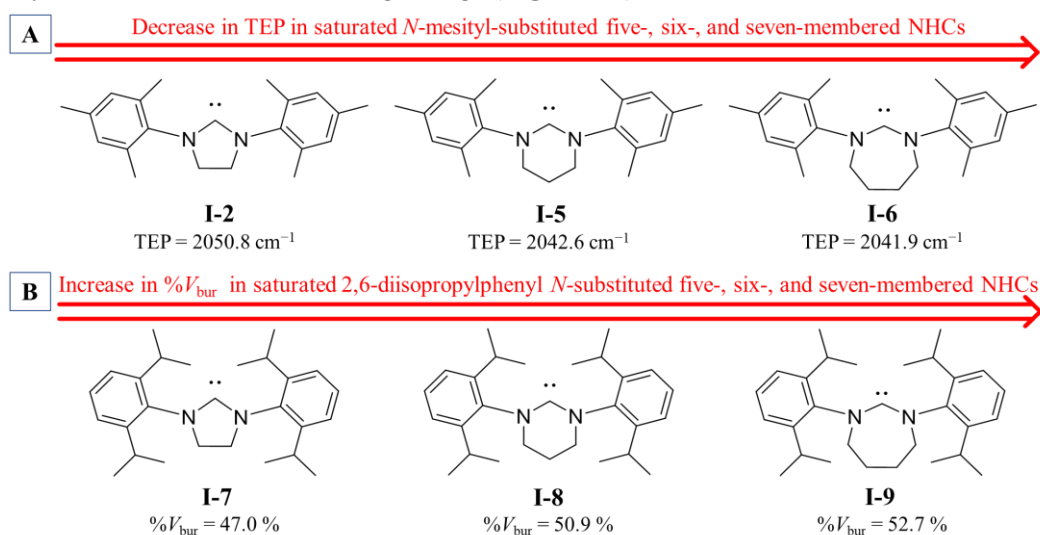
Figure 3. The effects of an increasing ring size from five- to seven- is shown in **A**) a scale showing a decrease in TEP and **B**) a scale showing an increase in percentage buried volume.

1.1.2   Quantifying Electronic and Steric Properties
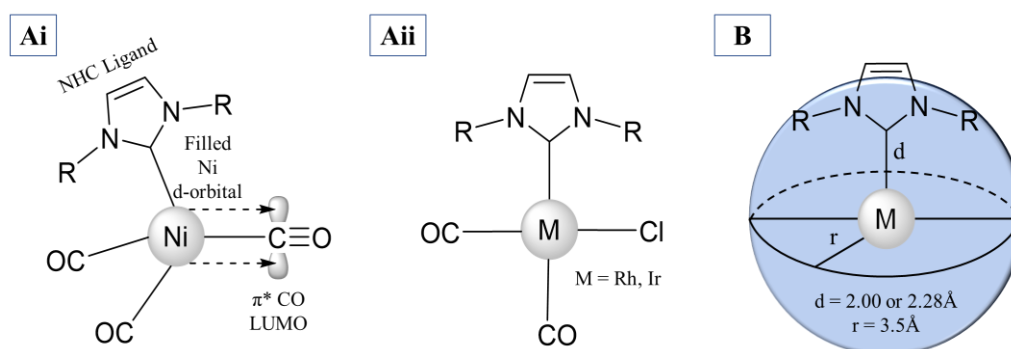
Figure 4. **A**) The measurement of Tolman Electronic Parameter (TEP) is conducted with either **i**) tetrahedral (NHC)Ni(CO)$_3$ or **ii**) square planar *cis*-(NHC)IrCl(CO)$_2$ or *cis*-(NHC)RhCl(CO)$_2$. **B**) The percentage buried volume (%V_{bur}) concept for characterizing the steric properties of NHC ligands. Figures adapted from literature.[15]

1.1.2.1   *Tolman Electronic Parameter*

Though many different methods of quantifying electronic properties of NHCs such as determining pKa, nucleophilicity parameter (N)[21] and Huynh electronic parameter (HEP)[22] exists, the Tolman electronic parameter (TEP) is by far the most commonly used to evaluate the electronic properties of NHCs.

Developed originally for phosphines,[23] the TEP was later adapted for NHCs. The TEP essentially correlates the infrared stretching frequency of carbon monoxide (CO) with the donor-acceptor properties of ligands in transition metal carbonyl complexes. The less electron donating is the NHC ligand, lower is the electron density at the metal centre.[7] This increases the electron donation between the metal centre into the π* antibonding orbital of CO ligand, weakening the CO triple bond and causing a lower frequency A_1 vibration in the complex's infrared (IR) spectrum.[15] A comparison of the obtained IR spectra enabled the possibility to indirectly evaluate the electron-donating ability of metal complexes depending on specific NHCs attached,[15] resulting in a compilation of a library of quantified NHC complexes.[21]

The TEP were earlier measured with the tetrahedral nickel(0) complex $(NHC)Ni(CO)_3$ (**Figure 4Ai**).[24] However, with growing concerns of the high toxicity and low boiling point of the complex, less toxic square planar complexes such as *cis*-$(NHC)IrCl(CO)_2$ or *cis*-$(NHC)RhCl(CO)_2$ were utilised (**Figure 4Aii**).[25-27] To standardize the different TEP values obtained with different metal complexes, mathematical equations (**Equation 1.1** and **1.2**) were used to correlate the different values of TEP measured. However, variations can still occur in the measured TEP values depending on the resolution of the infrared spectrometers and the solvent being used. As the range of wavenumber values for TEP is considerably small (v_{CO} ~2000-2100 cm^{-1}), IR spectrometers require higher resolution, while using common solvents such as hexane, CH_3Cl or CH_2Cl_2.[15, 22] Hence, comparison of TEP values should always be done between samples measured in the same conditions using the same solvent. To navigate through these limitations, computational methods were developed that not only successfully reproduce experimental data but also nullify the need to synthesize the metal complexes experimentally to measure TEP values.[28-31]

Rh to Ir: $v_{CO, Ir} = 0.8695\ v_{CO, Rh} + 250.7\ cm^{-1}$ eq. (**1.1**)

Ir to Ni: $TEP = 0.847\ v_{CO, Ir} + 336\ cm^{-1}$ eq. (**1.2**)

1.1.2.2 *Percentage Buried Volume*

Along with the electronic properties, the steric properties of NHCs are also important to understand their reactivity and stability. For this purpose, the percentage buried volume parameter (%V_{bur}) was developed by Hillier *et al*.[32] which quantified the steric properties of NHCs. As presented in **Figure 4B**, the %V_{bur} value refers to a metal-NHC complex in which the M = metal is at the centre of a sphere of a fixed radius (r). Depending on the percentage of the sphere "buried" by the ligand complex, the buried volume is the ratio between the volume occupied by the NHC ligand to the total volume of the sphere. The %V_{bur} is usually determined by theoretical calculations with the NHCs, or from crystallographic data, using fixed parameter for the metal-carbenic carbon bond (d) of 2.00 or 2.28 Å and a sphere radius (r) of 3.5 Å. Therefore, a comparison between different NHCs can only be made if the same approach is used to determine the %V_{bur} values due to the substantial influence of the coordination environment on bond lengths and ligand conformation.[33-35] Hence, linear gold(I) complexes [AuCl(L)] as standard sources have proved to be extremely useful for %V_{bur} calculations as their uncluttered coordination sphere avoids steric clashing with other ligands.[15] Nowadays, a free application on the Internet named Samb*V*ca[36] can be used easily to calculate %V_{bur} from uploaded crystal structure information.

1.1.3 Coordination Chemistry and Catalysis of Metal-NHC Complexes

Since one of the characteristics of NHCs is their ability to bond with main or transition group metal centres, understanding the nature of these bonds is of utmost importance. NHCs bind with metal centres

via dative or coordinate bonds, i.e., a bond in which both electrons come from the same atom (NHC in this case). The distance of such a bond, formed between the carbenic carbon of an NHC and a metal centre, inform about the ability of the metal to transfer any electron density to the carbene (called π back-donation) in any organometallic complexes.[37, 38] A key issue was understanding the degree of σ and π bonding between the NHCs and metal centres. In the context of NHCs, the main group elements (groups 1-2 and 13-17) lack the availability of partially filled d-orbitals required for effective back-donation and hence the NHCs bond with the metals mainly by σ bonding, while the π back-bonding is insignificant.[10] On the other hand, transition metals (groups 4-12[39-56]), typically late transition metals (groups 8-11), exhibit substantial π back-bonding from the metal to the NHC due to the partially filled d-orbitals that interact with the electron rich carbenic carbon of an NHC (**Figure 5**).[38] The extent of the contribution of the π back-bonding in the overall bonding energy was studied by Hu *et al*.[57] and Nemcsok *et al*.[58] In the former studies, other than the overall donation from the ligand to the metal in agreement to the expected σ bonding, Hu and coworkers reported significant π back-bonding interactions between the p_π orbitals of the carbene and the metal d_{xz} and d_{yz} orbitals of the NHC-Ag bond, approximately contributing 15-30 % of the complexes overall orbital interaction energies.[59] In the latter studies, Nemcsok and coworkers while working with M-NHC complexes of coinage metals (Ag, Au and Cu), quantified the π back-bonding contribution to about 20 %, highlighting its importance in NHC-metal bonding.[16]
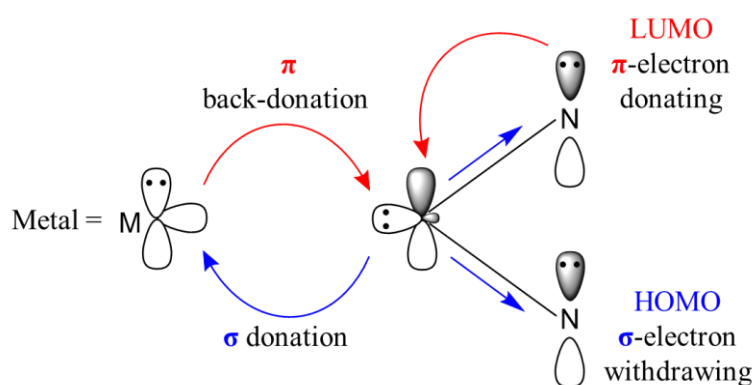
Figure 5. Bonding between metal and ligand within metal (M)-NHC complexes

One of the most important features of metal-NHC complexes is their ability to act as catalysts. A selection of metal-NHC complexes that have found such an application would be described thereafter.[60] Ruthenium (Ru)-based catalysts to perform olefin metathesis have been around since the 1990's.[61] However, due to their limited activity, effort was made to improve the catalytic species leading to the introduction of NHC-based Ru catalysts. The effort involved incorporating NHCs with different variations in terms of symmetry, substituents, heteroatoms in the backbone, ring size and presence of chirality.[16] To standardize the reactivity of new complexes, the Ru-based catalysts are usually investigated for the ring-closing metathesis (RCM) of diethyl diallylmalonate (**I-10**), the ring-opening metathesis polymerization (ROMP) of 1,5-cyclooctadiene (**I-11**) and the cross-metathesis (CM) of allylbenzene (**I-12**) and *cis*-1,4-diacetoxy-2-butene (**I-13**) (**Scheme 1B**).[62] One of the most important NHC-based series of metal catalysts are named Grubbs and Hoveyda–Grubbs complexes.[63-65] The catalyst have shown excellent activity in both ring closing metathesis of sterically hindered tri- and tetra-substituted olefins[66] and ring opening metathesis polymerization of sterically hindered olefins.[67, 68] NHC-based Ru catalysts have also found use in non-metathesis organic reactions which include transfer hydrogenation,[69-71] β-alkylation of secondary alcohols with primary alcohols[72] and C-H activation by arylation of functional arenes.[73, 74] Amidation of primary amines with primary

alcohols have also been possible with exceptional yields (**Scheme 1A**).[75, 76] In a relatively newly published work, Wang *et al.*[77] synthesized five different benzimidazole-derived Ru NHC complexes to cause a highly efficient dehydrogenation of aliphatic and aromatic alcohols to form carboxylic acids with a notably low Ru loading (125 ppm) (**Scheme 1C**).
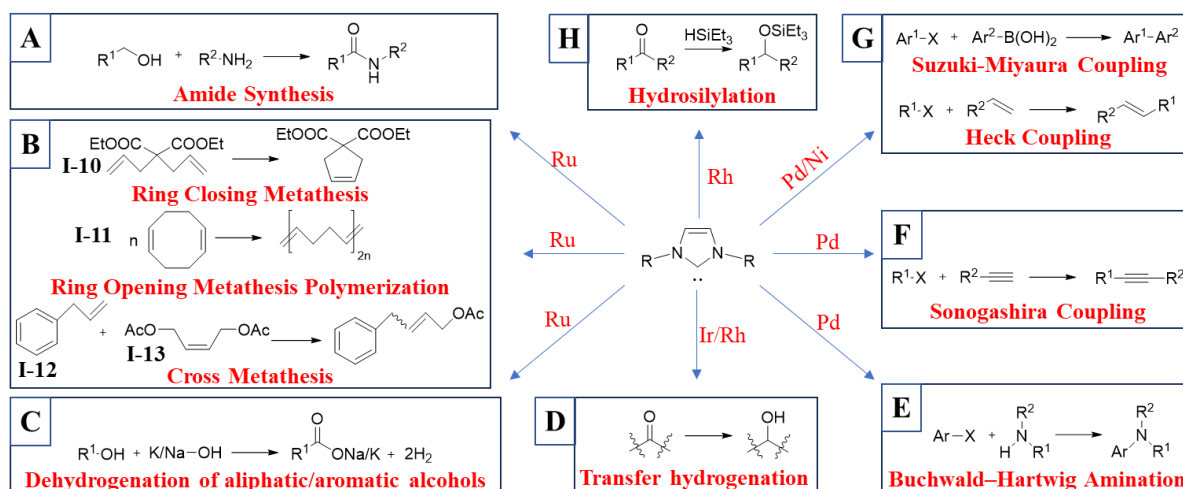
Scheme 1. Schematic figure displaying the different reactions possible with various metal-NHC complexes. Ru-based catalysts are used for **A**) amide synthesis, **B**) metathesis reactions and **C**) dehydrogenation of aliphatic/aromatic alcohols. **D**) Transfer hydrogenation is performed in the presence of Ir or Rh-based NHC complexes. Pd-NHC complexes are used during **E**) Buchwald-Hartwig amination, **F**) Sonogashira coupling and **G**) Heck coupling, which are performed also with Ni-based complexes. Finally, **H**) hydrosilylation is performed in the presence of Rh-based catalysts.

Along with ruthenium, rhodium (Rh) and iridium (Ir) catalyst complexes with NHC ligands have also been employed, largely for reduction and oxidation processes.[16] Iridium being less expensive and more efficient resulted in the Ir-complexes being utilised more than the traditionally used Rh-catalysts.[62] Rh and Ir-complexes have both shown extraordinary C-H activation possibilities while performing transfer hydrogenation (**Scheme 1D**) in the presence of isopropanol and a base.[78, 79] Rh-based NHC complexes have been used for hydrosilylation (**Scheme 1H**),[80] hydroboration,[81] and hydrogenation.[82] The catalytic hydrogenation of alkenes was achieved with both an iridium (Ir) NHC[83] and a Ru NHC.[84] Ruthenium aside, palladium stands out as one of the most extensively employed transition metals in NHC complexes utilized in catalysis. The amination of aryl halides in the presence of palladium, named Buchwald-Hartwig amination (**Scheme 1E**), is one such example utilising NHC-based Pd-complexes.[85, 86] Out of the many applications, the cross-coupling reactions take centre-stage since various Pd-NHC catalysts have been used in different reactions, including the Sonogashira (**Scheme 1F**),[87-89] Stille[90] and Negishi[91] couplings. Additionally, the effective use of Pd-NHC catalysts for Suzuki-Miyaura coupling reaction (**Scheme 1G**) between aryl halides and arylboronic acids are also well documented.[92-94] In one of the first reported application of metal-NHCs, Hermann *et al.*[95] reported on the first application of NHCs as ligands in transition-metal catalysis in 1995, demonstrating Heck coupling reactions (**Scheme 1G**) with an active palladium (Pd) bis(NHC) catalyst. Working with a series of Pd NHCs, Kaloğlu *et al.*[96] demonstrated a direct C–H bond activation for the C5-arylation of 1-methylpyrrole-2-carboxaldehyde by aryl bromides.

1.1.4 Catalysis by Copper (Cu) NHC complexes

With copper being an integral part of the history of chemistry, it would come as no surprise that copper (Cu) NHC complexes became the "best-seller" in organometallic chemistry.[97] Arduengo *et al.*[98] reported in 1993 the first NHC-based Cu catalyst in the form of a Cu(I) bis(NHC) complex, [(NHC)$_2$Cu][O$_3$SCF$_3$], a homoleptic two-coordinate complex. Thereafter, a Cu(I) mono(NHC) (or Cu(I) NHC interchangeably) was also synthesized within a year.[99] However, following a period of disinterest, the revival of interest in Cu NHC complexes occurred only in the early 2000s with the ethylation of enones.[100] Since then, a diverse variety of reactions have been successfully catalysed by employing Cu NHC complexes, some of which are schematically displayed in **Scheme 2**.

While previously hydrosilylation was mainly conducted using a copper hydride species [Cu(H)(PPh$_3$)]$_6$ (PPh$_3$ = triphenylphosphine), also known as "Stryker's reagent",[101] Nolan and coworkers investigated and presented the possibility of performing hydrosilylation reactions in the presence of a Cu NHC.[102] Since reported by Meldal[103] and Sharpless[104] in 2001, copper(I)-catalysed alkyne-azide cycloaddition (CuAAC) has had a number of successful copper systems catalysing the reaction, including Cu NHCs. Neutral complexes [Cu(X)(NHC)][105] as well as homoleptic systems of the cationic form [Cu(NHC)$_2$]X[106] have both performed exceedingly in its role as catalyst for CuAAC. Lebel *et al.*[107] described the olefination of aldehydes and ketones in the presence of a Cu NHC complex. Although olefinations with rhodium-based Wilkinson's catalyst had been documented,[108] the copper-based alternative provided a more cost-effective solution. The transfer of carbene using diazo compounds using Cu NHC was first published by Fructos *et al.*[109] and will be discussed more in **Chapter 1.1.4.1**. The contributions of Ohishi *et al.*[110] resulted in the development of Cu NHC-catalysed carbonylation of boronic esters, providing a new alternative to rhodium catalysts.
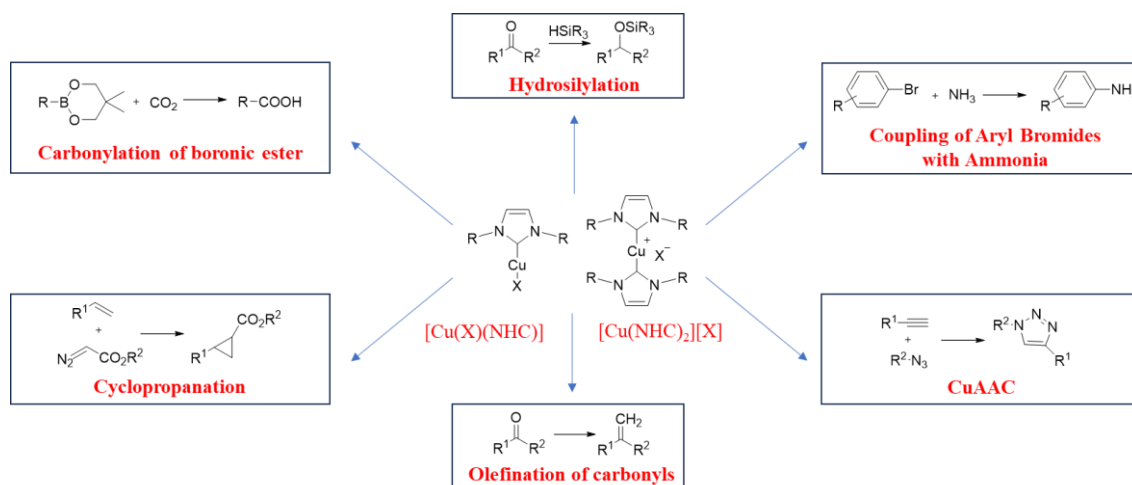
Scheme 2. Reactions catalysed by Cu NHC complexes.

1.1.4.1 *Cyclopropanation by Carbene Transfer*

Cyclopropanation of unsaturated moieties by generating carbenoids using diazo compounds in the presence of transition metal-catalysts is a particularly versatile method reported in literature, even if it is usually applied only for low molecular weight olefins.[111] Frequently used metal-catalysts based on palladium and rhodium,[112-115] but also Cu(I/II)-based catalysts were considered for these cyclopropanations.[116-119] Cyclopropanation of poly(diene)s, like poly(isoprene) or polybutadiene, are only rarely known examples in literature. For instance, a cyclopropanation of predominantly 1,2-syn-polybutadiene (1,2 linkage ~70 mol%) has been reported with methyl diazoacetate and a copper(I) triflate benzene complex ([CuOTf]·0.5 C$_6$H$_6$) as catalyst, achieving up to 33 mol% cyclopropane

modification corresponding to the polymer double bonds in DCM, albeit no preference to 1,2- or 1,4-linkages could be observed.[120] A more sophisticated approach used a [Tp^{Br3}Cu(NCMe)] catalyst (Tp^{Br3} = hydrotris(3,4,5-tribromo-1-pyrazolyl)borate) in the presence of ethyl diazoacetate to modify 1,2- and 1,4-*cis*-polybutadiene up to 100 % functionalization of the corresponding double bonds.[121] However, the synthesis of the catalyst [Tp^{Br3}Cu(NCMe)][122] proceeds *via* the highly toxic Tl[Tp^{Br3}] thallium precursor.[123] Though the obtained results are remarkable, the scale-up of the catalyst production is highly restrictive due to the toxicity of the thallium. Hence, it became of interest to find alternative metal catalysts that could achieve cyclopropanation with diazo esters.

Therefore, catalytic systems based on NHC ligand-metal complexes are important due to the minimal ligand dissociation related to the strong interactions between the NHC-ligand and the metal centre.[102] Metal-mediated cyclopropanation of unsaturated low molecular weight compounds with diazoacetates using Pd(0),[124] Au(I)[125, 126] and Cu(I)[109, 127] had been reported. However, most of those catalysts were applied only for low molecular weight compounds and not yet for polymers.

1.1.4.2 *Copper(I)-Catalysed Alkyne-Azide Cycloaddition*

Copper(I)-catalysed azide-alkyne cycloaddition, commonly referred to as CuAAC,[128-131] stands as a cornerstone in modern organic synthesis, enabling the rapid and efficient construction of complex molecules. Reported first by Meldal[103, 132] and Sharpless[104, 133, 134], the CuAAC represents a distinctive variant of the Huisgen's 1,3-dipolar cycloaddition,[135-137] in which terminal alkynes and alkyl/aryl azides engage in a [3+2] cycloaddition reaction to yield 1,4-disubstituted 1,2,3-triazole rings. In contrast, the thermally mediated Huisgen's 1,3-dipolar cycloaddition proceeds considerably slower by several orders of magnitude (up to ~10^{-6}) in comparison to CuAAC.[138] The formation of a carbon-heteroatom bond (C-X-C) was termed by Sharpless as "click" chemistry. This concept was accompanied by a stringent set of criteria that a reaction must satisfy to be categorized as such. The CuAAC fulfils almost all of these, such as: (a) the required characteristics to be achieved by "click" have a thermodynamic driving force higher than 20 kcal mol^{-1} (or 84 kJ mol^{-1}), (b) the reaction should be modular and wide in scope,[139-144] (c) achieve high yields, (d) generate no or easily removable byproducts, (d) simple product isolation *via* distillation or crystallization, (e) obtain stereospecific products, (f) the reaction conditions be mild and insensitive to oxygen and water, and (g) the usage of non-toxic solvents.[104] Along with homogeneous catalysts, "click" chemistry can be achieved using heterogeneous catalysts.[143, 145, 146]
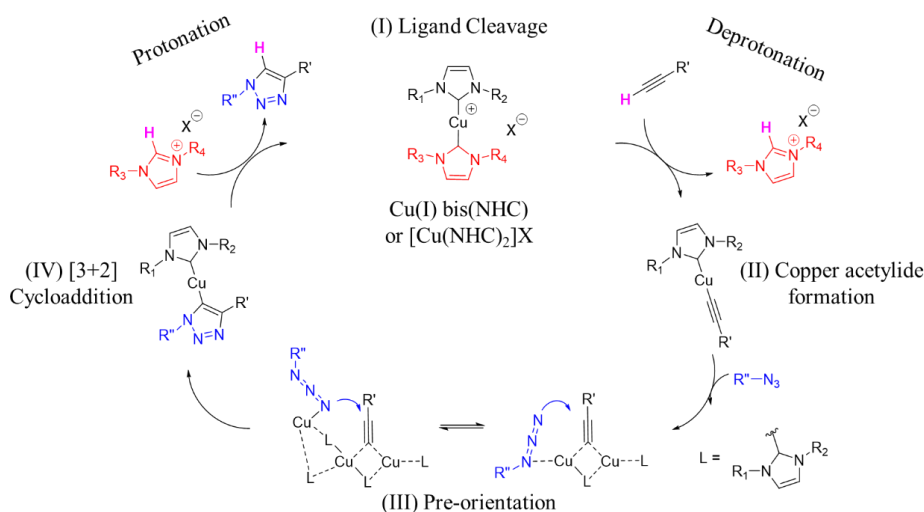
Figure 6. Mechanistic insight into the catalytic cycle of copper(I)-catalysed alkyne-azide cycloaddition (CuAAC).[147]

To investigate the mechanism of CuAAC, an intriguing starting point is the highly efficient and stable Cu(I) bis(NHC) or [Cu(NHC)$_2$]X (**Figure 6**).[148, 149] These cationic NHC-based complexes consists of two NHC ligands coordinated to a Cu(I) centre, exhibiting remarkable efficiency for CuAAC with high resistance to oxygen and water.[106] The mechanistic exploration begins with the initial step (**I**), encompassing two distinct processes. The first is the cleavage of the labile Cu-carbenic carbon bond of one of the two NHC ligand, which can then act as an internal base. The second is considered as the rate-determining step,[106, 150] and involves the basic NHC ligand deprotonating the alkyne to form copper(I) acetylide (**II**), while gaining the proton for itself. The coordination of the azide with the copper(I) acetylide involves certain mechanistic pre-orientations (**III**), which results in multiple Cu(I) centres forming binuclear/trinuclear complexes.[130, 151-154] Subsequently, the [3+2] cycloaddition reaction generates the 1,2,3-triazole intermediate bearing the Cu(I) moiety (**IV**). On protonation by the previously cleaved (and protonated) NHC, the final stereospecific 1,4-disubstituted-1,2,3-triazole is achieved. This also marks the regeneration of the initial Cu(I) bis(NHC), thereby concluding the catalytic cycle. The rate determining step is highly influenced based on the substituents and the saturation of the NHC in a Cu(I) bis(NHC) complex. As previously discussed in **Chapter 1.1.2**, the electronic and steric properties of the NHCs affect their reactivity and stability. Less bulky or electronic withdrawing groups like alkyl, *tert*-butyl (*t*-Bu) or cyclohexyl (Cy) have higher reactivity (albeit lower stability) than the more bulkier and electron donating groups like adamantly (Ad), mesityl (Mes) or 2,6-diisopropylphenyl (DIPP).[102, 155-159]

1.1.4.3 Recent Developments in Copper-NHC Catalysis

In the last five years (2018-2023), the expansion of literature based on Cu NHCs as catalysts has steadily continued. Cu(I) bis(NHC) and mixed NHC/phosphine copper complexes were used as efficient catalysts to enable copper-catalysed azide-alkyne cycloaddition (CuAAC) through [3+2] cycloaddition to form 31 different 1,4-disubstituted 1,2,3-sulfonyltriazoles in high yields (**Scheme 3A**).[160] These triazoles function as azavinyl carbene precursors in metal-catalysed transannulation but lack efficient synthesis methods as their synthesis is challenging due to the unwanted ring-opening side-reaction of the triazolyl-Cu intermediates. Previous attempts with other non-NHC copper-based catalysts were successful but required a strictly inert atmosphere. Hence, a novel preparation of *N*-sulfonyl-1,2,3-triazoles, in air and in the absence of base or additive, was achieved.[160]
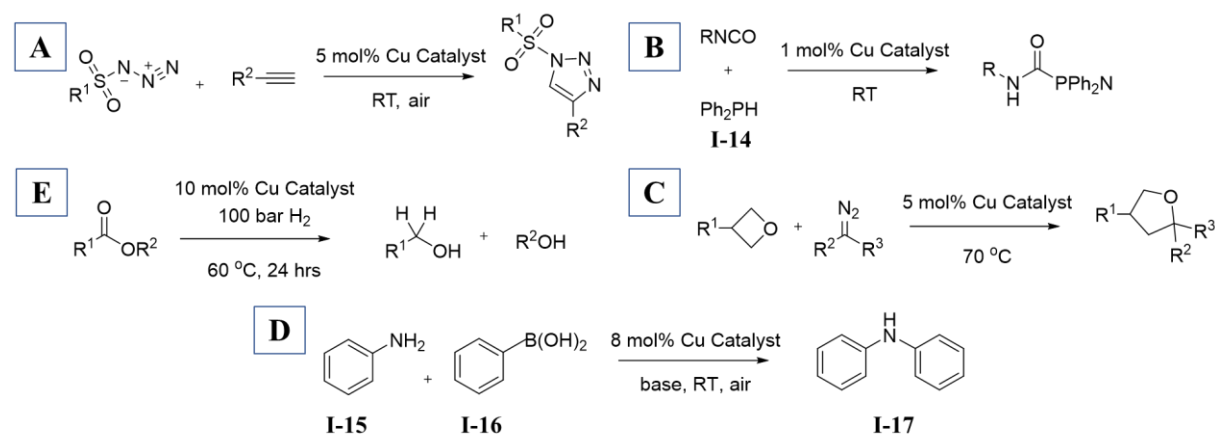
Scheme 3. Reaction schemes for **A**) CuAAC to form different 1,4-disubstituted 1,2,3-sulfonyltriazoles, **B**) catalytic hydrophosphination of different isocyanates, **C**) ring expansion of 3-substituted oxetanes to furans, **D**) Chan−Evans−Lam (CEL) coupling catalyst between aniline and phenylboronic acid, and **E**) activation of esters *via* hydrogen bonding.

The catalytic hydrophosphination of different isocyanates was conducted in the presence of (NHC)CuPPh$_2$ with diphenylphosphine (**I-14**) to form phosphinocarboxamides (**Scheme 3B**).[161] This is rather appealing as the hydrophosphination of isocyanates is rather underexplored compared to alkenes or alkynes due to challenges like competing side-reactions and limited substrates. Additionally, while catalyst-free isocyanate hydrophosphination is viable under strict neat conditions, it is largely restricted to small aromatic isocyanates. Astonishingly, compounds such as cyclohexyl isocyanate, which would not react under such conditions, achieved complete conversion within 30 min at a mere 1 mol% concentration of the copper catalysts, demonstrating their efficacy.[161] A catalytic pincer Cu(II) NHC was used to activate phenylboronic acids (**I-16**) in water to generate phenols by C-O bond formation. On many occasions, the activation of aryl boronic acids would inadvertently create byproducts such as benzene, anisole and diaryl compounds, but the widespread utility of phenols has rendered enhancing phenol synthesis from phenylboronic acids a key focus.[162] In another work, a set of Cu NHC complexes were employed for the ring expansion of 3-substituted oxetanes to furans with specifically symmetrical diazo compounds, with disubstituted oxetanes showing better reactivity than monosubstituted oxetanes (**Scheme 3C**).[163] A new and highly modifiable tetradentate Cu(II) NHC complex was utilized as a Chan−Evans−Lam (CEL) coupling catalyst between aniline (**I-15**) and phenylboronic acid (**I-16**) to obtain diphenylamine (**I-17**) by the formation of carbon-nitrogen bond (**Scheme 3D**). CEL reactions utilize (**I-16**) as a coupling agent for oxidative nucleophile-nucleophile coupling with amines or other nucleophiles. While commonly conducted with palladium, the authors wanted to explore copper for economic advantages. Additionally, usually reported CEL reactions conducted with copper required excess amounts of copper, which by definition would term the copper as reagents instead of catalysts. In the case of this study however, decent yields were achieved with only 8 mol% of the synthesized Cu(II) NHC complex at room temperature (RT) in methanol (MeOH), while optimizing reaction parameters only improved results. Hence, a novel tetradentate copper(II) complex with stability in protic solvents was introduced for CEL.[164] A bifunctional Cu(I) NHC complex achieved the activation of esters *via* hydrogen bonding and nucleophilic copper(I) hydride (Cu(I)H) generation from H$_2$ (**Scheme 3E**). This enabled catalytic hydride transfer to esters, facilitated by a guanidinium subunit for proton transfer. This approach stood out as Cu(I)H had not been reported previously for such transformations, as they require the use of "hard" stoichiometric metal hydrides which are associated with generation of metal waste and tedious work-ups, especially on a larger scale. Therefore, the approach not only broadened the applications of Cu(I)H, but also introduced a desirable catalytic hydrogenation of esters while mitigating the drawbacks of traditional methods.[165]

1.2 Mechanochemistry
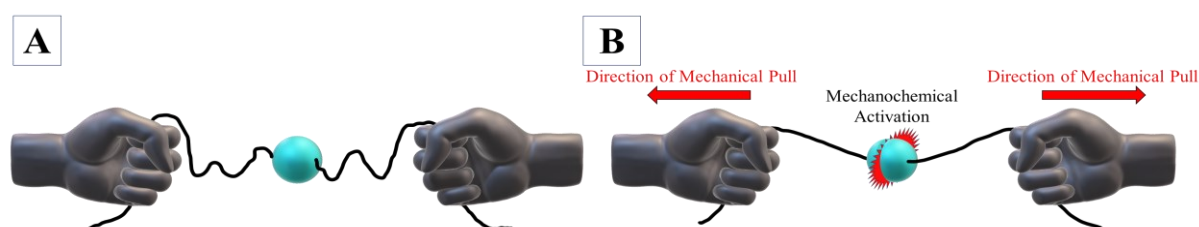
Figure 7. An illustrative depiction of a mechanophore as a bluish-green ball attached by its polymeric handles (black string) **A)** before force is applied and **B)** as force is applied (depicted by pulling).

Driven by an external force, mechanochemistry uniquely initiates chemical reactions by activation of mechanophores.[166-168] Mechanophores are defined as "*molecular units that produce a physical or*

chemical response when an applied mechanical force brings about a structural rearrangement (such as a conformational change or bond scission). The rearrangement results in a response that varies from a physical signal (such as a change in absorbance or emission of light) to a chemical signal (such as enhanced catalytic activity, formation of a reactive radical or the release of a small molecule)" (Mechanochemical tools for polymer materials, *Chem. Soc. Rev.* **2021**, *50*, 4100-4140).[169] In **Figure 7**, the bluish-green sphere is the mechanophore possessing mechanically labile bonds. The string attached to it is the polymeric part attached to a mechanophore that focuses and orients the applied force. Chemical transformations[170] occur on activation of a mechanophore under mechanical forces (depicted by the mechanical pull in **Figure 7B**). Such a force is applied by various mechanochemical activation methods (**Chapter 1.2.1**), and could lead to different functions of the mechanophore, similar to solid-state chemistry, where intramolecular bonds are mechanically broken[171] by an external force. Covalent chemical bonds in both thermoplastic and thermoset polymers can be broken by mechanical fields, leading to a reduction in either molecular weight and order, as reported by Staudinger as early as 1930's.[172] This behaviour is related to mechanochemistry, where the activation and rupturing of covalent chemical bonds is induced by mechanical energy, resulting in novel reaction pathways different from thermal or photochemical activation.[167, 168, 173-178]

The breaking of the labile bond by mechanic force can be explained by the thermally activated barrier scission (TABS) theory. The TABS theory proposes that chemical reactions occur when molecules overcome energy barriers due to thermal energy. It suggests that at higher temperatures, molecules possess sufficient energy to surpass these barriers and undergo reactions.[179-181] Conversely, increased energy through applied mechanical force should also lower the barrier, aiding mechanochemical activation at lower temperatures. Additional factors such as the length of the attached polymer backbone to the mechanophore[168, 182] and the mechanophore position in the polymer backbone (position at the midpoint of the polymer is ideal)[183] influences the efficiency of bond breakage. Furthermore, the balance of stiffness and flexibility of a polymer backbone for effective and efficient force transmission is also of utmost importance.[184, 185]
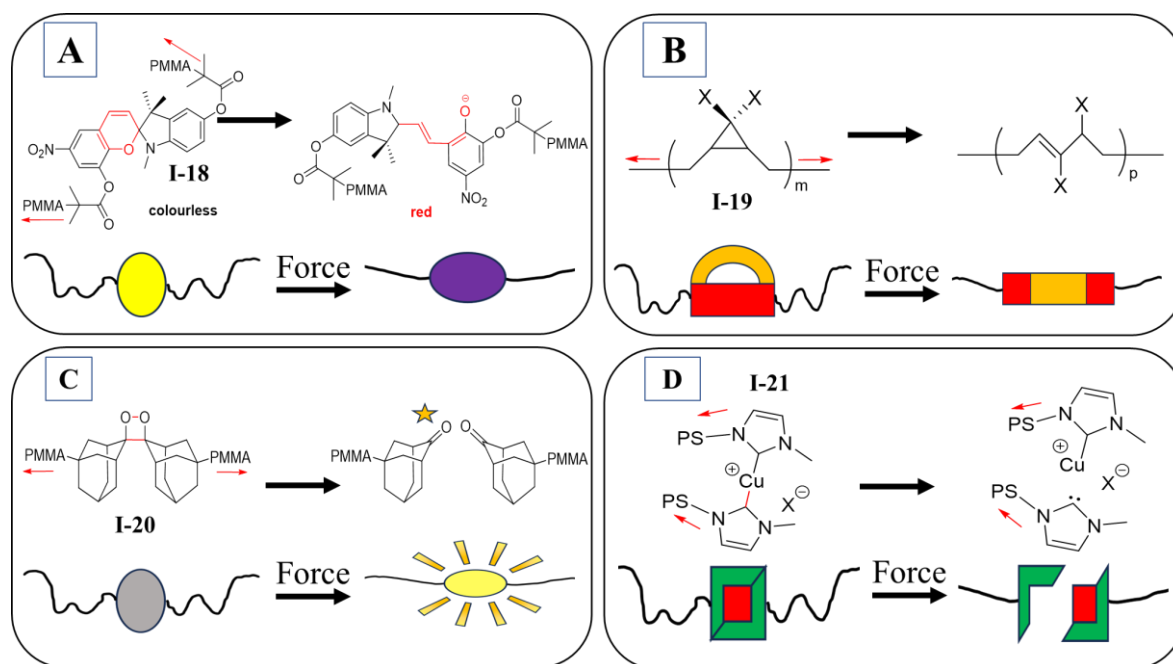
Figure 8. Generalized polymer-based mechanophores being subjected to mechanical force and subsequent responses such as: **A**) change in colour due to isomerization, **B**) cyclic mechanophores undergoing ring-opening, **C**) appearance of fluorescence and chemiluminescence, and **D**) activation of mechanocatalysts resulting in the creation of catalytic active sites. Adapted from literature.[147, 186]

In polymer science, there are several types of mechanophores, which transmit the applied external force to the chemical labile bonds (displayed as red bonds in **Figure 8**) *via* the attached polymer chains. The resulting cleavage of the labile bond leads to the formation of reactive species, a few of which are showed as examples in **Figure 8**.[186] **(A)** Mechanophores which display a visible colour change, caused by a change in absorption maximum due to bathochromic shift, have applications in stress sensor development and are termed as mechanochromophores. These include spiropyranes **(I-18)**,[187-190] anthracenes,[191-193] coumarins[194] and rhodamines.[195-197] **(B)** Some cyclic mechanophores are capable of releasing stress *via* ring-opening reactions, resulting in elongation of polymeric backbones (e.g., cyclopropanes **(I-19)**.[198, 199]) **(C)** Mechanophores that respond with the appearance of fluorescence/luminescence on application of mechanical stress, termed 'turn-on' response, are termed mechanoluminescent mechanophores (e.g., 1,2-dioxetanes **(I-20)**,[200-202] or rotaxanes[203]). **(D)** A selective scission of labile bonds between a metal centre and ligands attached to it could lead to at least one of the ligands being cleaved off, thus initiating a mechanochemically activated metal-catalysed reaction (**Chapter 2**). Termed as mechanocatalysts, **Figure 8D** shows such a creation of active centre on breaking of the labile bond between NHC ligands and metals in a Cu(I) bis(NHC) complex **(I-21)**, an important structural compound for further work in the scope of this thesis.

1.2.1 Mechanochemical Activation Methods

On incorporation of a mechanophore into a polymer, its activation by mechanical force could be investigated. The mechanochemical activation is usually first evaluated in a solution and then in solid bulk matrices. The following part provides an overview of the fundamental principles and applications of certain activation methods.

1.2.1.1 In Solution

In solution, mechanophores can be activated by different methods such as solvent swelling,[204, 205] freeze-thaw cycles[206-208] or turbulent and elongation flow exerting shear stress.[209, 210] However, ultrasonication[178, 211-218] remains the most common method for mechanochemical activation for polymers in solution, and hence this chapter would focus on that particularly.
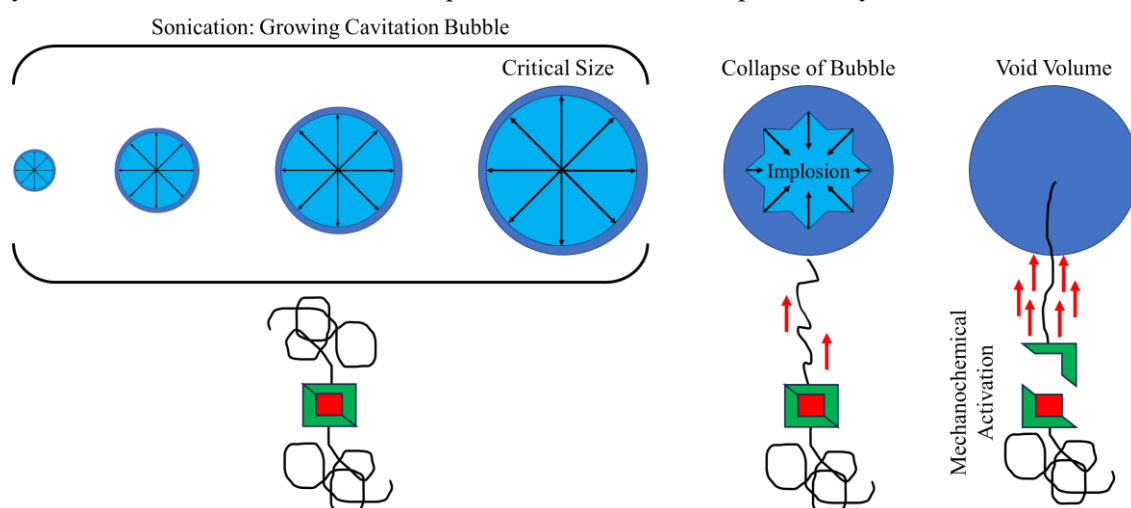
Figure 9. Polymeric mechanophores undergoing ultrasound-induced scission. Under ultrasound, cavitation bubbles form and grow until a critical size is reached after which they collapse by implosion and form a void volume. The void volume pulls in the nearby randomly coiled polymer into it, resulting in one end of a mechanophore being pulled faster, and leading to the cleavage of the weak labile bond.

Ultrasonication/Ultrasound is usually categorized into two types: high frequency (2-10 MHz) low intensity (max 0.5 W cm^{-2}) and low frequency (20 kHz-2 MHz) high intensity (min 10.0 W cm^{-2}).[219] While the former is termed non-invasive and used for medical applications, the latter is ideal for mechanochemistry.[220, 221] During ultrasonication (**Figure 9**), acoustic shockwaves induce the formation of cavity bubbles in the solvent. The bubbles increase in size as the surrounding volatile compounds or solvent migrate into it.[222] At a critical size, the cavitation bubbles implode rapidly on a timescale of microseconds, thus pulling in one end of the polymer handle attached to a mechanophore fast into the created void volume. The closer end of a polymer chain to a void volume is pulled in, causing the polymer random coils to be uncoiled and stretched till a certain limit is reached. Beyond this, the force generated by the stretching of the coil aggregates in the midpoint of the polymer chain, leading to the cleavage of the labile bond most close to the midpoint (optimal activation within ~15 % of the centre of the polymer chain).[220, 223] The high activation efficiency in ultrasonication is due to the high strain rates (10^6-10^8 s^{-1}) involved.[209, 219]

1.2.1.2 *In Bulk Materials*

It is of major importance to study mechanochemistry of mechanophores within bulk materials as most technical applications of polymeric materials are in the solid state. In solid bulk, mechanophores can be activated by grinding/ball milling,[208, 224-227] tensile testing,[228-230] compression[189, 231-233] or torsional shear force.[190] Although, solid-state methods have slower strain rates (1-100 s^{-1}) compared to ultrasonication, they are able to exert much higher maximum forces (10^5 N compared to 10^{-9} N in ultrasonication).[220] The two most common methods are compression tests or uniaxial tensile stress (**Figure 10A**). If the probed sample is stretchable and can withstand stress, tensile testing is more accurate to measure the toughness of a sample. However, if the samples are brittle, compression tests are a decent alternative. This is because it's challenging to determine the local stress between the sample and the force-exerting plate in compression testing, especially compared to the well-defined stress in elongation testing such as tensile stress.[169]

The basics of mechanochemical activation remain the same in either compression or elongation (uniaxial tensile testing or extensional oscillatory and rotational rheology instrumentation), i.e., the mechanophore within the matrix material is stretched continuously until a certain threshold, after which the labile bond is cleaved off (**Figure 10A**).[186] If the molecular weight of a mechanophore exceeds a certain value, the mechanophore could be efficiently activated even if it's only physically entangled.[234] The orientation of the mechanophore is more important in the solid-state as those oriented parallel to the applied force show higher activation (**Figure 10A**).[187, 229] The crystallinity of the polymer matrix also influences activation as mechanical force transmission is better through the crystalline parts of a polymer to reach labile bonds.[235]

The activation of mechanophores by compression was achieved by fixing the polymeric backbones attached to the mechanophores within a matrix material (**Figure 10A**),[147] either by covalent[236, 237] or supramolecular crosslinks.[238-240] The transmission of force is also observed to be improved by incorporation of the mechanophores within a network rather than in linear or chain-extended architectures (**Figure 10B**). Within a network, the mechanical force perpendicular to the orientation of the mechanophore is redirected, in turn increasing activation efficiency.[187, 229] This effect was studied in the case of spiropyran (**I-18**), comparing its activation within networks[238, 239, 241] and non-networks.[189, 228]

In an example of applying elongation stress *via* extension rheology instrumentation, Chen *et al.*[200] displayed the cycloreversion of bis(adamantyl)-1,2-dioxetane (**I-20**), observed as force activated chemiluminescence within a PMMA matrix. The experiment was conducted by fixing the 1,2-

dioxetane-embedded PMMA sample between two rotating drums which applied uniaxial stress by elongating the sample. The bright-blue chemiluminescence was observed optically with a charge-coupled device (CCD) detector to quantify the relationship between material properties and the mechanochemical activation.[147, 200] In general, such an optical response depends on the activation of the mechanophore and if the emitted light is detectable as visible light, fluorescence or luminescence. The use of different methods of optical detection is common and favoured due to its many advantages.
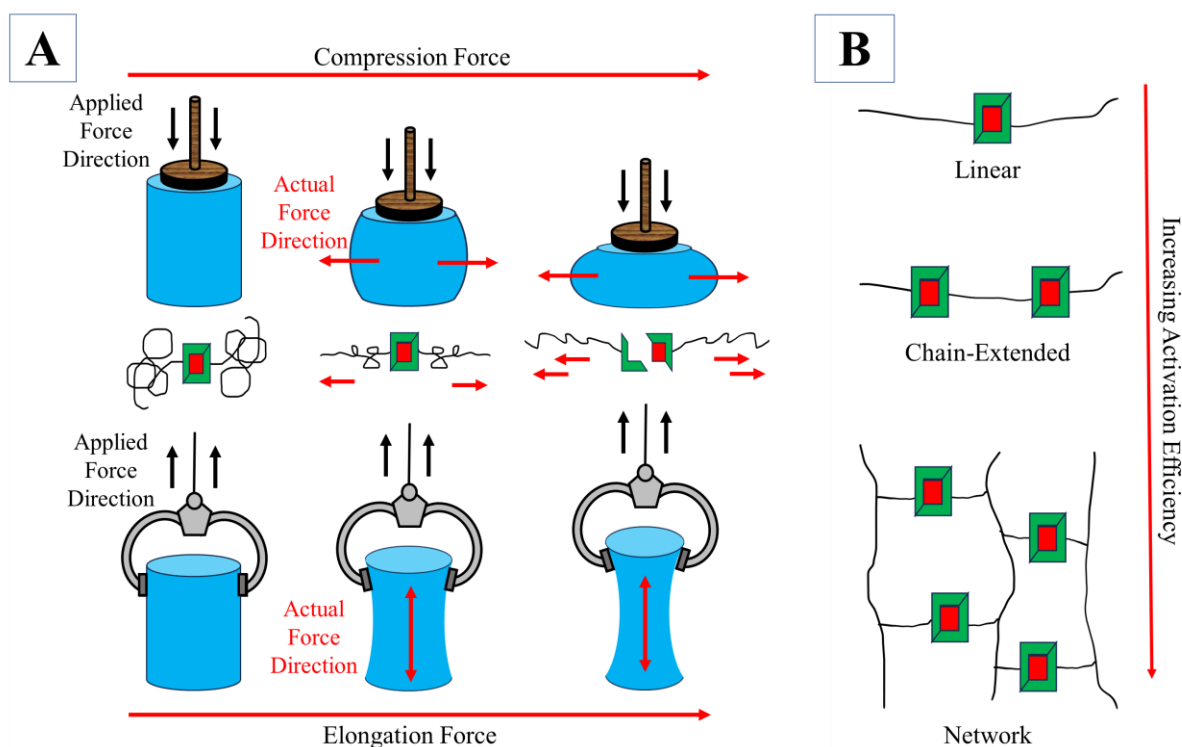
Figure 10. A) The application of compression or elongation force leads to the disentanglement of the coiled polymer chain resulting in its stretching and transmittance of the force to the weak labile bond of the mechanocatalyst. **B**) The activation efficiency of a mechanophore shows an increase, depending on the structure of the polymer chains in which it is embedded.

1.2.2 Mechanocatalysts

In addition to the above-mentioned chemical transformations in polymeric compounds, mechanochemistry with a variety of different metal complexes, termed mechanocatalysts, has also been reported. Metal complexes are only referred to as such if they are inactive or latent in their initial state. However, the mechanochemical activation of the initially latent complexes show significant catalytic effects. Such examples are also observed with *N*-heterocyclic carbenes (NHC), making metal-NHCs a promising group of mechanocatalysts.
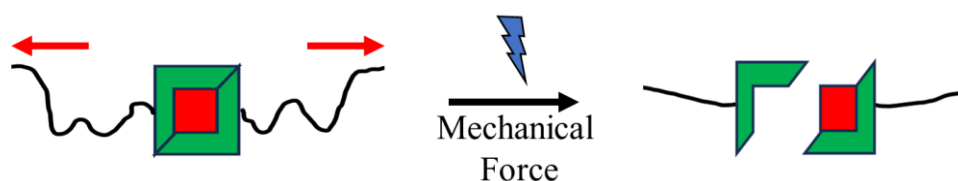
Figure 11. A general example for polymeric mechanocatalysts activated by mechanical force.[186]

1.2.2.1   Palladium (Pd)/Platinum (Pt)-Phosphane Mechanocatalysts

A palladium (Pd)-based mechanocatalyst was the first ever to be synthesized in 2004. Consisting of Pd-phosphine (P) coordination bonds, a reversible reduction in the molecular weight of the pTHF on ultrasonication was observed, displaying a preferential scission of the coordination bonds over covalent bonds.[242-245] Further work using a mixed Pd-P and Pt-P in pTHF also showed a the selectivity of the mechanochemical activation in which the weaker Pd-P bonds (~141 kJ mol^{-1}) broke three times faster than the stronger Pt-P bonds (~169 kJ mol^{-1}).[246] A pincer NHC−pyridine−NHC Pd complex has also been studied using atomic force microscopy (AFM)-based single-molecule force spectroscopy (SMFS) measurements. Although classed as mechanocatalysts, their catalytic activities have not been reported.

1.2.2.2   Iron (Fe)-based Mechanocatalysts

Di Giannantonio *et al.*[247] incorporated Fe-based ferrocene into polymethylacrylates (PMA) and polyurethanes (PU) for sensor and medical applications. On ultrasonication, the reduction of molecular weight was much faster in the Fe-containing PMA and PU compared to the polymers without Fe. Mechanochemical specificity was also observed with PMA showing a tenfold and PU a threefold preference for cleavage over C-C cleavage. Sha *et al.* synthesized mechanophoric Fe-5-methoxycyclooctene (MCO) copolymer (M_n = 111,000 g mol^{-1}) by incorporating Fe moieties.[248] On ultrasonication, the copolymer displayed molecular weight reduction until it reached its M_{lim} at 17,600 g mol^{-1} in two hours. Addition of isopropyl alcohol enhanced the cleavage significantly, demonstrating a specific cleavage of 97 %.[248]

1.2.2.3   Silver (Ag)-based Mechanocatalysts

The first mechanocatalysts that would show proven catalytic activity was synthesized and studied by the group of Sijbesma using silver (Ag) bis(NHC) complexes.[249-251] On sonication, the Ag(I) bis(NHC) embedded within pTHF follows the same path for labile bond cleavage as Cu(I) bis(NHC), as described in **Chapter 1.1.4.2**. Hence, either an NHC-Ag or an NHC with carbene would be obtained on cleavage. In the presence of this catalytic carbenic NHC species, benzyl alcohol and vinyl acetate underwent transesterification.[252] The reaction was also further studied to understand the catalyst concentration and molecular weight effects on the transesterification process.[253]

1.2.2.4   Ruthenium (Ru)-based Mechanocatalysts

Using commercially available ruthenium (Ru) based Hoveyda-Grubbs catalyst, a scalable application of mechanochemistry in olefin metathesis (cross metathesis- or ring-closing metathesis) has been employed to obtain high yields of products using different substrates *via* milling or liquid-assisted grinding (LAG).[254] A Ru-based bis(NHC) catalyst, similarly to the previously described Ag(I) bis(NHC), was also synthesized by the group of Sijbesma. As described previously, on sonication of Ru bis(NHC), two species would be obtained. However, contrary to the Ag(I) bis(NHC) species, in this case the NHC-Ru was the catalytic species. In the presence of it, ring-opening metathesis polymerization (ROMP) of cyclooctene and disubstituted norbornenes, as well as ring-closing metathesis (RCM) reactions of diethyl diallylmalonate (**I-10**) were conducted.[252, 255, 256]

The examples so far have largely been mechanocatalysis in solution. However, mechanocatalysis within a bulk state is also vital for developing effective strategies in polymers, which are usually applied in a solid form. One such rare example is of the embedding of a high molecular weight Ru bis(NHC) with polymeric pTHF side chains (M_n = 34,000 g mol^{-1}) together with mono- and bifunctional norbornene

monomers, into a semi-crystalline pTHF (M_n = 170,000 g mol^{-1}), thus enhancing the efficiency of transmission of mechanical force. The pTHF handles of the NHC co-crystallized with the pTHF matrix, forming additional crosslinking points to enhance the transmission even further. On applying five cycles of compression, the ROMP of norbornene was triggered, leading to crosslinked poly(norbornene) with up to 25 % conversion.[235]

1.2.2.5 Copper-NHC Mechanocatalyst

The concept of latent Cu(I) NHCs is not novel, as highlighted by Díez-González *et al.*[156], who identified [(SIPr)CuCl] (SIPr = *N,N*-bis(2,6-diisopropylphenyl)imidazolidin-2-ylidene) as a latent catalyst under very specific conditions. The catalyst remains dormant in those conditions until it is thermally activated at 60 °C to achieve CuAAC.[156] However, a homogeneous mechanochemical "click" system had not been previously developed. The combination of the previously discussed copper(I)-catalysed alkyne-azide cycloaddition with the concept of mechanocatalysts and mechanoactivation would allow our research group to achieve mechanically activated Cu(I) bis(NHC)s to catalyse CuAAC "click" reactions. Michael *et al.* introduced mechanochemical activation to an otherwise latent Cu(I) bis(NHC) catalyst[257] (more details in **Chapter 1.2.3**), resulting in varying studies of the many possibilities.

In further study of the Cu(I) bis(NHC)s, Micheal *et al.*[258] synthesized a series of them to study the effects of polymeric backbones (PIB and PS) in which the mechanocatalysts are embedded. It was observed that the rate of molecular weight degradation due to labile bond cleavage accelerated as the polymer chain length of synthesized PIB (17,200 g mol^{-1}) and PS (13,600 g mol^{-1}) increased, an effect attributed to an enhanced efficiency of force transmission. The catalytic activity investigated with CuAAC of benzylazide (**I-22**) with phenylacetylene (**I-23**) in solution showed sufficient latency with all three, i.e., PS, PIB or pTHF-based Cu(I) bis(NHC) without ultrasonication even after a week, at RT and at 65 °C. Catalytic activity increased with the initial polymer chain length. For PIB-based catalyst, "click" conversion rose from 11 % to 28 % with increasing molecular weight, while for PS-based, "click" conversion improved from 23 % to 52 %. Notably, PIB-based catalysts showed lower reactivity than PS-based counterparts even at a higher molecular weight, possibly due to the polar PS exhibiting better solvent-polymer interaction with THF, enabling higher efficiency in force transmission.[258]

Funtan *et al.*[259] further extended the concept to include peptides. In the foundational work, Cu(I) bis(NHC) catalysts bearing two carboxyl ([Cu(C$_{10}$COOH-NHC)$_2$]Br) or two amino groups ([Cu(C$_3$NH$_2$-NHC)$_2$]Br) were synthesized. The presence of N- and C-terminus allowed a classical peptide coupling between the two Cu(I) bis(NHC) catalysts to generate peptide-based mechanophores by the formation of amide bonds *via* polycondensation. Additionally, single amino acids glycine and L-valine were linked to ([Cu(C$_{10}$COOH-NHC)$_2$]Br) *via* peptide bonds. On sonication in the presence of benzylazide (**I-22**) with phenylacetylene (**I-23**) in solution, CuAAC was observed in (A) the low molecular weight mechanocatalysts ([Cu(C$_{10}$COOH-NHC)$_2$]Br) (3.5 %) and ([Cu(C$_3$NH$_2$-NHC)$_2$]Br) (4.8 %), (B) in the mechanocatalyst obtained by coupling ([Cu(C$_{10}$COOH-NHC)$_2$]Br) and ([Cu(C$_3$NH$_2$-NHC)$_2$]Br) (3.9 %), and (C) in glycine (6.9 %) and L-valine-linked (3.4 %) ([Cu(C$_{10}$COOH-NHC)$_2$]Br). These positive results opened up possibilities to couple peptides such as titin and elastin which are known for their "molecular spring" behaviour and elasticity.[259] After successfully establishing the possibility of using single amino acids glycine (G) and L-valine (V), elastin-like peptides (ELPs) such as the pentapeptide VPGVG was of special fascination because it is the most prominent amino acid sequence of native elastin (V = L-valine, G = glycine and P = proline).[260] A series of mechanocatalysts were synthesized by linking the amino acids (VG, VPG, VPGVG, (VPGVG)$_2$ and (VPGVG)$_4$) to ([Cu(C$_{10}$COOH-NHC)$_2$]Br). On sonication in the presence of benzylazide (**I-22**) with phenylacetylene

(**I-23**) in solution to invoke CuAAC, the "click" conversion increased steadily from the peptide-less catalyst ([Cu(C$_{10}$COOH-NHC)$_2$]Br) (3.4 %) to the longest elastin-like peptide chain-linked catalyst, a Cu(I) bis(NHC)-based ([Cu(C$_{10}$COOH–(VPGVG)$_4$–NHC)$_2$]Br) (5.6 %).[260]

1.2.3 Mechanophoric Damage-Sensing Approaches

The approach of achieving mechanically activated Cu(I) bis(NHC)s to catalyse CuAAC "click" reactions presented the opportunity to utilize the system in stress-sensing applications that employ 'turn-on' mechanisms. In this scheme, non- or weakly-fluorescent alkynes and azides could react to form fluorogenic products *via* fluorogenic "click" reaction.[261]

Michael *et al.*'s work[262] introduced mechanochemical activation to an otherwise latent Cu(I) bis(NHC) catalyst *via* ultrasound in solution and by compression force in solid polymer (pTHF). Their mechanocatalyst design integrated Cu(I) bis(NHC) complexes into the polymer backbones of flexible poly(isobutylene) (PIB) and rigid poly(styrene) (PS), with these polymers acting as substituents on the heterocycle. In solution, the model CuAAC system of phenylacetylene (**I-23**) and benzylazide (**I-22**) (**Figure 12Ai**) formed the corresponding 1,2,3-triazole ring only when ultrasonication was applied to this system, leading to the removal of one of the two shielding ligands. This further led to the formation of the active catalytic site which triggered the formation of copper(I) acetylide, further initiating the CuAAC process, as described in **Chapter 1.1.4.2**. The influence of structural difference was observed to be reflected in conversion of PS-based mechanocatalyst, which was higher than that of the PIB-based mechanocatalyst (44 % vs. 27 %), despite the lower M_n (13.1 kDa vs. 17.2 kDa).[262] Without sonication, however, only negligible "click" reaction occurred even when heated up to 60 °C, displaying the latency of the Cu(I) mechanocatalyst. This concept's extension involved solvent-free CuAAC activation within a semi-crystalline pTHF matrix (**Figure 12Aii**). A creative fluorogenic system consisting of non-fluorescent 3-azido-7-hydroxy-coumarin (**I-24**) and phenylacetylene (**I-23**) could undergo CuAAC to yield a highly fluorescent product only when the Cu(I) bis(NHC)s were mechanically activated by compression force. The fluorescence of the resulting "click" product enabled visualization and quantification of CuAAC within the polymer matrix.[257]

This methodology was furthered by the work of Biewend *et al.*[263] in which linear and chain extended PS polymers with embedded Cu(I) bis(NHC) were prepared. The molecular weight for the linear complexes ranged 12,000-50,500 g mol^{-1} while the chain-extended complexes ranged 15,000-31,000 g mol^{-1}. To investigate the catalytic activity of these complexes, the PS-based Cu(I) bis(NHC)s were embedded into a pTHF matrix ($M_{n(GPC)} = 112,000$ g mol^{-1}) together with a dye system consisting of non-fluorescent 3-azido-7-hydroxy-coumarin (**I-24**) and phenylacetylene (**I-23**). On application of compressive forces, the activated mechanocatalyst triggered a fluorogenic click reaction to form the fluorescent 7-hydroxy-3-(4-phenyl-1H-[1,2,3]triazole-1-yl)-coumarin dye (**I-25**). Such an activity is quantifiable *via* fluorescence spectroscopy. On compressing the linear complexes, the conversion increased from 11.1 % to 16.2 % with an increase of the molecular weight from 12,000 to 50,500 g mol^{-1}. Similarly, in the chain-extended complexes bearing more than one Cu(I) centre, the conversion increased from 16.1 % to 44.2 % with an increase of the molecular weight from 12,000 to 50,500 g mol^{-1}. In both the cases, this was attributed to the higher efficiency of force transmission on better anchoring of the PS handles to the pTHF matrix. Notable, the conversion of 50,500 g mol^{-1} of the linear complex is similar to that of 15,000 g mol^{-1} of the chain-extended complex, additionally confirming the effect described in **Chapter 1.2.1** regarding activation efficiency.[263]

Additionally, Biewend *et al.*[264] also displayed a stress-sensing application based on a low molecular weight Cu(I) bis(NHC) mechanocatalyst (**Figure 12B**). An approach was developed where the mechanocatalyst was embedded covalently into a crosslinked polyurethane (PU) foil, synthesized using

pTHF and hexamethylene-diisocyanate (HDI) with trimethylolpropane (TMP) as the crosslinker. A fluorogenic system consisting of precursors 8-azidonaphtalen-2-ol (**I-26**) and 3-hydroxyphenylacetylene (**I-27**), both non-fluorescents, were also covalently introduced inside the PU network. Application of mechanical force *via* oscillating tensile rheology cycles activated the latent mechanocatalyst inside the PU leading to the "click" reaction and the production of the highly fluorescent 8-(4-(3-hydroxyphenyl)-1,2,3-triazol-1-yl)naphthalen-2-ol dye (**I-28**) for stress quantification. A conversion of up to 17 % was achieved with an application of 80 % strain.[264]

Again, an important prerequisite for a stress-induced "click" reaction is to prevent any unintentional activation of a catalyst, namely the cleavage of an NHC ligand without external force (**Figure 12**). Such an untimely cleavage would initiate the catalytic cycle, leading to fluorescent reactions in the absence of stress and defeating its very purpose as a stress-sensor by indicating damage events. A strategy to prevent the cleavage is the attachment of polymer chains to the NHC ligands. These chains can inhibit the alkyne from coordinating to the Cu(I) centre by significantly enhancing the stability of the Cu(I) complex. Consequently, no activity is displayed until an external force leads to the scission of the bond between copper and the carbenic carbon of the NHCs.[245, 258, 265]
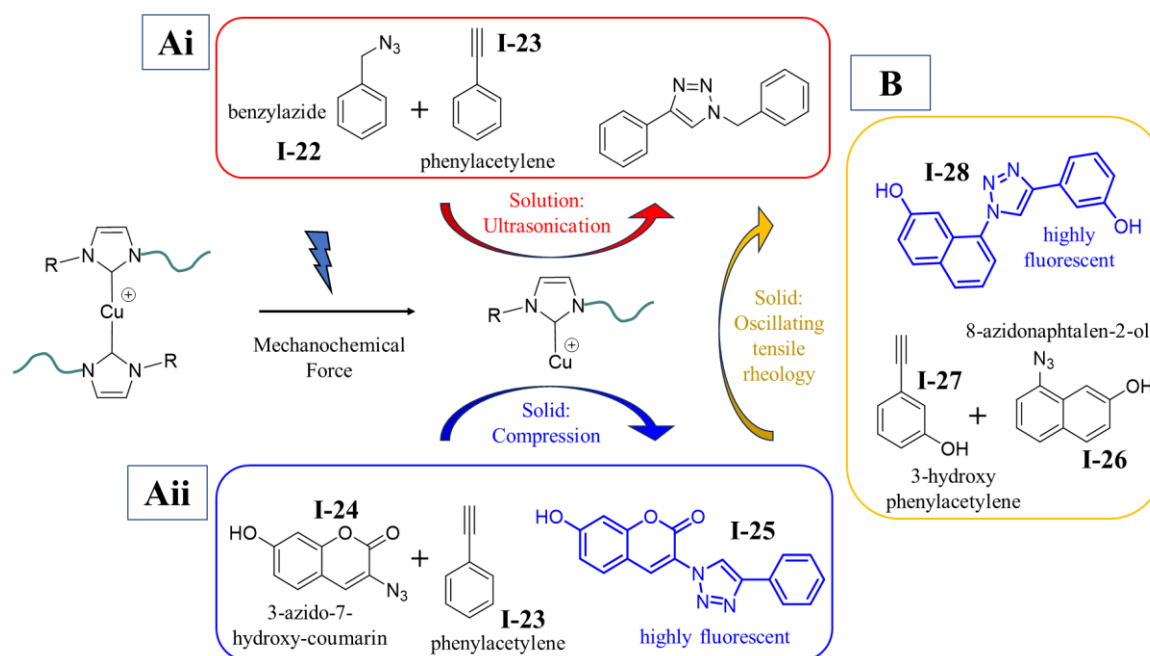
Figure 12. The mechanochemical activation of latent Cu(I) bis(NHC) conducted by **A**) Michael *et al.*[257] in **i**) solution by ultrasonication and **ii**) in solid polymer matrix by compression, and **B**) Biewend *et al.*[264] in solid polymer matrix *via* oscillating tensile rheology.

1.3 Metal Organic Frameworks (MOFs)

Metal-Organic Frameworks (MOFs) are one-, two-, or three-dimensional coordination networks,[266] produced by the formation of coordination bonds between metal cations, termed as secondary building units (SBUs) or nodes, and organic ligands, termed as linkers. In most cases, MOFs have geometrically and crystallographically well-defined framework structures.[267] Because of their porosity and their extended and ordered structures, MOFs are also termed as porous coordination polymers (PCPs). The length and functionality of the linker ligands determine the size of the resulting pores and hence can be easily tuned, resulting in structures with high surface area and good chemical tunability. One such class

of linkers, comprising imidazolium, triazolium, and benzimidazolium, is the azolium-containing ligands that are the precursors of *N*-heterocyclic carbenes (NHCs). The introduction of NHC's into MOFs is an important aspect as it was expected to boost the catalytic performance of the MOFs.[266]
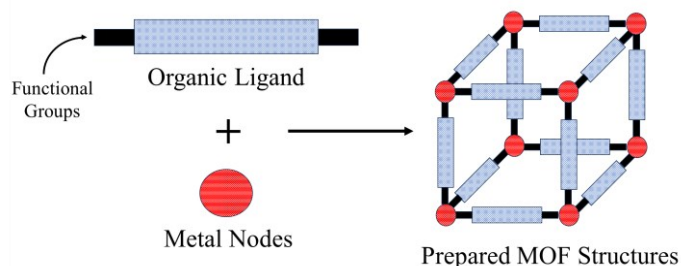
Figure 13. A schematic illustration of the components that constitute a metal-organic framework.

The first actual MOFs were reported independently by the working groups of Yaghi[268] and Williams,[269] both in 1999. Since then, MOFs have had a growing interest in them as potential materials in various uses, most significantly as storage media for gases based on being high adsorbents, as well as uses in membranes and catalysis.[270-274] Heterogeneous catalysis was among the earliest proposed purposes for crystalline MOF materials.[275] In comparison to transition metal salts catalyst which are widely used in industries, MOFs are easily recoverable, reusable, and minimize undesired waste, giving these heterogenous catalyst an advantage over homogenous catalysts.[273]

1.3.1 Structural and Functional Tunability of MOFs

1.3.1.1 Design Strategies

The question arises on why MOFs have had such a focussed development over the recent years even though it is hard to predict the final structural design of a MOF, especially when extended to much more complicated cases in terms of design. Moreover, the morphology and crystallinity of MOFs is affected by various factors such as substrate composition and concentration, temperature and solvent.[276] The straight-forward answer is that MOFs are extremely tailorable frameworks with controlled pore size, shape, and functionality for different applications.[276] Specifically, the architecture of a MOF is dictated by the structure and connectivity of a linker. Adjustments to the linker's geometry, length, ratio, and functional groups can be used to tailor the size, shape, surface area, and properties of a MOF.[276]

Among the MOF-74 family (MOF-74 = (Zn$_2$(dhbdc), dhbdc = 2,5-dihydroxy-1,4-benzenedicarboxylate), Mg-MOF-74 gained recognition on displaying exceptional performance in the low-pressure adsorption of CO_2, outperforming other metal-MOF-74s.[277] A persistent challenge has been creating crystals with pore openings large enough to accommodate substantial organic, inorganic, and biological molecules. Theoretically, extending the length of the linker in MOFs during synthesis should form larger pore apertures. In MOF-74, progressing from one to two, three, four, five, six, seven, nine, and eleven phenylene ring in the linker allows for the formation of an isoreticular (having the same topology) series of MOF-74 structures (IRMOF-74-I to -XI), with pore apertures ranging from 14 to 98 Å.[278]

In an example showcasing the influence of differently functionalized linkers on MOF properties, the aldehyde group-containing imidazolate-2-carboxyaldehyde (ICA) links, which connects zinc(II) centres in ZIF-90 (zeolitic imidazolate framework, a special class of MOFs) (**I-29**), underwent transformation to yield ZIF-91 (**I-30**) and ZIF-92 (**I-31**). This transformation involved reducing the aldehyde with NaBH$_4$ and reacting with ethanolamine in methanol under reflux conditions, respectively (**Figure 14A**).

Despite the strong reaction conditions, the integrity of the ZIF structure and its crystallinity remained throughout the synthesis.[279] The BET surface areas (pore volumes), assessed based on N_2 adsorption, calculated values 1198 m^2 g^{-1} (0.54 cm^3 g^{-1}) for ZIF-90 (**I-29**), 1024 m^2 g^{-1} (0.49 cm^3 g^{-1}) for ZIF-91 (**I-30**), and 42 m^2 g^{-1} (0.13 cm^3 g^{-1}) for ZIF-92 (**I-31**).[280] Significantly, ZIF-92 showed notably lower N_2 adsorption compared to ZIF-90, attributed to the ethanolamine functionalization of ZIF-92 at the ZIF-90 window, blocking the pore apertures. This effectively hindered N_2 molecules from accessing the pore interiors.[281]
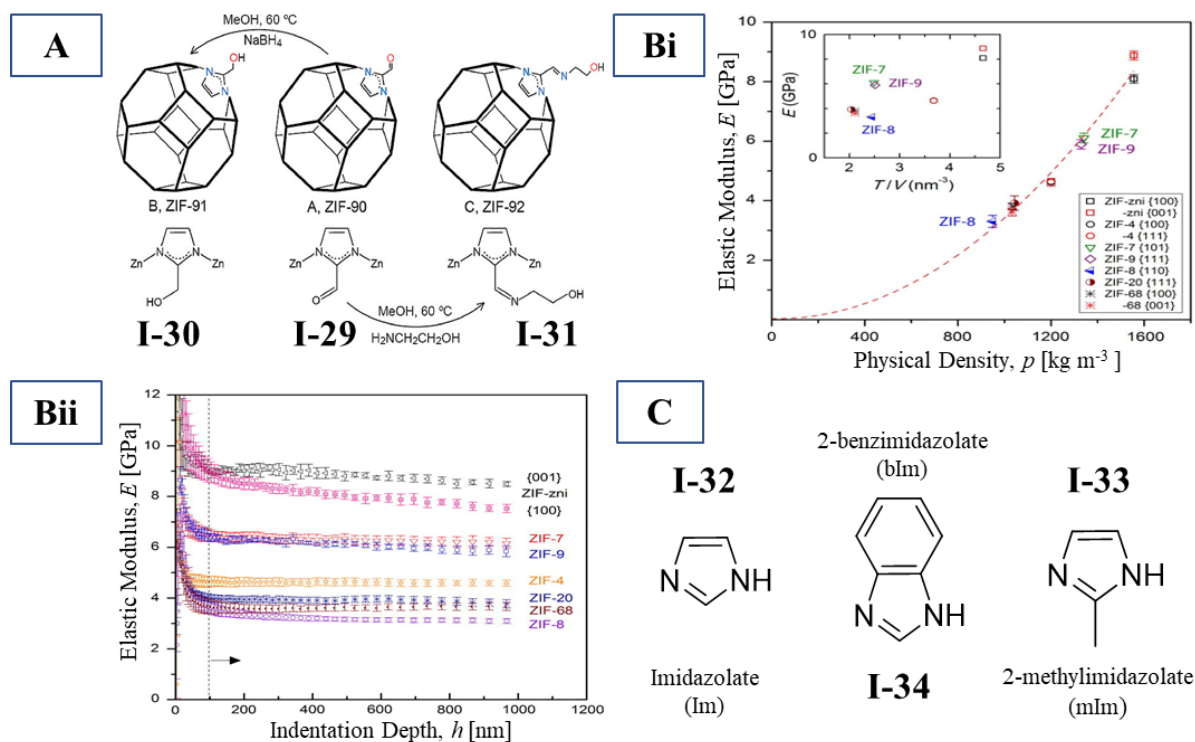
Figure 14. A) Transformation of ZIF-90 to ZIF-91 by reduction with $NaBH_4$ and to ZIF-92 by reaction with ethanolamine. Adapted with permission from "W. Morris, C. J. Doonan, H. Furukawa, R. Banerjee, O. M. Yaghi. Crystals as Molecules: Postsynthesis Covalent Functionalization of Zeolitic Imidazolate Frameworks. *J. Am. Chem. Soc.* **2008**, 130, 12626-12627."[279] Copyright 2008 American Chemical Society. **B)** The elastic moduli of different ZIFs **i)** as a function of the physical density and T/V (inset) and **ii)** as a function the nanoindentation depth. Adapted with permission from "J. C. Tan, T. D. Bennett, A. K. Cheetham. Chemical structure, network topology, and porosity effects on the mechanical properties of Zeolitic Imidazolate Frameworks. *P. Natl. Acad. Sci. USA* **2010**, 107, 9938."[282] **C)** Structures of different imidazolates used as organic linkers in some ZIFs.

Since this thesis expects to eventually use MOFs as mechanocatalysts, it would involve subjecting the MOFs to mechanical stresses and strains for which their mechanical properties are critical to reach practical implementations. The MOFs would require a sufficiently high elastic modulus to sufficiently induce high responsiveness and these too can be tuned by using different organic linkers.[282] The work of Tan *et al.*[283] utilized single crystal nanoindentation to investigate the mechanical properties of seven ZIFs in relation to their chemical structure, network topologies (zni, cag, sodalite (SOD), Linde Type A (LTA) and gmelinite (GME)), and porosity. The nanoindentation data revealed that the elastic stiffness increases as the ZIFs turn denser, albeit non-linearly (**Figure 14Bi**), similar to that predicted computationally for IRMOFs.[284] The densest ZIF structure, ZIF-zni [Zn(Im)$_2$] (Im: imidazolate, **I-32**

(**Figure 14C**)), exhibited the highest modulus of 8-9 GPa. The Young's moduli of ZIFs also displayed a strong inverse correlation with the internal accessible void space, defined as solvent accessible volume (SAV).[283] This suggests that the highly porous ZIFs, such as ZIF-8 [Zn(mIm)$_2$] (mIm: 2-methylimidazolate, **I-33** (**Figure 14C**)), display consistently lower elastic stiffnesses. Furthermore, ZIFs incorporating bulky imidazolate ligands were observed to be stiffer due to short-range ligand-ligand interactions, particularly while using large aromatic linkers that filled the pore regions. Among the three ZIFs of same network topology (SOD), ZIF-7 [Zn(bIm)$_2$] (bIm: 2-benzimidazolate, **I-34** (**Figure 14C**)) and ZIF-9 [Co(bIm)$_2$] exhibited Young's moduli two times higher than ZIF-8, primarily due to the sterically bulkier bIm (**I-34**) linkages compared to the mIm (**I-33**) in ZIF-8 (**Figure 14Bii**). Additionally, ZIF-7 and ZIF-9 displaying similar stiffnesses even with different metal centres (ZnN$_4$ v/s CoN$_4$) show that the rigid imidazolate linkers largely control the ZIF elasticity[283] and any flexibility would mainly come from organic linkers which rotate and bend.[285]

1.3.1.2   Structural Changes and Bond Breakage

1.3.1.2.1   In Liquids

For a MOF to be utilized as a mechanocatalyst, its behaviour under mechanical forces needs to be understood. In a liquid, application of ultrasonication produces different effects in a liquid-solid heterogenic system, depending on the size of the solid particle (such as a MOF). At a frequency of 20 kHz, the size of the cavitating bubbles is around 100–150 μm. If the solid particle size is at least twice the size of the bubble, the bubble collapses asymmetrically resulting in a microjet formation. This results in jets of high-speed liquids directed at the surface of the solid particles. The cavitation collapse also results in the formation of shock waves with magnitudes as high as 1 GPa. The shock waves generated by these microjets can cause significant damage to the surfaces of the solid particles, resulting in plastic deformation, surface defects or even new surfaces being formed and exposed.[212, 286]
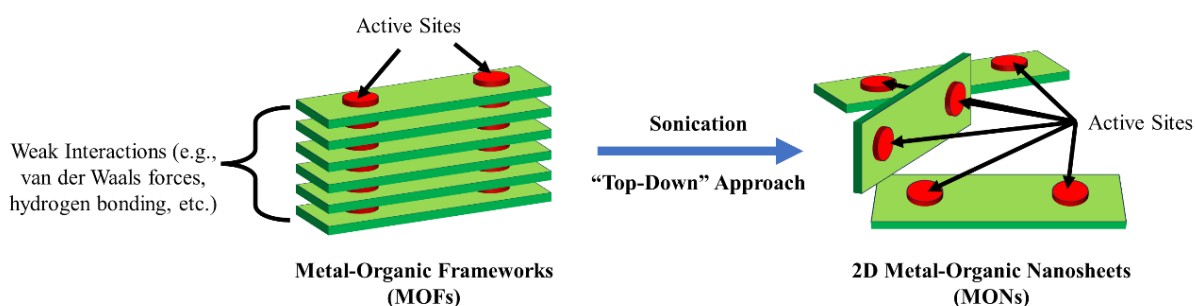
Figure 15. The "top-down" sonication approach utilized to obtain 2D MONs from MOFs.

The principle of using sonication resulting in rupturing bonds within the layers of a MOF was demonstrated by the synthesis of 2D metal-organic nanosheets/networks (MONs) from MOFs using the "top-down" approach (**Figure 15**).[287-300] The success of the top-down approach to disintegrate bulk materials relies on two requirements from the parent MOF. Firstly, weak interactions such as van der Waals forces, hydrogen bonding, etc. exists between the layers of the crystal structures. Secondly, the 2D structures should be able to bear sonication and other mechanical forces by virtue of their strong mechanical and chemical stability.[289] As the top-down method generates MONs by selectively disrupting interlayer bonding in bulk MOF crystals using external forces,[301] it is a form of bond breaking within MOFs, resulting in more active sites being exposed and an improvement of catalytic activity (**Figure 15**).

1.3.1.2.2 In Solids

Although formation of new surfaces is considered the main outcome in liquids, formation of crystal defects accounts higher in the direct mechanical activation of solids. Mechanical activation methods like ball milling, shock impact, or compression can induce stresses beyond the elastic limits of MOFs, leading to amorphization,[302-305] structural changes, defect accumulation, and bond breakage. These alterations in physicochemical properties enhance chemical reactivity in solid MOFs.[306, 307]

Nanocompression allows the determination of mechanical parameters and energy absorptions of individual nanocrystals.[308] A micrometre-sized flat punch applies uniaxial compression on a sample which records the load-displacement data, while videographing inside an electron microscope (**Figure 16Ai**).[308] On such an irreversible mechanical compression, the internal free space within porous materials tend to decrease, potentially leading to chemical effects. The ΔV (internal volume) decreases substantially while the ΔS (entropy) increases, caused by the internal space collapse and crystallinity loss. In the work by Su *et al.*,[309] a UiO-66 MOF (**I-35**) demonstrated endothermic bond breakage during a compression-induced collapse upon the reduction of its internal free volume. At compression of 1.9 GPa, the effective number of Zr-O bonds in UiO-66 (**I-35**) decreased from 4.0 to 1.9 (**Figure 16Aii**), as analysed by EXAFS. Additionally, IR spectra indicated the transformation of syn-syn bridging carboxylates into monodentate ligand (**Figure 16Aiii**), thus demonstrating the triggered mechanochemical reactions. Notably, the UiO-66 (**I-35**) nanocrystals absorbed substantial mechanical energy during compression, amounting to ~4 kJ g^{-1}. For context, a TNT (2,4,6-trinitrotoluene) explosive produces 4.2 kJ g^{-1} during explosion. Therefore, gram for gram, it could absorb as much energy as a high explosive would release.[309]
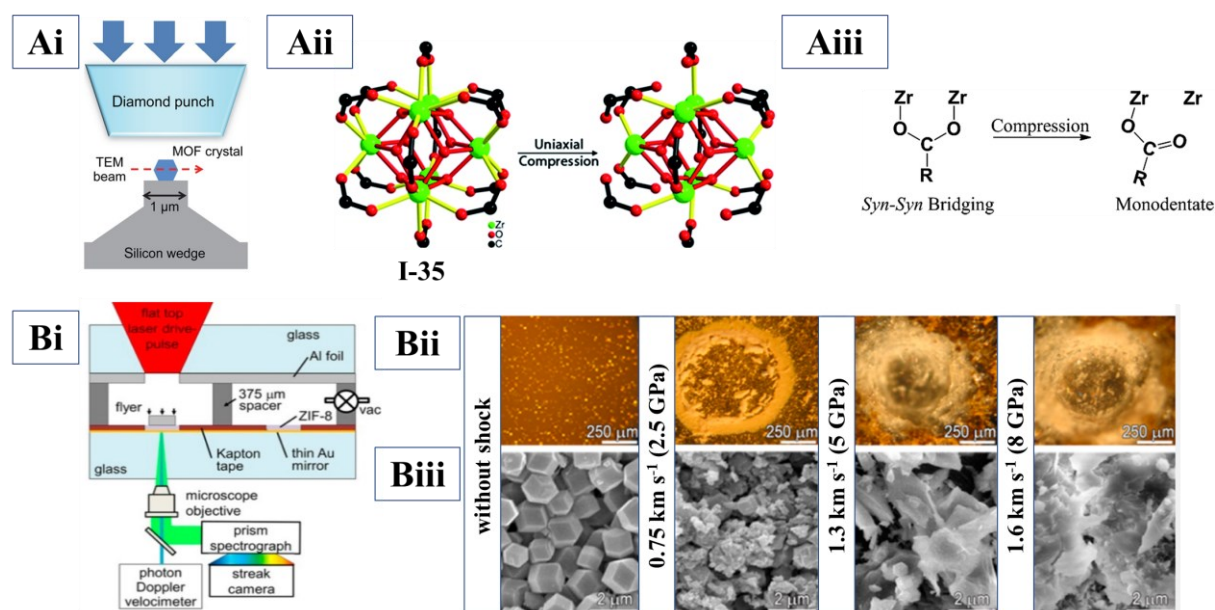
Figure 16. Ai) the setup for the uniaxial nanocompression (adapted with permission from Ref.[308]. Copyright 2018 Elsevier Inc.), **ii**) the decrease of the effective number of Zr–carboxylate oxygen (Zr-O) bonds in UiO-66 (**I-35**) decreasing from 4.0 to 1.9 and **iii**) resulting in the formation of monodentate ligands from syn-syn bridging carboxylates (**Aii** and **iii** are reproduced from Ref.[309] with permission from the Royal Society of Chemistry). **Bi**) The setup for microflyer plate apparatus, **ii**) optical images of ZIF-8 layer on glass substrate and **iii**) SEM images of ZIF-8 crystals after shock compression. Adapted with permission from "Z. Su, W. L. Shaw, Y.-R. Miao, S. You, D. D. Dlott, K. S. Suslick. Shock Wave Chemistry in a Metal–Organic Framework. *J. Am. Chem. Soc.* **2017**, 139, 4619-4622."[310] Copyright 2017 American Chemical Society.

A shock wave is a disturbance moving at supersonic speeds causing sudden increase in pressure, density, and internal energy. This creates a dynamic environment with rapid compression and high strain rates, damaging solid materials. MOFs respond uniquely to shock waves beyond their elastic limits due to their compressible free space, converting shock wave energy into heat for potential shock absorption (**Figure 16Bi**). In the investigation with shock compression of MOFs caused by the impacts of km s^{-1} flyer plate, Su *et al.*[310] reported the stability of the crystallinity of the MOF ZIF-8 below 2.5 GPa (at flyer plate velocities = 0.75 km s^{-1}). Thereon, ZIF-8 lost their long-range crystalline order at around 5 GPa (1.3 km s^{-1}) and faced complete structural collapse and the loss of local symmetry around 8 GPa (1.6 km s^{-1}) (**Figure 16Bii and Biii**).[310] Time-resolved in-situ photoluminescence and shock-induced emission indicated that the impacts of high-velocity shock waves on ZIF-8 were dissipated in two ways: through the nanoporous network collapse and endothermic shock-induced bond scission of chemical bonds.[310]

Hence, MOFs have shown the possibility of undergoing bond breakage on application of mechanical force in both liquids and solids. Therefore, their application as mechanocatalysts show immense scope and possibility.

1.3.2 CuAAC in MOFs

The previously presented CuAAC reactions were all based on homogeneous catalysts (**Chapter 1.2.3**). Although efficient, their preparation is often tedious and/or expensive. Additionally, homogenous Cu(I) catalysts do not allow easy removal and recycling without specialized steps. To solve these problems, considerable interest and efforts have been devoted to development of field of the heterogenization of homogeneous catalysts.[143, 311, 312] Therefore, MOFs with active sites, either at the metal nodes or at the organic linker ligands, have been investigated as solid counterparts of homogeneous catalysts.[313-315]

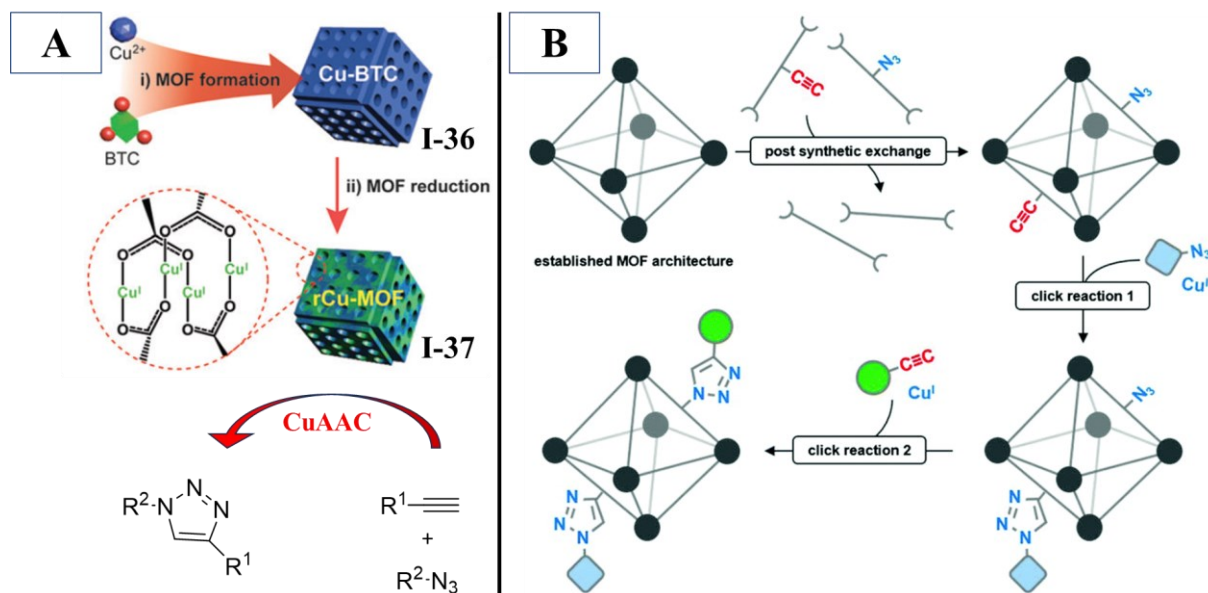**Figure 17. A**) Schematic illustration of formation and participation of a reduced copper metal-organic framework (rCu-MOF) in CuAAC reactions. Reproduced from Ref.[316] with permission from the Royal Society of Chemistry. **B**) Schematic route for utilizing post-synthetic modification (PSM) to achieve active sites within a MOF to use for CuAAC.[317] Published under a Creative Commons license CC BY 3.0 DEED.

In the work by Fu *et al.*,[316] a reduced copper metal-organic framework (rCu-MOF, (**I-37**)) was prepared by reducing Cu-BTC (**I-36**) (BTC: benzene tricarboxylate) MOF in the presence of hydroquinone (**Figure 17A**). Coupling reactions and polymer functionalization with quantitative yields *via* CuAAC were conducted in the presence of the catalytic MOF. The rCu-MOF (**I-37**) showed high activity, absence of heavy metal contaminants, easy recyclability, and structural stability for catalysis. It outperformed conventional copper halide catalyst, making it a promising, environmentally friendly choice for industrial applications, especially in polymer chemistry.[316] In another work,[318] various copper-containing MOFs, i.e., [Cu(im)$_2$], [Cu$_3$(BTC)$_2$], [Cu(2-pymo)$_2$] (2-pymo: 2-hydroxypyrimidinolate) and [Cu(BDC)] (BDC: benzene dicarboxylate) were synthesized. These Cu-MOFs displayed high activity and regioselectivity during the CuAAC reactions between benzylazide (**I-22**) and phenylacetylene (**I-23**), even comparable to various homogenous copper catalysts. Furthermore, solvent-free CuAAC was also achieved in excess phenylacetylene with advantages such as no solvent waste treatment, possibility of continuous operation with easy separation of the formed triazole, and the recycling of the phenylacetylene. Ultimately, Cu-MOF catalysts were employed to a one-pot two-step process in which the azide was generated "*in situ*" and promptly reacted with phenylacetylene.[318] Fluch *et al.*[317] employed post-synthetic linker (PSM) exchange to modify UiO-67 MOF and replace its native linkers with linkers bearing azide or acetylene groups (**Figure 17B**). Adding [Cu(CH$_3$CN)$_4$]PF$_6$ as copper catalyst, CuAAC was performed between the modified MOFs in a sequential and orthogonal manner. The quantification of the reaction showed that up to 50 % of the incorporated linkers could be converted to their "clicked" triazole products while the structure of UiO-67 remained unaffected. Therefore, this work offers an excellent demonstration for an effective use of PSM to create complex functionalities.[317]

Hence, these examples of CuAAC coupled with presented possibilities for mechanical activation in MOFs raise optimism to achieve a mechanochemically activated MOF performing CuAAC, in both liquid and solids.[319]

1.3.3 NHC-based MOFs

The flexibility to vary the metal nodes and organic linkers has resulted in the reporting and study of over 50,000 different MOFs in the past decades.[320, 321] In the past, quite a few MOFs utilizing *N*-heterocyclic carbenes (NHCs) as linkers have been reported with the majority being benzene-carboxylate groups due to their tendency to form rigid metal carboxylate clusters. The introduction of NHCs into a MOF structure not only increases the functionality of the frameworks and heterogenies the usually homogenous NHC complexes, but also synergises the catalytic potentials of both MOFs and NHCs.[266] Some of these NHCs are showed in **Figure 18** and further described below.

The work of Oisaki *et al.*[322] used the ligand 4,7-bis(4-carboxylphenyl)-1,3-dimethylbenzimidazium (**I-38**, **Figure 18A**) to initially form a metal-NHC complex [4,7-bis(4-carboxylphenyl)-1,3-dimethylbenzimidazol-2-ylidene](pyridyl)palladium(II) iodide. The complex was used to assemble structures that are isoreticular (having the same or similar structural topology) to MOF-5 (**I-39**, **Figure 19A**), a well-known primitive cubic MOF. The synthesised MOF consisting of Zn(II) nodes, IRMOF-77 (**I-40**, **Figure 19B**) (IRMOF = Isoreticular MOF), consisted of an NHC-Pd(II) linker positioned on every face of the cubic structure. The Pd(II)-pyridyl centres protrude into the pores of the MOF without blocking each other.[322] To examine the reactivity of the Pd(II) centre, a ligand exchange was carried out in a 4 % v/v quinoline/DMF solution for one day at RT. Conducted tests show the replacement of pyridine with quinoline in IRMOF-77 without changes in the structural order or the porosity of the MOF.[322] Wang *et al.*[323] utilized an innovative imidazolium tricarboxylate ligand, 3-(4-carboxybenzyl)-1-(3,5-dicarboxyphenyl)-1*H*-imidazolium chloride (**I-41**, **Figure 18B**), to synthesize a two-dimensional MOF with Zn(II) nodes. Despite the MOF's overall neutrality, it featured one-

dimensional channels within its structure that exhibited a charge-separated nature. DFT calculations indicated phenyl rings and imidazolium having positive charges, and negative charges were attributed to the carboxylate moieties. Remarkably, this MOF demonstrated selective adsorption capabilities for highly polarizable gas molecules like CO_2, H_2 and CH_4, while excluding N_2. The strong hysteresis observed indicated strong interactions between the MOF and the guest molecules (a molecule that is temporarily absorbed or trapped within a MOF). The MOF also displayed the importance of the anions accompanying an azolium/NHC as even trace amounts of Cl^- in the pores significantly altered sorption properties, allowing only CO_2 to enter the pore channels at higher pressures. Consequently, this MOF holds promise for various industrial applications such as selectively adsorbing and enriching H_2 from N_2/H_2 exhaust mixtures in ammonia synthesis.[324] Moreover, it encourages the development of new strategies for charge-separated adsorbents exhibiting hysteretic adsorption.[323] Although the adsorption selectivity may be influenced by preferential host-guest interactions in this case, various other factors, including pore size, molecular sieving, and interactions with metal centres, can also play a role.[325-329] The MOF prepared with 1,3-bis(2,6-dimethyl-3,5-carboxylphenyl) imidazolium chloride (**I-42**, **Figure 18C**), having Cu(II) nodes with paddlewheel-type coordination, also displayed selective sorption to separate CO_2 from CH_4, possibly due to the ionic environment created by the positively charged aromatic azolium components as well as interactions with open metal sites within the MOF.[330]
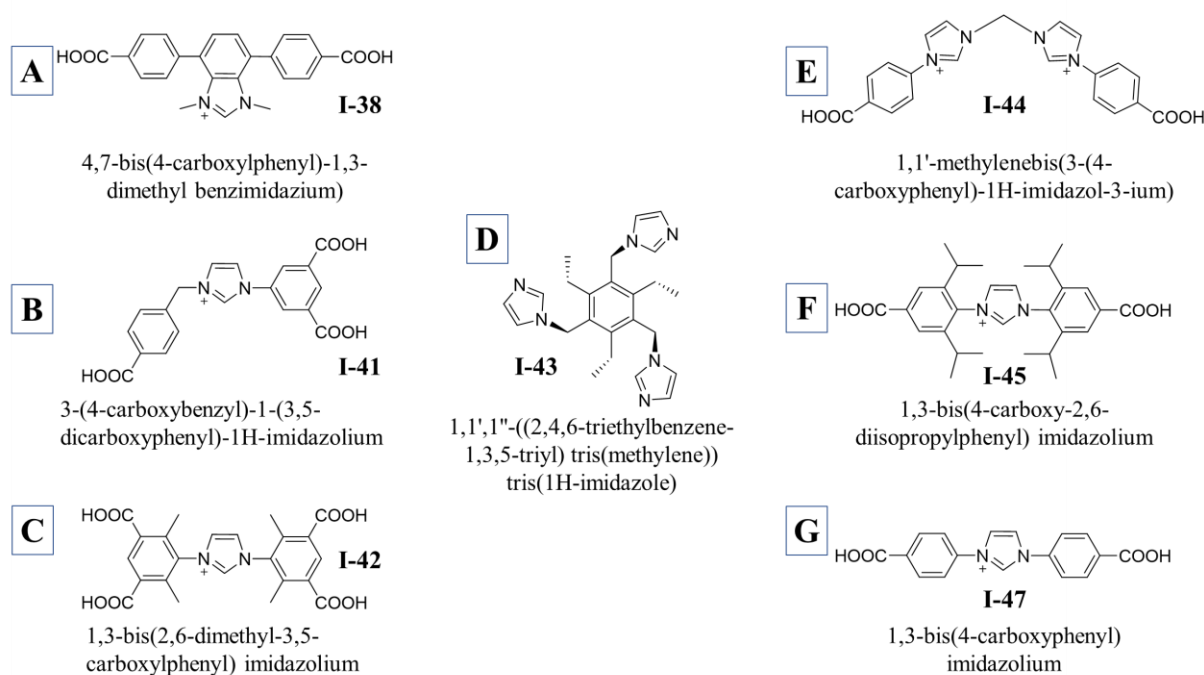
Figure 18. Different examples of NHCs that have been utilised as organic linkers within MOFs.

Despite numerous attempts, integrating *N*-heterocyclic carbenes (NHCs) into MOFs faced significant hurdles, including inaccessible carbene-precursor sites due to small pore sizes, MOF degradation when adding a base to deprotonate an imidazolium, and unintentional coordination of metal ions to carbene sites. However, a breakthrough occurred in 2012 when Lalonde *et al.*[331] successfully transformed a previously reported MOF, tripodal imidazolate framework-1 (TIF-1). Constructed using the ligand 1,1',1"-((2,4,6-triethylbenzene-1,3,5-triyl) tris(methylene)) tris(1H-imidazole) (**I-43**, **Figure 18D**),[332, 333] this transformation exposed NHC sites as catalysts, enabling the conversion of an α,β-unsaturated ketone into the corresponding ether in the presence of an alcohol. TIF-1 achieved an impressive 83 % conversion rate, compared to 72 % with the homogenous NHC catalyst IMes·HCl (IMes = 1,3-bis-

(2,4,6-trimethylphenyl)imidazol-2-ylidene).[334] Notably, TIF-1 reactions reached completion about ten times faster, establishing TIF-1 as a more efficient catalyst than IMes·HCl.[331] Kong *et al.*[335] has described the NHC precursor ligand 1,1′-methylenebis(3-(4-carboxyphenyl)-1*H*-imidazol-3-ium) (**I-44**, **Figure 18E**) to prepare a MOF [Cu₂L(NHC)₂(MeOH)₂]·4NO₃·H₂O. The imidazolium was deprotected to form NHCs and anchored concomitantly to palladium (Pd) *via* post-synthetic modification. In the presence of the catalytic active centre, the cross-coupling of phenylhalides with phenylboronic acids *via* the Suzuki–Miyaura reaction was quantitatively catalysed in heterogenous phases, depending on the donating or the electron-withdrawing properties of the two reactants.[335]
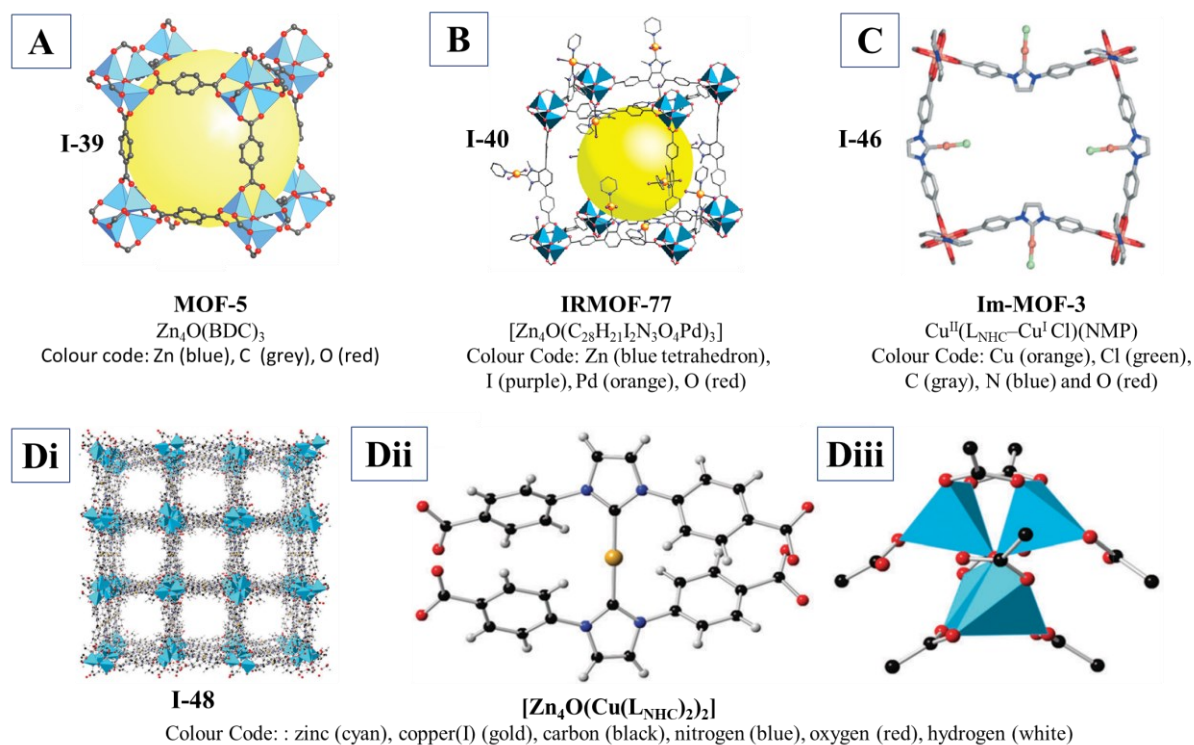
Figure 19. Crystal structures of **A**) MOF-5 (Adapted with permission from Ref.[336]. Copyright 2019 Wiley-VCH), **B**) IRMOF-77 (Adapted with permission from *"K. Oisaki, Q. Li, H. Furukawa, A. U. Czaja, O. M. Yaghi. A Metal−Organic Framework with Covalently Bound Organometallic Complexes. J. Am. Chem. Soc.* **2010**, 132, 9262-9264."[322] Copyright 2010 American Chemical Society), **C**) Im-MOF-3 (Reproduced from Ref.[337] with permission from the Royal Society of Chemistry), and **Di**) [Zn₄O(Cu(L(NHC))₂)₂]. **Dii**) represents the (Cu(L(NHC))₂) bis-NHC link and **Diii**) represents the coordination of the Zn₄O node (Reproduced from Ref.[338] with permission from the Royal Society of Chemistry). The yellow spheres represent the largest spheres that occupy the cavity without contacting the interior van der Waals surface for the MOFs.[322, 336]

With an interest in developing Cu(I)-based NHC complexes within MOFs, such examples were also identified.[339, 340] Chun *et al.*[341] reported the synthesis and self-assembly of 1,3-bis(4-carboxy-2,6-diisopropylphenyl) imidazolium (**I-45**, **Figure 18F**) and the further concomitant formation of copper-NHC complexes within the supramolecular networks. On treating with copper(II) nitrate with the NHC ligand, a supramolecular structure was assembled with two different copper species. First, Cu(II) formed paddlewheel structures to function as the metal nodes of the MOF. Second, the NHC had coordinated with copper, forming Cu(I) mono(NHC) chloride. Although the reduction of Cu(II) to Cu(I) was an interesting point, the authors require further specific evidence to identify the chemical species responsible for the reduction.[341] Lee *et al.*[337] described a MOF [Cu(II)(L(NHC)–Cu(I)

Cl)(NMP)]·(NMP)$_2$·(H$_2$O) (Im-MOF-3) (**I-46**, **Figure 19C**) made with the ligand 1,3-bis(4-carboxyphenyl) imidazolium (**I-47**, **Figure 18G**). Im-MOF-3 exhibited a 2D square-grid framework with Cu(II) paddlewheel nodes. The NHC also reacted with Cu(I) to form Cu(I) mono(NHC) chloride. However, in contrast to the previous case, the source of copper was Cu(I)Cl. Hence, Cu(I) was partially oxidized to form Cu(II), resulting in the formation of metal nodes of the MOF. In anticipation of Im-MOF-3 exhibiting catalytic behaviour as expected from a homogenous Cu(I) mono(NHC), preliminary borylation experiment conducted with 4-bromophenyl yielded 34 % of the final borylated biphenyl product.[337] Finally, in a publication that was the most interesting in terms of the MOF structure to the work for this thesis, Burgun *et al.*[338] reported the first example of the incorporation of Cu(I) bis(NHC) as a structural element within a MOF [Zn$_4$O(Cu(L$_{(NHC)}$)$_2$)$_2$] (**I-48**, **Figure 19D**) with Cu:Zn atomic ratio as 0.53:1. The Cu(I) bis(NHC) occupies and exists within the pores, with Zn(II) forming the metal nodes and 1,3-bis(4-carboxyphenyl) imidazolium (**I-47**, **Figure 18G**) being the organic linker of this unusual three-dimensional diamond-like framework. To investigate the catalytic potential of the MOF, activation of CO$_2$ *via* hydroboration at 35 °C was attempted. Conducted in the presence of pinacolborane, the obtained product HCO$_2$B(pin) was directly used as a formylating reagent for benzylamine.[338] A conversion of 92 % was already reached with 5 mol% Cu (1 mol% Cu = 0.5 mol% MOF) which remained constant even at 10 mol % Cu. Additionally, the recyclability advantage of heterogenous catalysts like MOFs over homogenous catalysts was displayed. A 5 mol% loading of the MOF was used over 5 cycles in which the conversion remained stable at 50 % after decreasing over the first two cycles.[338] Therefore, the Cu(I) bis(NHC) linkages within the MOFs were identified as active catalysts for the hydroboration of CO$_2$, similar to their related homogenous counterparts.[342] Intriguingly, to verify that the hydroboration reaction did not occur due to the formation of any homogenous NHC species in solution, the published work attempted to investigate "click" chemistry. It was noted that no catalytic reaction took place, the observation ascribed to an increased molecular size of the involved reactants and the heterogeneous nature of the MOF catalyst.[338] Therefore, there was considerable interest in investigating the potential use of Cu(I) bis(NHC)-containing MOFs as mechanocatalysts, following a similar approach as detailed in **Chapters 1.1.4.2** and **1.2.3**.

1.4   Thermoplastic Polyurethane (TPU)

Since the invention of polyurethane (PU) by the German Prof. Dr. Otto Bayer in 1937,[343] PUs are currently one of the most researched materials in the world. PUs are synthesized from a huge variety of sources with a wide range of specific applications, making it possible to group them into various different classes based on desired properties, one of them being thermoplastic polyurethanes (TPUs).[344] TPUs are typically linear segmented copolymers, synthesized by addition polymerization reaction of three components forming repeating urethane groups: a diisocyanate (aromatic or aliphatic),[345] a polyol (or macrodiol) and a chain-extender (usually a short organic diol or diamine).[346]

The synthesis of TPUs can be conducted by either a "one shot" or "two-shot" method. The "one shot" procedure involves all the reactants, i.e., the difunctional diisocyanate and diol, being mixed together in the desired stoichiometric ratios to cure and form an elastomer.[347, 348] In the "two-shot" procedure, also called "prepolymer method," involves the preparation of a prepolymer in the first step. The prepolymer is prepared by a reaction between diisocyanates and oligomers. In the second step, the chain extender and other additives (e.g., solvent, catalyst, etc.) is added to the prepolymer.[349-351] Both of the two possibilities, "one shot" or "two-shot" method, possess advantages and disadvantages. The "one-shot" method results in more random block polymers and are mainly employed in industry.[352] The "two-shot" method results in TPUs with higher molecular weight, low polydispersity (PDI), and better physical and mechanical properties, properties that are more suitable to be employed in research.[353]

1.4.1 Microphase Separation

Thermoplastic polyurethanes (TPUs) consist of alternating soft segments (SS) and hard segments (HS), chemically linked together along a macromolecular backbone. The reason for such naming is the different thermal behaviours displayed, where the T_g of SS is below ambient temperature, and the HS glass transition is above ambient temperature. The SSs are typically made of long hydroxyl-terminated polyols with a molecular weight of 1000-3000 g mol^{-1}, while the HSs are the reaction products of rigid isocyanate and chain extender moieties. Due to the presence of intermolecular hydrogen bonding, HSs act as stiff physical crosslinkers with the capability to alter mechanical properties of the material, whereas the SSs behave as soft and flexible elastomeric material. The two different segments, HS and SS, are thermodynamically incompatible with each other, resulting in a microphase separation. The structure-property relationship depends on the length and the chemical composition of HS and SS. The relationship can be utilised to impart specific properties to TPUs by properly choosing the chemical structure of the components and/or varying the molar ratio (concentration) of the HS and SS.[349, 354-358]
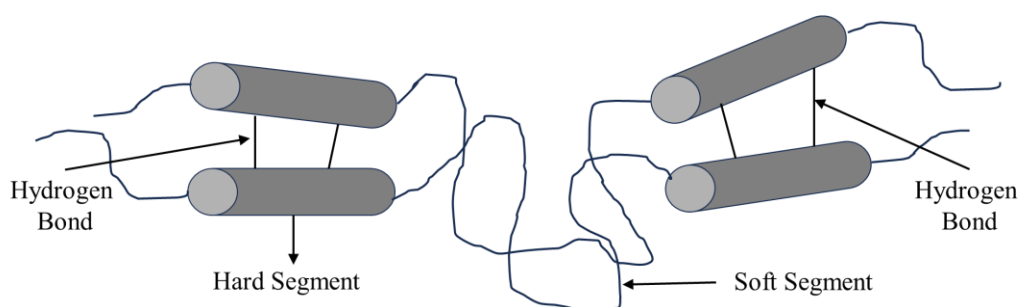
Figure 20. A pictorial description of soft/hard segments within a TPU.

1.4.1.1 Effect of Hard Segment Components

The incorporation of chain extenders as part of the hard segment has been significant for the production of TPUs. The chemical compositions and properties of these chain extenders have been widely studied.[359] These studies have pointed to the notable impact of these factors on the interactions between HSs and SSs. It was reported that 1,4-butanediol-based TPU exhibited superior thermal properties compared to 1,5-pentanediol and 1,3-butanediol TPUs due to its strong crystal structures.[360] Other studies pointed to a decrease in T_g of TPUs with longer chain extenders due to reduced polarity and increased flexibility. TPUs with an even number of -CH$_2$- in the diols exhibited superior mechanical properties.[361]
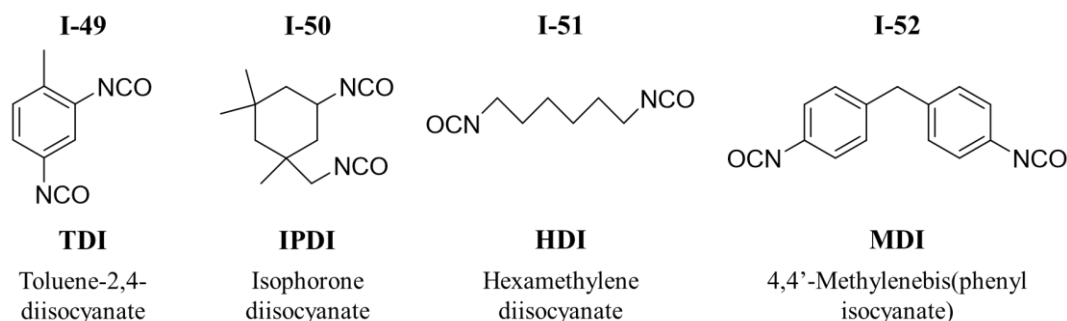
Figure 21. Structures of different isocyanates used in polyurethane synthesis.

The symmetry and planarity of diisocyanates are important parameters that influence HS crystallinity, and hence the mechanical properties.[362, 363] In a study with poly(ε-caprolactone)-based segmented polyurethanes (PCLUs), Ping et al.[364] investigated the impact of different diisocyanates (TDI (**I-49**), IPDI (**I-50**), HDI (**I-51**), and MDI (**I-52**)) (**Figure 21**) on material behaviour. It was observed that the rigidity was highest in HDI, followed by MDI and IPDI, with TDI-based structures displaying discrete domains. Initial stretching damaged hard domains, affecting recovery. Subsequent cycles did not damage hard domains, achieving 100 % recovery. Contracting stress measurements indicated hard segment frameworks significantly influenced stress relaxation, with the order of contribution being TDI < IPDI < MDI < HDI.[364]

1.4.1.2   *Effect of Hard Segment Concentration*

The relative weight fractions of the HSs and SSs contribute immensely to the structural, mechanical, and thermo-mechanical properties of the TPUs, especially in TPUs with HS content higher than 50 %. This was evidenced with the increasing Young's modulus and tensile strength of TPUs with increase in HS concentration, though the yield strength and elongation showed a decrease.[365] Koberstein et al. observed the effect of HS concentration on the T_g of the SS (T_{gSS}) and the heat capacity (ΔCp). With an increase in HS concentration, the T_{gSS} increased while the ΔCp decreased.[366] Klinedinst et al. presented a correlation between higher HS content and enlarged size of hard domains, as well as increased phase separation, resulting in increased temperature at which the HS melting occurred.[355] Additionally, testing with increasing HS content in PU-based polymer concretes displayed an enhancement of compressive strength, impact strength, modulus of static elasticity, flexural strength, and flexural modulus, effectively adjusting and engineering the performance of PU-based polymer concrete.[367] To develop a water barrier film, Kang et al.[368] also experimented with HS content variation from 0-40 %. The increasing hard domains resulted in resistivity to water permeability with the water vapor transmission rate (WVTR) measurements showcasing a decrease in water vapour permeability of the TPU films with varying HS content from 223.63 to 116.26 g m^{-2} day^{-1}.[368]

1.4.2   Shape Memory Polyurethane (SMPU)

Any polymer that is stimuli-responsive and returns from a temporarily deformed form to its original permanent form can be termed as a shape memory polymer (SMP). The external stimuli that trigger a shape memory includes thermal, pH, light, electric field, and humidity.[369-373] A polymer undergoes a transition from a glass-like to a rubbery-elastic state above its glass transition temperature (T_g).[374] Applying short-term uniaxial stress stores entropic energy because the movement of the entangled polymer chains is still largely restricted. Prolonged stress allows relaxation, causing chain slippage and bulk flow. Reversible deformation occurs using network chains as molecular switches, where flexibility is temperature-dependent at certain transition temperatures (T_{trans}). T_{trans} is usually equal to T_g in an amorphous SMPU or T_m in a crystalline SMPU.[374] External thermo-stimuli over T_{trans} enhances chain flexibility. Molecular motion freezing (in amorphous PU) or crystallization (in crystalline PU) fixes a programmed temporary shape when temperatures are again cooled below T_{trans}. Stability depends on macromolecular segment interaction and chain conformations. Reheating above T_{trans} allows chain relaxation and stable conformation formation. Such relaxation or shrinkage of the molecular chains, driven by the elastic strain energy produced during the deformation process, causes shape recovery in an SMPU (**Figure 22**).[374-376]

Due to the microphase separation present within PUs leading to hard and soft segments, PUs satisfies the most basic requirement of an SMP.[377, 378] Compared to other SMPs, PU-based SMPs (SMPU) are

easier to process, display large recovery strains up to 1000 %, and have an adjustable shape-recovery temperature range.[379, 380] Additionally, SMPUs have excellent chemical properties as well as biocompatibility.[381] Although SMPUs can be divided into two main categories, i.e., physically cross-linked thermoplastic (flexible and easily shapable) and chemically cross-linked thermoset (lack thermal plasticity, difficult to reprocess and/or recycle),[382, 383] the focus of this chapter will remain on thermoplastic polyurethanes (SMTPU).
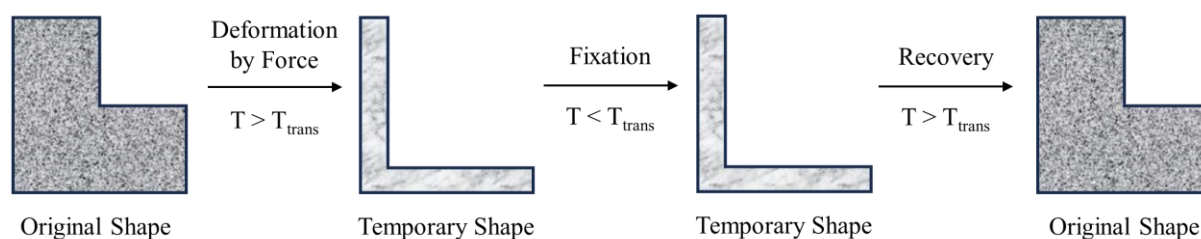
Figure 22. A pictorial description of the shape memory effect that is imparted due to the microphase separation of the hard and soft segments.[384]

In an SMPU, the SSs are glassy or semi-crystalline below T_g and are responsible for the temperature-sensitive shape recovery above T_{trans}, while the HSs fix the permanent shape by hydrogen bonding, Van der Waals, etc.[385] Hence, deformed SMPUs recover their original shape on heating over the T_g or the soft segment crystal melting temperature.[386] By changing the content ratio of HS and SS, the T_g can be adjusted to obtain tailored SMPUs.[387-390] However, PUs with HS content lower than 25-30 % cannot exhibit shape memory effect due to weak physical cross-linking. Although shape recovery properties increased with HS content, the HS content above 50 % exhibited poor recovery due to excessive physical crosslinks.[391-393] Hence, controlling the HS and SS structure and composition are extremely important to obtain the desired shape memory effect.

In **Chapter 1.2.3**, the significance of exploring mechanochemistry and force-responsive stress sensors has been emphasized. One of the objective of this thesis is to develop a stress-sensor system activated through mechanochemical processes, the real usefulness of which arises when incorporated within a polymeric material.[394] As **Chapter 1.4** would indicate, polyurethanes as bulk matrices for stress-sensor applications form a special interest for us in this thesis, as has been for other polymer scientists. Several examples of polyurethanes being used effectively widely with different mechanophores for such applications have been reported in literature.[395-399]

2   AIM OF THE THESIS

2.1   Objective and Motivation

The study of the catalytic activity and the mechanochemical responses of Cu(I) NHC complexes form the basis of this thesis. For this purpose, two routes should be explored. The first route would be the use of Cu(I) NHCs as homogenous catalysts to attempt cyclopropanation of poly(isoprene) by the implementation of functional groups into unsaturated polymers, while the second route would involve the use of Cu(I) NHCs as heterogenous mechanocatalysts in the form of metal-organic frameworks (MOFs).

While undertaking the first route, it is important to consider that the implementation of functional groups into unsaturated polymers is often a challenging task. In many cases a significant degradation of the polymer backbone must be considered, yielding polymers with significantly lower molecular weights. The chemical transformation of double bonds to cyclopropanes recommends usually the application of highly reactive species, such as carbenes, ylides and carbanions, or the assistance of metal catalysts.[400, 401] A prominent example is the metal-catalysed cyclopropanation,[120] which is known as a powerful tool to introduce different functional groups to small molecules as well as into the scaffold of poly(diene)s, enabling thus a broad variation of material properties. Hence, an attempt of cyclopropanations of poly(isoprene) using Cu(I) NHC catalysts would be undertaken to explore a pathway not extensively explored, enabling thus an easy access to modified poly(diene)s with ester or carboxylic groups. Therefore, the design of the pathway should involve choosing appropriate reactants, solvents, appropriate concentrations, and reaction conditions. In-depth study would also be required to predict the mechanism and determine the reaction rates to fully develop optimal conditions for the cyclopropanation reaction. The modified poly(isoprene) (PI) should be able to establish ionic interactions with cations or cationically modified polymers, or establish hydrogen bonds to form dynamic networks. This would thus offer the opportunity to be applied in the tyre/rubber industry, increasing durability and grip. Its potential for up-scaling should make approach feasible for an application in large-scale production processes such as for manufacturing of modified synthetic rubbers.

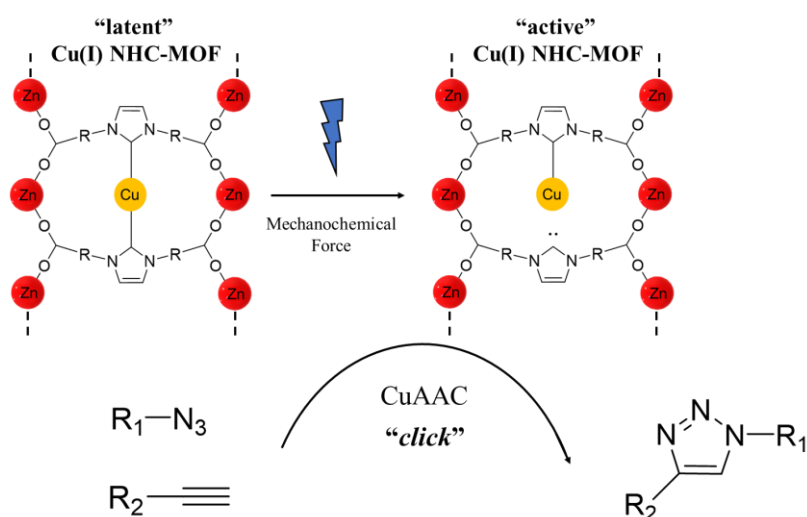
Figure 23. The mechanochemical activation of Cu(I) bis(NHC) containing MOF by cleavage of a shielding NHC to generate the catalytically active Cu(I) mono(NHC) which is able to trigger CuAAC ("click").

The second route should involve an extensive study into the application of Cu(I) NHCs as mechanocatalysts, expanding the previous work within the working group in which a latent Cu(I)-based

system had been developed as a mechanophore, capable of activation by mechanical forces transmitted *via* covalently attached polymer chains. Therein, a metal complex based on NHCs was used in the form of Cu(I) bis(NHC) complexes,[231, 258] embedded into polymer- and peptide-backbones[259, 260] to develop stress-sensing materials.[234, 264, 265] This would involve designing MOFs containing latent copper (I) bis(NHC) within the MOF structures which should have the possibility to be chemically activated by mechanical force causing one shielding ligand to be detached, thus generating a catalytic active site which would trigger a copper(I)-catalysed alkyne azide cycloaddition (CuAAC) (**Figure 23**). It is known that plastic deformations in MOFs can be initiated by mechanical treatments (bulk compression,[304, 305, 325, 402] shock impact,[310, 403] delamination by sonication[404-406]) to alter the chemical bonds and the crystal structures of the MOFs, resulting in modifications. Based on their extended structures, MOFs can also be regarded as highly ordered polymers, where repetitive elements are arranged in all different dimensions, thus forming a crystalline polymer-like structure, as a polymer chemists' definition could be. As MOFs are able to undergo both reversible elastic and irreversible plastic deformations, mechanochemistry in MOFs is an attractive perspective, as force should be transmitted efficiently from nodes inside the MOF, wherein the mechanochemically active metal-NHC-bonds are placed into.

The ability of the activation of the obtained Cu(I) within a MOF to trigger a CuAAC "click" reaction would be first investigated in solution using ultrasonication of the model benzylazide and phenylacetylene reaction. The purpose of this step is to gain preliminary insights into the feasibility of employing MOFs as mechanocatalysts. If successful, the MOF's application would be extended to thermoplastic polyurethane (TPU) bulk material to fulfil its application as a fluorogenic stress-sensing system. This would result in the development of a potential three-in-one TPU system embedded with MOF which would: 1) undergo mechanochemical activation in the presence of an embedded Cu(I) bis(NHC)-containing MOF, enabling CuAAC within a bulk system, 2) function inside a shape memory TPU material (SMPU), allowing shape recovery upon reheating due to the thermodynamically driven phase separation, and 3) allows to monitor the mechanochemical activation process *via* a fluorogenic dye system that facilitates early detection of material failure and identifying specific failure areas, enabling quick and cost-effective replacement of polymeric materials.
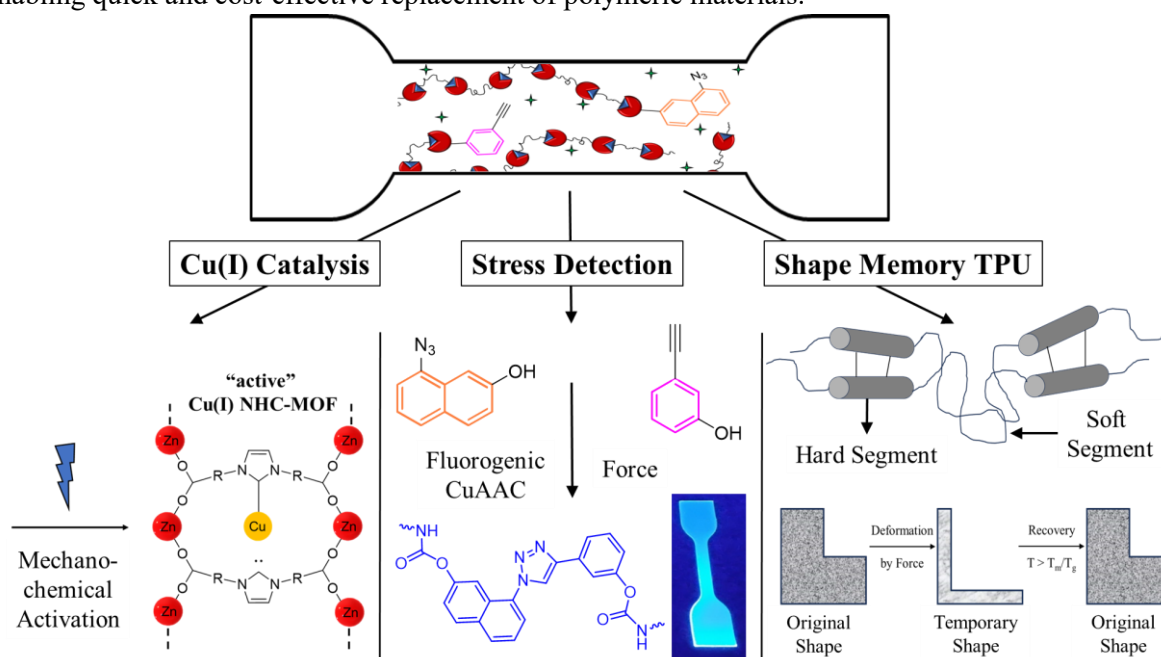

Figure 24. The ultimate aim of the thesis is to develop a potential three-in-one TPU system embedded with NHC-MOF, namely observing Cu(I) catalysis resulting in CuAAC, observing fluorescence to use it as a stress-sensing system and accomplishing a shape memory TPU (SMTPU).

2.2 Concept

To achieve the thesis's objective, the conceptualization involved the first route of employing Cu(I) *N*-heterocyclic carbenes (NHCs) initially as conventional catalysts. Predominantly *cis*-1,4-PIs (90 : 8 = 1,4-PI : 3,4-PI; 65 : 25 = 1,4-*cis* : 1,4-*trans*) (PI) (**3**) would be reacted in the presence of commercially available Cu(I) NHC catalysts with diazoacetates (EDA/*t*-BDA) (**4/5**) to generate ester-substituted cyclopropane along the PI backbone. This would be conducted using two approaches, APPROACH A1 with Cat. **1** [(IPr)CuCl] and APPROACH A2 with Cat. **2** [(IMes)CuCl] (**Figure 25A**), with the ratio of diazoacetate (DA) per PI double bond set to 1:2. The progress of the reactions would be monitored using ^{1}H NMR spectroscopy. Copper was selected as the transition metal as it is less toxic than thallium and less expensive compared to palladium or gold. Moreover, Cu-mediated cyclopropanations are known to be conducted under mild reaction conditions.[111]

A   **Cu(I)-catalysed cyclopropanation of poly(isoprene) with diazoacetates**

B   **Deprotection of cyclopropanated poly(isoprene)**
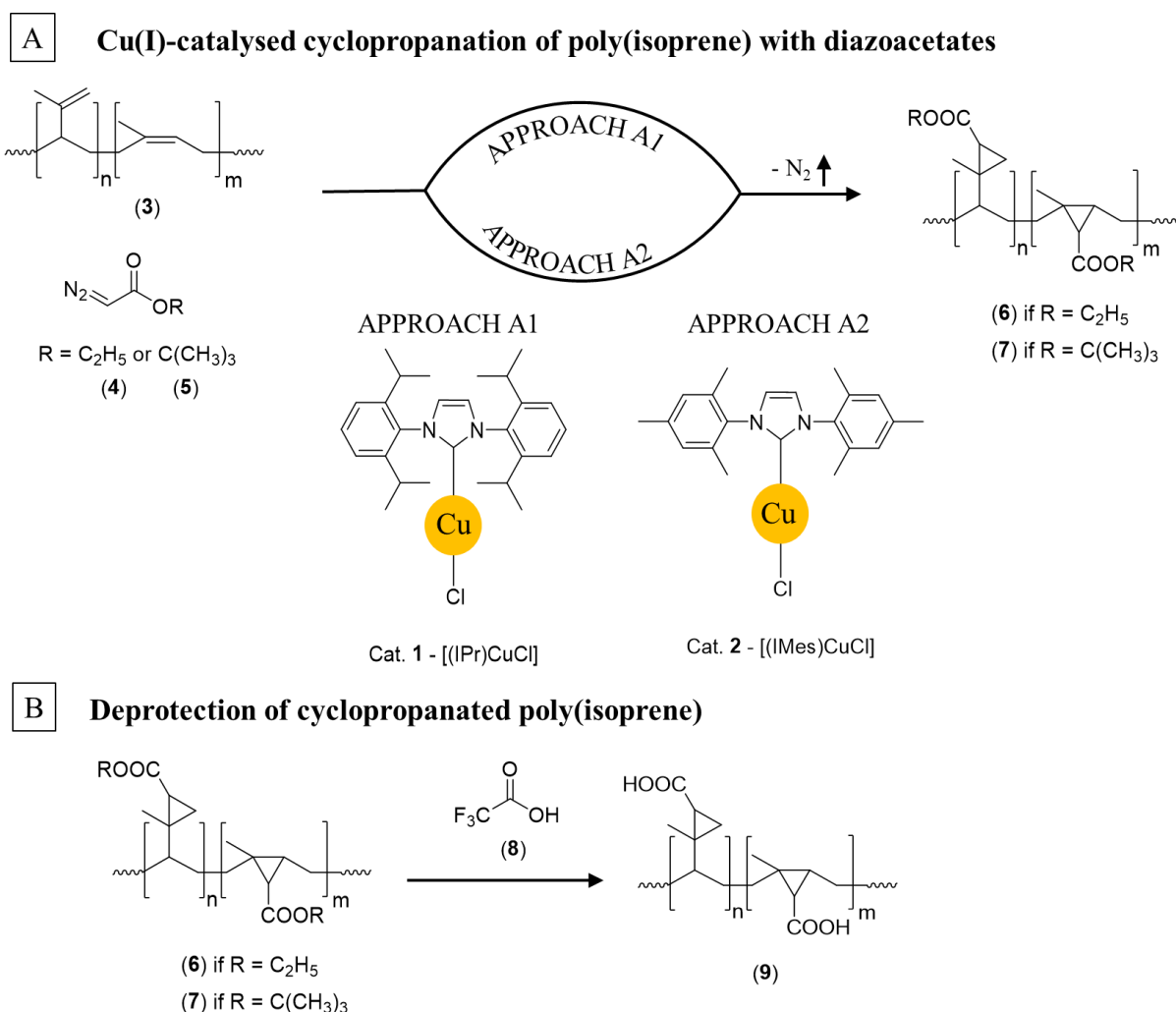
Figure 25. A graphical representation of the concept displaying **A**) Cu(I)-catalysed cyclopropanation of PI with diazoacetates and **B**) the deprotection of the cyclopropanated PIs.

The first set of experiments should involve optimizing the catalyst amount and the reaction temperature. The solvent for this set of experiments would be fixed to cyclohexane with a PI concentration (solid content) of 1.3 wt.%. The use of cyclohexane as a solvent was of special interest as usually non-polar solvents are used in industrial PI synthesis *via* living anionic polymerization. The diazoacetate to be used would remain EDA (**4**) for further optimization reactions until stated otherwise. The next set of experiments would target the investigation of the influence of solvent polarities towards the

modification yield. For this purpose, the cyclopropanation would be performed in tetrahydrofuran (THF), dichloromethane (DCM), and cyclohexane. Further set of experiments would explore the effects of changes in the PI solid content (e.g., 10 wt.%, 15 wt.%, 20 wt.%, …, etc.) until an increase does not affect the modification yield and a maximum is achieved. The kinetics of the cyclopropanation of PI with EDA (**4**) would be performed to serve two purposes; to know the time taken for the reaction to cease and to investigate differences in the reactivity of Cat. **1** and Cat. **2**, possibly resulting in one of the two approaches (APPROACH A1 or A2) to be favoured (**Figure 25A**). As all optimization with (**4**) would have been completed, the optimized reaction conditions would be transferred to the cyclopropanation using *tert*-butyl diazoacetate (*t*-BDA) (**5**). The thus obtained modified PIs, either with (**4**) or (**5**), should be characterized using ^{1}H NMR spectroscopy, GPC and DSC. In the final step, the deprotection of the cyclopropanated PIs would be conducted (**Figure 25B**). Deprotection experiments would be accomplished to transform the cyclopropyl ester-bearing PIs into those with free carboxylic groups, which should be able to establish ionic interactions or hydrogen bonds. The deprotection experiments would be conducted for both ethyl and *tert*-butyl ester modified PIs. The obtained product should be investigated using IR and rheology experiments to understand the changes in the chemical and structural properties, hence achieving a meaningful application of manufacturing modified synthetic rubbers for tyre/rubber industry.
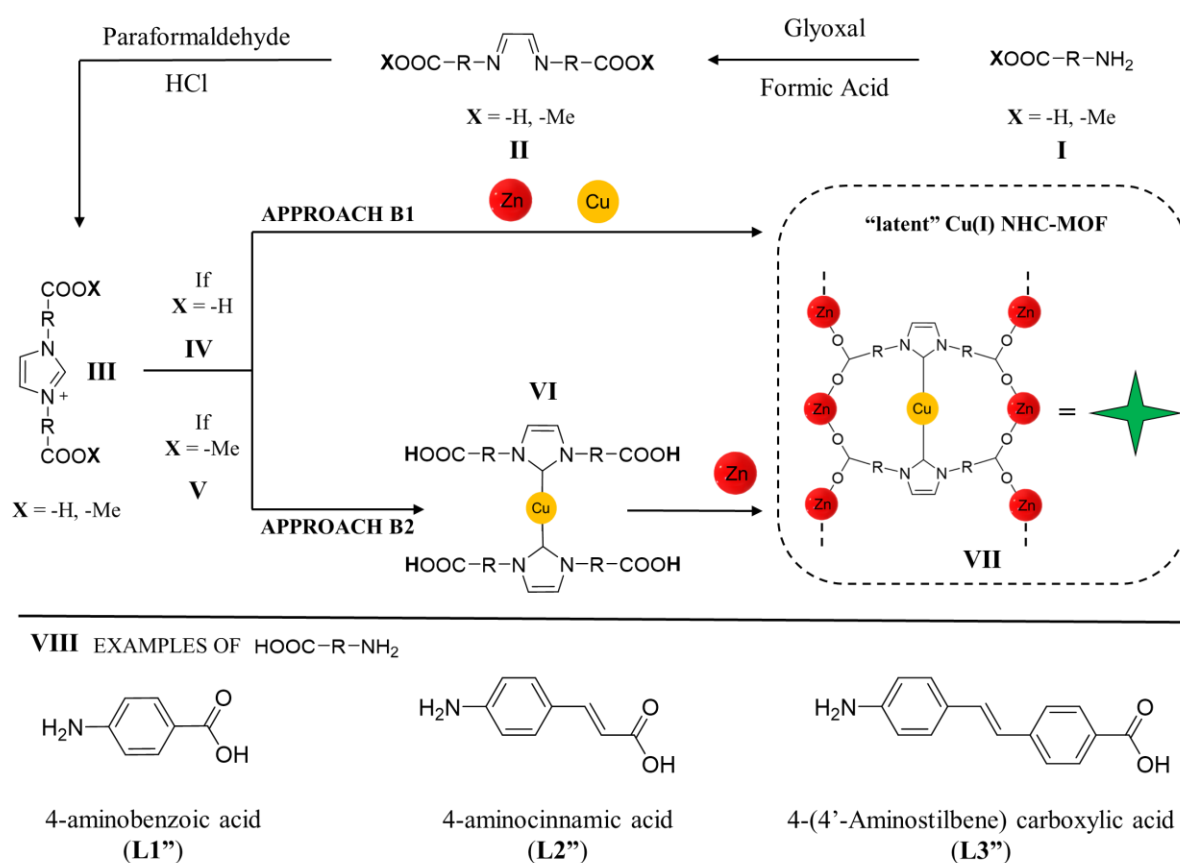
Figure 26. A graphical representation of the synthesis of NHC-MOFs using the two proposed approaches.

As part of the second route, Cu(I) NHCs would be employed as mechanocatalysts in the form of metal-organic frameworks (MOFs). For this purpose, a bifunctional compound (-NH$_2$ and -COOX (H/Me)) would serve as the starting point for the preparation of the NHC-MOFs (**I**, **Figure 26**). These bifunctional compounds should initially be utilized to synthesize an *N*-heterocyclic carbene (NHC)

ligand (**II** and **III**) which would be the organic linker of the NHC-MOFs. Once an NHC would be obtained, the preparation of the NHC-MOFs could follow two methodologies. In the case of X = H (**IV**), APPROACH B1 would be followed in which the NHC ligand is further used to synthesize a MOF, ideally forming a Cu(I) bis(NHC) in the pore (**VII**) with Zn(II) as the metallic nodes, as per the procedure described by Burgun *et al.*[338] In the case of X = Me (**V**), APPROACH B2 would be followed which involves the synthesis of a Cu(I) bis(NHC) which would be deprotected to obtain -COOH group (**VI**). This, along with Zn(II), could be then used to synthesize the NHC-MOFs (**VII**). These would be characterized using powder X-ray diffraction (PXRD), infrared spectroscopy (IR), thermogravimetric analysis (TGA), and flame atomic absorption spectroscopy (FAAS). It has already been stated that based on the extended structures of MOFs, they could be regarded as highly ordered polymers. An investigation into whether MOFs, with their higher rigidity compared to linear polymers or polymeric networks, should lead to an efficient activation by ultrasound or upon embedding into a polymer matrix is an interesting prospect that would be explored. Different organic linkers lead to changes in the physical density, the porosity, and the pore architecture of MOFs. With such variations, the mechanical properties, such as elastic moduli, are noticeably affected, signalling an intricate relationship between structure and mechanical properties.[282] For this reason, there would be three possible bifunctional compounds in contention (**VIII**). Due to their varying structure, each of them should influence the rigidity of the NHC-MOF differently. Hence, R is the key (see **Figure 26**) and a balance between rigid and soft components become necessary as the transmittance of force requires stiffness, but too stiff and the entire MOF could collapse due to bond breakage.[309] Hence, tuning the MOF so it survives procedures such as ultrasonication and extensional oscillatory and rotational rheology is necessary and possible.

Once synthesized, the NHC-MOFs would be subjected to ultrasonication experiments in solution. The use of ultrasound (or any other mechanical stress) is expected to activate the latent Cu(I) bis(NHC) complexes as described previously.[234, 258-260, 264, 265] On application of an external force, one of the two NHC ligands shielding and attached to the Cu(I) should be cleaved, rupturing the mechanochemically labile bond present between the NHC-carbon and the Cu(I) which allows the first step, a coordination of the alkyne-ligand with the available Cu(I) to form copper(I) acetylide,[260] to eventually form an 1,2,3-triazole product. The progress of this would be monitored using ^{1}H NMR spectroscopy to understand the catalytic efficiency of the NHC-MOFs. Previously in **Chapter 1.3.1.2.1**, the principle of using sonication resulting in bonds rupturing within the layers of a MOF to form 2D metal-organic networks (MONs) was discussed. Also, effects of ultrasonication on a solid, like MOF, in a liquid-solid heterogenic system were discussed. The formation of microjet and shock waves should result in plastic deformation, surface defects or even new surfaces being formed and exposed.[212, 286] It could be hypothesized that a catalytic activity would be gained due to newly formed surfaces of the cracked MOF by ultrasonication causing at least a partial destruction of the MOFs.

Once the ^{1}H NMR spectroscopy informs of the most efficient and catalytically active NHC-MOF, it would be selected to embed within a thermoplastic polyurethane (TPU) matrix. The thermoplastic polyurethane (TPU) would be initially synthesized by a multicomponent polyaddition reaction involving pTHF and MDI in the presence of catalytic amount of 1,8-diazabicyclo[5.4.0]undec-7-ene, generating pre-condensed soft block segments. Subsequent addition of the chain extender 1,4-butanediol (BDO) would result in the formation of hard block segments, leading to the formation of alternating soft/hard blocks. These supramolecular crosslinked elastomeric polyurethane networks would be fabricated as foils of varying ratios of the soft/hard block segments. The chosen ratio of the soft/hard blocks should influence the physical properties of the TPU. These changes in properties would be measured using extensional rotational rheology with oscillating stress-strain experiments to obtain the Young's modulus, as well as with DSC to provide crucial information regarding the physical and

chemical properties of the TPUs. Once a TPU foil of an appropriate soft/hard segment ratio is chosen, it would be necessary to combine mechanophoric behaviour with CuAAC "click" reaction within the TPU matrix in order to ultimately form a three-in-one stress sensing system. For this, the mechanochemically activated NHC-MOF can act as a trigger for the CuAAC of the covalently embedded compounds 8-azidonaphthalen-2-ol (**13**) and 3-hydroxyphenylacetylene (**14**), forming the fluorescent 8-(4-(3-hydroxyphenyl)-1,2,3-triazol-1-yl)naphthalen-2-ol (**15**) (**Figure 27**) *via* a fluorogenic "click"-reaction after stress has been imparted on the TPU. Tensile oscillatory rheology would then be performed on the resulting foils to study the shape memory effect (SME) and the mechanochemical activation of the TPU foils (see **Figure 27**). The SME of the TPU is caused by the microphase separation of its thermodynamically immiscible hard and soft segments. The hard segments act as anchor points for shape recovery, while the soft segments absorb any external stress applied. To study the mechanochemical activation of the MOF, the mechanochemical response should be correlated with the increase in the fluorescence intensity that should be observed when the highly fluorescent 8-(4-(3-hydroxyphenyl)-1,2,3-triazol-1-yl)naphthalen-2-ol (**15**) dye is formed *via* CuAAC (**VI, Figure 27**). The successful achievement of all three applications within the TPU matrix, namely observing Cu(I) catalysis resulting in CuAAC, correlating fluorescence to applied mechanical force, and accomplishing a shape memory TPU (SMTPU), will lead to the realization of a three-in-one fluorogenic stress-sensing system.
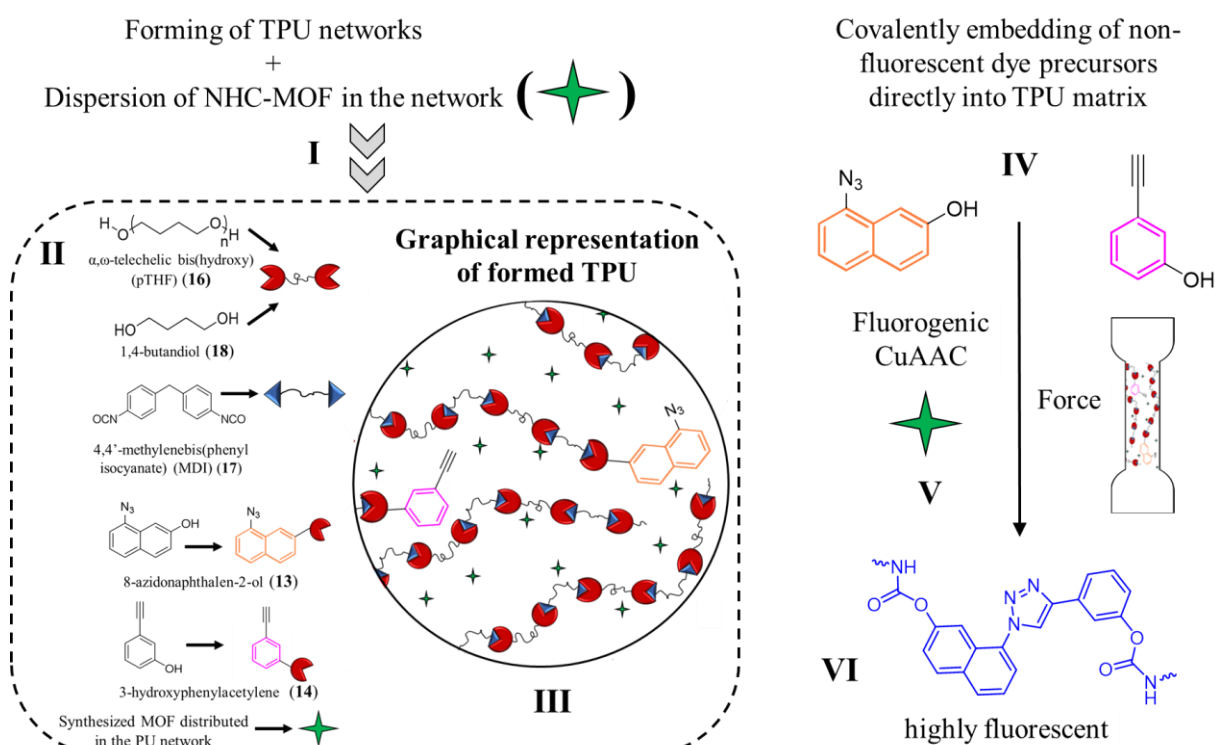

Figure 27. A graphical representation of the formed TPU foils as well as the CuAAC that could be observed within a TPU matrix.
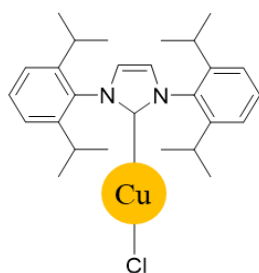
3 RESULTS and DISCUSSION

3.1 Cu(I) NHCs as Catalysts for Cyclopropanation

Published in "Shinde KS, Michael P, Rössle M, Thiele S, Binder WH. Cyclopropanation of poly(isoprene) using NHC-Cu(I) catalysts: Introducing carboxylates. *J Polym Sci*. **2020**; 58: 2864-2874."[407]

3.1.1 Cu(I)-catalysed Cyclopropanation of Poly(isoprene) with Diazoacetates
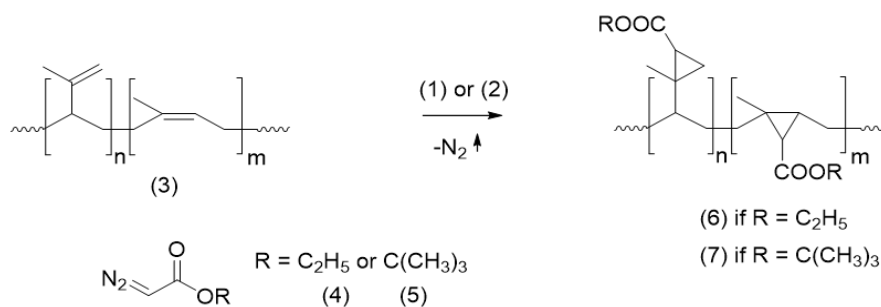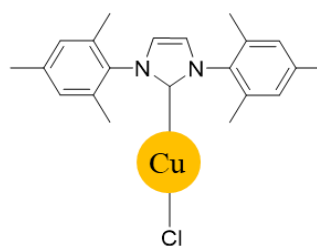
Scheme 4. Metal-catalysed cyclopropanation of a predominantly *cis*-1,4-poly(isoprene) with the NHC-Cu(I)-based catalyst (**1, 2**) and the diazoacetates (**4, 5**).

In a first set of experiments, the catalytic cyclopropanations of predominantly *cis*-1,4-poly(isoprene)s (90 : 8 = 1,4-PI : 3,4-PI; 65 : 25 = 1,4-*cis* : 1,4-*trans*) (PI) (**3**) were conducted using ethyl diazoacetate (EDA) (**4**) utilizing two different approaches, Cu(I) NHC catalysts Cat. **1** [(IPr)CuCl] in APPROACH A1 and Cat. **2** [(IMes)CuCl] in APPROACH A2 (see **Scheme 4**). The ratio of EDA per PI double bond was set to 1:2 and the solvent was fixed to cyclohexane with a PI concentration of 1.3 wt.%. The use of cyclohexane as a solvent is of special interest as usually non-polar solvents are used in industrial PI synthesis *via* living anionic polymerization. The reaction conditions were subsequently optimized in terms of the catalyst amount and the reaction temperature (**Table 1**). The ratio of the catalysts was varied from 0.002 to 0.05 eq. per double bond of PI, where 0.05 eq. was determined as best with modifications of 3 % (Cat. **1**) and 2 % (Cat. **2**), respectively (determined *via* ^{1}H NMR spectroscopy, for details see **Chapter 5.2.2**). Investigating the influence of the reaction temperature from room temperature to 40 °C revealed no significant effect towards the modification yield, which remained around 3 % for both catalysts (for details see **Table 1**, **Ent 7** and **8**). Hence, the reaction temperature was kept constant at room temperature.

Table 1. Variations in catalyst amounts as well as a singular change of temperature to ascertain suitable reaction conditions.

Ent	Ratio (Cat.:PI:EDA)	Catalyst	T °C	% Modification [a]
1	0.002:1:2	Cat. **1**	RT	0.5
2		Cat. **2**		0.4
3	0.02:1:2	Cat. **1**	RT	3.0
4		Cat. **2**		2.0
5	0.05:1:2	Cat. **1**	RT	3.0
6		Cat. **2**		2.0
7	0.05:1:2	Cat. **1**	40 °C	3.0
8		Cat. **2**		3.0

The reactions were performed in cyclohexane with the solid content (wt.%) of PI in cyclohexane set at 1.3 %. Reactions performed for 48 h. [a]Calculated according to the ratio of the signals at the peaks at 5.10 ppm and 4.80-4.63 ppm belonging to 1,4- and 3,4-poly(isoprene) respectively as well as the new peak after modification at 4.10 ppm belonging to the methylene protons of the $-CO_2CH_2CH_3$ moiety of the cyclopropane appearing in ^{1}H NMR spectroscopy (for details see **Chapter 5.2.2**).

In the next set of experiments, the influence of solvent polarities towards the modification yield was investigated (**Table 2**, **Ent 6a**). Therefore, the cyclopropanation was performed in tetrahydrofuran (THF), dichloromethane (DCM), and cyclohexane (see **Figure 28A**). The best modification of 10 % was obtained with Cat. **2** in DCM (see **Table 2**, **Ent 6a.i**), while THF and cyclohexane revealed only low PI modification (2-3 %) (see **Table 2**, **Ent 6a.ii** and **6a.iii**). The low modification in cyclohexane was expected because both the catalysts showed a lack of solubility in it. The limited solubility of the catalysts in cyclohexane led naturally to lower reaction rates and thus to a lower overall conversion.[408] Albeit the solubility in THF was good, its strong coordination to the copper caused a strong shielding of the catalytic active centre, resulting finally in lower yields. Weakly coordinating polar solvents such as DCM are preferred for cyclopropanation reactions *via* carbenes to avoid significant solvent effects.[409] Hence, further reactions were conducted with DCM as the most suitable solvent as well as with cyclohexane because of its industrial relevance.

Table 2. Calculated % modification for cyclopropanated 1,4-PI with different parameters.

Ent		Parameters	Solvent	Solid Content (wt.%)	% Modification [a]	
					Cat. 1	Cat. 2
1		Virgin PI (**3**)	-		-	-
6a	i	Solvent Variation	DCM	1.3	3	10
6a	ii		THF		2	2.5
6a	iii		Cyclohexane		3	2
6b	i	Solid Content (wt.%) Variation	Cyclohexane	1.3	3	2
6b	ii		Cyclohexane	10	1.5	3
6b	iii		Cyclohexane	15	1.5	5
6b	iv		Cyclohexane	20	2.5	5
6c	i		DCM	15	-	17
6d	i		DCM	10	2	4

| 6d | ii | Cyclopropanation with *t*-BDA | | 15 | - | 5 |
| 6e | | Cyclopropanation with EDA **(4)** in 1,2-DCE | 1,2-DCE | 15 | 5 | 4 |

The ratio of the catalyst to per double bond of the PI to diazoacetate is set at 0.02:1:2 for **Ent. 6a** and 0.05:1:2 for all other experiments. The PDI of all above listed experiments vary from 1.1-1.2 and the ratio of 1,4- / 3,4-PI isomers remain approximately 9. [a]Calculated according to the ratio of the signals at the peaks at 5.10 ppm and 4.80-4.63 ppm belonging to 1,4- and 3,4-poly(isoprene) respectively as well as the new peak after modification at 4.10 ppm belonging to the methylene protons of the -CO$_2$*CH$_2$*CH$_3$ moiety of the cyclopropane appearing in ^{1}H NMR spectroscopy (for details see **Chapter 5.2.2**).
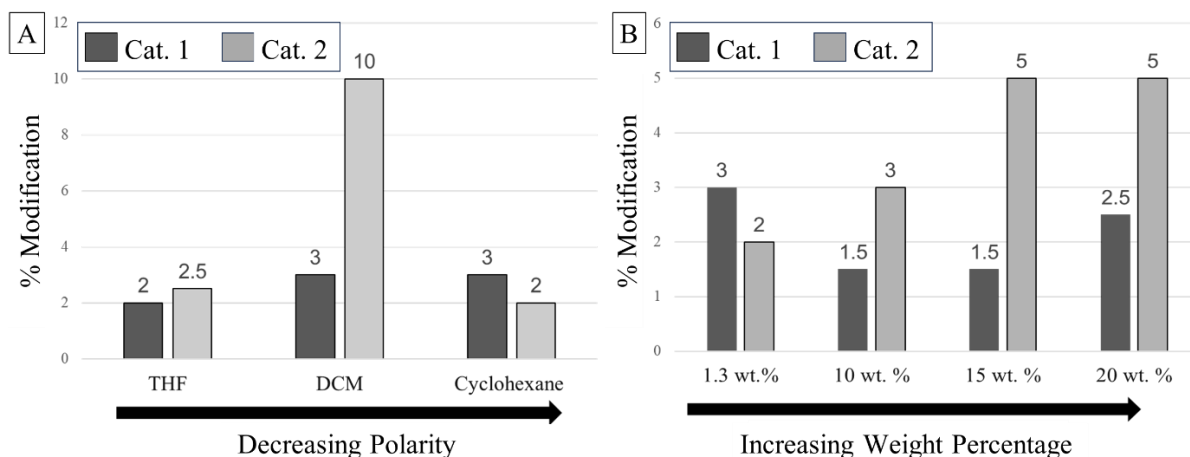
Figure 28. Dependency of cyclopropanation of PI with EDA and Cu(I) NHC catalysis on **A)** the solvent polarity at 1.3 wt.% solid content and **B)** different concentration of PI (solid content in wt.%) in cyclohexane.
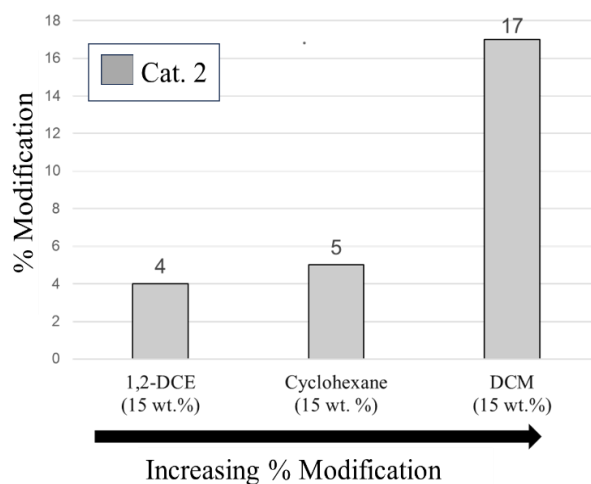
Figure 29. Comparison of the % modification for 15 wt.% of solid content in chlorinated solvents, 1,2-DCE and DCM compared to cyclohexane. The Cat:PI:EDA per double bond ratio is 0.05:1:2 and the % modification was determined by ^{1}H NMR spectroscopy (for details see **Chapter 5.2.2**).

To further optimize the reaction conditions, the PI solid content (wt.% in solvent) was varied (see **Table 2**, **Ent 6b**) from 1.3 wt.% to 20 wt.% to increase the effective concentration of the reactive compounds, PI as well as EDA, expecting higher reaction rates and thus finally higher modification efficiencies. Accordingly, the modification yields increased in case of Cat. **2** from 2 % for 1.3 wt.% up to 5 % for 15 wt.% in cyclohexane (see **Table 2**, **Ent 6b.i and 6b.iii**, see **Figure 28B**). A further increase to

20 wt.% showed no additional enhancement of the % modification. However, for the higher concentrated solutions (15-20 PI wt.%, **Table 2**), a violent bubbling was observed, which was on one hand the result of the faster reaction and thus stronger heat development due to the exothermic nature of the reaction, and on the other hand a result of the faster release of a larger amount of evolved N_2, gas generated in the course of the reaction. Hence, a slow, dropwise addition of the diazoacetates was necessary to avoid an uncontrolled explosion which occurred at higher concentrations than 20 wt.%, thus limiting the test range.

Acknowledging that the initial experiments conducted with Cat:PI:EDA per double bond ratio of 0.02:1:2 had the highest modification degree of 10 %, obtained with DCM with a solid content of 1.3 wt.% (**Table 2**, **Ent 6a.i**) with Cat. **2**, a variation of 15 wt.% solid content of PI was also conducted in DCM (see **Figure 29**) with a ratio of 0.05:1:2. An effort was also made with another chlorinated solvent, 1,2-dichloroethane (1,2-DCE) to observe the possible % modification (**Table 2**, **Ent 6e**). However, DCM with a solid content of 15 wt.%, showed a much superior modification of 17 %, achievable with Cat. **2** (**Table 2**, **Ent 6c.i**), compared to a modification of 4-5 % achieved with both 1,2-DCE and cyclohexane respectively, with a comparable solid content.
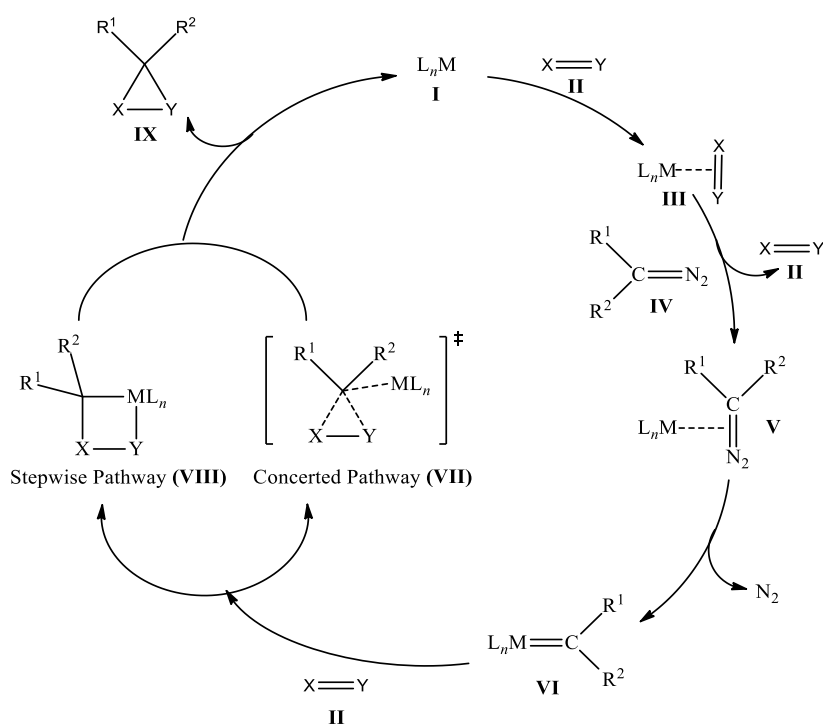
Scheme 5. Mechanism of the metal-catalysed cyclopropanation of olefins with diazo compounds.[117, 409-411]

Kinetic studies of the cyclopropanation of PI with EDA (**4**) were performed in cyclohexane at 20 wt.% (as technical relevant conditions) to investigate differences in the reactivity of Cat. **1** and Cat. **2** (**Table A1**). The reaction was monitored *via* ^{1}H NMR spectroscopy revealing the maximum conversion after 24 h for Cat. **2** to be 4 % and 48 h for Cat. **1** to be 1.5 % (**Figure A1**). In order to understand the difference in modification yields by the two catalysts, it is important to consider the mechanistical pathways of the Cu(I)-catalysed cyclopropanation reactions.[410, 412] After an initial formation of a pre-catalyst due to the affinity of the active Cu(I) catalyst for the unsaturated substrate[116, 409-411, 413, 414] (**Scheme 5, III**), the cyclopropanation proceeds further *via* complexation of a metal and a carbene (**VI**), formed by expelling N_2 from the diazo compound (**V→VI**), which is determined as the rate determining step.[116] The ring closing step itself is known to proceed either *via* a one-step concerted pathway (**VII**)

as a direct-carbene insertion, or *via* a two-step process, proceeding by a metallocyclobutane intermediate (**VIII**),[409, 411, 415] depending on the diazo compound, the ligand (L_n) and the transition metal (M).

Considering these theoretical assumptions, a possible explanation of the different reactivity of both catalysts can be found in the different donor properties of the NHC ligands. The pKa values are reported as 21.1 for Cat. **1** and 20.8 for Cat. **2** respectively.[21] Even though the difference in the values is minimal, the pKa value of Cat. **1** could indicate to a higher electron density on the copper instead of the carbenic carbon in the case of Cat. **2**. Hence, Cat. **2** would act as a more efficient catalyst as the strength of backdonation from the Cu(I) to the incoming diazoacetate to form (**VI**) (see **Scheme 5**) would be higher, in consequence enhancing its reactivity. The steric effects of the catalyst could possibly have more influence on the reactivity of the catalysts. The percent buried volume (%V_{bur}) is reported as 47.6 % for Cat. **1** and 36.3 % for Cat. **2** respectively for M-NHC length at 2.00 Å,[33] showing that Cat. **1** is bulkier compared to Cat. **2**. Therefore, the bulkier Cat. **1** could affect the mechanism, as suggested in **Scheme 5**, in two ways; by affecting the coordination of the diazoesters to the catalysts as suggested in (**VI**), as well as hindering the cyclopropanation itself, indicated by step (**VII/VIII**), making Cat. **2** a more effective and efficient catalyst.

However, it was wondered why the overall modification yield was at a relatively low level. A feasible explanation was found in a potential premature decomposition of the diazo compound. Albeit literature has reported no decomposition of the EDA (**4**) in the presence of the [(IPr)CuCl] (Cat. **1**) until an unsaturated substrate was added,[109] it was determined that dimerization took place *via* ^{1}H NMR spectroscopy (**Figure 30**). In the presence of catalyst **1** or **2**, the EDA (**4**) (ratio of 40:1 to catalyst) underwent dimerization to form diethyl maleate and fumarate (in solvent DCM-d_2), also in the absence of an unsaturated substrate, similar to other Cu(I) catalysts.[416] To study if the presence of PI mitigates this dimerization, further *in situ* NMR investigations were conducted, revealing that the presence of PI does not hinder the dimerization (**Figure A2**). Also, a slowed addition of EDA as well as the addition in several portions did not prevent the dimerization, which is thus to be considered as a major reason for the low modification yields.

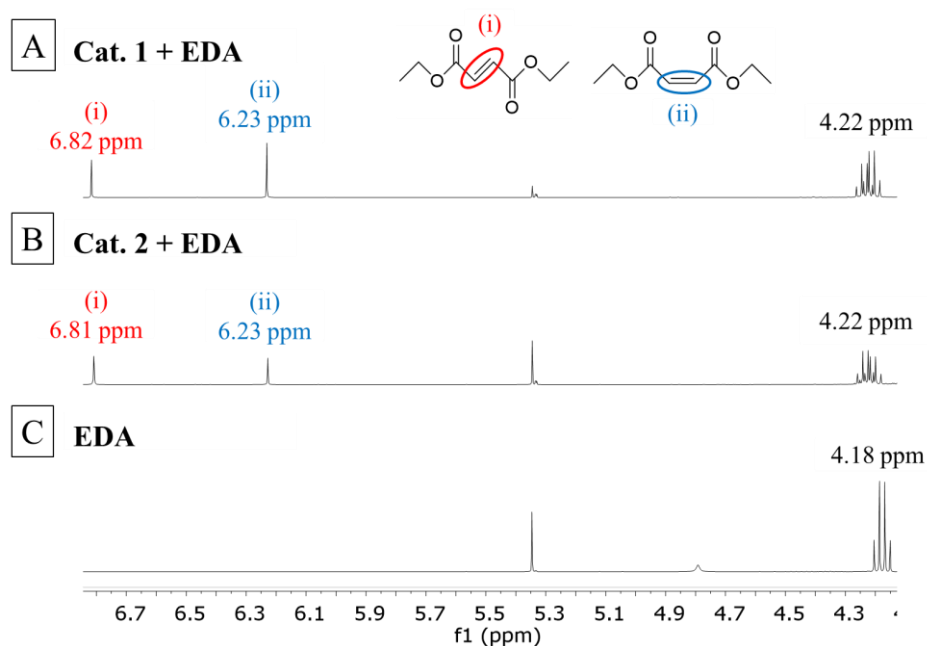**Figure 30.** ^{1}H NMR spectra for EDA in the presence of **A**) Cat. **1** and **B**) Cat. **2**. The spectrum **C**) is of EDA without a catalyst. All NMR were measured in the solvent DCM-d_2.

The optimized reaction conditions of **Table 2**, **Ent 6c.i** were transferred to the cyclopropanation of *tert*-butyl diazoacetate (*t*-BDA) (**5**) yielding optimized modification yields of 4-5 % (see **Table 2**, **Ent 6d**).

The characterization of the modified PIs was accomplished *via* GPC, ^{1}H NMR and IR spectroscopy and selected results are summed-up in **Table 3**. The reported values of M_n and PDI are both obtained from GPC. The M_n shows in general an increase after modification while the PDI essentially remains the same and is an indication that chain scission associated with many similar post-polymerization reactions did not appear.[121]

The effect of the modification onto the glass transition temperature T_g was investigated by DSC as it is of special importance for the desired tyre application (**Table 3**). There appears to be a reduction in the segmental mobility due to reduction in rotation around the -CH_2- bonds in the backbone of the macromolecules, corresponding to the increase in the number of polar ester groups,[120, 417] as the T_g of the virgin PI (**3**) shows an increase from -67 °C to -61 °C and -58 °C for 5 % modified PI, cyclopropanated by EDA (**4**) and *t*-BDA (**5**), respectively. On further increase of modification to 17 % (**Table 3**, **Ent 6c.i**), the T_g of the cyclopropanated PI shows an increase of ~23 °C to -44 °C. The regioselectivity of 1,4- and 3,4-PI was also investigated *via* ^{1}H NMR spectroscopy (**Figure 59A)** revealing an almost constant ratio between both isomers before and after the modification. This observation indicated that the Cu(I)-catalysed cyclopropanation of diazo esters on double bonds showed no regioselectivity and is thus in good compliance with the literature.[120] However, a stereoisomeric effect of *cis* and *trans* 1,4-PI could be determined. The average ratio of *cis*/*trans* isomers (determined from NMR, **Figure 59B**) showed a decrease from 65 : 25 *cis*/*trans* 1,4-PI (2.5) in the case of virgin PI to 55 : 25 *cis*/*trans* 1,4-PI (2.2) after 3-5 % modification. In case of 17 % modification yield, the ratio was decreased to 50 : 25 *cis*/*trans* 1,4-PI (2), showing a strong preference of *cis*-1,4-PI for the cyclopropanation.

**Table 3.** Selected examples for characterization data of diazoacetate modified PIs.

Ent	Reactants	Solvent	Solid Content (wt.%)	$M_{n,GPC,corr}$[a] (g mol^{-1})	PDI	% Modification [b]	T_g (°C)
1	Virgin PI (**3**)	-	-	2900	1.1	-	-67
6b.iii	Cat. **2**:PI:EDA	Cyclohexane	20	3100	1.1	5	-61
6c.i	Cat. **2**:PI:EDA	DCM	15	3700	1.1	17	-44
6d.i	Cat. **2**:PI:*t*-BDA	DCM	10	3200	1.1	4	-58
6e	Cat. **1**:PI:EDA	1,2-DCE	15	2600	1.2	5	N/A

The ratio of the catalyst to per double bond of the PI to diazoacetate is set at 0.05:1:2 for all experiments and the ratio of 1,4-/ 3,4-PI isomers remain approximately 9. [a]Correction factor of 0.58 used for M_n obtained by GPC. [b]Calculated according to the ratio of the signals at the peaks at 5.10 ppm and 4.80-4.63 ppm belonging to 1,4- and 3,4-poly(isoprene) respectively as well as the new peak after modification at 4.10 ppm belonging to the methylene protons of the -CO_2*CH_2*CH_3 moiety of the cyclopropane appearing in ^{1}H NMR spectroscopy (for details see **Chapter 5.2.2**).

3.1.2 Deprotection of Cyclopropanated Poly(isoprene)

Deprotection experiments were accomplished to transform the cyclopropyl ester-bearing PIs into those with free carboxylic group (**Scheme 6**), which are able to establish ionic interactions or hydrogen bonds. However, in case of the ethyl ester modified PIs (**Table 2, Ent 6c.i**), all attempts resulted in very low deprotection when applying e.g. sodium hydroxide, phosphoric acid[418] or trifluoroacetic acid (TFA) (**8**).[419, 420] Therefore, a change in the diazoester to *tert*-butyl diazoacetate (**5**) instead of ethyl

diazoacetate (**4**) was considered, as the *tert*-butyl groups can be cleaved more efficiently[418, 419, 421] under weakly acidic conditions.
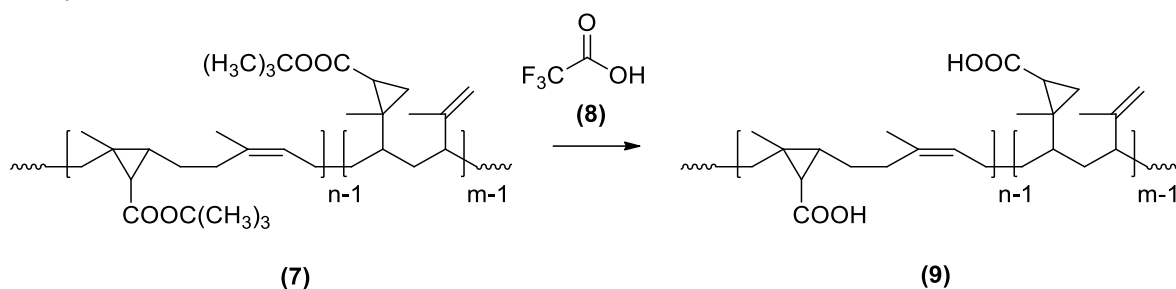
Scheme 6. Deprotection of (**7**) with trifluoroacetic acid (TFA) (**8**).
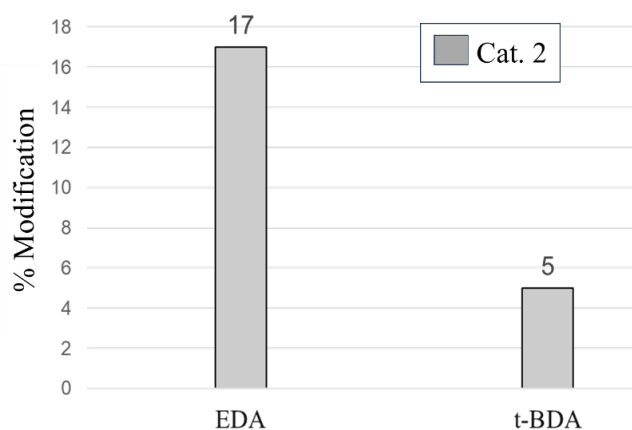
Figure 31. Cu(I)-catalysed cyclopropanation of PI with *tert*-butyl diazoacetate. The Cat:PI:EDA/*t*-BDA per double bond ratio is 0.05:1:2. The solid content (wt.%) of the PI in both the reactions with EDA (**4**) and *tert*-BDA (**5**) is 15 wt.% in DCM.

To obtain cyclopropane rings substituted with -CO$_2$C(CH$_3$)$_3$, *tert*-butyl diazoacetate (**5**) (*t*-BDA) was chosen according to the optimized reaction conditions in the case of EDA (**4**) with DCM as solvent. However, the modification yield with *t*-BDA was only 4-5 % for (**7**) (**Table 2, Ent 6d**) and is thus much lower compared with EDA in DCM (**Figure 31**). A reason for this could be that the PI used is a predominantly *cis*-polymer and hence modifications in successive repeating units could potentially be hindered by the presence of the much-bulkier -CO$_2$-*tert*-butyl groups substituted on the cyclopropane rings compared to the -CO$_2$-ethyl groups.

Figure 32. Images of *t*-BDA modified PI (**7**) (see **Table 2, Ent 6d.ii)** before deprotection (**7***) and after deprotection (**9***). (**7***) and (**9***) are the image form of (**7**) and (**9**) as seen in **Scheme 6**.

The deprotection of the sample **Table 2, Ent 6d.ii** (**7**) was conducted using TFA (**8**) using a modified method from literature.[420] The deprotected 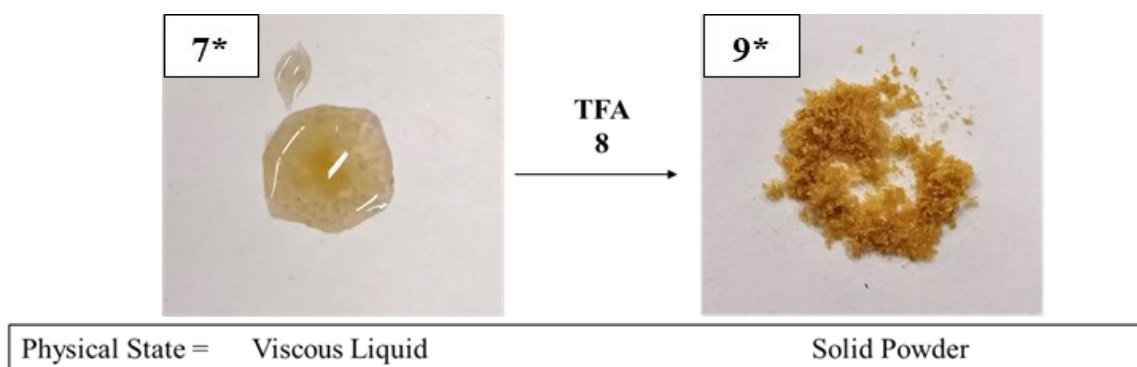sample (**Figure 32** (**9***)) was a solid powder when compared to the pre-deprotected sample (**Figure 32** (**7***)), which was a viscous liquid. To confirm that the obtained powder was in fact the polymer, GPC was conducted (**Table 4**). As can be observed, the M_n values remain firmly in the 2700-3200 g mol^{-1} range confirming the powder was in fact the modified polymer.

Table 4. A comparison of $M_{n,GPC}$ pre-(**7***) and post-deprotection (**9***) of *t*-BDA modified PI.

Ent.	Sample	M_n (GPC) (g mol^{-1})	$M_{n,GPC,corr}$ [a] (g mol^{-1}) (≈ 0.58)	PDI
1	Virgin PI	5000	2900	1.1
2	7*	5500	3200	1.1
3	9*	4700	2700	1.5

[a]Correction factor of 0.58 used for M_n obtained by GPC.
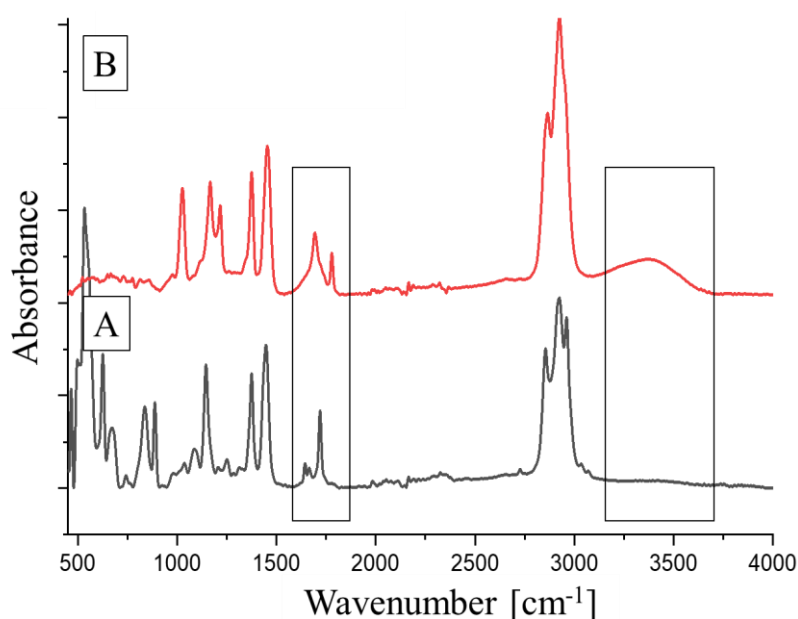
Figure 33. ATR-FTIR spectrum of **A**) *t*-BDA modified PI (**7***) and **B**) modified PI after deprotection (**9***).

ATR-FTIR-spectroscopy was conducted (**Figure 33**) for both, the pre- and post-deprotected samples (**7***) and (**9***) (**Figure 32**) respectively. On comparison of the two spectra, two important differences were noted. First is the emergence of a broad peak in the range of 3300-3500 cm^{-1} in the deprotected sample which could be attributed to the acidic -OH. The other is the shift in the peak attributed to the ester (-COOC(CH$_3$)$_3$) of the modified PI at 1720 cm^{-1} to a lower wavenumber at 1700 cm^{-1} attributed to the deprotected carboxylic acid moiety (-COOH).

Preliminary rheology experiments were conducted at different temperatures (**Figure A3**) with a shear strain of 5 %. The sweep could not be performed at temperatures below 130 °C as there was slippage at high frequencies and at temperatures above 170 °C, decomposition of the deprotected PI was observed.

Further rheology measurements revealed, as expected, a frequency dependency for all PIs, the virgin, the cyclopropyl ester-modified as well as the deprotected COOH PI, as can be seen in **Figure 34A**. At higher frequencies, the individual moduli are higher, and the material appears to be stiffer. A comparison between the virgin and the modified PI at room temperature indicates an increase in the storage modulus by a magnitude of almost 10^4, while the loss modulus remains the same, indicating that the cyclopropyl ester modification caused a significant stiffer material even at modification rates of only 5 %. At a frequency of 10 Hz, the loss factor tan(δ) is 20,000 and 11 (**Table A2**) for the virgin PI (3000 g mol^{-1}) and 5 % modified PI, respectively. Hence, the graph clearly indicates that the loss factor tan(δ) is much higher than 1 in the case of virgin PI compared to that of modified PI, and hence the modulus is dominated by the viscous properties of the material, also indicated by the more liquid-like behaviour of the virgin PI. Similarly, at a frequency of 10 Hz, the loss moduli of the deprotected PI (480,000 Pa) were determined at magnitudes of about 10^4 higher than that of protected PI (68 Pa) (see **Figure 34A**) even at elevated temperatures of 140 °C, which was necessary to melt the COOH-PI by removing the established hydrogen bonds. Comparing loss modulus of the deprotected PI (480,000 Pa) with that of high molecular weight (HMW) virgin PI of the range 150,000 g mol^{-1} (69,000 Pa, **Figure 34B**) shows some strong aggregates were indicated due to hydrogen bond dimers of COOH, causing finally an internal network formation and adopting thus a behaviour analogous to the HMW PI. A rigid internal supramolecular network was already established at low modification yields of 5 % per individual PI chain, which makes a further deliberate increase in modification yield unrequired as it would prevent an application of the designed material in tyre industry.
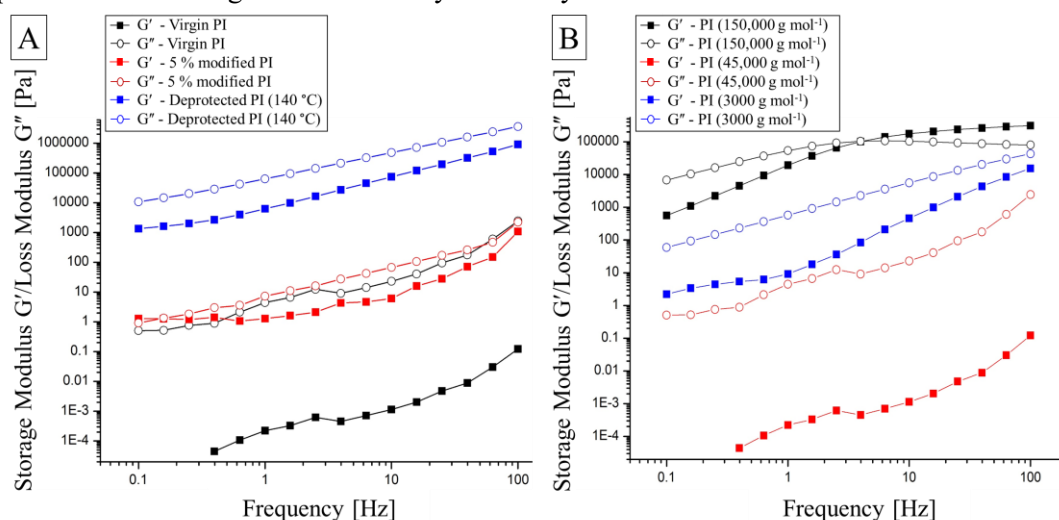
Figure 34. Frequency sweep of **A**) virgin, a 5 % modified and deprotected PI and **B**) virgin PI of different molecular weights at room temperature (25 °C).

3.2   Cu(I) NHCs as Mechanocatalysts within Metal-Organic Frameworks (MOFs)

Partially published in "Shinde, K. S., Michael, P., Fuhrmann, D., Binder, W. H, A Mechanochemically Active Metal-Organic Framework (MOF) Based on Cu-Bis-NHC-Linkers: Synthesis and Mechano-Catalytic Activation. *Macromol. Chem. Phys.* **2023**, 224, 2200207."[422]

3.2.1   Synthesis of Bifunctional Ligands

As previously mentioned in **Chapter 2**, two potential approaches were proposed for the preparation of *N*-heterocyclic carbene (NHC) ligands for the eventual synthesis of metal-organic frameworks (MOFs) (**Scheme 7**). Copper(I) NHCs exist as neutral [Cu(X)(NHC)][105] as well as cationic [Cu(NHC)$_2$]X[106,

[147] complexes. The first approach (APPROACH B1) involved using bifunctional compounds with -NH$_2$ and -COOH groups to form NHCs, subsequently reacting with metallic components to form bis-NHC complexes in the MOF pores. The second approach (APPROACH B2) involved protecting the bifunctional compounds with methylation, synthesizing ester-based NHCs, and then bis-NHCs. These methyl-protected bis-NHCs would subsequently undergo deprotection by cleavage of the ester to obtain carboxylic acid groups. Three starting bifunctional compounds, namely 4-aminobenzoic acid (**L1"**), 4-aminocinnamic acid (**L2"**), and 4-(4'-aminostilbene) carboxylic acid (**L3"**), were considered for the purpose of optimizing the preparation of organic linkers for the MOFs (**Scheme 7**). These compounds provided different levels of molecular rigidity. MOFs are highly tuneable, and their rigidity can be adjusted by using organic linkers with different properties. This is demonstrated by the elastic moduli which varies depending on the linker and can affect the physical density, porosity, and pore architecture of a MOF.[279, 282] Therefore, achieving an optimal balance between rigid and soft components of the NHC ligand is crucial, as the stiffness of the MOF may affect its ability to transmit mechanical force. The MOF may collapse if it is too stiff, while the transmission of mechanical force may not be effective if it is too soft. Thus, it is important to tune the MOF to survive procedures such as ultrasonication, compression, or tensile testing, achievable through careful adjustment of the organic linker used.
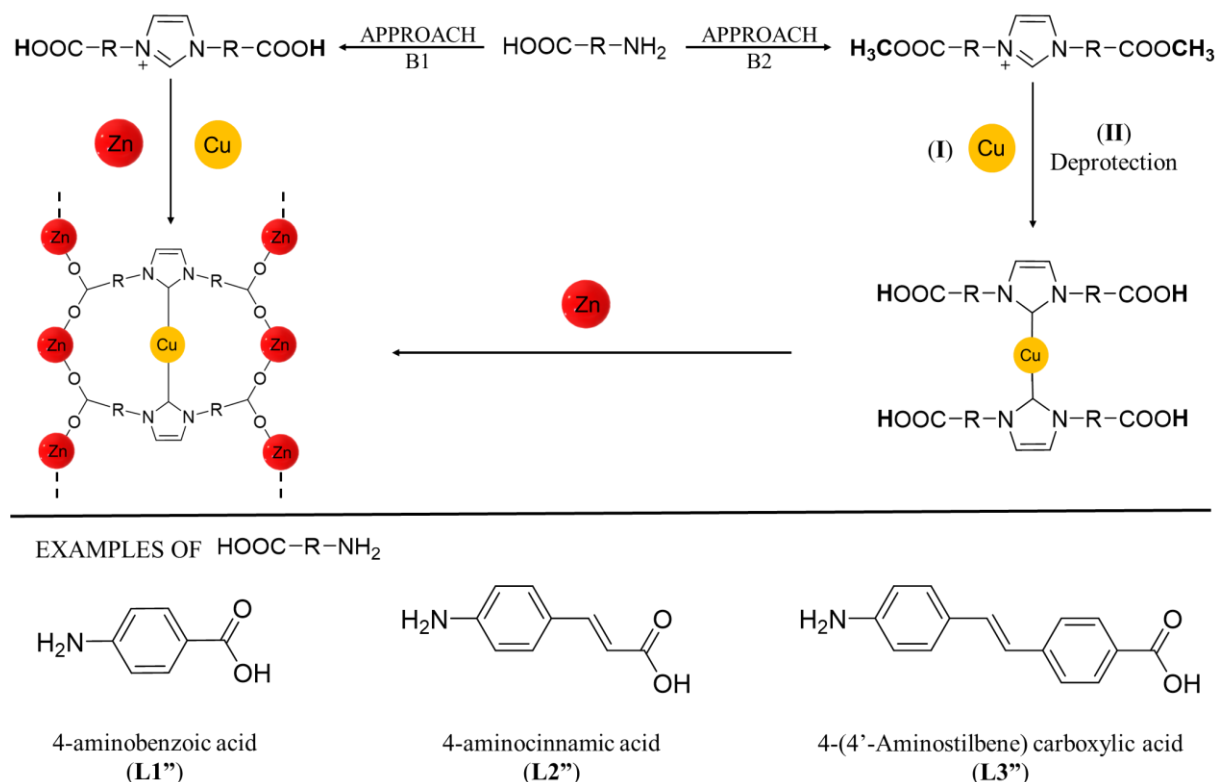
Scheme 7. The schematic depiction of the two approaches to synthesize NHC-MOFs as well as examples of the starting bifunctional compounds.

3.2.1.1 Preparation for APPROACH B1

Prior to the start of APPROACH B1, there was an intention to synthesize **L2"** and **L3"**. However, attempts to prepare **L2"** by reducing 4-nitrocinnamic acid (10.0 mmol) using hydrazine hydrate (10 mL) and zinc dust (20.0 mmol) were unsuccessful, as documented in **Chapter 5.3.6**. As a result, it was decided to obtain **L2"** commercially in order to focus on NHC preparation. On the other hand, **L3"** was

prepared by conducting a Heck's coupling reaction between 4-vinyl aniline (VA, 26.0 mmol) and 4-iodobenzoic acid (IBA, 26.0 mmol) in the presence of palladium(II) acetate (0.25 mmol)) as catalyst and triethylamine as base, described in **Chapter 5.3.12**. This palladium-catalysed cross-coupling reaction successfully yielded the desired product **L3"**, as observed by the peaks in the ^{1}H NMR spectrum belonging to the characteristic double bond of a stilbene in the range of 6.83-7.10 ppm (**Figure A33**). This is further supported by characterization *via* ^{13}C NMR spectroscopy and ESI-TOF spectrometry analysis, as seen in **Chapter 7.2.10**.

3.2.1.2 Preparation for APPROACH B2

In order to proceed with APPROACH B2, it was necessary to perform esterification to methylate the -COOH group in all of the starting compounds. The schematic representation of this process for each compound is illustrated in **Figure 35**, while the detailed procedures are described in different **Chapters** mentioned in **Table 5**. The emergence of new peaks in the range 3.67-3.96 ppm, attributed to the -CH$_3$, provided proof of the success of the conducted procedures. These were additionally supported by ^{13}C NMR spectroscopy, ESI-TOF spectrometry and/or IR measurements to have a complete set of characterization analysis, seen in **Appendix**. When attempting to methylate **L1"**, two different methods were used (see **Chapter 5.3.3**). Methylation using methanesulfonic acid produced **Me-L1"** with low yields (46 %). In contrast, conc. H$_2$SO$_4$ resulted in a higher yield (94 %) through the Fischer esterification process. Therefore, only the latter attempt is presented in **Table 5** and **Chapter 7.2.3**.
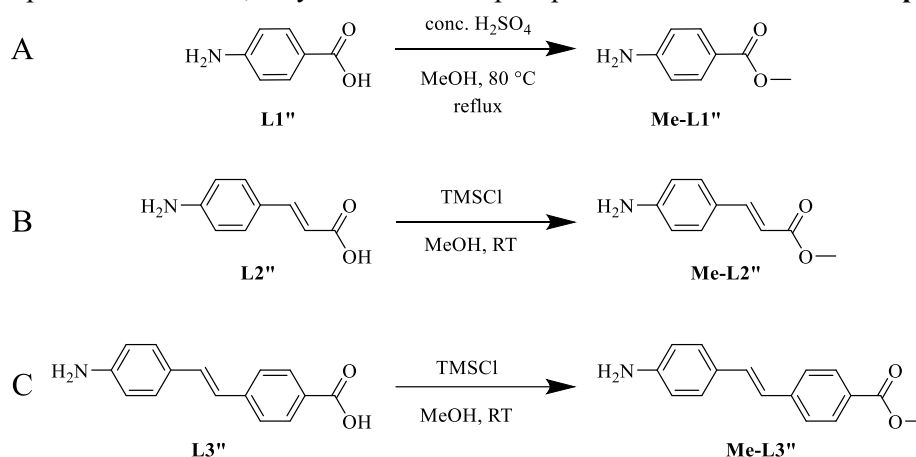
Figure 35. A schematic representation of the methylation of the starting compounds **A)** **L1"**, **B)** **L2"** and **C)** **L3"**.

Table 5. Summary of all the starting compounds synthesized for both APPROACH B1 and B2.

Ent	Starting Chemical Compound	Type	Synthesized Chemical Compound			Code
			Structure	Yield [%]	Chapter	
1	L1"[a]	X=H		-	-	L1"[a]
2		X=Me		94	5.3.3	Me-L1"
3	L2"[a]	X=H		-	-	L2"[a]
4		X=Me		97	5.3.9	Me-L2"
5	VA+IBA[a,b]	X=H		33	5.3.12	L3"
6	L3"	X=Me		97	5.3.14	Me-L3"

[a]The compounds marked are commercially obtained. [b]The compounds are vinyl aniline (VA) and 4-iodobenzoic acid (IBA).

3.2.2 Synthesis and Characterization of NHC Ligands

The synthesis of NHC ligands for use as mechanocatalysts was achieved through a two-step process. The first step involved the synthesis of ethylenediamine-based ligands (*N,N*-ligands), followed by the synthesis of NHC ligands in the second step.

3.2.2.1 Synthesis of Ethylenediamine-based Ligands (N,N-Ligands)

$$XOOC-R'-NH_2 \xrightarrow[\text{Formic Acid (Cat.)}]{\text{40\% Glyoxal}} XOOC-R'-N \diagdown \diagup N-R'-COOX$$

where **X** = -H, -Me | where **X** = -H, -Me
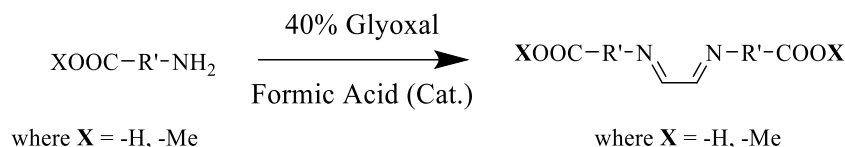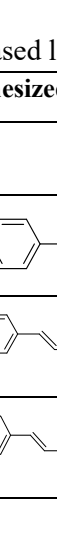
Scheme 8. A general scheme representing the synthesis of ethylenediamine-based ligands.

The synthesis of the ethylenediamine-based ligands (*N,N*-ligands) was conducted by reacting the bifunctional reactants (1 eq.) with 40 % glyoxal (0.5 eq.) and formic acid in catalytic amounts, as shown schematically in **Scheme 8**. The reaction was conducted in MeOH over 48 h. The different reaction conditions and the chapters for detailed procedures are summarized in **Table 6**.

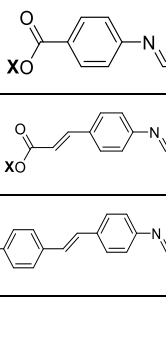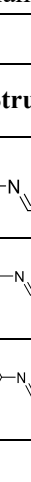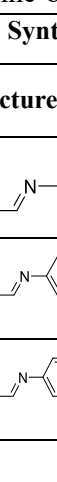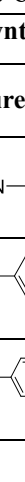**Table 6.** A summary of the syntheses of ethylenediamine-based ligands.

Ent	Starting Compound	T [°C]	Synthesized Ligand				
			Type	Structure	Code	Yield [%]	Chapter
1	L1"	RT	X=H		L1'	63	5.3.1
2	Me-L1"	35	X=Me		Me-L1'	68	5.3.4
3	L2"	35	X=H		L2'	47	5.3.7
4	Me-L2"	35	X=Me		Me-L2'	66	5.3.10
5	L3"	RT	X=H		L3'	10	5.3.13
6	Me-L3"	-	X=Me		Me-L3'	-	-

The synthesis of *N,N*-ligand from **Me-L3"** (**Table 6, Ent 6**) was not carried out due to time constraints as the project timeline required a more focused approach on the preparation of MOFs and their eventual use as mechanocatalysts. The *N,N*-ligand of **L2"** (**Table 6, Ent 3**) was prepared with a yield of 47 % but not only were the NMR spectroscopy results inconclusive, furthermore, the solubility of **L2'** was poor in most solvents, except partially in DMSO (see **Table 16** for solubility information). Therefore, the ESI-TOF analysis could not be conducted. Furthermore, it would also affect the next step of the NHC preparation which is typically conducted in THF. Despite these challenges, the next step was undertaken to observe if **L2** could still be synthesized from **L2'**. This approach was consistent for all synthesised *N,N*-ligands, i.e., use for further synthesis as was obtained.

3.2.2.2 Synthesis and Characterization of NHC Ligands

The procedures for synthesizing NHC ligands from *N,N*-ligands were generally similar across all cases. To prepare the NHCs, the *N,N*-ligands (1 eq.) were reacted with paraformaldehyde (1.25 eq.) and 12 N HCl (1.5 eq.) in anhydrous THF for 48 h, as seen schematically in **Scheme 9**. Further details on the summarized results as well as the chapters for detailed procedures are presented in **Table 7**.
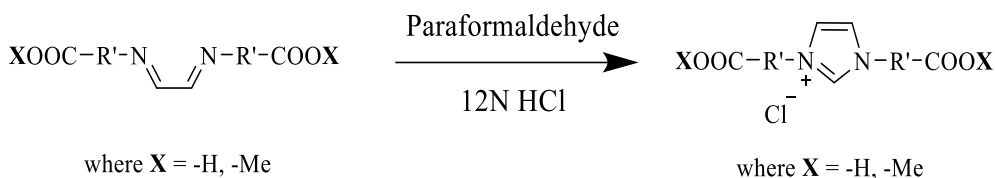
Scheme 9. A general scheme representing the synthesis of NHC ligands.

Following the completion of the reactions, certain observations need to be noted. The synthesis of **L2** from **L2'** (**Table 7, Ent 3**) was unsuccessful. Despite collecting a precipitated powder, it was insoluble in most solvents, rendering NMR (^{1}H and ^{13}C) spectroscopy and ESI-TOF analysis impossible. Regarding the preparation of **L3** from **L3'** (**Table 7, Ent 5**), it was deemed unfeasible as it was not viable to do so considering the low yield (10 %) while preparing **L3'**. Hence, neither were considered further.

The success of the other synthetic procedures was analysed using both ^{1}H and ^{13}C NMR, IR spectroscopy, and ESI-TOF MS to complete the set of characterization analyses (see **Appendix**). In the ^{1}H NMR spectrum, the two characteristic signals to look for while identifying an NHC are the peaks in the region of 10.5 to 11.0 ppm, arising from the proton on the carbon between the two nitrogen heteroatoms, and in the region of 8.5 to 9.0 ppm with a coupling constant of around 1-2 Hz, arising from the protons on the double-bonded carbon atoms adjacent to the nitrogen atoms (marked in red and blue respectively in **Table 7**).
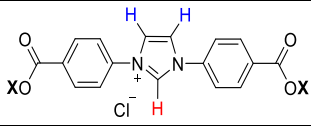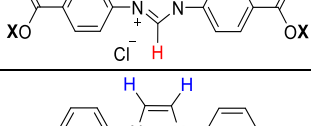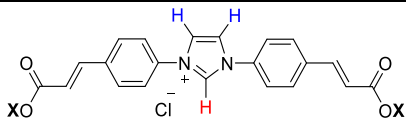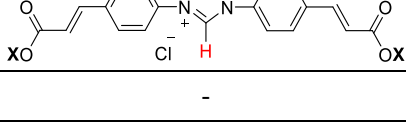
Table 7. A summary of the synthesis of NHC ligands.

Ent	Starting Ligand	T [°C]	Synthesized Ligand				
			Type	Structure	Code	Yield [%]	Chapter
1	L1'	RT	X=H		L1	67	5.3.2
2	Me-L1'	35	X=Me		Me-L1	61	5.3.5
3	L2'	35	X=H		L2	-	5.3.8
4	Me-L2'	35	X=Me		Me-L2	77	5.3.11
5	L3'	-	X=H	-	L3	-	-

Hereon, the focus was shifted solely on the creation of NHC-MOF with **L1** using APPROACH B1, to conduct mechanochemical activation experiments initially in solution with ultrasound, followed by exploring the possibility of achieving the same in bulk. Consequently, moving forward, only **L1** will be utilized and referred to.

3.2.3 Synthesis of NHC-MOFs

The Cu(I) bis(NHC) catalytic site-containing NHC-MOFs were synthesized using a solvothermal approach (for details, see **Chapter 5.3.15** and **Table 18**). The process involved the use of **L1**, along with Zn(NO$_3$)$_2$·6H$_2$O (1 eq.) and [Cu(CH$_3$CN)$_4$]PF$_6$ (0.5 eq.) (see **Scheme 10**), dissolved in dry DMF and stirred at 120 °C for 10 d, after which the reaction mixture was cooled to RT. The cooling rate was also controlled at 10 °C min^{-1}, as it affects the crystal structure and morphology.[423] The Cu(I) bis(NHC) complex was synthesized following the free-carbene route which is induced by deprotonation of **L1** in the presence of a base such as dimethylamine, formed by the *in situ* decomposition of DMF.[423] The

NHC-MOF was synthesized inside a closed headspace vial and finally obtained as a powder by directly precipitating. However, it should be noted that the synthesis of **NHC-MOFI** and **II** (**Table 18**, **Ent 6** and **7**) were conducted separately by research partners from the group of Prof. Dr. Harald Krautscheid at the Institute of Inorganic Chemistry, Universität Leipzig, who carried out the synthesis using Teflon-lined autoclaves. Further information can be found in **Chapter 7.2.13**.

The powder obtained from the synthesis was found to be insoluble in water or common organic solvents. This is typical of MOFs due to their crystallinity and porous structure. The strong metal-ligand bonds in MOFs make them extremely stable, resulting in their very low solubility in most conventional solvents.[424] Consequently, NMR and mass spectrometry techniques become almost impossible for their characterization. In addition, since single crystals were not obtained, it was not possible to perform single crystal X-ray analysis to definitively confirm their structure. Therefore, characterization of the NHC-MOFs was limited to PXRD, IR, FAAS, and TGA analyses. These techniques provided some information regarding the crystal structure changes and composition of the MOFs. As only **NHC-MOF1**, **NHC-MOF3**, **NHC-MOFII** and **NHC-MOF5** (**Table 18**) were used later in sonication experiments, characterizations of only these are presented further.
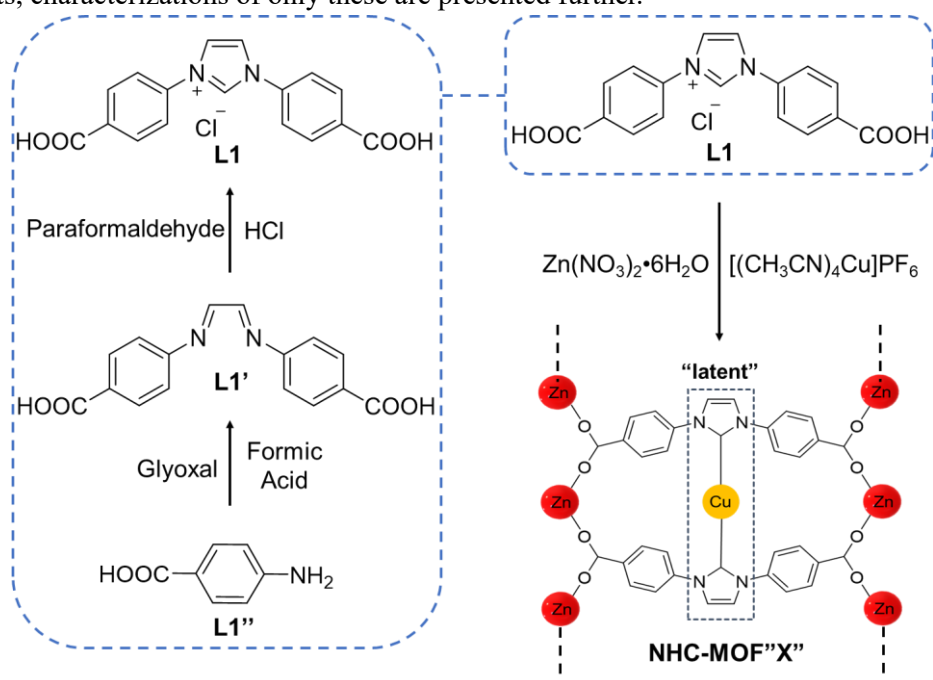
Scheme 10. Schematic concept for the synthesis of latent NHC-MOFs before mechanochemical activation is applied.

3.2.3.1 Characterization by PXRD

The 2θ diffraction patterns obtained on conducting powder X-ray diffraction (PXRD) of the MOFs **NHC-MOF1**, **NHC-MOF3**, **NHC-MOFII** and **NHC-MOF5** (**Table 18**) with organic linker (**L1**) and metal ligands (Zn(II) and Cu(I)) are presented in **Figure 36**. MOF synthesis can be sensitive to minor changes in reaction conditions and therefore parameters such as reaction temperature, time, solvent composition, and pH are crucial and can significantly affect the formation of MOFs, their structures or morphologies.[425-428] Hence, it turned out to be challenging to reproduce the MOFs, and therefore also their PXRD patterns. The crystallinity of **NHC-MOF3** was low. This could be due to the removal of solvent by drying, as literature [429, 430] has described the collapsing of MOF crystal structures, causing a "crystal-to-amorphous" transformation on the removal of guest molecules (solvent molecules that are present within a MOF structure), leading to **NHC-MOF3** being amorphous.
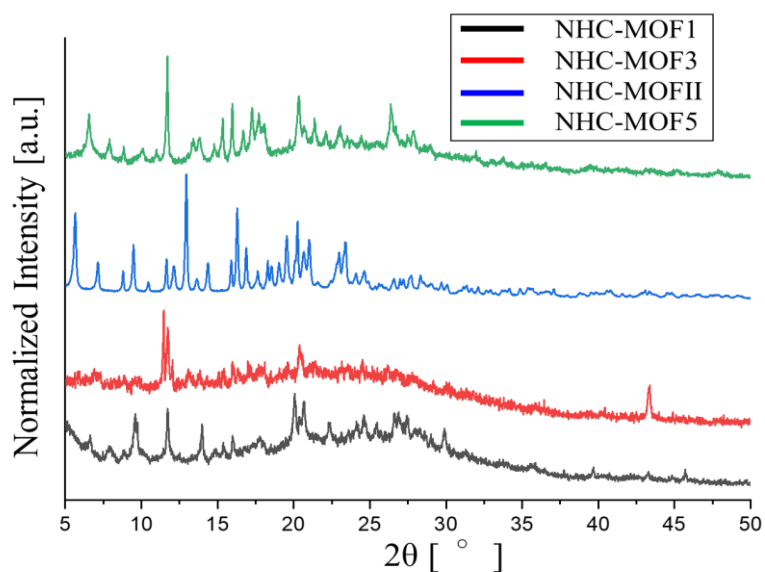
Figure 36. PXRD patterns (Cu-K$_{\alpha 1}$ radiation, α = 154.060 pm) of **NHC-MOF1**, **NHC-MOF3**, **NHC-MOFII** and **NHC-MOF5**.

3.2.3.2   Characterization by IR
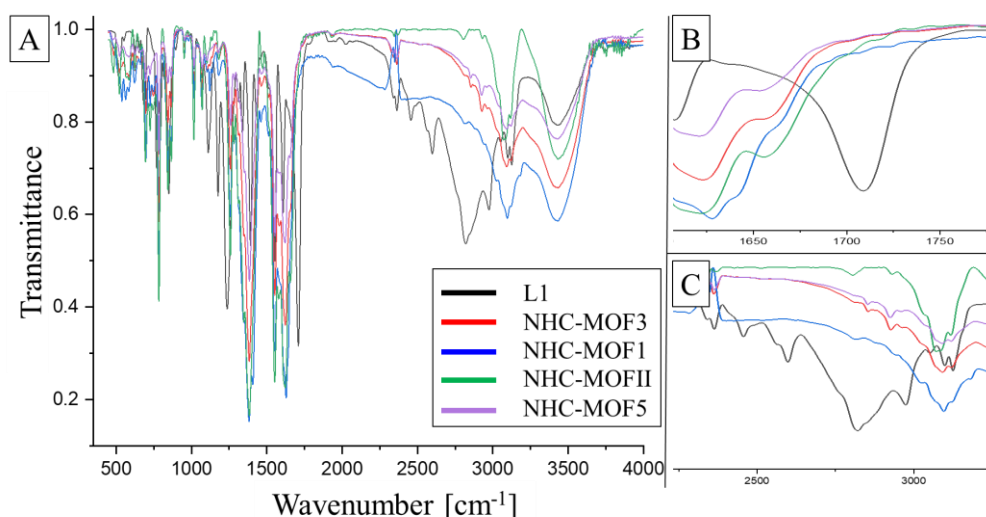
Figure 37. A) IR spectra of the NHC ligand **L1** and the NHC-MOFs with the relevant regions enlarged to show the differences between the NHC-ligand and the NHC-MOFs in peaks of the carboxylic acid group **B**) at 1710 cm^{-1} belonging to the C=O stretching and **C**) in the 2400-3075 cm^{-1} region belonging to the O-H stretching-bands.

A comparison of the IR spectra of the precursor **L1** and the NHC-MOFs (**Figure 37**) showed two differences indicative of the successful formation of a MOF. The strong and broad peak in the 2400 to 3075 cm^{-1} region (**Figure 37C**) and the strong peak at 1710 cm^{-1} (**Figure 37B**) belong to the O-H stretching and the C=O stretching-bands of the carboxylic acid, respectively. These two peaks disappeared in the NHC-MOFs, indicating the absence of free carboxylate groups and the successful coordination of Zn^{2+} with both of the -OH and the C=O of the precursor (**L1**). The individual IR measurements can be viewed in **Chapter 7.2.14** (**Figure A44**).

3.2.3.3   Characterization by TGA

Ent	Code	Temperature at start of decomposition [$T_{deco,str}$]	Mass Loss up to $T_{deco,str}$	Temperature at end of decomposition [$T_{deco,end}$]	Mass Loss between $T_{deco,str}$ & $T_{deco,end}$	Total Mass Loss at 500 °C
1	NHC-MOF1	275	- 17 %	384	- 44 %	- 67 %
2	NHC-MOF3	320	- 20 %	420	- 36 %	- 60 %
3	NHC-MOFII	245	- 14 %	382	- 43 %	- 62 %
4	NHC-MOF5	320	- 23 %	402	- 43 %	- 73 %

Figure 38. A comparison of the thermogravimetric analysis (TGA) conducted of the NHC-MOFs.

The TGA of NHC-MOFs indicated an average mass decrease of up to 19 % until the temperature at the start of decomposition ($T_{deco,str}$) was reached, which ranged from 245 to 320 °C for different NHC-MOFs (depicted in **Figure 38**). **NHC-MOF3** and **NHC-MOF5** displayed higher thermal stability than the other NHC-MOFs with a $T_{deco,str}$ of 320 °C. However, **NHC-MOF3** exhibited better overall stability with a total mass loss of approximately 60 %, compared to a loss of approximately 73 % for **NHC-MOF5**, at 500 °C. The individual TGA measurements can be seen in **Chapter 7.2.15** (**Figure A45**). It can be inferred from these results that primordial thermal destruction prior to the desired mechanochemical activation can be excluded, as also exemplified later during the sonochemical experiments.

3.2.3.4   Characterization by FAAS

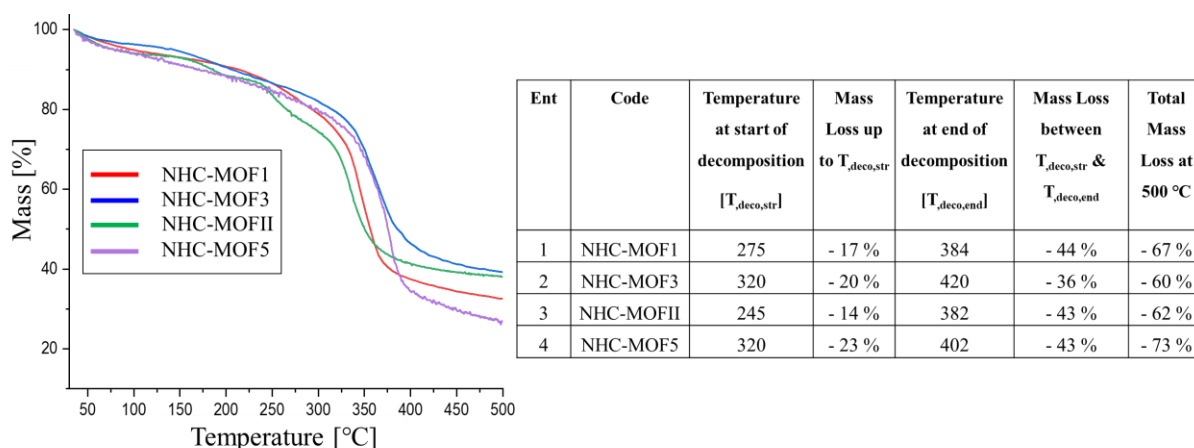To determine the amounts of copper (Cu) and zinc (Zn) in the different NHC-MOFs, flame atomic absorption spectroscopy (FAAS) was utilized for quantification. The results for the synthesized NHC-MOFs are available in **Chapter 5.3.16** in detail while **Table 8** presents the results for selected NHC-MOFs. The measurements for **NHC-MOF3** were particularly interesting. The measurements were calibrated for Cu and Zn with a correlation coefficient (R^2) of 0.9977 and 0.9946, respectively, while the relative standard deviation (% RSD) was 1.1 % and 1.6 %, respectively (**Figure A46**). Upon measurement of **NHC-MOF3**, the weight percentage of Cu was determined to be 4.66 % while the percentage of Zn was 8.97 %. The corresponding atomic ratio of Cu and Zn was ~ 0.53:1, similar to the expected atomic ratio of 0.53:1 in the literature for an analogous MOF ([$Zn_4O[Cu(L)_2]_2$]).[423]

Table 8. The atomic ratio of Zn and Cu for selected NHC-MOFs determined by FAAS.

Ent	NHC-MOF	Copper (Cu)		Zinc (Zn)		Cu:Zn Atomic Ratio
		Wt.%	Atomic Ratio	Wt.%	Atomic Ratio	
1	NHC-MOF1	3.75	0.13	11.75	0.39	0.33 : 1
2	NHC-MOF3	4.66	0.16	8.97	0.30	0.53 : 1
3	NHC-MOFII[a]	2.40	0.08	10.50	0.35	0.24 : 1
4	NHC-MOF5	2.12	0.07	8.97	0.30	0.24 : 1

[a]Synthesis of NHC-MOFII was conducted separately by research partners from the group of Prof. Dr. Harald Krautscheid at the Institute of Inorganic Chemistry, Universität Leipzig, who carried out the NHC-MOF preparation using Teflon-lined autoclaves (see **Chapter 7.2.13** for more details).

3.2.4 Mechanochemical Activation of NHC-MOFs by Ultrasonication

After synthesizing the Cu(I) bis(NHC)-MOFs (**NHC-MOF"X"**), their catalytic properties were tested with regards to their activation by mechanical force using CuAAC reaction. Sonochemistry through ultrasound was used to activate the dispersed MOF in solution. Sound waves propagate into the liquid, resulting in alternating high and low pressure cycles, transmitting mechanical energy to break molecular bonds in solution.[431] This allowed for the cleavage of one shielding NHC-ligand of a Cu(I) bis(NHC) and the generation of a free coordination site on the copper, which would introduce catalytic activity (**NHC-MOF"X"****) (**Scheme 11**).
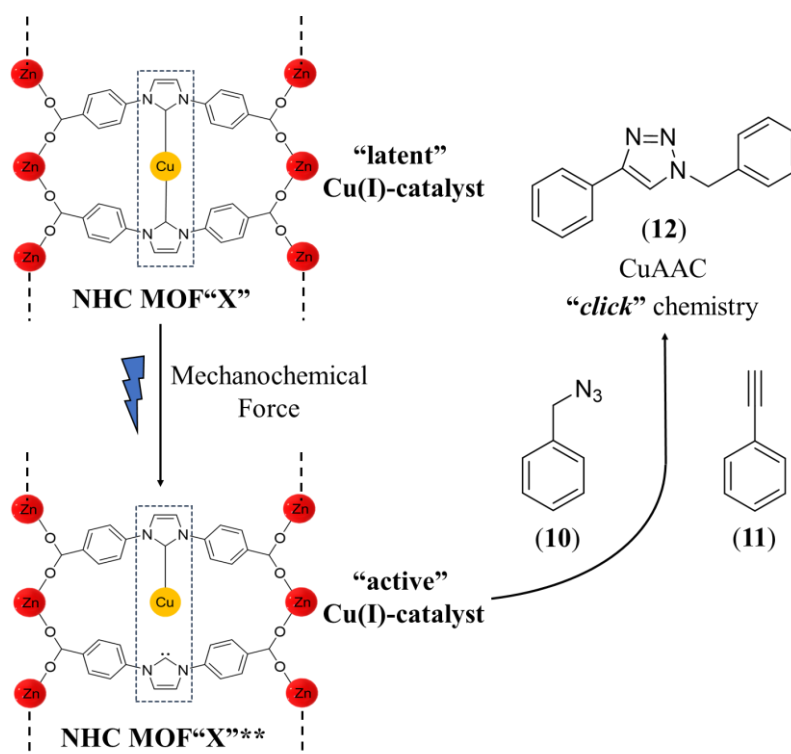
Scheme 11. Proposed mechanochemical activation of the NHC-MOFs containing Cu(I) bis(NHC), triggered through the applied mechanochemical force, i.e. ultrasonication in solution, leading to the scission of the labile Cu(I)-NHC bond and the cleavage of one shielding NHC-ligand, generating thus a catalytic active site.

3.2.4.1 Sonication Thermal Control

To ensure that the conversion obtained during ultrasonication at room-temperature in the presence of NHC-MOFs is clearly *via* mechanochemical activation and not by thermal processes, a sonication thermal control was monitored over multiple cycles of sonication experiments to check eventual temperature changes (**Figure 61**). A single sonication cycle runs for 90 min. Hence, cooling was conducted *via* two different approaches, first named as *1ce cool*, i.e., cooled at the very beginning, and the second named as *2ce cool*, i.e., cooled once at the beginning and once after 45 min, at an average room temperature (RT) of 22 °C. The ultrasonication experiment conducted with all the NHC-MOFs used the *2ce cooling* system. The average temperature with *1ce cooling* was measured to be 26 °C while in *2ce cooling* it was 18.5 °C. This proves that a maximum of 26 °C is reached and therefore the CuAAC conversion that might be achieved through sonication is based entirely on mechanochemical activation and was not thermally induced. To define an actual reaction temperature, an average of 18.5 and 26 °C was considered, i.e., 22 °C.

3.2.4.2 ^{1}H NMR Investigations of Mechanochemical Activation and Control Experiments
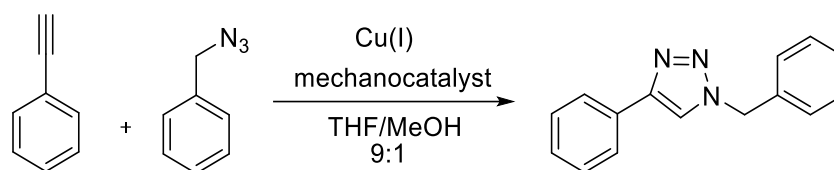
Scheme 12. Model "click" reaction of phenylacetylene (**11**) with benzylazide (**10**) in order to determine the activation of latent mechanocatalyst NHC-MOFs by *in situ* ^{1}H NMR spectroscopic investigations.

To investigate the catalytic activity of mechanochemically activated NHC-MOFs, ultrasonication experiments were conducted in a solution using a copper(I)-catalysed azide alkyne cycloaddition (CuAAC) model reaction between benzylazide (**10**) and phenylacetylene (**11**) in a 1:1 ratio. The experiments were conducted by subjecting the mixture to multiple cycles of sonication at an amplitude of 30 % of the maximal amplitude of 125 µm, thus applying an energy of 20 kJ per sonication cycle, which corresponded to a sonication intensity of 8.34 W cm^{-2}. This was accomplished with an applied sequence of 5 s pulse and 10 s break for 30 min (90 min total). Each cycle was followed by a rest time of 45 min (see **Chapter 5.3.18** for more details). The temperature of an entire sonication cycle remained at approximately 22 °C due to external cooling to avoid any undesirable thermal effects. The sonication experiment was conducted in THF-d_8:MeOH (9.67:0.33) with the added NHC-MOF (10 wt.% of the total weight of (**10**) + (**11**)). MeOH was added to the solution because previously conducted experiments with pure THF had resulted in lower activation, suggesting that MeOH is capable of protonating the cleaved free carbene NHC, thereby preventing the possible back reaction with the Cu(I) mono(NHC) (as shown in **Scheme 13**).[186]
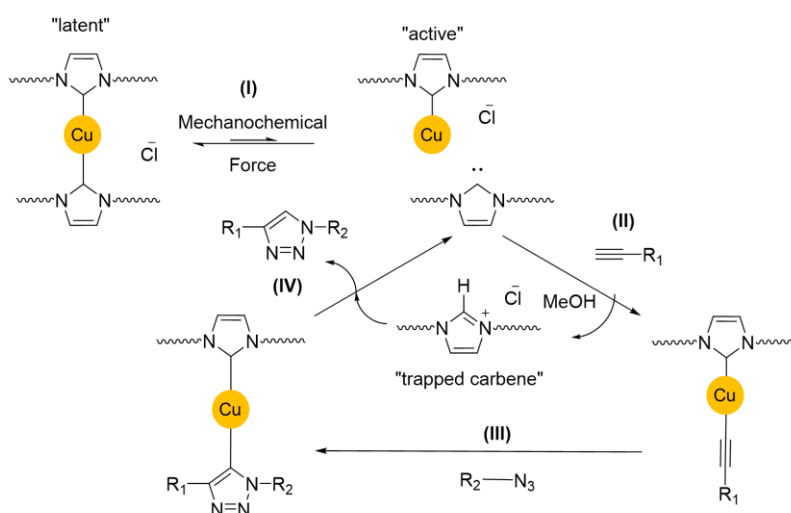
Scheme 13. Mechanochemical activation of the latent Cu(I) bis(NHC) inside the NHC-MOF by application of force resulting in the cleaving of one shielding NHC-ligand to obtain an active Cu(I) mono(NHC) as well as a free NHC (**I**). The free carbene is protonated by the presence of MeOH to form a "trapped carbene" while the Cu(I) mono(NHC) forms a monocarbene copper(I) acetylide structure (**II**), which subsequently undergoes cycloaddition with the azide compound (**III**). This then is protonated by the trapped carbene to form the final triazole product (**IV**). Adapted from literature.[186]

To ensure the validity of the results, three control experiments without ultrasonication were also conducted using the benzylazide-phenylacetylene model system. The first control experiment was conducted to check for any catalytic activity in the absence of NHC-MOF at 60 °C, which showed no conversion (**Table 9, Ent 1**). The other two controls were conducted in the presence of NHC-MOFs at

room temperature (RT) and 60 °C (see **Table 9** and **Figure A52**). The formation of the 'click' product, 1-benzyl-4-phenyl-1*H*-1,2,3-triazole (**12**), was monitored *in situ* by ^{1}H NMR spectroscopy before, during, and after sonication and control experiments. This was done by monitoring the increasing triazole resonance at 8.11 ppm (marked by the blue box) and the shift of the CH_2 resonance from 4.34 (marked by the red box) to 5.58 ppm (marked by the green box) over time (time-dependent ^{1}H NMR spectra are presented in **Chapter 7.2.17**). The results obtained were summarized in **Table 9**.

Table 9. Time and sonication cycle dependent investigation of click reaction from benzylazide (**10**) and phenylacetylene (**11**) using different NHC-MOFs.

Ent	Son. No.	NHC-MOF involved	Type of activation[a,b]	T [°C]	t_{End} [h]	US cycles[c]	final conversion [%][d]
1	-	-	No catalyst	60	25.0	**off**	0
2			Mech. Act.	22	22.5	10	61
3	Son1		Cont. Exp.	60	50.0	**off**	75
4		NHC-MOF1		RT	168.0	**off**	6
5	Son2		Mech. Act.	22	22.5	10	0
6	Son3[e]		Mech. Act.	22	33.8	15	98
7			Mech. Act.	22	45.0	20	25
8	Son4	NHC-MOF3	Cont. Exp.	60	55.0	**off**	10
9				RT	50.0	**off**	2
10			Mech. Act.	22	45.0	20	3
11	Son5	NHC-MOFII	Cont. Exp.	60	50.0	**off**	1
12				RT	65.0	**off**	0
13	Son6	NHC-MOF5	Mech. Act.	22	56.3	25	0

[a]For all reactions, an equimolar mixture of (**10**) and (**11**) in THF-*d8*/MeOH 9.67:0.33 was used together with 10 wt.% of **NHC-MOF1**, **3**, **5** or **II**. [b]The type of activation is either mechanochemical activation (Mech. Act.) or control experiments (Cont.Exp.). [c]Each ultrasonication cycle consists of 90 min sonication with 30 % of amplitude with pulse sequence of 5 s on, 10 s off and 45 min rest time corresponding to a sonication power intensity of 8.34 W cm^{-2} and an energy input of 20 kJ per US cycle. [d] ^{1}H NMR spectroscopy monitored in THF-*d8* by observing the increasing triazole resonance at 8.11 ppm as well as the shift of the CH_2 resonance from 4.34 to 5.58 ppm. [e]3 eq. of NaAsc. was used for "click" reaction of (**10**) and (**11**).

3.2.4.2.1   Investigations of NHC-MOF1

Three different ultrasonication experiments (Son1, Son2, and Son3 (see **Table 9**) were conducted to assess the ultrasonication performance of **NHC-MOF1**. Son1 and Son2 involved subjecting **NHC-MOF1** to ten ultrasonication (US) cycles (22.5 h total), while Son3 involved subjecting NHC-MOF1 to 15 US cycles (33.8 h total). Each ultrasonication cycle lasted 135 min and was carried out using the reaction conditions detailed in **Chapter 3.2.4.2**, **Table 9, Ent 2, 5**, and **6**, and **Figure 39**.

After five US cycles in Son1, a 15 % conversion was achieved, which increased to a final conversion of 61 % after 10 US cycles (totalling 22.5 h) (see **Figure 39A** and **Chapter 7.2.17.1** for ^{1}H NMR spectroscopy measurements), probably due to the rapid formation of new MOF surfaces in agreement with the hypothesis presented in **Chapter 2**. The PXRD analysis revealed a collapse of crystalline peaks after sonication (see **Chapter 7.2.17.2** for more details), confirming a structural collapse. The control experiments for Son1 (**Figure 39B**) conducted at room temperature (Son1.Cont.RT) exhibited

negligible conversion of 1 % over 50 h (time taken for 22 US cycles), while a poor conversion of 6 % was observed over a week, highlighting the latency of the MOF over a longer period without the application of ultrasound or thermal treatment. However, at 60 °C (Son1.Cont.60C), the conversion of 60 % over 25 h (time taken for ~10 US cycles) was nearly equivalent to the conversion achieved through 10 US cycles with ultrasound, suggesting thermal activation of NHC-MOF1.

Figure 39. The increase of the % conversion of (**12**) formed from a 1:1 mixture of (**10**) and (**11**) *via* CuAAC **A**) with sonication cycle dependent investigations into the mechanochemical activation of **NHC-MOF1** by ultrasonication and **B**) with time dependent control experiments conducted at room temperature and 60 °C.

After more than a year, an attempt was made to replicate the results of Son1 in Son2. However, due to the poor storage conditions that **NHC-MOF1** had been stored for over a year, a noticeable change in colour from dark grey to light green (seen in **Figure 40**) was observed, possibly due to the oxidation of Cu(I) to Cu(II) within the NHC-MOF. This was also observed experimentally as no product signals were observed in ^{1}H NMR spectroscopy (**Figure A47B**). Subsequently, all other synthesized NHC-MOFs were stored in a glovebox to maintain an oxygen- and moisture-free environment.
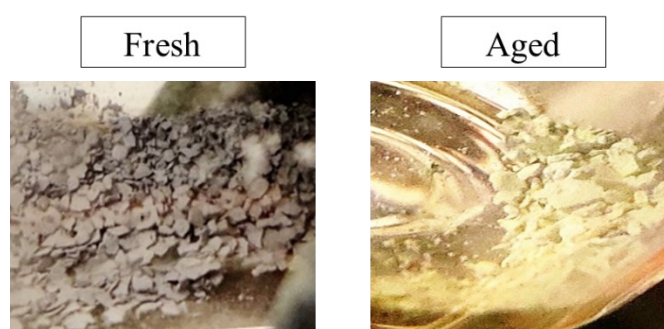
Figure 40. The visual difference between a freshly synthesized and an aged (over a year) **NHC-MOF1** stored under normal conditions.

An additional sonication experiment (Son3) was conducted with 3 eq. sodium ascorbate (NaAsc) (**Table 9, Ent 6**) while utilizing the copper(II)/ascorbate system (see **Chapter 7.2.17.3** for details). ^{1}H NMR spectra were recorded before sonication and after the 5th, 10th, and 15th US cycle (see **Figure A47C** for NMR spectra). The results indicate that the conversion of Son3 over the period of ten US cycles (53 %) is lower than that of Son1 (61 %), while the final conversion achieved after 15 US cycles was 98 %. This confirms that **NHC-MOF1**'s poor performance in Son2 was due to Cu(I) oxidation. However, this

also meant that **NHC-MOF1** cannot be activated without a reducing agent such as NaAsc, and as there is no plan to introduce reducing agents in polyurethane (PU) bulk systems during future mechanochemical activation with our NHC-MOFs, **NHC-MOF1** was not suitable for further use despite achieving high conversions *via* CuAAC.

3.2.4.2.2 *Investigations of NHC-MOFII and NHC-MOF5*

The ultrasonication performances of **NHC-MOFII** and **NHC-MOF5** were evaluated by subjecting them to 20 (Son5, 45 h total) and 25 cycles (Son6, 56.3 h total) of sonication, respectively, using the reaction conditions described in **Chapter 3.2.4.2** and **Table 9, Ent 10** and **13**, and depicted in **Figure 41**. To track the conversion rate during ultrasonication, ^{1}H NMR spectra were recorded before and after the 5th, 10th, 15th, and 20th cycles in Son5 and Son6, and additionally after the 25th cycle in Son6 (with each cycle lasting 135 min) (**Figure A50**). Until the 15th cycle, neither Son5 nor Son6 showed any conversion, but Son5 experienced an increase in conversion up to 3 % afterward, while Son6 continued to exhibit no conversion even after the 25th cycle, indicating poor performance by both NHC-MOFs.
Due to the poor performance of **NHC-MOF5** in Son6, control experiments were only conducted with **NHC-MOFII**. These experiments were carried out in the presence of a benzylazide-phenylacetylene model system without sonication and presented in **Figure 41B**. The conversion was found to be negligible at room temperature (Son5.Cont.RT) over 65 h (time taken for 29 US cycles), while a conversion of 1 % was observed at 60 °C (Son5.Cont.60C) over 50 h (time taken for 22 US cycles).
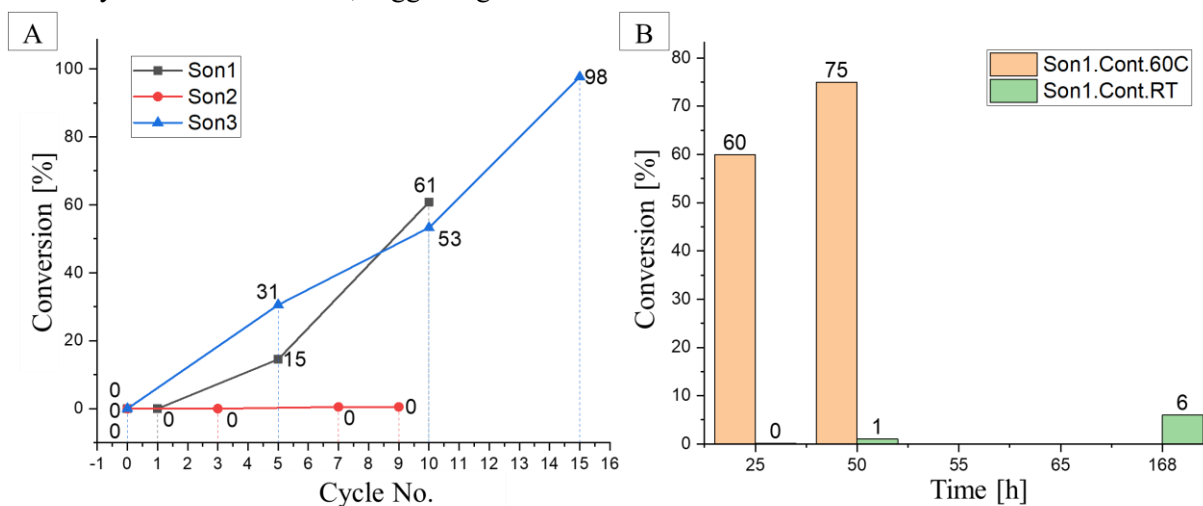

Figure 41. The increase of the % conversion of (**12**) formed from a 1:1 mixture of (**10**) and (**11**) *via* CuAAC **A**) with sonication cycle dependent investigations into the mechanochemical activation by ultrasonication of **NHC-MOFII** in Son5 and **NHC-MOF5** in Son6 (**Chapter 7.2.17.5** for more details) and **B**) with time dependent control experiments conducted at room temperature and 60 °C for Son5.

3.2.4.2.3 *Investigation of NHC-MOF3*

The mechanocatalyst **NHC-MOF3** was subjected to 20 cycles of sonication (Son4, 45 hours total) using the reaction conditions mentioned in **Chapter 3.2.4.2** and **Table 9, Ent 7**. To monitor the conversion percentage during ultrasonication, ^{1}H NMR spectra were determined before and after the 4th, 8th, 15th and 20th cycles (each cycle taking 135 minutes). **Figure 42A** presents the conversion percentage during ultrasonication, and the corresponding NMR spectra are shown in **Figure A49**. The conversion percentage showed a gradual increase until the 8th cycle after which the increase was much sharper, likely due to a faster rate of formation of new surfaces by cracking of the NHC-MOF, as shown in **Chapter 1.3**. The proton signal from (**10**) (4.34 ppm) declined over the 20 cycles of sonication, while peaks associated with (**12**) 5.58 ppm (green box) and 8.11 ppm (blue box)) increased (see **Figure A49**),

indicating an increasing conversion of the products formed by the CuAAC. The highest conversion percentage of 25 % was obtained after 20 sonochemical cycles, with the conversion plateauing after the 15th cycle.

Control experiments were performed by stirring **NHC-MOF3** in the presence of a benzylazide-phenylacetylene model system without sonication. At room temperature (Son4.Cont.RT), a conversion of 2 % was observed after 50 h (equivalent to the time taken to perform 22 cycles of ultrasonication), demonstrating the stability of the NHC-MOF and its latent nature as a mechanocatalyst without the application of ultrasound or thermal treatment. At 60 °C (Son4.Cont.60C), a conversion of up to 10 % after 55 h (equivalent to the time taken to perform 24 cycles of ultrasonication) was observed.
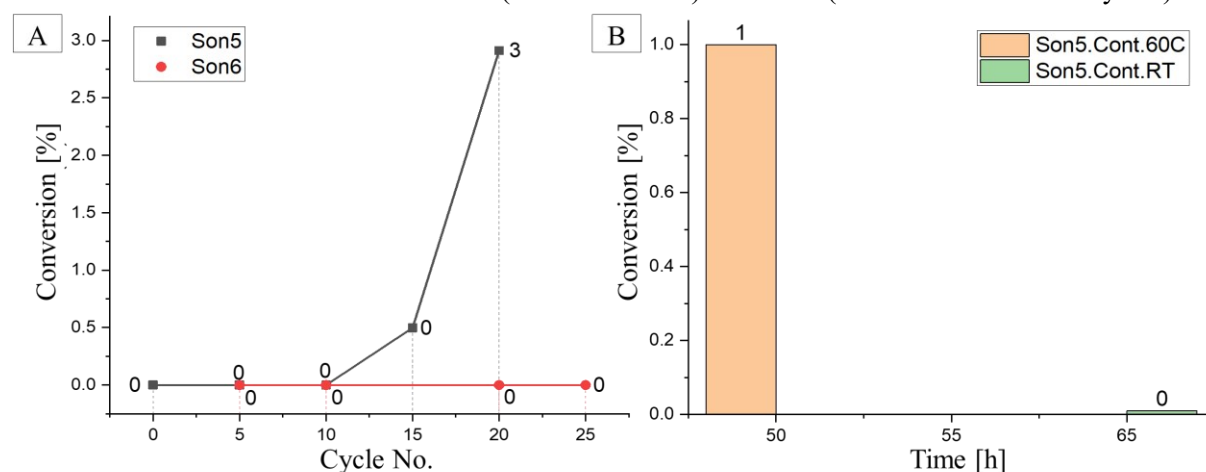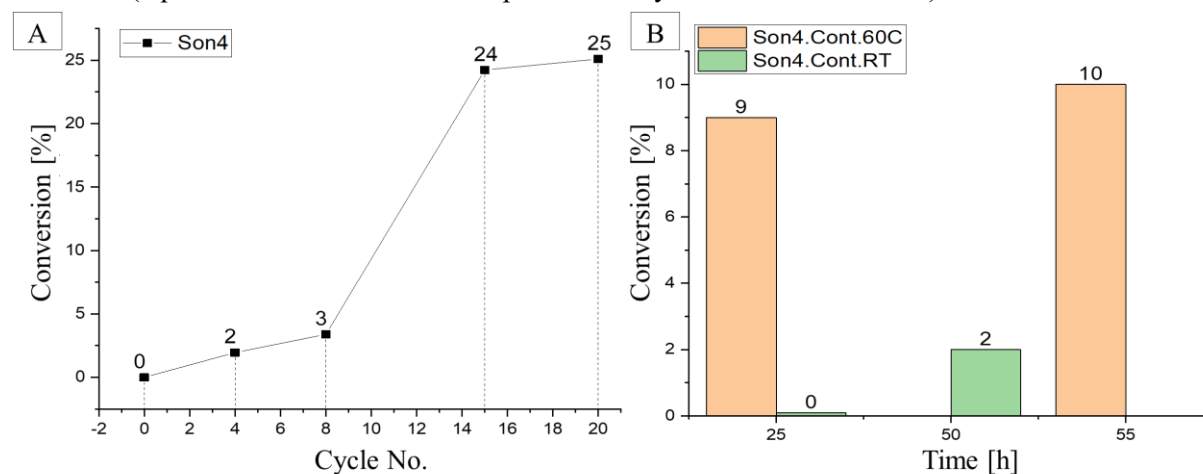

Figure 42. The increase of the % conversion of (**12**) formed from a 1:1 mixture of (**10**) and (**11**) *via* CuAAC **A**) with sonication cycle dependent investigations into the mechanochemical activation by ultrasonication of **NHC-MOF3** in Son4 (see **Chapter 7.2.17.4** for more details) and **B**) with time dependent control experiments conducted at room temperature and 60 °C.

3.2.4.3   *Further Investigation of Mechanochemical Activation of NHC-MOF3*

NHC-MOF3 exhibited remarkable results in the sonication experiments, indicating that it is a better candidate than the other NHC-MOFs for further experiments involving mechanochemical activation in bulk. However, prior to conducting these experiments, a detailed investigation was performed into the ultrasound-induced mechanochemical activation of **NHC-MOF3**, to understand its fate before and after sonication. It was previously hypothesized that sonication would lead to at least a partial destruction of the MOF (**Chapter 2**). This is now also indicated by its catalytic activity. Thus, scanning electron microscopy (SEM), atomic force microscopy (AFM) and PXRD measurements of the NHC-MOF before and after ultrasound-induced mechanochemical activation were conducted. The microscopy images displayed in **Figure 43** reveal that the original **NHC-MOF3** had larger structures that were broken into smaller, more disordered particles after 20 cycles of sonication, leading to its activation (**NHC-MOF3****). In PXRD, as the diffraction pattern was already poor in crystallinity, no noticeable changes could be observed (**Figure 44A**) other than the multiple new peaks observed at higher 2θ values in the sonicated **NHC-MOF3**** which were not visible in the MOF that underwent thermal control at 60 °C. Initial studies seem to point to the formation of CuH, formed due to sonication in the presence of water (see **Chapter 7.2.17.6** for more details). This indicates that the structure of the NHC-MOF was partially destroyed, leading to the appearance of new peaks. Moreover, the additional signals appearing in the ^{1}H NMR spectrum at 5.35 ppm, 7.78 ppm, and 7.98 ppm (**Figure A49**) suggest the decomposition of not only the NHC-MOF structure but also the NHC ligand itself.
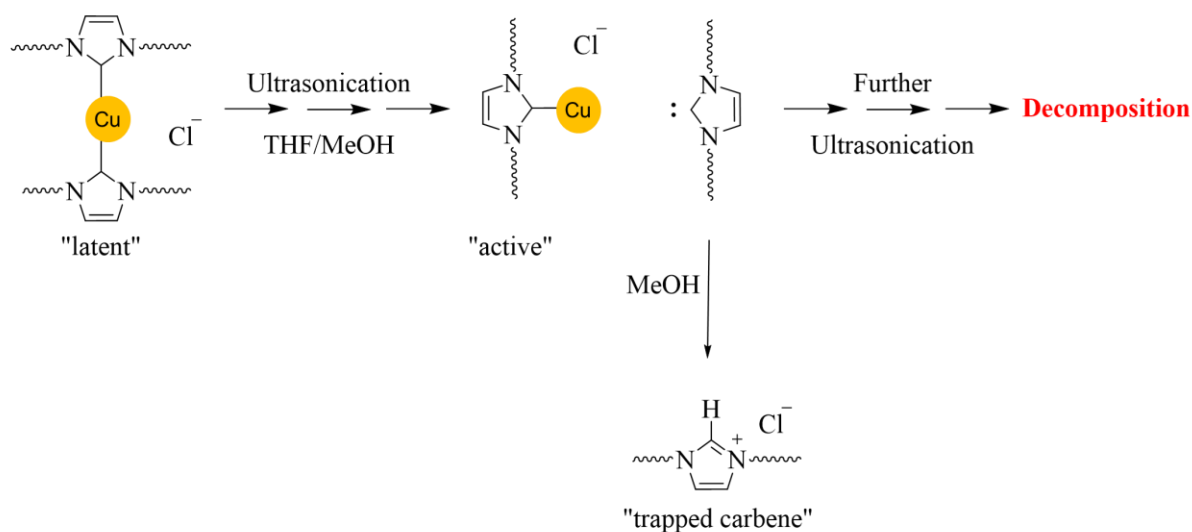
Scheme 14. The scission of the labile Cu(I)-NHC bond of the Cu(I) bis(NHC) within an NHC-MOF by ultrasonication to generate the active Cu(I) mono(NHC) and the free carbene NHC which is trapped by the addition of MeOH. However, continuous ultrasonication indicates a potential decomposition of the NHC moieties. Adapted from literature.[186]

Additionally, the TGA conducted for the sonicated **NHC-MOF3**** at Cycle 8 and Cycle 20 shows a mass loss of 15 % and 30 % till 320 °C, respectively. The TGA curves at 500 °C show ~45 % and ~6 % of mass still left at Cycle 8 and Cycle 20 of sonication, respectively (**Figure 44B**). Previous studies working with different Cu(I) bis(NHC)s have shown that ultrasonication activates the latent biscarbene complex to form the Cu(I) mono(NHC). However, many cycles of sonication resulted in a destructive pathway leading to the decomposition of the NHC ligand as well.[186, 258] This is consistent with our findings and shown schematically in **Scheme 14**. The achieved conversion of 3 % at Cycle 8 of sonication showed a mass change at 500 °C that was similar to that of the native **NHC-MOF3**. Thus, it could be assumed that the structure of the NHC-MOF was at least partially retained at this point while acting as a catalyst for the "click" reaction. The conversion percentage increased continuously till Cycle 15 (an increase of conversion from 3 % to 24 %), after which the conversion to form the click product plateaued, corresponding to the destruction of the NHC-MOF structure. Consequently, this leads to a limitation in the achievable percent conversion and could further explain the plateauing curve of conversion beyond Cycle 15 as seen in **Figure 42A**, and would also indicate that the powder collected after sonication predominantly consisted of organic material, most likely the decomposed ligand.
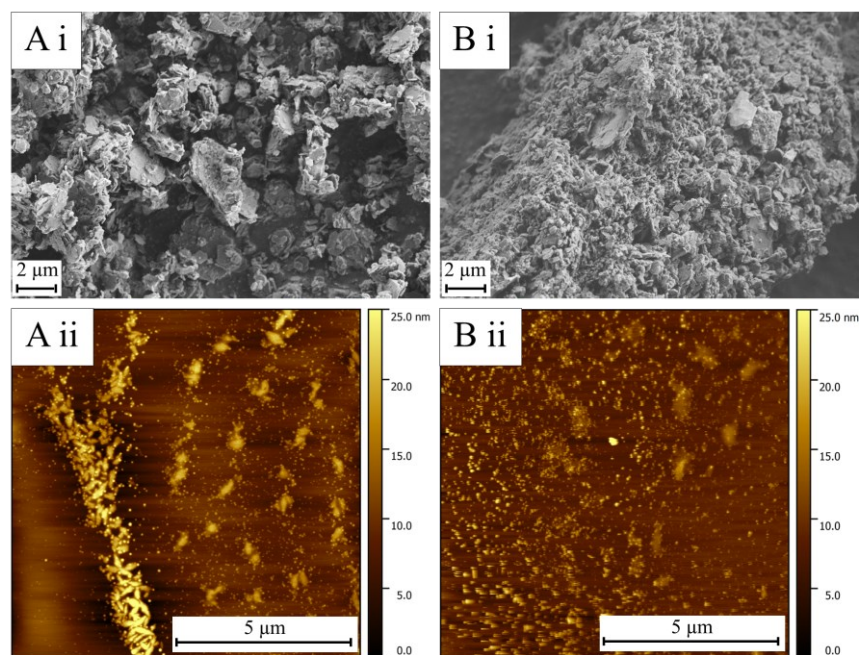
Figure 43. Microscopy images with **i)** SEM and **ii)** AFM for **A)** native **NHC-MOF3** and **B)** the sonicated **NHC-MOF3**** after 20 cycles of sonication.
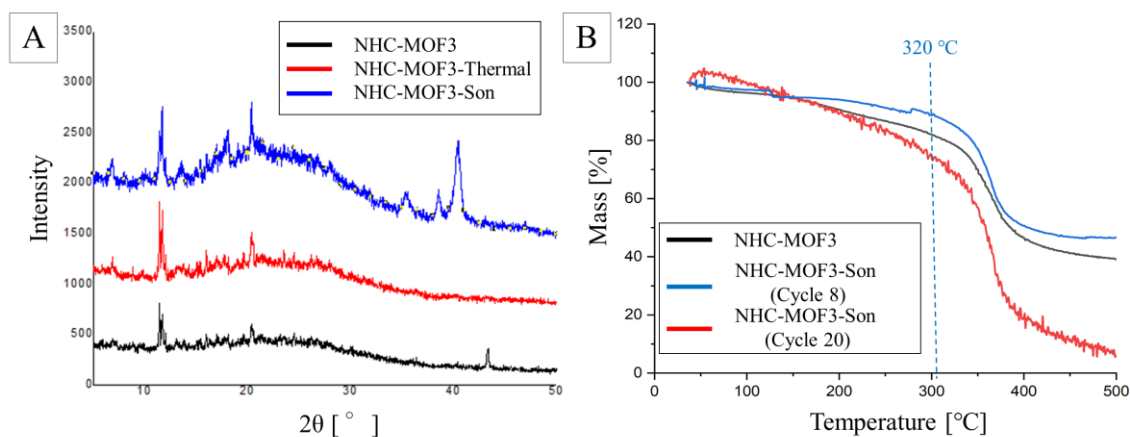
Figure 44. A comparison of the NHC-MOF pre (**NHC-MOF3**) and post (**NHC-MOF3****) sonication *via* **A)** PXRD and **B)** TGA.

In a nutshell, **NHC-MOF3** has not only shown a good thermal stability of up to 320 °C in TGA and was the only NHC-MOF to display an atomic ratio of Cu:Zn as 0.53:1, but it also produced remarkable results of 25 % conversion when used in investigations of ultrasound-induced mechanochemical activation in a model benzylazide-phenylacetylene system without any reducing agents. Additionally, the control experiments showed latency at room temperature and much lower thermal activation (10 %) at 60 °C. Hence, **NHC-MOF3** was chosen to be further embedded in a polyurethane (PU) matrix to conduct experimentation of mechanochemical activation in bulk.

3.3 Mechanochemically Active Thermoplastic Polyurethane (TPU) Systems

Partially published in "K. S. Shinde, P. Michael, W. H. Binder, Mechanochemical Activation of a Metal–Organic Framework Embedded within a Thermoplastic Polyurethane Matrix: Probing Fluorogenic Stress-Sensing. *Macromol. Chem. Phys.* **2023**, 224, 2300297" [432]

3.3.1 Synthesis of a Fluorogenic Naphthalene-based Dye

To create TPU foils capable of functioning as stress-sensing systems, a naphthalene-based dye approach was pursued. The process involved combining 8-azidonaphthalen-2-ol (**13**) and commercial 3-hydroxyphenylactylene (**14**) to produce a highly fluorescent 8-(4-(3-hydroxyphenyl)-1,2,3-triazol-1-yl)naphthalen-2-ol (**15**) to serve as the sensor dye.
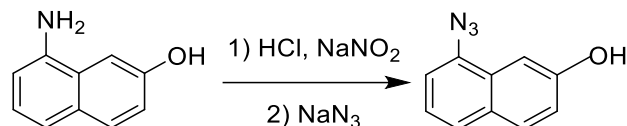
Scheme 15. The synthesis of 8-azidonaphthalen-2-ol (**13**).

To begin, (**13**) had to be synthesized as per **Scheme 15** with a procedure described in **Chapter 5.4.6** by diazotization of 8-aminonaphthalen-2-ol, generating a diazonium salt that was subsequently substituted with sodium azide. (**13**) featured a hydroxyl group that could react with isocyanates, covalently integrating it into a poly(urethane) network. To obtain the "click" dye (**15**) needed for system calibration, (**13**) and (**14**) were subjected to a CuAAC reaction which is discussed in **Chapter 5.4.7**.

3.3.2 Synthesis and Characterization of TPU
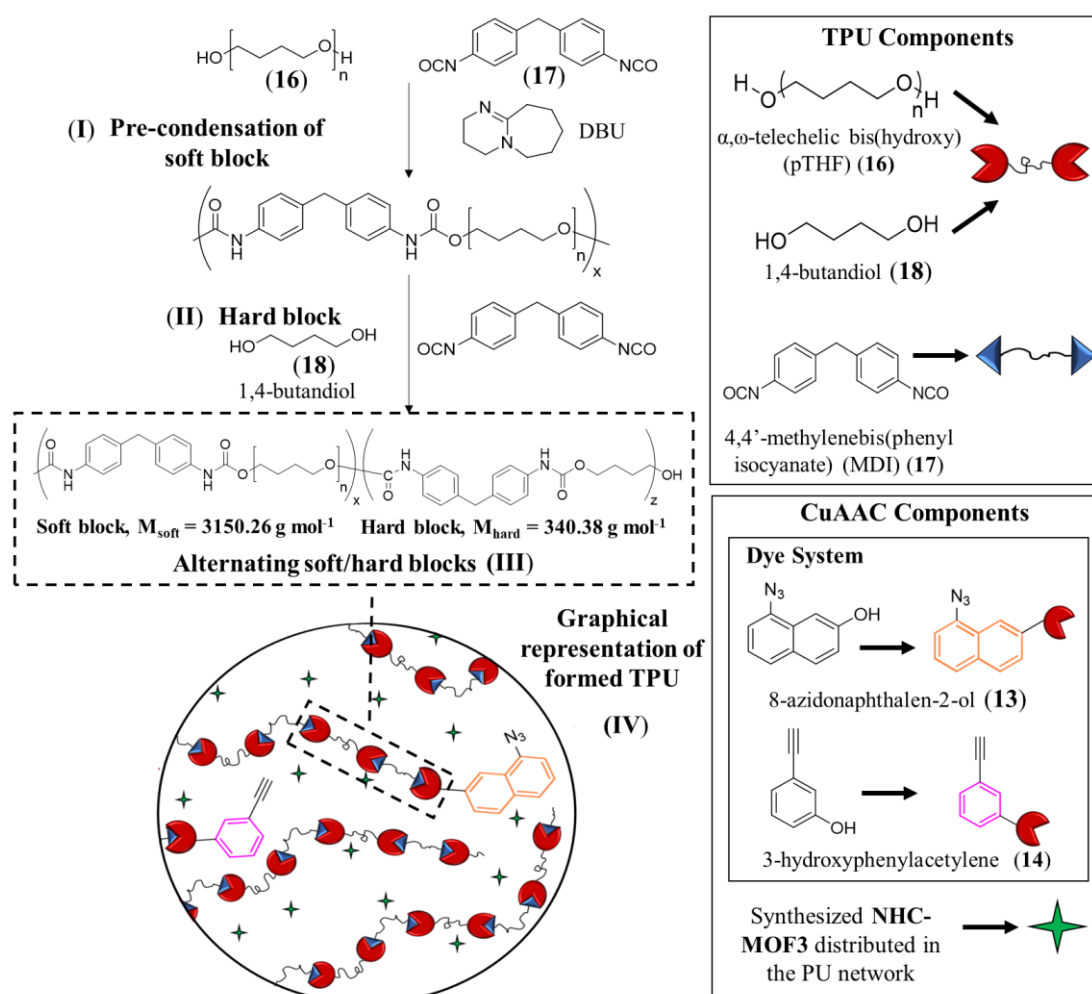
Scheme 16. Schematic concept for the synthesis of a stress-sensing thermoplastic polyurethane (TPU) consisting of TPU components and components necessary to conduct a copper-catalysed click chemistry (CuAAC).

In an expansion of the previous work, **Scheme 16** demonstrates the integration of the mechanochemically active **NHC-MOF3** into a polymeric system of thermoplastic polyurethane (TPU). The components for the TPU, including the fluorogenic dye precursors, are also depicted. The process begins with the polyaddition reaction between α,ω-telechelic bis(hydroxy) poly(tetrahydrofuran) (pTHF) (**16**) with a molecular weight of 2900 g mol^{-1} and 4,4'-methylenebis(phenyl isocyanate) (MDI) (**17**) in the presence of catalytic amounts of 1,8-diazabicyclo[5.4.0]undec-7-ene (DBU). This reaction resulted in the formation of pre-condensed soft block segments (**Scheme 16**, (**I**)). The subsequent addition of the chain extender 1,4-butanediol (BDO) (**18**) led to the formation of hard block segments and ultimately alternating soft/hard blocks (**Scheme 16**, (**III**)). This process creates a supramolecular crosslinked network based on strong hydrogen bonding among the urethane linkages and pi-pi bonding.[433]

The process leading up to **Scheme 16**, (**III**) was conducted during Development Stages 1 and 2 (DS1 and DS2), detailed in **Chapters 5.4.2** and **5.4.4**, respectively. During DS1, the production of TPU (O-TPU) was not up to the desired standards. GPC measurements (see **Chapter 5.4** for details on how to calculate) indicated that the molecular weight (M_n) (**Table 10**) was inconsistent. This possibly was due to the final step of stirring of 15 min after the addition of (**18**) being fixed but the extent of reaction completion varying possibly due to factors such as temperature, moisture, and storage of starting materials. The conversion rate ranged from 95 to 97 %, which is unflattering for a step-growth polymerization. DSC measurements (**Figure A65A**) also revealed that the O-TPUs produced were modestly formed. While a melting point for the soft segment ($T_{m,soft}$) was observed at 23 °C, there was no melting point for the hard segment ($T_{m,hard}$) even for TPUs with higher hard segment ratios (e.g. O-TPU60 or O-TPU70), calling into question the formation of hard-soft segments.

A modified procedure of DS1, as described in **Chapter 5.4.2**, was used to conduct a kinetic study of TPU50 in order to understand the kinetics of the polyaddition reaction leading to a TPU. Samples for GPC measurements (see **Chapter 5.4.3** for details) were taken every 5 min in three sections and showed two peaks (**Figure A61**). The peak at 7.5 mL shifted to lower retention volumes with an increase of M_n, while the second peak at 9.5 mL with a molecular weight of 280 g mol^{-1}, similar to the molecular weight of (**17**) (250.26 g mol^{-1}), decreased in intensity as the reaction proceeded and (**17**) was consumed. Despite the addition of catalytic DBU, kinetic studies showed a lack of substantial progress during the consumption of (**17**) (**Table A3**). It was suspected that (**17**) was undergoing hydrolysis as Karl Fischer titration revealed that (**18**) had 4200 ppm of water, leading to the need for DS2 for TPUs.

Two major changes were incorporated in DS2. Firstly, the starting materials were extensively treated to remove any moisture (see **Chapter 5.4.4** for more details). Secondly, the final step after addition of (**18**) was changed, i.e., the stirring was continued till the reaction mixture turns viscous, rather than a time-fixed procedure (15 min in DS1). These changes brought substantial differences in the characterization results. The GPC measurements of the new TPU showed remarkable molecular weights with consistent high conversions in the 97-98 % range (**Table 10**). The DSC measurements also showed $T_{m,hard}$ peaks at 195 °C from TPU60 onwards in addition to the previously observed $T_{m,soft}$ at 23 °C, proving the existence of hard domains in the TPU (**Figure A65B**).
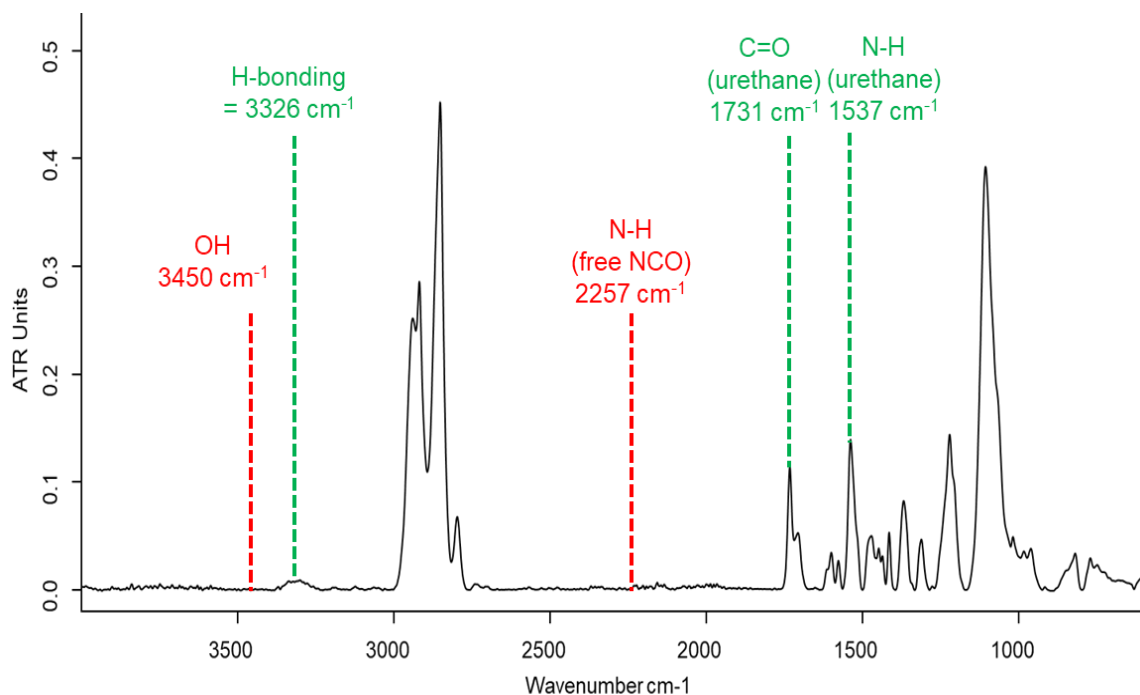
Figure 45. IR(ATR) spectrum of TPU50 foil synthesized as per procedure of Development Stage 2 (DS2, see **Chapter 5.4.4** for more details).

Furthermore, DSC and FTIR spectroscopy were performed on the synthesized TPU50 to confirm the success of the reaction. DSC (**Figure A65**) revealed a $T_{m,soft}$ of ~23 °C with a melting enthalpy of $\Delta H_{soft} = 37.4$ J g^{-1}, indicating a degree of crystallization of 22 % (ΔH_{m0} (pTHF) = 172 J g^{-1})[434] (see **Chapter 5.4.8.2** for crystallinity determination). In **Figure 45**, the presence of urethane groups was confirmed by the detection of C=O stretching and N-H bending bands at 1731 cm^{-1} and 1537 cm^{-1}, respectively. The absence of 3450 cm^{-1} -OH groups and 2257 cm^{-1} -NCO free groups suggested that all (**17**) had reacted. The N-H hydrogen-bonding peak at 3326 cm^{-1} was barely detectable as a small shoulder.

Table 10. Reaction conditions and characterization data of TPU synthesized in Development Stage 1 (DS1) and 2 (DS2).

Ent	TPU"X"	Soft/Hard (mol ratio)	$M_{hard/Soft}$[a] [g mol^{-1}]	M_n[b] [kDa]		PDI[b]		Degree of Polymerization (DP)[c]		Conversion [%][d]	
				DS1	DS2	DS1	DS2	DS1	DS2	DS1	DS2
1	TPU30	70:30	2310	52	**76**	1.85	**1.90**	23	**33**	95.5	**97.0**
2	TPU40	60:40	2025	60	**60**	1.85	**1.85**	30	**30**	96.5	**96.5**
3	TPU50	50:50	1745	40	**60**	1.90	**1.90**	23	**34**	95.5	**97.0**
4	TPU60	40:60	1465	49	**61**	1.90	**1.90**	34	**42**	97.0	**97.5**
5	TPU70	30:70	1185	24	**51**	1.90	**1.90**	20	**43**	95.0	**98.0**
6	TPU80	20:80	902	-	**40**	-	**2.10**	-	**44**	-	**98.0**

[a]Calculated from eq. (**5.1**). [b]Measured using GPC with THF as solvent and polystyrene (PS) standards with a molecular weight range from 1,050 to 115,000 g mol^{-1}. [c]Calculated from eq. (**5.2**). [d]Calculated from eq. (**5.3**).

After confirming the success of DS2, the next phase of development, Development Stage 3 (DS3), was initiated to incorporate CuAAC components (illustrated in **Scheme 16**) into the multicomponent polyaddition reaction of α, ω-telechelic bis(hydroxy) poly(tetrahydrofuran) (pTHF) (M_n = 2900 g mol^{-1}) (**16**), 4,4'-methylenebis(phenylisocyanate) (MDI) (**17**), and 1,4-butanediol (BDO) (**18**). The CuAAC components included the physically dispersed mechanocatalyst **NHC-MOF3** (4.66 % Cu in **NHC-MOF3**, 0.06 eq. of Cu) and the covalently linked dye system consisting of 3-hydroxyphenylacetylene (**14**) and 8-azidonaphthalen-2-ol (**13**), resulting in an elastomeric poly(urethane) material that satisfies all requirements for use as a stress-sensing material. To embed the insoluble **NHC-MOF3**, a simple dispersion method was used, where it was dispersed into the TPU solution before it solidified. Three different foils were synthesized using DS3, namely TPU50_1, 2, and 3 (**Table 25**). AFM imaging of TPU50_1 and TPU50_3 (**Figure 46**) revealed minute particles of **NHC-MOF3** with protruding heights of up to 14 nm for the former and up to 85 nm for the latter, providing rough estimates of the NHC-MOF size. Gel permeation chromatography (GPC) analysis of the native TPU50 without **NHC-MOF3** yielded a molecular weight M_n of ~65 kDa, with a polydispersity index (PDI) of 1.95. Due to the insolubility and small size of the dispersed **NHC-MOF3** in the foil causing difficulty in its filtration, GPC of these samples was not possible and it was assumed that the values were similar to those of native TPU50. The DSC of the foils TPU50_1, 2 & 3 (**Figure A66**) did not show any remarkable difference to that of a virgin TPU50, signalling no effect of the **NHC-MOF3** on the structural properties of the TPU.
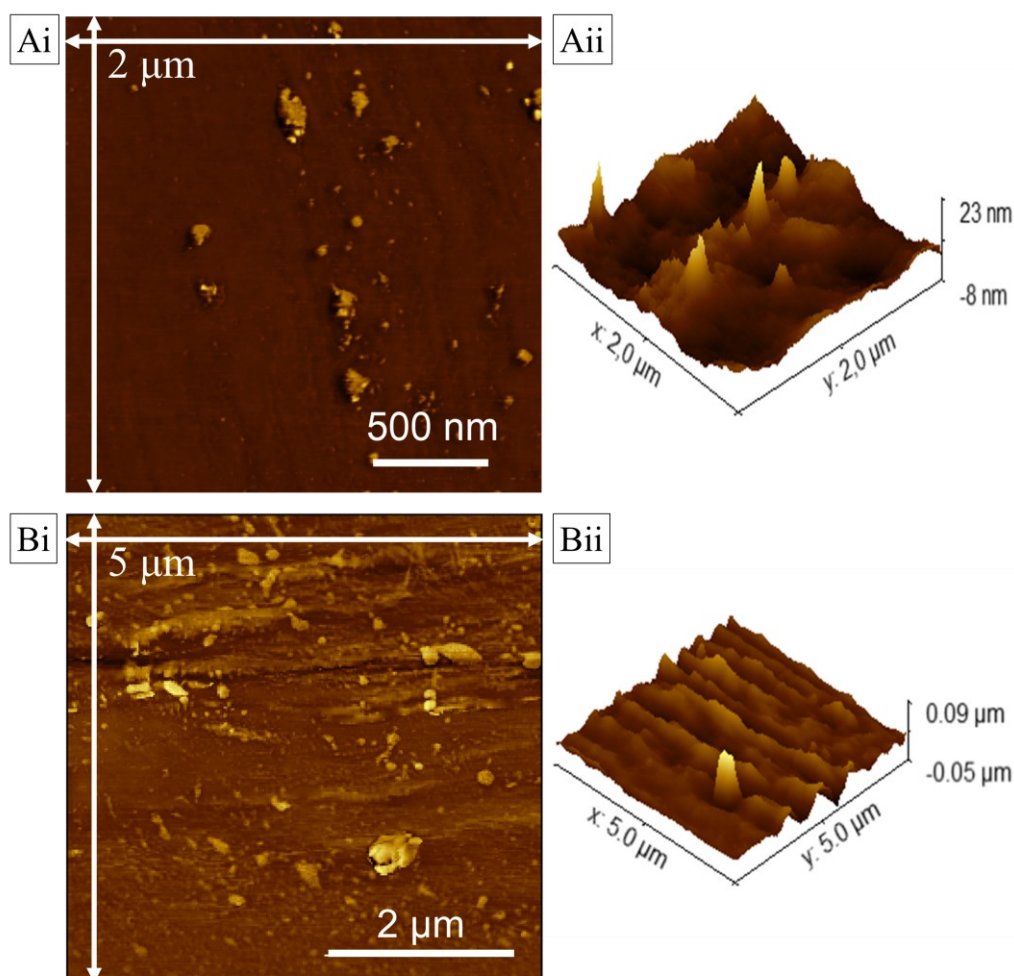

Figure 46. AFM images of the dispersed **NHC-MOF3** within the polyurethane of **A)** TPU50_1 and **B)** TPU50_3 during **i)** phase image, and **ii)** height image in 3D form to better estimate the height of the **NHC-MOF3** particles.

3.3.3 Determination of Mechanical Properties

The physical properties of TPU are affected by the ratio of soft/hard blocks. An increasing percentage of hard blocks leads to an increased tensile strength and Young's modulus, thus resulting in an increasing rigidity.[365, 435] To examine the material properties of the synthesized TPUs, dumbbell-shaped samples of dimensions 20 x 4 mm were obtained by cutting foils of the TPUs' synthesized in DS2 using a sample cutter. Experiments were conducted with extensional rotational rheology, performed on the samples using the Universal Extensional Fixture (UXF) sample holder (**Figure 48A**). For measuring the Young's (E) modulus, oscillating stress-strain experiments were conducted with an increase of strain up to 5.00 % (see **Chapter 5.4.8.1** for more details). For measuring tensile storage (E') modulus, oscillating tensile rheology was conducted over multiple cycles, following the procedure described in **Chapter 5.4.9.1**.

3.3.3.1 Investigating TPU30 and TPU70

For virgin TPU30 and TPU70 (virgin = DS2 TPU's without CuAAC components (**Scheme 16**)), an E modulus of 0.002 MPa and 0.033 MPa (**Figure A62**) was measured, respectively. However, while conducting oscillating tensile rheology, it was observed that the TPUs composed of a low hard segment ratio (30 %, TPU30) ruptured almost immediately under force and it was necessary to cool the sample to 4 °C for approximately an hour to make it rigid enough to mount on the UXF, introducing moisture to the TPU. Conversely, the high hard segment ratio TPUs (70 %, TPU70) could not be measured accurately with oscillating tensile rheology due to its rigidity, as seen in **Figure 47B**. Therefore, a soft/hard ratio of 50:50 (TPU50) was chosen for the embedding of the components necessary for CuAAC, which includes the dye system and the mechanochemically active NHC-MOF.
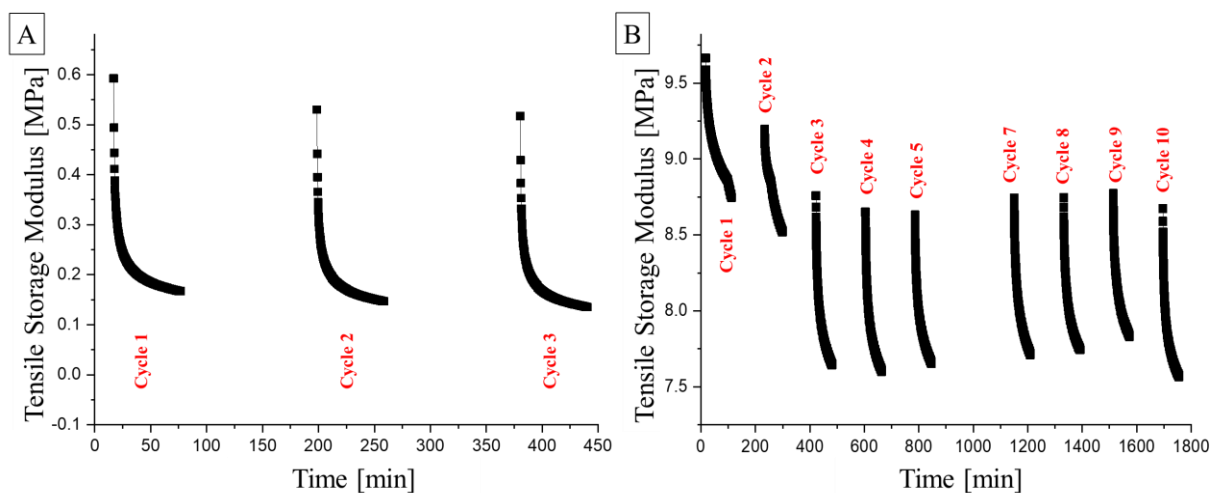

Figure 47. Determination of the initial and end tensile storage modulus of each cycle of stretching conducted *via* Universal Extensional Fixture (UXF) at 25 °C with the strain rate set at 0.5 Hz and the deformation set at ε = 40 % of **A**) TPU30 and **B**) TPU70.
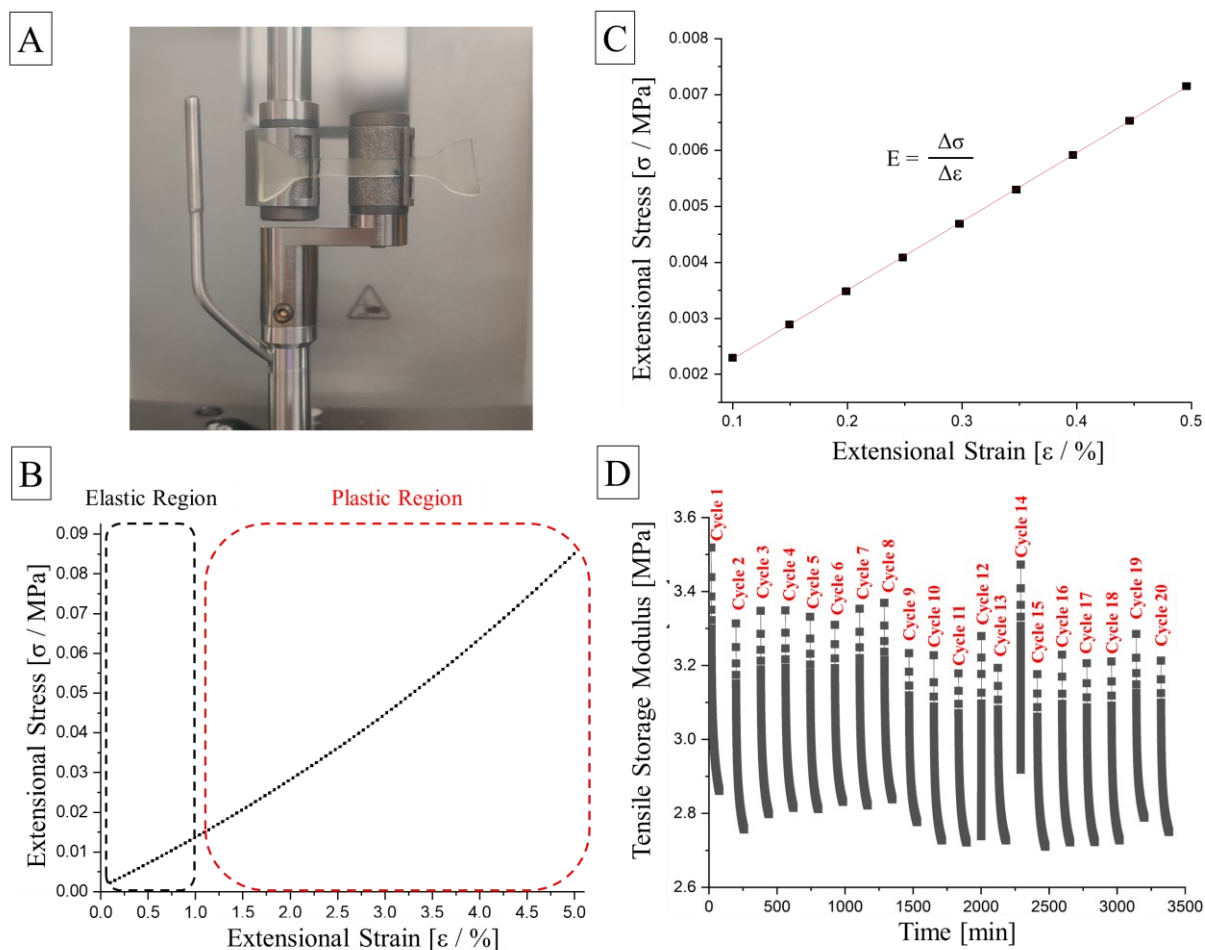
Figure 48. A) Experimental setup of extensional rotational rheology experiments with TPU foils fixed with the Universal Extensional Fixture (UXF) at 25 °C with the strain rate set at 0.5 Hz and the deformation set at ε = 40 %. **B)** The classification of the linear elastic and plastic region which is then used to **C)** determine the Young's modulus, calculated by using the slope of the linear regression in the low strain range from 0.01 % to 0.50 %. **D)** Determination of the initial and end tensile storage modulus of each cycle over 20 cycles. This graph was generated from an average of two different measurements to ensure higher accuracy and was used to conduct shape memory and recovery efficiency measurements (see **Chapter 5.4.9**).

3.3.3.2.1 Determination of the Young's (E) Modulus

To ensure accurate measurement of TPU50, the values of virgin TPU50, TPU50_1 and TPU50_2 was averaged. Oscillating stress-strain experiments were conducted until strains of up to 5 %. Initially, the stress increased linearly with the increasing strain, displaying a linear elastic behaviour until about 1 % strain, after which a plastic behaviour was observed (**Figure 48B**). The region between 0.01 % to 0.5 % strain was used to calculate the Young's modulus (**Figure 48C**), which is the slope of the stress-strain curve. From this, an E modulus of 0.013 MPa was determined for TPU50 (**Chapter 5.4.8.1** for details).

3.3.3.2.2   Determination of Shape-Memory Effect (SME)

Figure 49. A pictorial description of soft/hard segments within a TPU and the shape memory effect that is imparted due to the microphase separation of the segments.
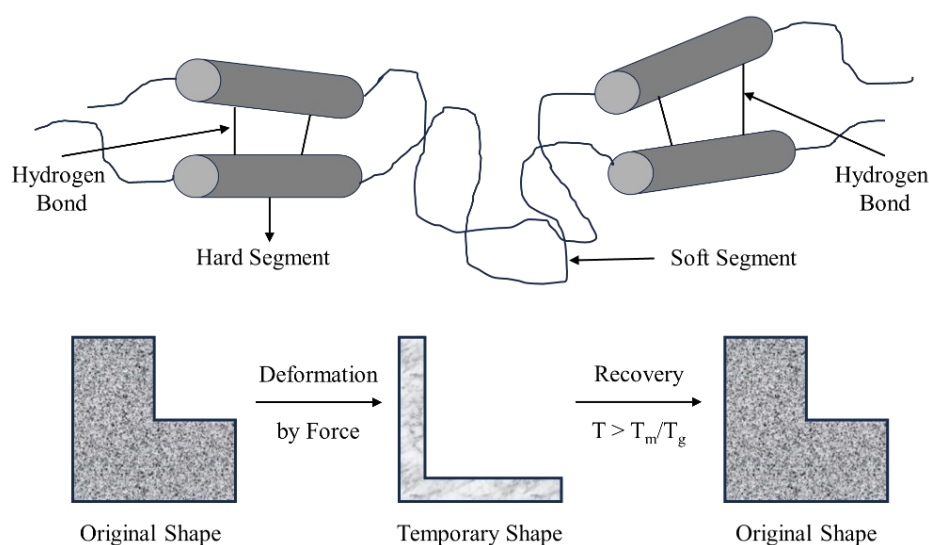
The TPU50 foils embedded with **NHC-MOF3** in dumbbell-shaped samples were subjected to oscillating tensile rheology, henceforth called stretching experiment (SE). These experiments served a dual purpose, first to briefly study the shape memory effect (SME) of TPU (measurement is the average of TPU50_1 and TPU50_2), and second to test the mechanochemical activation of **NHC-MOF3** within a TPU-fluorogenic dye system (**Chapter 3.3.4**). To study the first purpose, it is important to understand that SME is not an inherent property of any PU, but is a characteristic of segmented PUs like TPU, and is triggered by various external stimuli.[369] Segmentation is caused by microphase separation which arises from the incompatibility between internal phases in TPU, resulting in the formation of soft and hard block segments. In summary, the hard segments serve as pivot points that fix the permanent shape, while the soft segments absorb the applied external stress and are responsible for the SME when the deformed materials are heated above the T_g/T_m of the soft block (**Figure 49**).[381, 384]

A single cycle of the stretching experiments (SE) was designed such that the stretching (stressing/damaging) was conducted for 60 min at 25 °C with a deformation of 40 % and a frequency of 0.5 Hz. This was followed by 30 min of heating at 50 °C directly inside the oven of the UXF to recover material properties by melting the soft block of the TPU, triggering shape-memory behaviour. Subsequently, a waiting period of further 75 min at 25 °C was observed to recover properties of the TPU. The shape memory efficiency and recovery efficiency were measured over 20 cycles using the **Equations 5.5** and **5.6**. Two different samples of TPU50, namely TPU50_1 and TPU50_2, were used. Each were embedded with the precursor dyes (**13**) and (**14**), and **NHC-MOF3**. The independently conducted experiments provided two sets of data which were averaged to enhance accuracy. Over 20 cycles, the shape memory efficiency remained in the 90-96 % range (**Figure 48D**) while the recovery efficiency remained in the 80-100 % range (**Table A4**), thus excluding the possibility that the mechanochemical activation might be induced by any changes of the physical properties of the TPU.

3.3.4 Mechanochemical Activation Of **NHC-MOF3** In TPUs
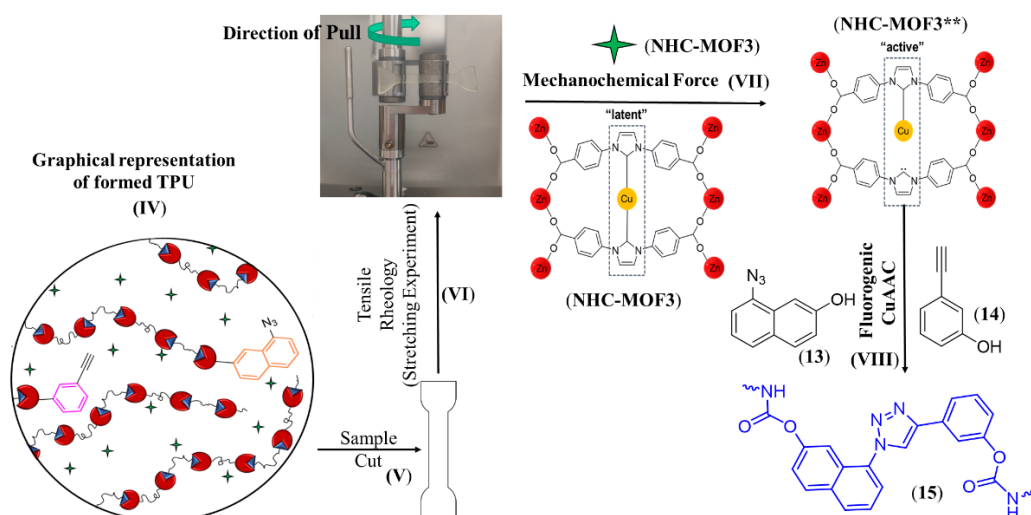
Scheme 17. Schematic concept for the mechanochemical activation of a latent **NHC-MOF3** within a solid thermoplastic polyurethane (TPU) to catalyse a subsequent fluorogenic copper-catalysed click chemistry (CuAAC) to form the highly fluorescent 8-(4-(3-hydroxyphenyl)-1,2,3-triazol-1-yl)naphthalen-2-ol dye (**15**).

The second purpose of the SEs was the mechanochemical activation of **NHC-MOF3** within a TPU-fluorogenic dye system. As previously described for **NHC-MOF3** in solution (**Chapter 3.2.4.2.3**), **NHC-MOF3** should undergo activation to form **NHC-MOF3**** (**Scheme 17**, (**VII**)) on application of the repeated oscillatory stress. The stretching experiments (SE) were performed using an UXF instrument by applying stress repeatedly over multiple cycles with each cycle comprised of a 60 min stretching (damaging) phase at 25 °C with a deformation of 40 % and a frequency of 0.5 Hz, followed by a 30 min heating phase at 50 °C *via* the UXF oven to recover material properties by triggering the shape-memory behaviour. The sample was then left for a further 75 min at 25 °C to recover properties after which a new cycle would begin. The mechanochemically activated **NHC-MOF3**** would catalyse the dye precursors to undergo CuAAC (**Scheme 17**, (**VIII**)) to form the highly fluorescent 8-(4-(3-hydroxyphenyl)-1,2,3-triazol-1-yl)naphthalen-2-ol dye (**15**), allowing it to be quantified *via* fluorescence measurements.
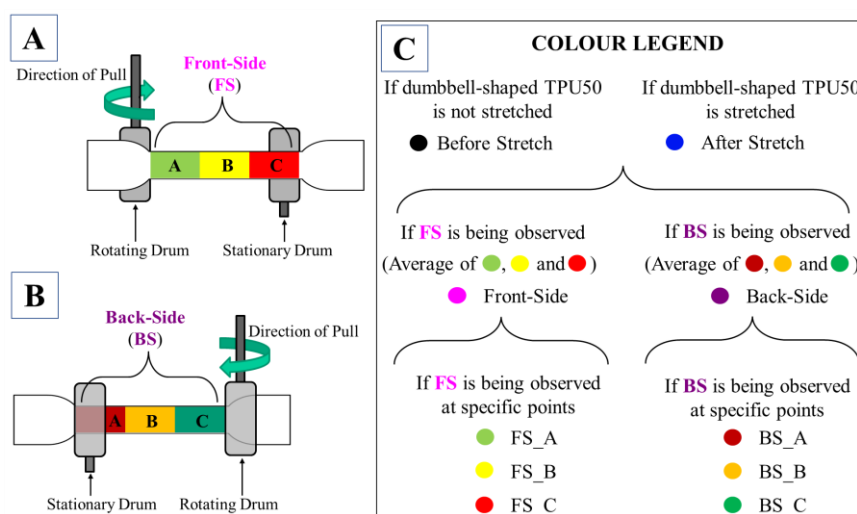

Figure 50. Illustrative depiction of the stretching regions to describe the areas on which fluorescence spectrometry was conducted in a dumbbell-shaped TPU50 sample.

3.3.4.1 Quantification of Fluorogenic "Click" Reaction

For the fluorescence measurements, the excitation wavelength (λ_{ex}) of 377 nm was chosen based on previously conducted optical measurements of the click dye (**15**) (UV-vis and fluorescence measurements in solution).[264] Based on a calibration of the obtained fluorescence intensity as described in **Chapter 5.4.10.1**, an increasing fluorescence at λ_{em} = 458 nm is observed with increasing concentrations of (**15**) (**Figure 63**). This was referenced for the quantification during different stretching experiments (SE) (**Table 11**). The **Equation 5.7** (**Chapter 5.4.10.1**) was used to calculate the conversion % from the measured fluorescence intensity. Each side of the dumbbell-shaped sample (Front-Side (FS) and Back-Side (BS)) was subjected to fluorescence measurement at different positions (positions A, B and C) (**Figure 50**). The labelling of the sides and positions was fixed for all samples, ensuring uniformity. **Figure 50** provides an illustrative representation of the stretching terms used to describe the different terms of a sample clamped to the rheology system, which consists of two drums, one stationary and one rotating/pulling.

Table 11. A summary of all the stretching experiments conducted and the type of the conversion % that is reported (see **Chapter 5.4.10.1** for more details).

Ent	SE Code	TPU50		Sample Thickness [mm]	Type of conversion %[a]	Chapter
		Code of Foil Used	Chapter			
1	EXP1	TPU50_1	5.4.5	0.71	*Estimated*	3.3.4.2
2	EXP2			0.52	*True*	3.3.4.3
3	EXP3	TPU50_2		0.50	*True*	3.3.4.3
4	EXP4			0.72	*Estimated*	3.3.4.3
5	EXP5	TPU50_Ref50%	5.4.10.1	0.51	*True*	3.3.4.4
6	EXP6	TPU50_3	5.4.5	0.68	*Estimated*	3.3.4.5

[a]For further details, refer to **Chapter 5.4.10.1**

3.3.4.2 Stretching Experiment 1

For EXP1, a dumbbell-shaped sample with dimensions 20 x 4 x 0.71 mm from the TPU50_1 foil was selected. As the sample's thickness is 0.71 mm, all calculated conversion percentages in **Table 12** are *estimated* values (for further details, refer to **Chapter 5.4.10.1**). The mode of embedding **NHC-MOF3** into the TPU proved important: the first attempts used mechanical stirring (refer to **Chapter 5.4.5** for further details), TPU50_1, to disperse the MOF before introducing within TPU50, resulting in an already primordial fluorescence (**Figure 51A**) of 12 % conversion (Average-Side) (**Table 12**, **Ent 1**) at λ_{em} = 458 nm (at λ_{ex} = 377 nm). This is attributed to the methodology of suspending the MOF by stirring, resulting in the formation of an already activated **NHC-MOF3**** (**Scheme 17**), with a visible CuAAC in the TPU solution. Since TPU foils take at least 5 days to solidify, it remains in a solution, a state where **NHC-MOF3** has already demonstrated CuAAC.[422]
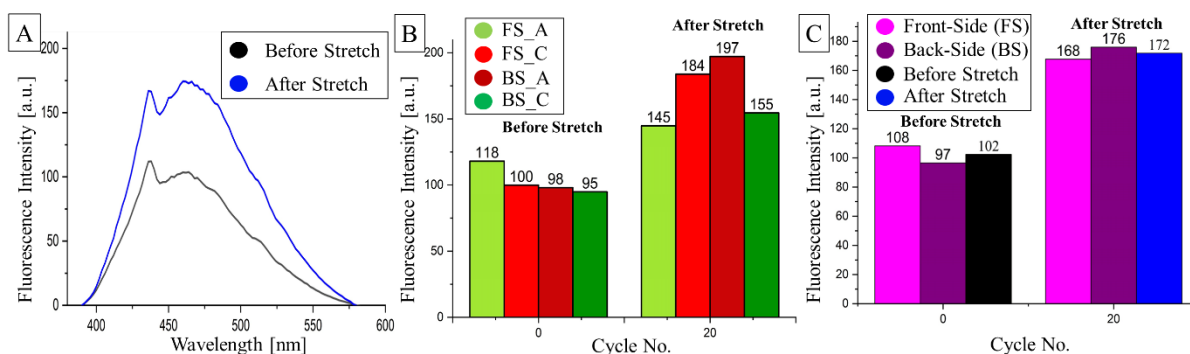
Figure 51. Oscillating tensile rheology of TPU50_1 in EXP1 resulted in quantifiable fluorescence intensities, achieved with $\lambda_{ex} = 377$ nm and at $\lambda_{em} = 458$ nm. These are displayed in the form of a before and after **A**) fluorescence spectrum of the stretching experiment, **B**) graph displaying fluorescence observed across the different positions on the two sides, and the **C**) graph displaying fluorescence intensities. The colours correspond to the colours indicated in stretching terms in **Figure 50**.

In the conducted SE experiment (EXP1), the mechanophore-containing dumbbell-shaped TPU50_1 was subjected to oscillating tensile rheology which involved applying defined stress rates and deformations, as detailed in **Chapter 5.4.9.1**. On mechanochemical activation, its fluorescence intensities were measured at λ_{ex} of 377 nm and $\lambda_{em} = 458$ nm, and the **Equation 5.7** (**Chapter 5.4.10.1**) was used to calculate the conversion % from the measured fluorescence intensities.

Table 12. Reported values for the *estimated* conversion % across the two sides (Front-Side (FS) and Back-Side (BS)) at different positions (A, B, C) after 20 cycles of stretching in EXP1.

Ent	Cycle No.	Conversion [%][a]								
		FS_A	FS_B	FS_C	BS_A	BS_B	BS_C	Front-Side	Back-Side	Avg.-Side
Colour Code[b]										
1	0	14	12	11	11	11	10	**13**	**10**	**12**
2	20	19	24	26	28	24	21	**23**	**24**	**24**
Difference		+5	+12	+15	+17	+13	+11	**+10**	**+14**	**+12**

[a]As the sample's thickness is 0.71 mm, all calculated conversion percentages are *estimated* values.
[b]Colour code as per **Figure 50**.

Following 20 cycles of stretching, the conversion % showed an increase of 12 percentage points (Average-Side), as evidenced by the fluorescence intensity which rose from 102 to 172 a.u. (refer to **Figure 51C**). However, it was unclear whether this increase could be attributed to the SE or if there were independent CuAAC reactions occurring within the TPU50_1, indicated by the initial high fluorescence intensity. To address this concern, refer to **Figure 50** which depicts the arrangement of the oscillation rheometer's two drums - one stationary and the other pulling UXF- that clamp the dumbbell-shaped TPU50_1. Since the TPU50 has the most physical contact with the stationary drum, it can be assumed that the force exerted on FS_C is greater than that on FS_A on the Front-Side. Similarly, on the Back-Side, the force exerted on BS_A is assumed to be greater than that on BS_C. It can also be assumed that BS_A experiences more force than FS_C at the point of the stationary drum as it is in direct contact with the drum. These assumptions were found to be valid in EXP1 (refer to **Figure 51** and **Table 12**, **Ent 2**), where after 20 cycles the position FS_C (26 %) showed a higher intensity than FS_A (19 %), while BS_A (28 %) showed a higher intensity than BS_C (21 %). Notably, BS_A also

displayed a higher conversion than FS_C. These variations in intensities are remarkable if compared to the intensities before stretching as then the intensities were quite similar (**Table 12**, **Ent 1**) and form an excellent comparable starting point. Thus, this validates the conceptual idea of the impact of stretching in promoting the mechanochemical activation of **NHC-MOF3**, within the polyurethane matrix, as successful.

3.3.4.3   Stretching Experiments 2, 3 and 4

A sample made of TPU50_1 foil with dimensions of 20 x 4 x 0.52 mm was chosen for EXP2, while for EXP3 and EXP4, samples made from the TPU50_2 foil with dimensions of 20 x 4 x 0.50 mm and 20 x 4 x 0.72 mm respectively, were selected. It should be noted that since the sample thickness is 0.72 mm in EXP4, all the conversion percentages calculated for it in **Table 13** are *estimated* values. In contrast, the conversion percentages for EXP2 and EXP3 are *true* values (for details, refer to **Chapter 5.4.10.1**). During the investigation of reproducibility of EXP1 in EXP2, stretching over 16 cycles of a sample with thickness 0.52 mm showed, curiously, a decrease of the fluorescence intensity over the many stretching cycles. Initially neglecting the result as a one-time occurrence, it was decided to synthesize a new foil, TPU50_2 (see **Chapter 5.4.5** for description). Dumbbell samples of thicknesses 0.50 mm and 0.72 mm from this foil were selected and used to conduct EXP3 and 4, respectively. As TPU_1 had shown an initial fluorescence before EXP1 (**Table 12**), the initial fluorescence of EXP 2 with 37 % conversion (*true* conversion %) was expected. However, even the samples from the TPU50_2 foil, prepared using a different methodology of **NHC-MOF3** suspension before embedding, showed an initial fluorescence corresponding to 23 % (*true* conversion %) and 30 % (*estimated* conversion %) prior to EXP3 and 4, respectively. In both cases, the results were similar to EXP2, showing a decrease in fluorescence intensity with an increase in the number of stretching cycles. **Figure A63** and **Table 13** illustrate that in EXP2, Front-Side experienced a higher decrease in percentage points compared to Back-Side while the opposite trend was observed in EXP3, and the decrease was similar on both sides in EXP4. As a result, it was challenging to determine any significant interrelation between the samples to comprehend the observed trends, although some theories were proposed.
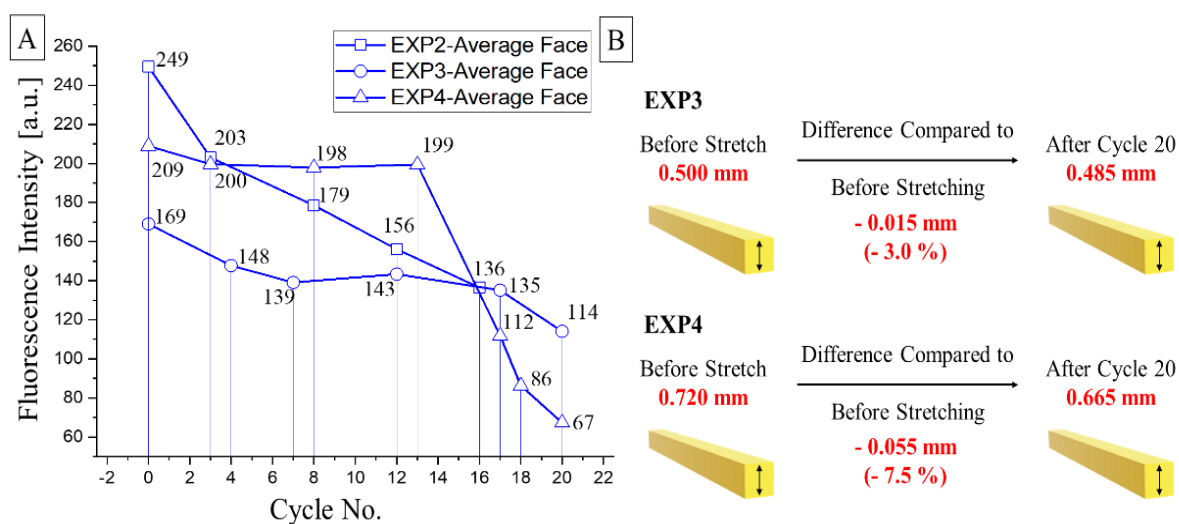
Figure 52. A) Fluorescence intensities averaged over the two sides to obtain the Average-Side intensities of the samples in EXP2, 3 and 4 over multiple cycles. The fluorescence intensities were measured with λ_{ex} = 377 nm and at λ_{em} = 458 nm. **B**) The change in the thickness of the dumbbell samples after the stretching experiments EXP3 and 4 are displayed.

Table 13. Reported values for either the *true* or *estimated* conversion % across the two sides (Front-Side (FS) and Back-Side (BS)) at different positions (A, B, C) after EXP2, 3 and 4.

Ent	Cycle No.	Conversion [%]								
		FS_A	FS_B	FS_C	BS_A	BS_B	BS_C	Front-Side	Back-Side	Avg.
Colour Code[c]										
					EXP2[a]					
1	0	41	37	38	34	34	38	**39**	**35**	**37**
2	16	17	15	17	19	21	15	**17**	**18**	**17**
Difference		-21	-22	-21	-15	-13	-23	**-22**	**-17**	**-20**
					EXP3[a]					
1	0	24	22	22	25	23	22	**23**	**23**	**23**
2	20	18	18	15	11	10	10	**17**	**10**	**14**
Difference		-6	-4	-7	-14	-13	-12	**-6**	**-13**	**-9**
					EXP4[b]					
1	0	33	29	29	32	29	28	**30**	**30**	**30**
2	20	7	6	7	4	5	4	**7**	**4**	**5**
Difference		-26	-23	-22	-28	-24	-24	**-23**	**-26**	**-25**

[a]The sample thickness for EXP2 and EXP3 were 0.52 and 0.50 mm and therefore the conversion percentages are *true* values.
[b]The sample thickness for EXP4 was 0.72 mm and therefore the conversion percentages are *estimated* values.
[c]Colour code as per **Figure 50**.

A preliminary theory was that the initial high conversion % observed before the SE's of EXP2, 3 and 4 were the maximum achievable conversions for the samples, and that stretching caused a decrease in fluorescence intensity due to a change in sample thickness. However, as depicted in **Figure 52B**, the thickness of the samples changed only slightly by -3 % and -7.5 % in EXP3 and EXP4, respectively, and should not realistically affect the fluorescence intensities.

The second theory proposed is that the decrease in fluorescence intensity was due to the ageing of the system itself, which includes the **NHC-MOF3**, TPU and the fluorogenic dye precursors. To test this hypothesis, EXP5 was conducted with TPU50_Ref50% foil which was part of the study for the fluorescence measurements conducted for the calibration experiment described in **Chapter 5.4.10.1**. Hence, it contains only the dye system without the mechanophore **NHC-MOF3** (**Scheme 16**).

3.3.4.4 Stretching Experiment 5

EXP5 was conducted using a dumbbell-shaped sample with dimensions 20 x 4 x 0.51 mm from the TPU50_Ref50% foil. As the sample's thickness is 0.5 mm, all calculated conversion percentages listed in **Table 14** are *true* values (for details, refer to **Chapter 5.4.10.1**). During EXP5, the dumbbell sample was subjected to oscillating tensile rheology, which involved applying defined stress rates and deformations as detailed in **Chapter 5.4.9.1**. Following mechanochemical activation, the fluorescence intensities were measured with λ_{ex} of 377 nm at $\lambda_{em} = 458$ nm. The conversion % was calculated from the measured fluorescence intensity using **Equation 5.7** (**Chapter 5.4.10.1**).
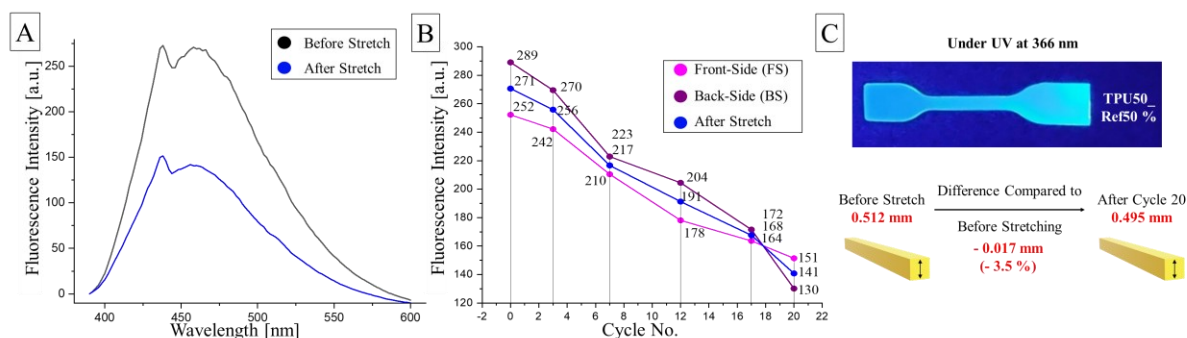
Figure 53. Oscillating tensile rheology of TPU50_Ref50% in EXP5 resulted in quantifiable fluorescence intensities, achieved with $\lambda_{ex} = 377$ nm and at $\lambda_{em} = 458$ nm. The colours correspond to the colours indicated in stretching terms indicated in **Figure 50**. These are displayed in the form of a **A)** fluorescence spectrum before and after the stretching experiment and a **B)** graph displaying the decrease in fluorescence intensities on both the sides. **C)** Since the dumbbell sample is from foils used for calibration of 50 % conversion, it glows under UV light (366 nm). Additionally, the change in the thickness of the dumbbell sample after the stretching experiment EXP5 ended is displayed.

Table 14. Reported values for the *true* conversion % across the two sides (Front-Side (FS) and Back-Side (BS)) at different positions (A, B, C) after 20 cycles of stretching in EXP5.

Ent	Cycle No.	Conversion [%][a]								
		FS_A	FS_B	FS_C	BS_A	BS_B	BS_C	Front-Side	Back-Side	Avg.
Colour Code[b]										
1	0	36	37	39	41	46	45	**37**	**44**	**41**
2	20	16	16	28	17	19	12	**20**	**16**	**18**
Difference		-20	-21	-11	-24	-27	-33	**-17**	**-28**	**-23**

[a]The sample thickness for EXP5 was 0.51 mm and therefore the conversion percentages are *true* values.
[b]Colour code as per **Figure 50**.

The change in the sample thickness after 20 cycles of stretching was -3.5 %, comparable to that of EXP3 which had a similar thickness of 0.50 mm. The conversion % decreased by 23 percentage points, with a more pronounced decrease in Back-Side (-28 %) than in Front-Side (-17 %) (**Table 14**), although no effect of the presumed higher force exerted on FS_C or BS_A could be clearly observed.

A couple of observations were made from the results of EXP5. Firstly, with the more obvious effect of ageing on fluorescence intensities, is the initial conversion % of the dumbbell sample. The sample was previously used for calibration of a fluorescence intensity having 50 % conversion. However, the sample exhibited a fluorescence intensity of 41 % before stretching, indicating an impact on the fluorescence intensity of the TPU foils due to ageing. Secondly, the decrease in fluorescence intensity in EXP5 was consistent with the trend observed previously, suggesting that the presence or absence of **NHC-MOF3** was not the reason for this behaviour of the TPU system, with the effect of stretching being identical in EXP 2, 3, 4 and 5. Hence, the remaining two components of the system, the TPU and the fluorogenic dye precursors, were needed to be tested.

3.3.4.5 Stretching Experiment 6

With ageing being the primary suspect for the effect on the fluorescence of the TPU systems, the most logical step was to synthesize a new TPU50 foil, albeit with some more modifications regarding the

methodology of suspension of the **NHC-MOF3** before it is added into the TPU solution. Therefore, another strategy was chosen for dispersion, i.e., by dispersing the MOF *via* ultrasonication in an ultrasonication bath for only 10 s (TPU50_3, see **Chapter 5.4.5** for more details). Shorter ultrasonication times (10 s) resulted in a low level of this primordial activation in the sample TPU50_3. Hence, the methodology proved to be effective as the initial fluorescence in TPU50_3 showed a 72 % decrease over TPU50_1 (29 a.u. in TPU50_3). From TPU50_3, a sample of dimension 20 x 4 x 0.68 mm was cut to conduct EXP6, conducted from the 7th day onwards, thus negating any ageing effects.

For EXP6, calculated conversion percentages listed in **Table 15** are *estimated* values as the sample's thickness is 0.68 mm (for details, refer to **Chapter 5.4.10.1**), which is much more pronounced in this experiment as the new methodology for **NHC-MOF3** dispersal worked. The fluorescence intensities for the samples for EXP6 showed a very low initial fluorescence intensity compared to any sample from EXP1-4. This, however, resulted in an unusual initial conversion %, as can be seen in **Table 15**. Hence, it becomes more important to remember that the calibration was performed specifically for samples of thicknesses 0.50 mm (see **Chapter 5.4.10.1** for more details). Due to the unusual values of the conversion %, the difference in the conversion between Cycle 1 to Cycle 20 was focussed on.

Table 15. Reported values for the estimated conversion % across the two sides (Front-Side (FS) and Back-Side (BS)) at different positions (A, B, C) after 20 cycles of stretching in EXP6.

Ent	Cycle No.	Conversion [%][a]								
		FS_A	FS_B	FS_C	BS_A	BS_B	BS_C	Front-Side	Back-Side	Avg.
Colour Code[b]										
1	0	-1	-2	-2	0	-1	-2	**-2**	**-1**	**-1**
2	20	-1	0	3	6	2	-2	**0**	**2**	**1**
Difference		0	+2	+5	+6	+3	0	**+2**	**+3**	**+2**

[a]The sample thickness for EXP6 was 0.68 mm and therefore the conversion percentages are *estimated* values.
[b]Colour code as per **Figure 50**.

After 20 cycles of stretching, the thickness of the sample decreased by about 5 % (**Figure 54D**). The conversion % showed an increase of 2 percentage points as the fluorescence intensity increased from 29 a.u. to 43 a.u. (**Figure 54C**). Furthermore, **Figure 54A** shows that in the case of the Front-Side, the difference in the conversion % was zero percentage points in the case of FS_A, while FS_C showed an increase of 5 percentage points. In the case of Back-Side (**Figure 54B**), BS_C showed an increase of zero percentage while BS_A showed an increase of 6 percentage points. Comparing FS_C and BS_A, the difference in the percentage point was one higher for BS_A. Hence, all assumptions made previously in **Chapter 3.3.4.2** regarding the effect of stretching on the mechanophoric **NHC-MOF3**-containing TPU hold their ground. Overall, the effect of increase in fluorescence by an external application of stress to activate the latent **NHC-MOF3** embedded within TPU demonstrated that they can be used as a fluorogenic stress-sensor. Additionally, the areas of the TPU receiving higher stress showed higher fluorescence, assisting in pin-pointing specific areas within the TPU with an increased possibility of material failure.

The variation in the increase of the *estimated* conversion values after stretching between EXP1 (12 %, see **Table 12**) and EXP6 (2 %, see **Table 15**) may be attributed to the different methods of dispersing the NHC-MOF in the TPU50 solution. It resulted in different sizes of the **NHC-MOF3** in TPU50_1 (14 nm, utilized in EXP1) and TPU50_3 (85 nm, utilized in EXP6), as observed in the AFM measurement (**Figure 46**). Since the **NHC-MOF3** particles in TPU50_3 are approximately 6 times

larger than those in TPU50_1, they cannot be dispersed as effectively as in the case of TPU50_1. Consequently, it clearly indicates that TPU50_3 with its larger particles exhibited a lower initial catalytic behaviour.[422]
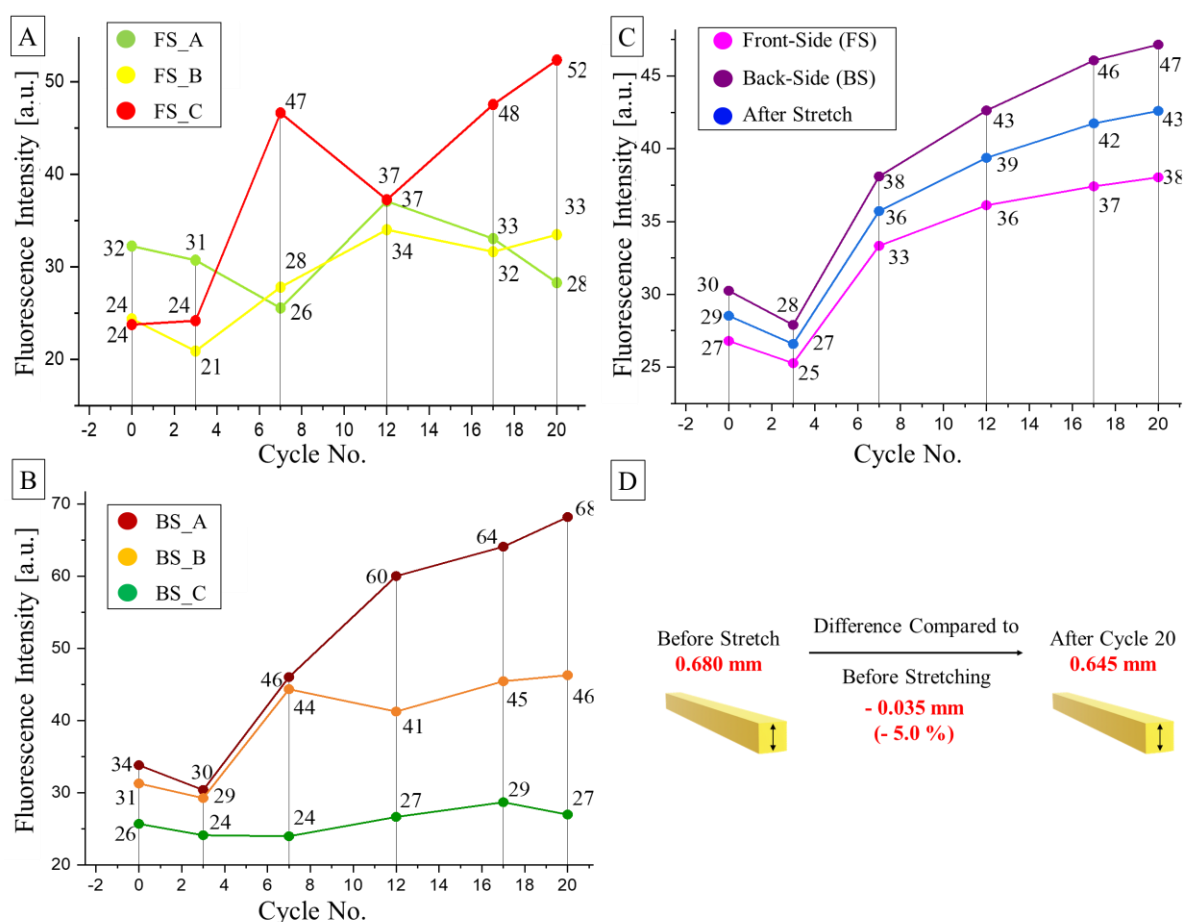

Figure 54. Oscillating tensile rheology of TPU50_3 in EXP6 resulted in quantifiable fluorescence intensities, achieved with λ_{ex} = 377 nm and at λ_{em} = 458 nm. The colours correspond to the colours indicated in stretching terms indicated in **Figure 50**. These are displayed in the form of graphs of **A)** three positions on Front-Side, **B)** three positions on Back-Side, and the **C)** average increase in fluorescence intensities across the sample. **D)** The change in the thickness of the dumbbell sample after the stretching experiments EXP6 ended is displayed.

3.3.5   Investigations on Sample Ageing

In the case of the TPU, DSC and wide-angle X-ray diffraction (WAXD) measurements were conducted of the dumbbell sample used in EXP4 and EXP6 to see any changes in the structural properties of the TPU. In DSC, the crystallinity of the samples was calculated by measuring the area under the curve of the peak of $T_{m,soft}$ (ΔH_{m0} = 172 J g^{-1} for pTHF at 100 % crystallinity[434]). It did not show any change before or after the stretching experiments (**Table 29**). WAXD measurements conducted on the sample TPU50_3 before and after a three-month period showed no relevant change in the azimuthal integrated 1D scattering pattern. Two Bragg reflections are observed at q ~14.2 nm^{-1} and 17.3 nm^{-1} superimposed with diffuse amorphous scattering (**Figure 55**). The crystallinity is determined using the ratio of the area of the Bragg reflections A_{Bragg} to the total area ($A_{total} = A_{Bragg} + A_{amorphous}$) of the 1D scattering pattern in the WAXD region (10 nm^{-1} < q < 20 nm^{-1}). The crystallinity remains nearly constant at 13-15 %, showing no significant deterioration in the chemical structure of the TPU.
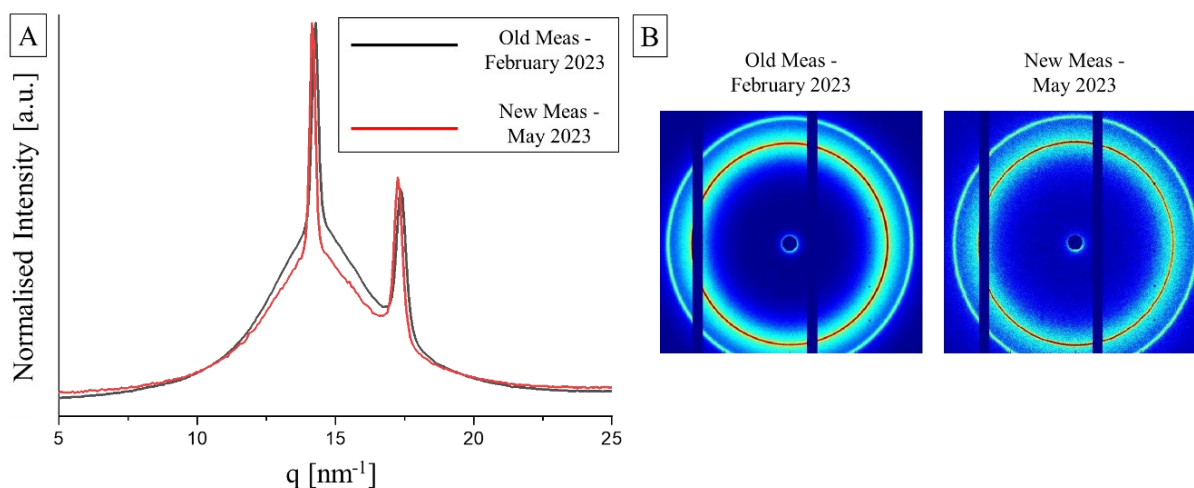
Figure 55. WAXD measurements conducted for TPU50_3 before and after a three-month period to obtain **A**) 1D scattering intensity as function of scattering vector q and **B**) 2D scattering pattern.

The final suspect were the precursor dyes, particularly 8-azidonaphthalen-2-ol (**13**), which had previously shown deterioration and had also changed colours from brownish-white to dark brown solid due to improper storage. For this purpose, the TPU50 calibration samples were checked and a visual deterioration of TPU50 calibration samples was noted, as shown in **Figure A64**. The dumbbell samples previously were transparent and uncoloured when freshly synthesized, but turned brownish despite being stored in ideal conditions. The higher colouration of the TPU50_Ref0% with the highest (**13**) concentration, and a decrease in colouration with a decrease in (**13**) concentration, further supported the theory of deterioration of (**13**) over time within the TPU samples. In the most basic of cases, the darkening of a solid sample will cause it to absorb more incident (excitation) light during fluorescence spectrometry. This reduced transmission of excitation light results in lower excitation intensity reaching the fluorophores within the sample, leading to reduced fluorescence emission. Hence, a more detailed study is required into the trends observed in EXP2-5 but is well out of scope of this thesis.

4   SUMMARY

The objective of this thesis was to investigate the catalytic activity and mechanochemical response of Cu(I) *N*-heterocyclic carbenes (NHCs). This investigation led to the utilization of Cu(I) NHCs as catalysts for the cyclopropanation of predominantly *cis*-1,4-poly(isoprene) (PI) using diazo compounds. Furthermore, Cu(I) NHCs were employed as mechanocatalytic metal-organic frameworks (MOFs) to facilitate CuAAC "click" reactions in solution. This approach was later extended to the development of a three-in-one stress sensing system which would: 1) undergo mechanochemical activation in the presence of an embedded Cu(I) bis(NHC)-containing MOF, enabling CuAAC within a bulk system, 2) function inside a shape memory TPU material (SMPU), allowing shape recovery upon reheating, and 3) allow the monitoring of the mechanochemical activation process *via* a fluorogenic dye system that facilitates early detection of material failure and identifying specific failure areas.
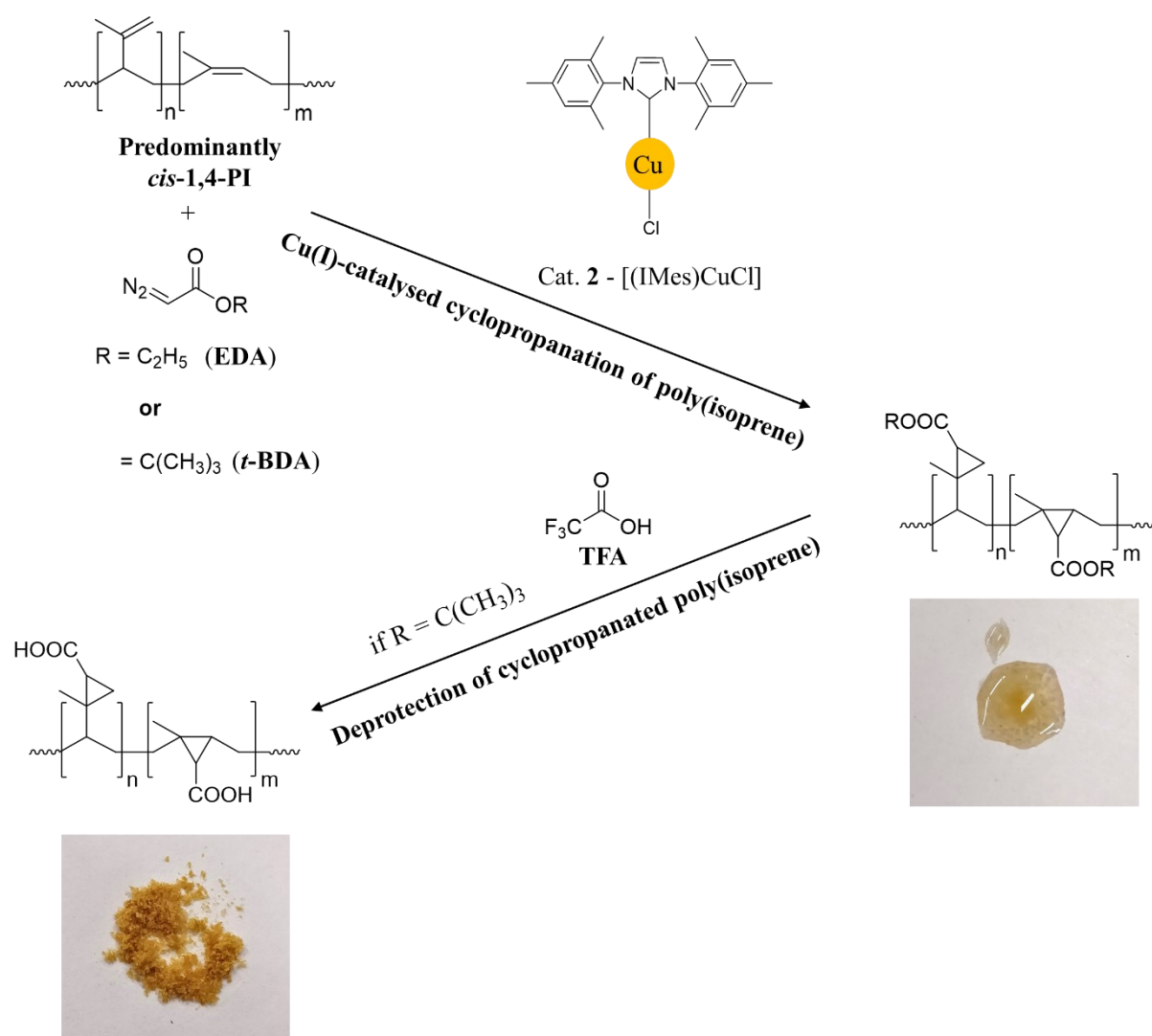
Figure 56. A summary of *cis*-1,4-poly(isoprene)s being altered with ester groups *via* cyclopropanation. Deprotected esters facilitated supramolecular networks, applicable to tyre industry modifications.

The cyclopropanation of predominantly *cis*-1,4-poly(isoprene) (PI) was conducted with two approaches: APPROACH A1 using Cat. **1** [(IPr)CuCl] and APPROACH A2 using Cat. **2** [(IMes)CuCl] (**Figure 56**). The modification yield was determined *via* ^{1}H NMR spectroscopy. The initial experiments focused on optimizing the reaction parameters such as solvent polarity, catalyst concentration, reaction

temperature and the PI concentration (solid content) in selected solvents. While probing solvents of different polarities, the best result was determined with Cat. **2** in DCM with ethyl diazoacetate (EDA) (**Figure 56**) with a molar ratio of 0.02:1:2 (catalyst:PI:EDA) per double bond of the PI. The modification yield in cyclohexane and THF was low with both the catalysts, probably due to their limited solubility in cyclohexane and the strong coordination of THF with copper. However, even though weakly coordinating polar solvents like DCM were preferable for cyclopropanation reactions to minimize solvent effects, cyclohexane was still utilized alongside due to the importance of such non-polar solvents in industrial PI synthesis *via* living anionic polymerization. During the optimization of the catalyst concentration, 0.05 eq. of catalyst to 1 eq. of PI was identified as optimal and used for all subsequent experiments. The investigation into the influence of the reaction temperatures from room temperature to 40 °C revealed no significant effect towards the modification yield, leading to the decision to conduct the reaction at room temperature. Further optimization involved varying the PI solid content in the solvent. Increasing the solid content up to 15 wt.% in cyclohexane led to a gradual increase in the modification yield (up to 5 %). In DCM, however, a solid content of 15 wt.% resulted in a much superior 17 % modification yield using Cat. **2**, with limitations on further increment. Based on the initial experiments, it was determined that the chlorinated solvent DCM was the most effective. Hence, another chlorinated solvent, 1,2-dichloroethane (1,2-DCE), was also tested with both approaches, resulting in a modification yield comparable to cyclohexane. Therefore, DCM remained the most effective solvent for the cyclopropanation (**Figure 56**).

To further understand the reactivities of Cat. **1** and Cat. **2**, kinetic studies of the cyclopropanation of PI with EDA in cyclohexane were undertaken, displaying a higher activity for Cat. **2**. Along with the mechanistic pathways of Cu(I)-catalysed cyclopropanation reactions, chemical and steric effects of the catalysts were also considered. The different reactivities of both catalysts could be attributed to the different donor properties of the NHC ligands. The steric effects could have had more influence on the reactivities as Cat. **1** is bulkier than Cat. **2**, potentially affecting both the coordination of the diazoesters to the catalyst and the cyclopropanation itself, making Cat. **2** a more effective and efficient catalyst.

To understand as to why the overall modification remained relatively low, experiments were conducted that showed that one possibility was due to the premature decomposition of the diazo compound. Although literature reports no decomposition of EDA in the presence of Cat. **1** until an addition of an unsaturated substrate, experiments showed a dimerization even in the absence of PI. The presence of PI did not hinder the dimerization, and it was identified as a major factor contributing to the low modification yields.

The final set of cyclopropanation experiments involved the modification of PI with *tert*-butyl diazoacetate (*t*-BDA, (**Figure 56**)) in DCM, with low modification yields (4-5 %). This difference in yield compared to an EDA modified PI in DCM could be due to the predominantly *cis*-polymer nature of the PI used. This might have hindered modifications in successive repeating units due to the bulkier *tert*-butyl groups substituted on the cyclopropane rings. In the case of both the diazoacetates, the M_n values from the GPC generally had increased after modification, while the PDI values remained constant, suggesting that chain scission had not occurred. The DSC was utilized to study the effect of the modifications on the glass transition temperature (T_g). The modifications reduced the segmental mobility within the cyclopropanated PIs with an increase of the polar ester groups. The T_g of virgin PI (-67 °C) increased to -61 °C and -58 °C for 5 % modification with EDA and *t*-BDA, respectively. At the higher modification yield of 17 %, the T_g further increased to -44 °C. The ^{1}H NMR spectroscopy was utilized to study the regioselectivity of the reaction. The Cu(I) NHC catalysed cyclopropanation reactions showed no regioselectivity. However, a stereoisomeric effect was observed between the *cis*- and *trans*-1,4-PI. The average ratio of *cis*/*trans* isomers decreased from 65 : 25 in virgin PI to 55 : 25 with lower modification, and further decreased to 50 : 25 at 17 % modification yield, indicating a preference for cyclopropanation of *cis*-1,4-PI.

Deprotection experiments were conducted to convert the cyclopropyl esters to carboxylic acid groups, allowing establishment of ionic interactions or hydrogen bonds. However, the use of NaOH, H$_3$PO$_4$, or TFA resulted in very low yields for PIs modified with EDA. The PIs modified with *t*-BDA showed the wanted results with TFA (**Figure 56**), as these groups could cleave more efficiently in acidic conditions. GPC analysis confirmed that the obtained powder was the deprotected PI (**Figure 56**), with M_n values remaining in the range of 2700-3200 g mol^{-1}. ATR-FTIR showed the expected differences when comparing the pre- and post-deprotected samples. Rheology experiments were performed on the different PIs. The storage modulus of the modified PI was significantly higher than the virgin PI, indicating a much stiffer material even at low modification yields (5 %). The loss factor tan(δ) was lower for the modified PI, suggesting that the modulus was dominated by the material's viscous properties. The deprotected PI exhibited a higher loss modulus compared to the protected PI, even at elevated temperatures of 140 °C, indicating the formation of an internal supramolecular network due to hydrogen bond dimers. This network resembled the behaviour of high molecular weight PI, making further modification by cyclopropanation redundant for the tyre industry as it would prevent an application of the designed material.
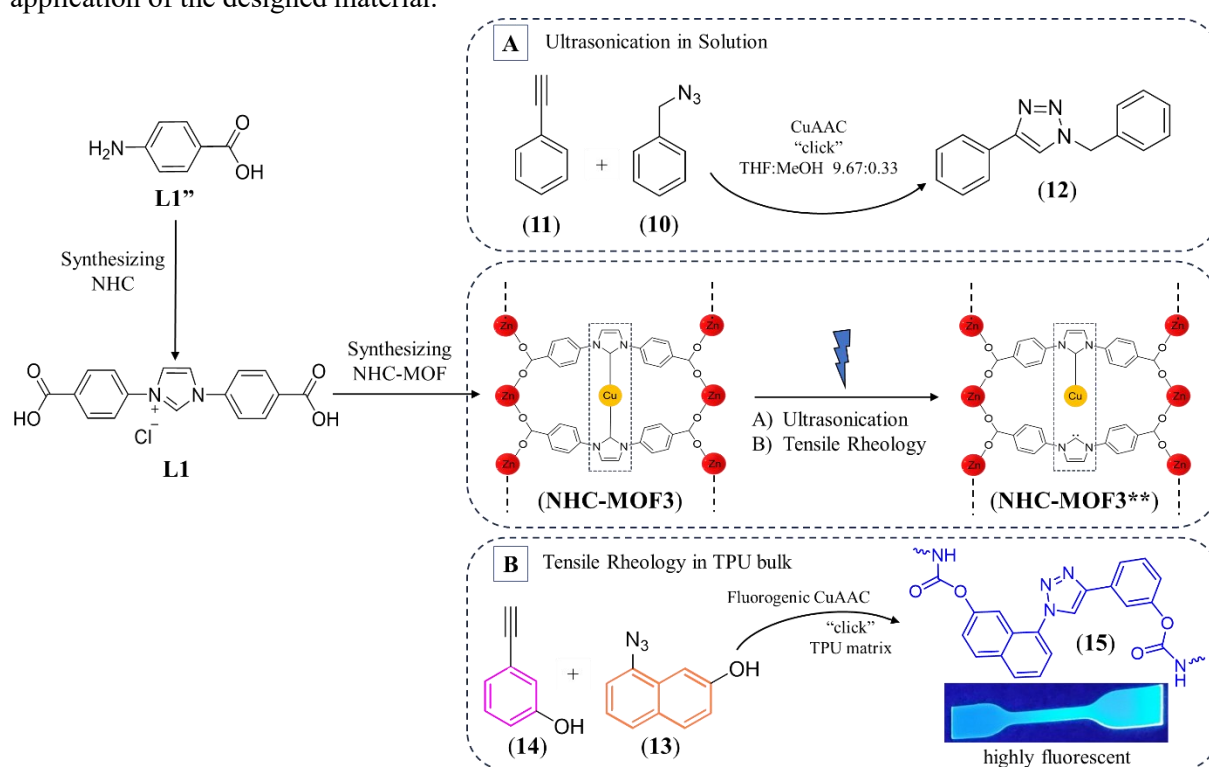
Figure 57. A summary of the undertaken mechanochemical activation of **NHC-MOF3** by **A)** ultrasonication in solution and **B)** tensile rheology in TPU bulk.

Regarding the aim to ultimately develop a three-in-one stress sensing system by combining mechanophoric behaviour with CuAAC "click" reaction within a TPU matrix, the first objective involved the development and characterization of *N*-heterocyclic carbene based metal-organic frameworks (NHC-MOFs) that behaved as latent mechanocatalysts. These NHC-MOFs could be activated under mechanical force through ultrasonication in solution and then by extensional oscillatory and rotational rheology (tensile rheology) machine in bulk.

Two approaches were undertaken to prepare the NHC-MOFs: bifunctional compounds with -NH$_2$ and -COOH groups were used to form NHCs, which further reacted with metallic components to create MOFs containing Cu(I) bis(NHC)s within their structure (APPROACH B1). The second approach

involved protecting the compounds with methylation, synthesizing ester-based Cu(I) bis(NHC)s, cleaving the ester to obtain carboxylic acid groups, and finally reacting them with Zn(II) to form the NHC-MOF (APPROACH B2). 4-aminobenzoic acid (**L1"**, **Figure 57**), 4-aminocinnamic acid and 4-(4'-aminostilbene) carboxylic acid were considered as organic linkers to optimize the NHC-MOF preparation. The variation in organic linkers aimed to achieve a balance between rigid and soft components to enhance the MOF's ability to withstand ultrasonication or tensile rheology. In the end, the **L1"**-based NHC (**L1**, **Figure 57**) was chosen to synthesize the NHC-MOFs using APPROACH B1 and analysed using various techniques. The characterization using PXRD (powder X-ray diffraction) conveyed a rather well-known challenge of MOFs in general, the difficulty of reproducibility. The NHC-MOFs, all with the same composition and synthetic procedure, did not exhibit any similarity. Also, as a match could not be established in the Cambridge Structural Database (CSD), the structure itself could not be identified for the obtained NHC-MOFs. However, comparing the IR of **L1** and the obtained NHC-MOFs indicated the successful formation of a MOF. The TGA (thermogravimetric analysis) demonstrated a wide range of stability among the NHC-MOFs, with decomposition temperatures ranging from 245 to 320 ℃. Among them, **NHC-MOF3** (**Figure 57**) exhibited better overall stability. FAAS (flame atomic absorption spectroscopy) analysis provided the Cu:Zn atomic ratios for the different NHC-MOFs. The atomic ratio of 0.53 : 1, as expected per the literature,[423] was demonstrated by **NHC-MOF3**, with the weight percentage of Cu and Zn determined to be 4.66 % and 8.97 %, respectively. The mechanochemical activation of the synthesized MOFs was accomplished by subjecting them to ultrasonication in solution containing model CuAAC "click" reaction precursors phenylacetylene (**11**) and benzylazide (**10**) (**Figure 57A**). The two NHC-MOFs **NHC-MOF1** and **NHC-MOF3** exhibited significant mechanochemical activity. After 10 and 20 ultrasonication cycles, respectively, **NHC-MOF1** showed an average conversion of 57 %, while **NHC-MOF3** displayed a conversion of 25 %. Control experiments tracked using ^{1}H NMR spectroscopy demonstrated the true latent nature of **NHC-MOF1** and **NHC-MOF3**, as minimal conversions were observed at room temperature. However, thermal activation at 60 ℃ was observed with conversions of 75 % and 10 %, respectively. It was hypothesized that a catalytic activity could be gained due to newly formed surfaces of the cracked MOF by ultrasonication, causing an at least partial destruction of the MOF structure to obtain Cu(I). This hypothesis was supported by PXRD, revealing a collapse of its crystalline structure in the case of **NHC-MOF1** and the appearance of new peaks at higher 2θ values, indicating the formation of CuH. Due to oxidation over time, the mechanochemical activity of **NHC-MOF1** could not be reproduced until sodium ascorbate, a reducing agent, had been added to the sonication mixture. As the use of reducing agents in the bulk system was not planned, **NHC-MOF1** was excluded from further consideration and the focus was shifted to **NHC-MOF3** (**Figure 57**).

SEM and AFM images of post-sonicated **NHC-MOF3** confirmed the partial destruction of the larger NHC-MOF structures into smaller, disordered particles. Additionally, the appearance of additional signals in the ^{1}H NMR spectrum after sonication suggested the decomposition of **NHC-MOF3** and additionally the NHC itself. The TGA before and after sonication showed a significant mass difference at 500 ℃, indicating that the posts-sonication **NHC-MOF3** mostly consisted of decomposed organic material, likely the ligand itself, additionally confirming the hypothesis. Consequently, **NHC-MOF3** was selected for further experimentation in a thermoplastic polyurethane (TPU) matrix to investigate mechanochemical activation in bulk, as it seemed to be the most promising candidate based on its activation potential (see **Figure 57B**).

To investigate the mechanochemical activation of **NHC-MOF3** in bulk, thermoplastic polyurethane (TPU) was developed over three stages, enabling a simple tunability of mechanical properties by varying the hard/soft segment ratios within the TPU. The soft segment consisted of α, ω-telechelic bis(hydroxy) pTHF and half of the added MDI (M_{soft} = 3150.26 g mol^{-1}), while the hard segment

consisted of BDO as well as the other half of added MDI (M_{hard} = 340.38 g mol^{-1}). DBU was used as a catalyst in the polyaddition reaction to form a supramolecular crosslinked network based on strong hydrogen bonding among the urethane linkages, and pi-pi bonding. With the MDI concentration kept constant and the tuning of the concentration of pTHF and BDO to have a [OH:NCO] ratio of 1:1, Young's moduli ranging from 0.002 MPa to 0.033 MPa were obtained. This offered a possibility to test different stiffnesses and hence the mobility for subsequent mechanochemical activation of TPU for tensile rheology. However, the TPU30 and TPU70 proved too soft and too rigid, respectively, to be handled and utilized. Hence, TPU50 with a Young's modulus of 0.013 MPa was chosen for all subsequent experiments.

In the final stage, the components required for the fluorogenic "click" reaction were embedded within the TPU50 matrix. The precursor dyes (8-azidonaphthalen-2-ol (**13**) and 3-hydroxyphenylacetylene (**14**), **Figure 57B**) were covalently linked, while **NHC-MOF3** was physically dispersed in the TPU. This allowed for the formation of a suitable TPU material for a three-in-one approach.

The shape memory effect (SME) of TPU50 was investigated through oscillating tensile rheology over 20 cycles of stretching. It demonstrated high shape memory efficiency and recovery efficiency, indicating that mechanochemical activation was not influenced by changes in the TPU's physical properties as the tensile storage modulus almost regained to its original value before the beginning of a new cycle. The catalytic activity of **NHC-MOF3** was tested within TPU50 by applying mechanical force using extensional oscillating rheology. The fluorescence intensity of the highly fluorescent 8-(4-(3-hydroxyphenyl)-1,2,3-triazol-1-yl)naphthalen-2-ol dye (**15**), formed by the conversion of the precursor dyes *via* CuAAC (**Figure 57B**), was measured with fluorescence spectrometry. Based on calibrations performed in the absence of **NHC-MOF3**, a linear fit equation was determined. The measured fluorescence intensities were then plugged into the equation to calculate the conversion, taking the sample thickness into consideration as the calibration was performed only for 0.5 mm thicknesses and the thickness of a sample affects its fluorescence intensities. An initial experiment showed a successful increase of 12 percentage points. However, subsequent experiments exhibited a curious trend of decreasing fluorescence after stretching. Changes in sample thickness were ruled out as a probable cause as the change of thicknesses before and after stretching were only slight and should not affect the fluorescence intensities.

The ageing of the system was considered as the possible issue, requiring detailed scrutiny. To investigate the effect of **NHC-MOF3**, an experiment was conducted with the calibration sample representing 50 % conversion. However, it showed a similar trend of decreasing fluorescence. Furthermore, it was also noted that the conversion of the sample had decreased before the stretching, indicating that **NHC-MOF3** was not responsible for the observed trend. Hence, ageing of the TPU or the precursor dyes became the primary suspects. To address this, a new TPU50 foil was synthesized, and a stretching experiment was conducted immediately to negate any ageing effects. After 20 cycles of stretching, an increase of 2 percentage points was observed. The difference in the increase of percentage points, compared to the very first stretching experiment, was attributed to the different methods of dispersing the NHC-MOF. The different dispersion methods caused the **NHC-MOF3** particles to be ~6 times larger than those in the first sample, and hence they could not be dispersed as effectively. Consequently, the discrepancy in dispersion likely influenced the conversion results. With the ageing question persisting, DSC was conducted before and after stretching. WAXD measurements were also conducted for an unstretched foil over a three-month period. However, no changes were observed in the TPU crystallinity using both methods, and hence ruled out as the problem. The next suspect were the precursor dyes, particularly (**13**) (**Figure 57B**), which had previously shown deterioration when stored in ambient conditions. A visual observation of the calibration samples (after almost six months from synthesizing) showed a browning of the samples compared to the fresh foils which were transparent

and colourless. The higher colouration of the TPU50 foil with the highest concentration of (13) further supported the theory of deterioration of it over time within the TPU samples. In the most basic of cases, the darkening of a solid sample causes it to absorb more incident (excitation) light, leading to reduced fluorescence emission.
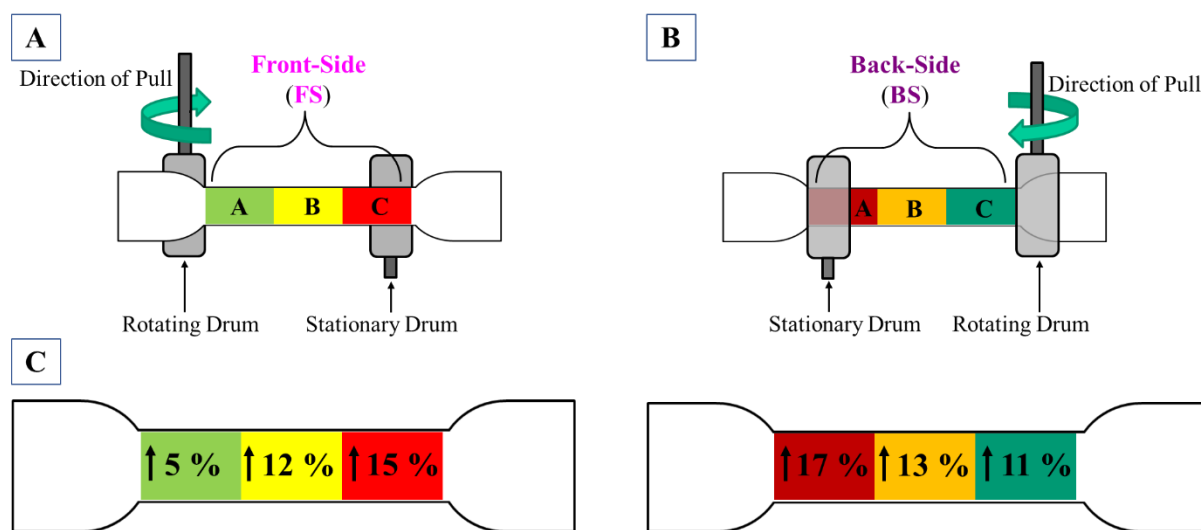

Figure 58. Illustrative depiction of the stretching regions describing the areas on which fluorescence spectrometry was conducted in a dumbbell-shaped TPU50 sample on **A**) the Front-Side (FS) and the **B**) Back-Side (BS). **C**) Certain areas of the TPUs showed higher florescence on receiving higher stress, assisting in pin-pointing specific areas within the TPU with an increased risk of material failure.

Despite the challenges faced, it can be concluded that a successful three-in-one system was achieved. The TPU displayed shape memory effect, while Cu(I) catalysis occurred within the bulk system, leading to the formation of the fluorescent dye (**15**). In terms of achieving a fluorogenic stress sensor system, stretching experiments demonstrated quantifiable fluorescence upon application of mechanical force. Furthermore, observations show that stretching experiments not only induced stress which resulted in an increase of fluorescence, but additionally the areas of the TPU receiving higher stress showed higher fluorescence, assisting in pin-pointing specific areas within the TPU with an increased risk of material failure (**Figure 58**). This supports the use of the tested material as a fluorogenic stress sensor, as the stress history is stored in the material through the generated fluorescence.

.

5 EXPERIMENTAL PART

5.1 Methods

Nuclear magnetic resonance (NMR) spectra were measured on a Gemini 2000 FT-NMR spectrometer by Varian and deuterated solvents were used for the measurements. The chemical shifts are given in parts per million (ppm) and referred to the remaining solvent signals of THF-d_8 at 1.73 and 3.58 ppm (^{1}H NMR), DMSO-d_6 at 2.50 ppm (^{1}H NMR) and 39.5 ppm (^{13}C NMR), CDCl$_3$ at 7.26 ppm and DCM-d_2 at 5.34 ppm. The obtained spectra were analysed using MestReNova (14.0).

Analytic GPC was performed on a Viscotek GPCmax VE 2002 using a column set of a H$_{HR}$H Guard-CLM3008 and a GMH$_{HR}$-N-18055 main column in tetrahydrofuran (THF) with a flow rate of 1 ml min^{-1} and a column temperature of 22 °C. Detection was accomplished by refractive index with a VE 3580 RI detector of Viscotek at 35 °C. External calibration was done using polystyrene (PS) standards with a molecular weight range from 1,050 to 115,000 g mol^{-1} were used.

Fourier-transform infrared spectroscopy measurements were done on a Bruker Tensor VERTEX 70 spectrometer and Opus 6.5 was used for data analysing. For attenuated total reflection-infrared (ATR-FTIR), a Golden Gate Heated Diamond ATR Top-plate was equipped while in the case of KBr measurements (FT-IR-KBr), the KBr pellet method of preparation was used.

Differential scanning calorimetry (DSC) was performed on a differential scanning calorimeter 204F1/ASC Phoenix from Netzsch (Selb, Germany). Crucibles and lids made of aluminium were used. Measurements were performed in a temperature range of −100 °C to 180 °C from using a heating rate of 10 K min^{-1}. As purge gas, a flow of dry argon or nitrogen was used. For evaluation of data, the Proteus Thermal Analysis Software (Version 5.2.1, NETZSCH-Geraetebau GmbH, Selb, Germany, 2011) was used.

ESI-ToF MS measurements were performed using a Bruker Daltonics microTOF. The sample was dissolved in HPLC grade solvents. All spectra were obtained by means of direct injection with a flow rate of 180 μL h^{-1} in either the positive or negative mode with an acceleration voltage of 4.5 kV.

Thermogravimetric Analysis (TGA) measurements were performed on a TGA Netzsch T210. Measurements were done under a flow of nitrogen (20 mL min^{-1}) and a heating rate of 10 K min^{-1} in the range 40-600 °C.

Atomic force microscopy (AFM) measurements were performed using a nanosurf CoreAFM with Tap190AI-G Cantilevers in the phase-contrast mode. The samples were dispersed in milipore water at concentrations of 50 μg mL^{-1}. The dispersion was dropped on the mica surface, incubated for 60 s and removed with a soft tissue before measurements. Images were created using Gwyddion 2.53 (freeware, http://gwyddion.net/).

Scanning electron microscopy (SEM) measurements were performed with Zeiss Gemini 500.

Ultrasonication experiments were conducted in a 10 mL reaction vessel with two additional side necks attached to a VCX 500 ultrasonic processor (Sonics & Materials, CT, USA) equipped with a long full-wave solid probe and an internally threaded stainless-steel adapter. To the mixture, successive cycles of pulsed ultrasound with a frequency of 20 kHz using 30 % of the maximal amplitude of 125 μm was applied, thus applying an energy of 20 kJ per sonication cycle, which corresponded to a sonication intensity of 8.34 W cm^{-2}. This was accomplished with a sequence of 5 s pulse and 10 s break for 30 min were applied (90 min total). Each cycle was followed by a rest time of 45 min.

Powder X-Ray Diffraction (PXRD) measurements were carried out on a STOE STADI-P diffractometer equipped with a sealed Cu X-ray tube, a germanium (111) monochromator crystal (λ(Cu-Kα1) = 154.060 pm) and a Dectris MYTHEN 1k detector. Samples were grinded with a agate mortar, filled in glass capillaries (Hilgenberg, outer diameter 0.5 mm) and measured in Debye-Scherrer mode.

Data handling was done with STOE WinXpow software [STOE & Cie GmbH, WinXpow Version 3.5.0.2, Darmstadt 2018.]

Flame Atomic Absorption Spectrometry (FAAS) measurements were carried with Analytik Jena novAA® 350 atomic absorption spectrometer (Analytik Jena GmbH, Jena, Germany) with a slit width of 1.4 mm for Cu, with a 5 mA Cu hollow cathode lamp (Heraeus, Hanau, Germany) operating at 324.8 nm. Slit width for measurement of Zn was 0.5 mm using a 5 mA Zn hollow cathode lamp at 213.9 nm. Samples were atomized using an acetylene/air gas mixture (C/O ratio 0.075) with a constant flow of 50 L h^{-1}. For sample preparation, exactly weighed catalyst powders were reduced to ashes at 550 °C for 20 h. Residues were taken up in 10 mL of 20 % nitric acid, transferred into a 100 mL volumetric flask and filled up using double-distilled water. Resulting samples were directly injected in the AAS or if necessary, after dilution with 2 % nitric acid. Quantitation was realized *via* external calibration. Here, stock solutions between 1.0 and 5.0 mg L^{-1} were evaluated in triplicate (AAS standard solution, Rotistar, Carl Roth GmbH, Karlsruhe, Germany). Calibration curves were generated by linear regression.

Rheology was performed on an oscillatory plate rheometer MCR 301/SN 80753612 from Anton Paar (Graz, Austria). All measurements were performed using a PP08 measuring system (parallel plated, diameter 8 mm). Oscillatory frequency sweep was conducted with 5 % strain and frequency range from 100 to 0.1 Hz with a decadal logarithmic ramp of 5 pt/dec.

Extensional oscillatory and rotational rheology experiments of thin films were conducted on Anton Paar (Physica) MCR 101/SN 80753612 *via* Universal Extensional Fixture (UXF) at 25 °C. Therefore, the films were cut into a dumbbell shape (containing Cu = 6 mol% of 8-azidonaphthalen-2-ol (**13**)/3-hydroxyphenylacetylene (**14**)) were fixed in the UXF sample holder and subjected to oscillating stretch experiments. To investigate the shape memory effect of the TPU and the mechanochemical activation of the Cu(I) bis(NHC) catalysts within TPU,[422] the frequency was set at 0.5 Hz while keeping the deformation at ε = 40 %.

Fluorescence measurements were carried out in the bulk state on a Cary Eclipse fluorescence spectrometer of Agilent, fixing the samples with a solid sample holder. Emission spectra were recorded in fluorescence mode after excitation at 377 nm and collecting between 390 nm to 650 nm with a maximum at 458 nm and repeated at least three times at different positions per side. The selected voltage was 585 V.

Sample Cutting of the TPU films into dumbbell shaped samples was done with hydraulic cutting press in accordance with DIN 53504 type 3a/ISO 37 type 3.

Wide-angle X-ray diffraction (WAXD) measurements were performed in transmission mode using a SAXSLAB laboratory setup (Retro-F) equipped with an AXO microfocus X-ray source and an AXO multilayer X-ray optic (ASTIX) as monochromator for Cu Kα radiation (λ = 1.54 Å). A DECTRIS PILATUS3 R 300K detector was used to record the 2D scattering patterns. The 2D WAXD pattern were integrated *via* SAXSGUI in order to obtain 1D WAXD pattern. The sample to detector distance was about 10 cm. A twin pinhole system was used for the measurements with an aperture size of about 0.9 mm and 0.4 mm.

5.2   Cu(I) NHCs as Catalysts for Cyclopropanation

5.2.1   Cu(I)-Catalysed Cyclopropanation of Poly(isoprene) with Diazoacetates

All reactions were carried out under inert conditions using common Schlenk techniques and all solvents were degassed freshly by at least three freeze-pump-thaw cycles prior use. Poly(isoprene) (6 g; corresponding to 88.0 mmol functional groups; $M_{n,GPC,corr}$ = 2900 g mol^{-1}, DP = 42) were dissolved in dry solvents (1,2-DCE, cyclohexane, DCM or THF). The copper(I) catalysts (Cat. **1/2**) (0.05 eq. per double bond (DB), 4.5 mmol) were added as a solution. If the reaction solvent was cyclohexane, the

catalysts were added in DCM (minimum volume required to solubilize the catalyst) which was later removed by vacuum. Subsequently, the diazoacetate (DA) (EDA (**4**)/*t*-BDA (**5**), 2 eq. per DB, 180 mmol) was added as diluted solution in the appropriate solvent (either 1,2-DCE, DCM, THF or cyclohexane) by a dropping funnel over a period of 4 h. A water bath at RT was used to keep the exothermicity in check. The final total volume of the solvents was based on the concentrations of 1.3 wt.%, 10 wt.%, 15 wt.% or 20 wt.% of PI, as desired. The reaction was stirred for 48 h at room temperature. Unless the reaction was conducted in cyclohexane, the solvent was removed under vacuum and the contents of the flask were re-solubilized in cyclohexane. The crude product was purified by precipitating thrice in cold methanol (-50 °C), collected, and dried in high vacuum giving (**6/7**) in 60-65 % yields.

For EDA modified PI (6) =

PDI = 1.1.

^{1}H NMR (400 MHz, CDCl$_3$) δ 5.10 (dt, *J* = 15.0, 6.4 Hz, 29H), 4.80 – 4.63 (m, 7H), 4.09 (dqt, *J* = 9.7, 7.2, 3.1 Hz, 17H), 2.03 (q, *J* = 15.7, 12.3 Hz, 110H), 1.67 (d, *J* = 7.6 Hz, 69H), 1.58 (s, 15H), 1.28 – 1.18 (m, 32H), 0.88 (t, *J* = 6.6 Hz, 3H).

For *t*-BDA modified PI (7) =

$M_{n,\text{GPC,corr}}$ = 3200 g mol^{-1}, PDI = 1.1.

^{1}H NMR (400 MHz, CDCl$_3$) δ 5.11 (dt, *J* = 14.9, 6.4 Hz, 37H), 4.79 – 4.63 (m, 8H), 2.12 – 1.94 (m, 151H), 1.68 (s, 74H), 1.64 (d, *J* = 11.8 Hz, 13H), 1.44 (s, 17H), 0.88 (t, *J* = 6.7 Hz, 3H).

ATR-FTIR: ν (cm^{-1}) = 2960 (s), 2925 (s), 2853 (s), 1720 (m, ν$_{CO}$), 1645 (w), 1445 (s), 1375 (s), 1145 (s), 1085 (w), 858 (m), 836 (m), 672 (m), 625 (s), 534 (s), 464 (s).

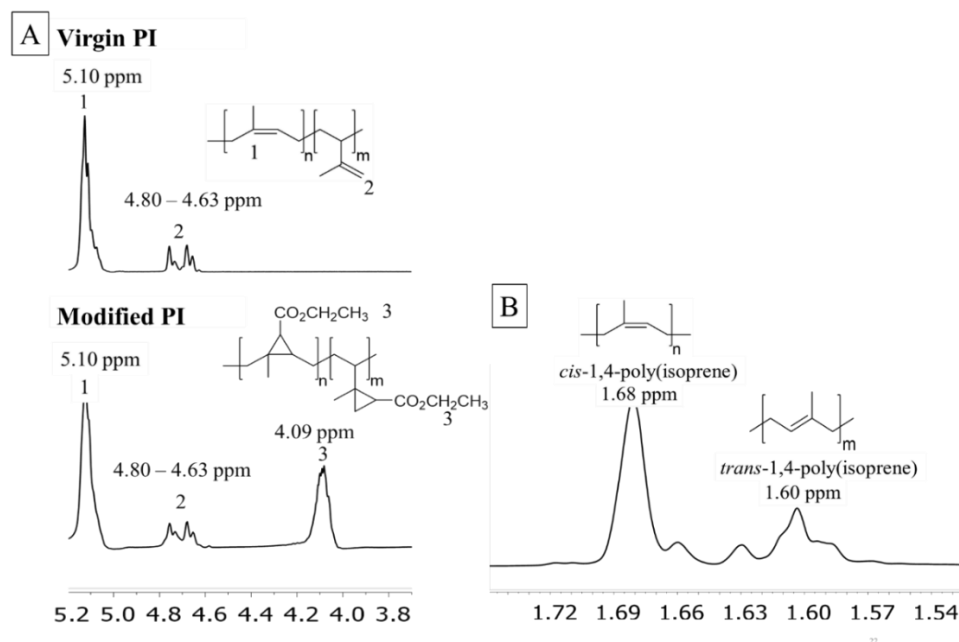### 5.2.2   Determination of Percentage Modification of Cyclopropanation

Figure 59. ^{1}H NMR spectra of **A**) a virgin predominantly *cis*-1,4-PI (**3**) and a modified PI (**6**), and **B**) peaks assigned to *cis*-1,4-PI and *trans*-1,4-PI.

The percent modification of all cyclopropanations was determined using the relative integrals in ^{1}H NMR spectra as indicated in **Figure 59**, which show the modification of PI (**3**) with EDA (**4**). The spectra show the changes before and after modification, with the peaks at 5.10 ppm and 4.80-4.63 ppm

assigned to 1,4-poly(isoprene) and 3,4-poly(isoprene), respectively, as well as the new peak at 4.10 ppm after modification belonging to the methylene protons of the -CO$_2$***CH$_2$***CH$_3$ moiety of the cyclopropane.[121]

5.2.3 Cu(I)-Catalysed Decomposition of Ethyl Diazoacetate (EDA)

All reactions were carried out in a glovebox and the DCM-d_2 was opened and used as obtained inside the glovebox. The Cu(I) catalyst (**Cat. 1** = 10.8 mg/ **Cat. 2** = 9 mg) (1 eq.) was added to a glass vial and dissolved in DCM-d_2 (0.2 mL). Subsequently, the EDA (**4**) (40 eq.) was added dropwise. The reaction was stirred for 24 h at room temperature after which samples were collected and sent for NMR.
For Cat. 1 - ^{1}H NMR (400 MHz, DCM-d_2) δ 6.82 (s, 1H$_{trans}$), 6.23 (s, 1H$_{cis}$), 4.22 (dq, J = 9.7, 7.1 Hz, 4H), 1.36 – 1.16 (m, 6H).

For Cat. 2 - ^{1}H NMR (400 MHz, DCM-d_2) δ 6.81 (s, 1H$_{trans}$), 6.23 (s, 1H$_{cis}$), 4.22 (dq, J = 9.8, 7.1 Hz, 4H), 1.36 – 1.14 (m, 6H).

### 5.2.4 Deprotection of Cyclopropanated Poly(isoprene)

The deprotection of (**7***) (0.2 g; 0.0625 mmol; $M_{n,\text{GPC,corr}}$ = 3200 g mol^{-1}, DP = 42; corresponding to 3 mmol functional groups) was accomplished treating a solution of (**7***) in DCM (5 mL) with trifluoroacetic acid (TFA) (**8**) (30 mmol) under vigorous stirring for 24 h. The solvent and remaining TFA were removed under vacuum. The crude product was dissolved in cyclohexane and precipitated into cold methanol (-50 °C) for at least three times. The final product (**9***) was obtained after drying in high vacuum.
ATR-FTIR: ν (cm^{-1}) = 3370 (w, ν$_{OH}$), 2925 (s), 2865 (s), 1778 (m), 1700 (m, ν$_{CO}$), 1455 (m), 1375 (m), 1217 (m), 1167 (m), 1026 (m).

5.3 Cu(I) NHCs as Mechanocatalysts within Metal-Organic Frameworks (MOFs)

5.3.1 Synthesis of *N,N′*-Bis(4-carboxyphenyl)ethylenediimine (**L1'**)

The synthesis was conducted according to the described literature with slight modifications.[340]
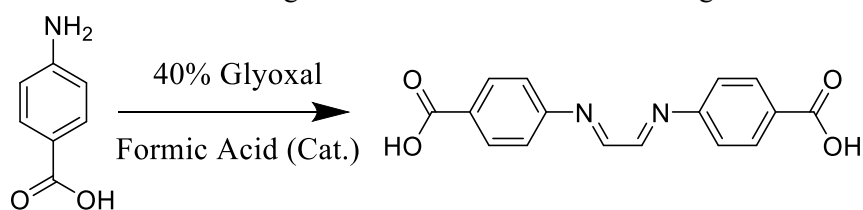
Scheme 18. Synthesis of *N,N′*-bis(4-carboxyphenyl)ethylenediimine (**L1'**).

In 30 mL methanol, 4-aminobenzoic acid ((**L1"**), 10 g, 2.0 eq.) was dissolved. To this solution, 10 drops of formic acid were added, followed by a dropwise addition of glyoxal (40 % aqueous solution, 4 mL, 1.0 eq.). After stirring the solution for 48 h at room temperature, the formed precipitate was collected using vacuum filtration. It was then washed with cold methanol (stored at 2 °C for 60 min) and dried, first in air and then under high vacuum to obtain the product (yield: 6.53 g, 63 %). It was used as obtained without further purification.

5.3.2   Synthesis of 1,3-Bis(4-carboxyphenyl)imidazolium chloride (**L1**)

The synthesis was conducted according to the described literature with slight modifications.[340]
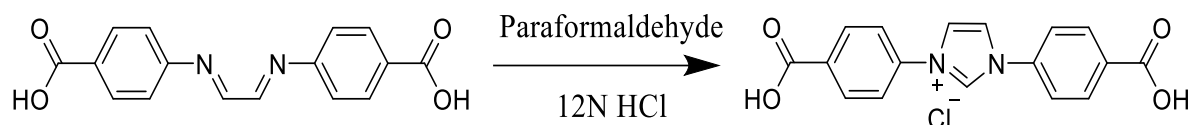
Scheme 19. Synthesis of 1,3-Bis(4-carboxyphenyl)imidazolium chloride (**L1**).

Paraformaldehyde (635 mg, 21.16 mmol, 1.25 eq.) was dissolved in 12 N HCl (2.1 mL, 25.33 mmol, 1.5 eq.) in dioxane (4 mL). This solution was added dropwise to a solution of **L1'** (5 g, 16.9 mmol) dissolved in anhydrous THF under argon atmosphere at 0 °C. The reaction mixture was then stirred at room temperature for 24 h. The precipitated light pink solid was collected by vacuum filtration, washed with THF and then with diethyl ether, and subsequently dried in vacuum (yield: 3.5 g, 67 %).

^{1}H NMR (500 MHz, DMSO-d_6, δ): 13.31 (s, 2H), 10.62 (s, 1H), 8.69 (d, $J = 1.7$ Hz, 2H), 8.22 (d, $J = 8.3$ Hz, 4H), 8.08 (d, $J = 8.2$ Hz, 4H).
**^{13}C NMR (126 MHz, DMSO-d_6, δ)**: 166.60, 138.14, 135.92, 132.57, 131.62, 131.57, 122.59, 122.41.
ESI-TOF m/z: (positive mode, MeOH, m/z) [M]$^+$ calc. for $C_{17}H_{13}N_2O_4$, 309.0870; found 309.0821.
IR (KBr): ν = 521 cm^{-1} (w), 626 cm^{-1} (w), 652 cm^{-1} (w), 690 cm^{-1} (w), 769 cm^{-1} (m), 793 cm^{-1} (w), 850 cm^{-1} (m), 895 cm^{-1} (w), 952 cm^{-1} (w), 1015 cm^{-1} (w), 1069 cm^{-1} (w), 1112 cm^{-1} (w), 1176 cm^{-1} (m), 1236 cm^{-1} (s), 1337 cm^{-1} (w), 1392 cm^{-1} (m), 1432 cm^{-1} (w), 1553 cm^{-1} (m), 1609 cm^{-1} (m), 1710 cm^{-1} (s), 2364 cm^{-1} (w), 2458 cm^{-1} (w), 2598 cm^{-1} (w), 2822 cm^{-1} (m), 2975 cm^{-1} (m), 3122 cm^{-1} (m), 3433 cm^{-1} (w).

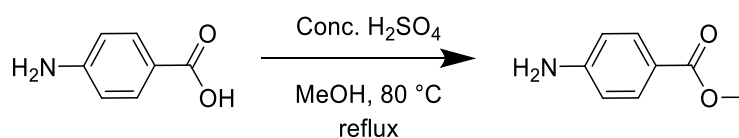### 5.3.3   Synthesis of Methyl 4-Aminobenzoate (**Me-L1"**)

5.3.3.1   Using Methanesulfonic Acid
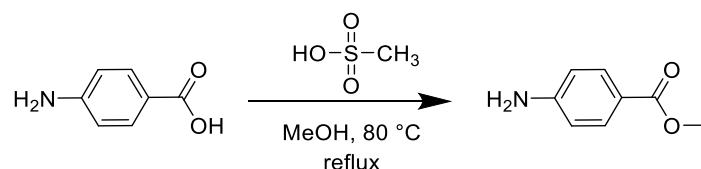
Scheme 20. Synthesis of methyl 4-aminobenzoate (**Me-L1"**) using methanesulfonic acid.

4-Aminobenzoic acid (5.0 g, 36.46 mmol) was dissolved in MeOH (50.0 mL) and subsequently catalytic amounts of methanesulfonic acid were added. The mixture was refluxed for 48 h at 80 °C after which a white powder could be seen deposited on the walls of the flask. The powder was then vacuum filtered and washed with cold MeOH to obtain methyl 4-aminobenzoate (**Me-L1"**) in 46 % yield. Though the synthesis was successful, the low yield motivated a change of acid and hence another synthesis with concentrated H_2SO_4 was attempted.

5.3.3.2   Using Concentrated H_2SO_4

Scheme 21. Synthesis of methyl 4-aminobenzoate (**Me-L1"**) using concentrated H_2SO_4.

The synthesis was conducted according to the described literature with slight modifications.[436]

To a solution of 4-aminobenzoic acid (10 g, 0.073 mol) in methanol (160 mL), H_2SO_4 (21.45 g, 0.218 mol) was added dropwise. The reaction mixture was stirred at 80 °C for 24 h under argon atmosphere after which white solid could be observed deposited on the flask walls. After the reaction mixture was cooled to room temperature, it was neutralized with 10 M NaOH solution until neutral pH was observed on pH strips. The solid was filtered and washed with methanol. The filtrate was concentrated under reduced pressure. The crude product was diluted with water and the aqueous layer was extracted three times with ethyl acetate. The combined organic layers were washed with brine, dried over $MgSO_4$ and filtered. Solvent was removed under reduced pressure to afford the product in 94 % yield.

^{1}H NMR (400 MHz, DMSO-d_6) δ 7.65 – 7.62 (m, 2H), 6.58 – 6.55 (m, 2H), 5.95 (s, 2H), 3.73 (s, 3H).

^{13}C NMR (101 MHz, DMSO-d_6) δ 166.34, 153.47, 131.05, 115.73, 112.65, 51.10

ESI-TOF m/z: (positive mode, MeOH (1 mL) + formic acid (1 μL), m/z) $[M+H]^+$ calc. for $C_8H_9NO_2$, 152.0706; found 152.0705.

IR (KBr): v = 508 cm^{-1} (w), 613 cm^{-1} (w), 639 cm^{-1} (w), 700 cm^{-1} (w), 771 cm^{-1} (m), 843 cm^{-1} (w), 973 cm^{-1} (w), 1118 cm^{-1} (m), 1175 cm^{-1} (m), 1199 cm^{-1} (m), 1287 cm^{-1} (s), 1315 cm^{-1} (m), 1436 cm^{-1} (s), 1514 cm^{-1} (m), 1598 cm^{-1} (s), 1638 cm^{-1} (m), 1686 cm^{-1} (s), 2942 cm^{-1} (w), 3228 cm^{-1} (m), 3340 cm^{-1} (m), 3411 cm^{-1} (m).

5.3.4 Synthesis of Dimethyl 4,4'-(((1E,2E)-ethane-1,2-diylidene) Bis(azaneylylidene)) Dibenzoate (Me-L1')
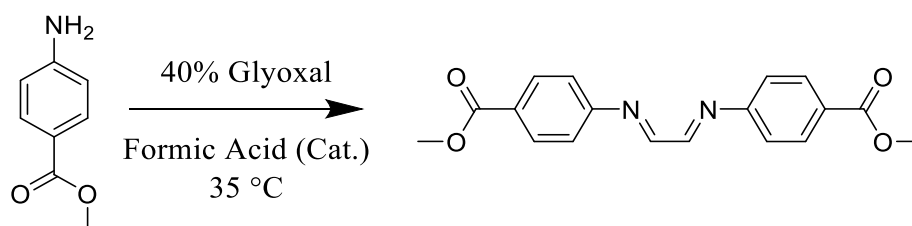
Scheme 22. Synthesis of dimethyl 4,4'-(((1E,2E)-ethane-1,2-diylidene) bis(azaneylylidene)) dibenzoate (**Me-L1'**).

In 15 mL methanol, methyl 4-aminobenzoate ((**Me-L1''**), 0.5 g, 3.3 mmol, 2.0 eq.) was dissolved. To this solution, 10 drops of formic acid were added, followed by a dropwise addition of glyoxal (40 % aqueous solution, 0.2 mL, 1.7 mmol, 1.0 eq.). After stirring the solution for 48 h at 35 °C, the formed precipitate was collected using vacuum filtration. It was then washed with cold methanol (stored at 2 °C for 60 min) and dried, first in air and then under high vacuum to obtain the product (yield: 0.38 g, 68 %). It was used as obtained without further purification.

5.3.5 Synthesis of 1,3-Bis(4-(methoxycarbonyl)phenyl)-1H-imidazol-3-ium Chloride (**MeL1**)
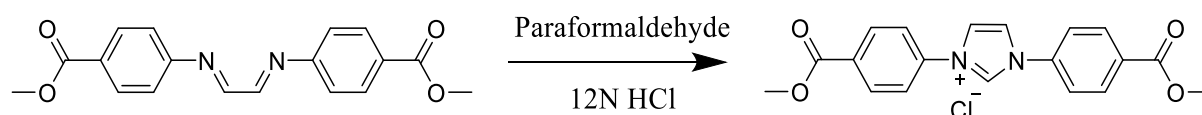
Scheme 23. Synthesis of 1,3-bis(4-(methoxycarbonyl)phenyl)-1H-imidazol-3-ium chloride (**MeL1**).

Paraformaldehyde (21.0 mg, 0.70 mmol, 1.25 eq.) was dissolved in 12 N HCl (72.0 μL, 0.83 mmol, 1.5 eq.) in dioxane (0.15 mL). This solution was added dropwise to a solution of **Me-L1'** (0.18 g, 0.55 mmol) dissolved in anhydrous THF (3.5 mL) under nitrogen atmosphere at 0 °C. The reaction

mixture was then stirred at room temperature for 48 h. The precipitated solid was collected by vacuum filtration, washed with THF and then diethyl ether, and then dried under vacuum (yield: 0.11 g, 61 %).

^{1}H NMR (500 MHz, DMSO-d_6) δ 10.76 (s, 1H), 8.74 (d, J = 1.5 Hz, 2H), 8.28 – 8.22 (m, 4H), 8.19 – 8.13 (m, 4H), 3.94 – 3.90 (m, 6H).

^{13}C NMR (126 MHz, DMSO-d_6) δ 164.22, 137.05, 134.71, 130.08, 129.88, 121.34, 120.99, 51.69.

ESI-TOF m/z: (positive mode, MeOH (1 mL), m/z) [M]$^+$ calc. for $C_{19}H_{17}N_2O_4$, 337.1183; found 337.1234.

IR (KBr): v = 508 cm^{-1} (w), 622 cm^{-1} (w), 688 cm^{-1} (w), 766 cm^{-1} (s), 829 cm^{-1} (w), 862 cm^{-1} (m), 965 cm^{-1} (m), 1016 cm^{-1} (m), 1070 cm^{-1} (m), 1121 cm^{-1} (s), 1195 cm^{-1} (m), 1258 cm^{-1} (s), 1305 cm^{-1} (s), 1436 cm^{-1} (m), 1554 cm^{-1} (s), 1607 cm^{-1} (m), 1702 cm^{-1} (s), 1724 cm^{-1} (s), 1943 cm^{-1} (w), 2149 cm^{-1} (w), 2853 cm^{-1} (m), 2893 cm^{-1} (m), 2954 cm^{-1} (m), 3106 cm^{-1} (m), 3168 cm^{-1} (m), 3408 cm^{-1} (w)
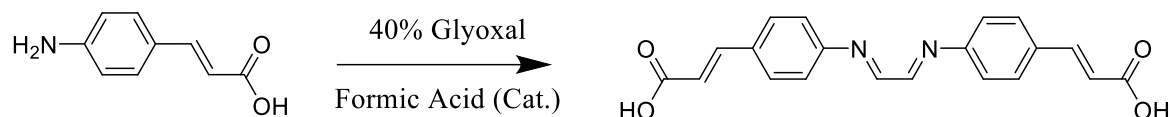
5.3.6   Synthesis of 4-Aminocinnamic Acid (**L2"**) from 4-Nitrocinnamic Acid
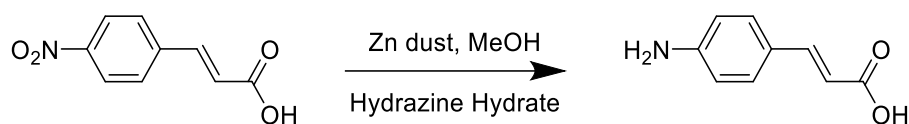
Scheme 24. Synthesis of 4-aminocinnamic acid (L2") from 4-nitrocinnamic acid.[437]

A suspension of 4-nitrocinnamic acid (1.93 g, 10 mmol) and Zn dust (11.3 g, 20 mmol) in methanol (10 mL) was stirred under N$_2$ with hydrazine hydrate (55 %, 10 mL) at RT. After 10 h of reaction, it was filtered through celite. The organic layer was evaporated, and the residue was dissolved in CHCl$_3$. It was then washed with brine (saturated NaCl) to remove excess hydrazine hydrate. The organic layer was evaporated and dried to try to obtain the desired product. However, no product was obtained.

5.3.7   Synthesis of (2E,2'E)-3,3'-((((1E,2E)-ethane-1,2-diylidene) Bis(azaneylylidene)) Bis(4,1-phenylene))diacrylic Acid (**L2'**)

Scheme 25. Synthesis of (2E,2'E)-3,3'-((((1E,2E)-ethane-1,2-diylidene) bis(azaneylylidene)) bis(4,1-phenylene))diacrylic acid (**L2'**).

In 10 mL methanol, 4-aminocinnamic acid ((**L2"**), 3.0 g, 2.0 eq.) was dissolved. To this solution, 10 drops of formic acid were added, followed by a dropwise addition of glyoxal (40 % aqueous solution, 1.1 mL, 1.0 eq.). After stirring the solution for 48 h at room temperature, the formed precipitate was collected using vacuum filtration. It was then washed with cold methanol (stored at 2 °C for 60 min) and dried, first in air and then under high vacuum to obtain the black solid product (yield: 0.98 g, 47 %). It was used as obtained without further purification while showing major solubility issues.

IR (ATR): v = 535 cm^{-1} (w), 674 cm^{-1} (w), 828 cm^{-1} (w), 981 cm^{-1} (w), 1017 cm^{-1} (w), 1177 cm^{-1} (s), 1264 cm^{-1} (m), 1307 cm^{-1} (m), 1379 cm^{-1} (m), 1418 cm^{-1} (m), 1514 cm^{-1} (s), 1598 cm^{-1} (s), 1631 cm^{-1} (s), 1686 cm^{-1} (s), 2583 cm^{-1} (w), 2926 cm^{-1} (m), 3036 cm^{-1} (m), 3398 cm^{-1} (m)

Table 16. The solubility status of **L2'** tested with different solvents.

| Ent	Solvent	Solubility Status	Ent	Solvent	Solubility Status
1	THF	No	7	H_2O	No
2	MeOH	No	8	DCM	No
3	$CHCl_3$	No	9	HFIP	No
4	DMSO	Yes, partially	10	EtAc	No
5	DMF	No	11	Hexane	No
6	Toluene	No			

5.3.8   Synthesis of 1,3-Bis(4-((E)-2-carboxyvinyl)phenyl)-1H-imidazol-3-ium Chloride (**L2**)
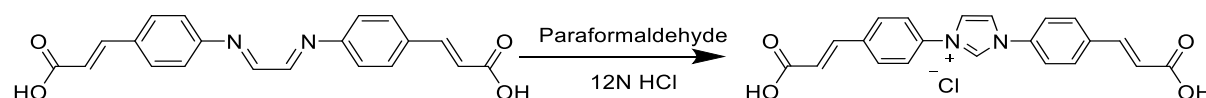
Scheme 26. Synthesis of 1,3-bis(4-((E)-2-carboxyvinyl)phenyl)-1H-imidazol-3-ium chloride (**L2**).

Paraformaldehyde (33.0 mg, 1.13 mmol, 1.25 eq.) was dissolved in 12 N HCl (45 μL, 1.36 mmol, 1.5 eq.) in dioxane (80 μL). This solution was added dropwise to a solution of **L2'** (0.32 g, 0.91 mmol) dissolved in anhydrous THF under argon atmosphere at 0 °C. The reaction mixture was then stirred at room temperature for 24 h. The precipitated brownish-black powder was collected by vacuum filtration, washed with THF and then diethyl ether, and then dried in vacuum. However, the powder was insoluble in most solvents and hence characterization with NMR or ESI-TOF was not possible.

IR (KBr): v = 589 cm^{-1} (w), 671 cm^{-1} (w), 802 cm^{-1} (w), 872 cm^{-1} (w), 1024 cm^{-1} (w), 1097 cm^{-1} (w), 1158 cm^{-1} (w), 1262 cm^{-1} (w), 1402 cm^{-1} (w), 1459 cm^{-1} (m), 1509 cm^{-1} (m), 1542 cm^{-1} (m), 1560 cm^{-1} (m), 1636 cm^{-1} (m), 1870 cm^{-1} (w), 2342 cm^{-1} (m), 2364 cm^{-1} (m), 2853 cm^{-1} (m), 2923 cm^{-1} (m), 2960 cm^{-1} (m), 3434 cm^{-1} (s).

5.3.9   Synthesis of Methyl (E)-3-(4-aminophenyl)acrylate (**Me-L2"**)
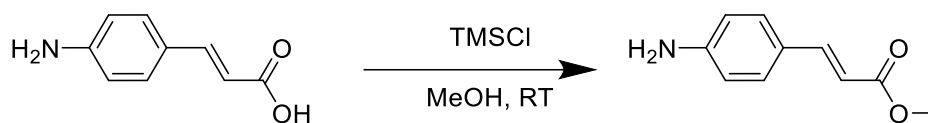
Scheme 27. Synthesis of methyl (E)-3-(4-aminophenyl)acrylate (**Me-L2"**).

The synthesis was conducted according to the described literature with slight modifications.[438]
L2" (5.00 g, 30.64 mmol) was mixed in methanol (50 mL) in a two-neck flask round bottom flask under nitrogen, to obtain a mixture in suspended state. TMSCl (7.6 mL, 60 mmol, 2 eq.) was added dropwise with constant stirring at room temperature. The mixture became clear after complete addition of TMSCl and after some time the solid started separating out. The mixture was stirred for 24 h at room temperature. The solvent was evaporated, and crude sample was dried under vacuum. Thus, prepared compound was treated with ammonia and the compound was extracted with ethyl acetate. The collecting ethyl acetate organic layer was dried over $MgSO_4$, and it was then evaporated. Thus, compound obtained was found to be **Me-L2"** (yield: 5.3 g, 97 %). TLC analysis (CH_2Cl_2/MeOH, 13:1)

¹H NMR (400 MHz, DMSO-*d₆*) δ 7.48 (d, *J* = 15.8 Hz, 1H), 7.41 – 7.33 (m, 2H), 6.60 – 6.49 (m, 2H), 6.22 (d, *J* = 15.8 Hz, 1H), 5.75 (s, 2H), 3.67 (s, 3H).

¹³C NMR (101 MHz, DMSO-*d₆*) δ 167.38, 151.57, 145.54, 130.19, 121.22, 113.53, 110.56, 50.96.

ESI-TOF m/z: (positive mode, MeOH (1 mL) + formic acid (1 μL), m/z) [M+H]⁺ calc. for $C_{10}H_{11}NO_2$, 178.0863; found 178.0859.

IR (KBr): *v* = 520 cm⁻¹ (m), 579 cm⁻¹ (w), 825 cm⁻¹ (m), 978 cm⁻¹ (m), 1012 cm⁻¹ (w), 1173 cm⁻¹ (s), 1307 cm⁻¹ (s), 1328 cm⁻¹ (m), 1434 cm⁻¹ (s), 1515 cm⁻¹ (s), 1594 cm⁻¹ (s), 1625 cm⁻¹ (s), 1690 cm⁻¹ (s), 2948 cm⁻¹ (w), 3222 cm⁻¹ (w), 3355 cm⁻¹ (s), 3444 cm⁻¹ (m)

5.3.10 Synthesis of Dimethyl 3,3'-(((((1E,2E)-ethane-1,2-diylidene) bis(azaneylylidene)) bis(4,1-phenylene))(2E,2'E)-diacrylate (**Me-L2'**)
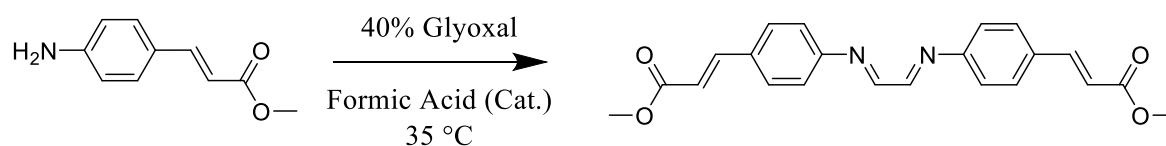

Scheme 28. Synthesis of dimethyl 3,3'-(((((1E,2E)-ethane-1,2-diylidene) bis(azaneylylidene)) bis(4,1-phenylene))(2E,2'E)-diacrylate (**Me-L2'**).

In 15 mL methanol, methyl-4-aminocinnamate ((**Me-L2''**), 0.5 g, 3.0 mmol, 2.0 eq.) was dissolved. To this solution, 10 drops of formic acid were added, followed by a dropwise addition of glyoxal (40 % aqueous solution, 0.16 mL, 1.5 mmol, 1.0 eq.). After stirring the solution for 48 h at 35 °C, the formed precipitate was collected using vacuum filtration. It was then washed with cold methanol (stored at 2 °C for 60 min) and dried, first in air and then under high vacuum to obtain product (yield: 0.37 g, 66 %). It was used as obtained without further purification.

ESI-TOF m/z: (positive mode, THF, m/z) [M] calc. for $C_{22}H_{20}N_2O_4$, 376.1418; found 376.2739.

IR (KBr): *v* = 516 cm⁻¹ (w), 821 cm⁻¹ (s), 859 cm⁻¹ (w), 981 cm⁻¹ (s), 1066 cm⁻¹ (s), 1168 cm⁻¹ (s), 1267 cm⁻¹ (s), 1365 cm⁻¹ (s), 1435 cm⁻¹ (s), 1516 cm⁻¹ (s), 1600 cm⁻¹ (s), 1709 cm⁻¹ (s), 2363 cm⁻¹ (w), 2838 cm⁻¹ (w), 2947 cm⁻¹ (m), 2993 cm⁻¹ (m), 3357 cm⁻¹ (m)

5.3.11 Synthesis of 1,3-Bis(4-((E)-3-methoxy-3-oxoprop-1-en-1-yl)phenyl)-1H-imidazol-3-ium chloride (**Me-L2**)
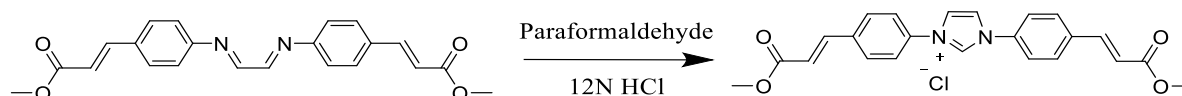
Scheme 29. Synthesis of 1,3-bis(4-((E)-3-methoxy-3-oxoprop-1-en-1-yl)phenyl)-1H-imidazol-3-ium chloride (**Me-L2**).

Paraformaldehyde (15.0 mg, 0.6 mmol, 1.25 eq.) was dissolved in 12 N HCl (0.06 mL, 0.7 mmol, 1.5 eq.) in dioxane (150 μL). This solution was added dropwise to a solution of **Me-L2'** (0.15 g, 0.4 mmol) dissolved in anhydrous THF under argon atmosphere at 0 °C. The reaction mixture was then stirred at room temperature for 24 h. The precipitated solid was collected by vacuum filtration, washed with THF and then diethyl ether, and then dried in vacuum (yield: 0.12 g, 77 %).

¹H NMR (400 MHz, DMF-*d₇*) δ 10.93 (t, *J* = 1.7 Hz, 1H), 8.83 (d, *J* = 1.6 Hz, 2H), 8.29 – 8.20 (m, 4H), 8.18 – 8.10 (m, 4H), 7.83 (d, *J* = 16.1 Hz, 2H), 6.85 (d, *J* = 16.1 Hz, 2H), 3.82 (s, 6H).

¹³C NMR (101 MHz, DMF-*d₇*) δ 166.89, 142.98, 136.45, 136.33, 135.51, 130.36, 122.84, 122.44, 120.49, 51.65.

ESI-TOF m/z: (positive mode, MeOH, m/z) [M] calc. for $C_{23}H_{21}N_2O_4$, 389.1496; found 389.1512.

IR (KBr): v = 523 cm⁻¹ (w), 821 cm⁻¹ (w), 983 cm⁻¹ (w), 1173 cm⁻¹ (s), 1203 cm⁻¹ (s), 1327 cm⁻¹ (m), 1435 cm⁻¹ (m), 1512 cm⁻¹ (m), 1549 cm⁻¹ (m), 1600 cm⁻¹ (s), 1637 cm⁻¹ (s), 1709 cm⁻¹ (s), 2948 cm⁻¹ (m), 3415 cm⁻¹ (s)

5.3.12 Synthesis of 4-(4'-Aminostilbene) Carboxylic Acid (L3")
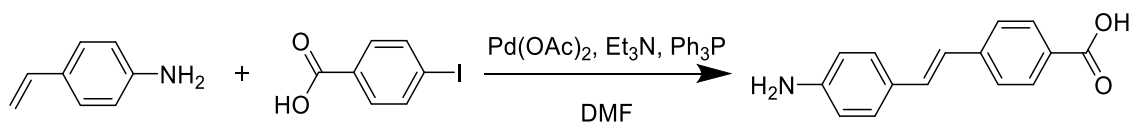
Scheme 30. Synthesis of 4-(4'-aminostilbene) carboxylic acid (**L3"**).[439]

4-Vinyl aniline (90 %, 3.5 g, 26.0 mmol) and 4-iodobenzoic acid (6.5 g, 26.0 mmol) were dissolved in DMF (30.0 mL) and triethylamine (30.0 mL). The solution was refluxed in the presence of triphenylphosphine (70.7 mg, 0.25 mmol) and palladium(II) acetate (58.32 mg, 0.25 mmol) for 48 h. After removing the solvent, ethyl acetate (200 mL) was added, and the soluble part was extracted with 2 M hydrochloric acid solution (100 mL x 3). Neutralizing the aqueous layer with an aqueous sodium hydroxide solution yielded a precipitate of 4-(4'-aminostilbene) carboxylic acid (yellow powder, 2.08 g, 33.0 %), while showing major solubility issues.

¹H NMR (400 MHz, DMSO-*d₆*) δ 7.84 (d, *J* = 7.8 Hz, 2H), 7.40 (d, *J* = 7.9 Hz, 2H), 7.27 (d, *J* = 8.1 Hz, 2H), 7.10 – 6.83 (m, 2H), 6.56 (d, *J* = 8.1 Hz, 2H), 5.32 (s, 2H).

¹³C NMR (101 MHz, DMSO-*d₆*) δ 170.90, 149.28, 138.91, 129.93, 129.66, 128.08, 125.07, 123.18, 114.36.

ESI-TOF m/z: (negative mode, MeOH, m/z) [M-H]⁻ calc. for $C_{15}H_{13}NO_2$, 238.0863; found 238.0781.

IR (ATR): v = 531 cm⁻¹ (w), 648 cm⁻¹ (w), 697 cm⁻¹ (w), 781 cm⁻¹ (w), 818 cm⁻¹ (m), 850 cm⁻¹ (m), 895 cm⁻¹ (w), 962 cm⁻¹ (w), 1015 cm⁻¹ (w), 1180 cm⁻¹ (m), 1280 cm⁻¹ (m), 1386 cm⁻¹ (s), 1518 cm⁻¹ (s), 1540 cm⁻¹ (s), 1574 cm⁻¹ (s), 1681 cm⁻¹ (w), 2850 cm⁻¹ (w), 2923 cm⁻¹ (w), 3354 cm⁻¹ (s)

Table 17. The solubility status of **L3"** tested with different solvents.

Ent	Solvent	Solubility Status	Ent	Solvent	Solubility Status
1	THF	No	7	1,4-dioxane	No
2	MeOH	Yes, partially	8	DCM	No
3	CHCl₃	No	9	Et₂O	No
4	DMSO	Yes, partially	10	EtAc	No
5	DMF	No	11	Hexane	No
6	Toluene	No	12	ACN	No

5.3.13 Synthesis of 4,4'-((1E,1'E)-((((1E,2E)-ethane-1,2-diylidene) bis(azaneylylidene)) bis(4,1-phenylene))bis(ethene-2,1-diyl))dibenzoic acid (L3')
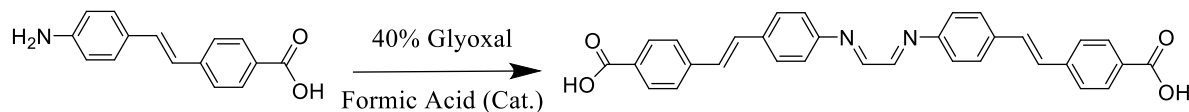
Scheme 31. Synthesis of 4,4'-((1E,1'E)-((((1E,2E)-ethane-1,2-diylidene) bis(azaneylylidene)) bis(4,1-phenylene))bis(ethene-2,1-diyl))dibenzoic acid (**L3'**).

The 4-(4'-aminostilbene) carboxylic acid (**L3"**) was insoluble in different solvents (see **Table 17**) other than in MeOH in which the solubility was partial. After making solubility tests, the solubility of **L3"** in MeOH was ascertained to be 1 g per 150 mL. Hence, in 15 mL methanol, **L3"** (0.1 g, 0.4 mmol, 2.0 eq.) was dissolved. To this solution, 10 drops of formic acid were added, followed by a dropwise addition of glyoxal (40 % aqueous solution, 21 µL, 0.2 mmol, 1.0 eq.). After stirring the solution for 48 h at RT, the formed precipitate was collected using vacuum filtration. It was then washed with cold methanol (stored at 2 °C for 60 min) and dried, first in air and then under high vacuum to obtain product (yield: 0.02 g, 10 %).

^{1}H NMR (400 MHz, DMSO-d_6) δ 12.82 (s, 2H), 7.90 (d, J = 8.4 Hz, 4H), 7.67 (d, J = 8.5 Hz, 4H), 7.57 (d, J = 8.7 Hz, 4H), 7.35 (d, J = 16.3 Hz, 2H), 7.12 (q, J = 7.2 Hz, 4H), 4.99 (s, 3H).
^{13}C NMR (101 MHz, DMSO-d_6) δ 204.15, 167.55, 149.53, 131.16, 130.20, 128.34, 126.55, 117.34, 111.57, 84.86, 54.86.
IR (ATR): v = 537 cm^{-1} (w), 597 cm^{-1} (w), 769 cm^{-1} (w), 815 cm^{-1} (w), 930 cm^{-1} (m), 1056 cm^{-1} (m), 1182 cm^{-1} (m), 1287 cm^{-1} (m), 1513 cm^{-1} (m), 1595 cm^{-1} (s), 1674 cm^{-1} (s), 2530 cm^{-1} (w), 2825 cm^{-1} (w), 2931 cm^{-1} (w)

5.3.14 Synthesis of Methyl (E)-4-(4-aminostyryl)benzoate (Me-L3")
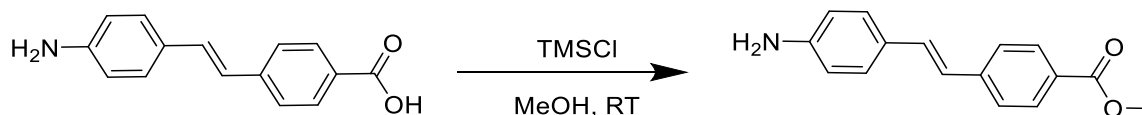
Scheme 32. Synthesis of methyl (E)-4-(4-aminostyryl)benzoate (**Me-L3"**).

The synthesis was conducted according to the described literature with slight modifications.[438]
L3" (0.5 g, 2.1 mmol) was mixed in methanol (10 mL) in a two-neck flask round bottom flask under nitrogen, to obtain a mixture in suspended state. TMSCl (0.53 mL, 4.2 mmol, 2 eq.) was added dropwise with constant stirring at room temperature. The stirring was continued for 5 days during which some of the solid started separating out. The solvent was evaporated, and crude sample was dried under vacuum. Though the compound obtained was found to be **Me-L3"**, the prepared compound needed further purification. (yield: 5.3 g, 97 %). TLC analysis (CH$_2$Cl$_2$/MeOH, 13:1).

^{1}H NMR (400 MHz, DMSO-d_6) δ 7.92 – 7.85 (m, 2H), 7.61 (d, J = 7.9 Hz, 2H), 7.36 – 7.26 (m, 6H), 7.21 (s, 1H), 6.96 (d, J = 16.6 Hz, 1H), 6.67 (s, 5H), 6.58 (s, 2H), 5.43 (s, 2H), 3.96 – 3.74 (m, 3H).
^{13}C NMR (101 MHz, DMSO-d_6) δ 171.43, 149.40, 142.98, 132.17, 129.55, 128.20, 125.69, 121.36, 113.84, 51.92.
ESI-TOF m/z: (positive mode, THF:MeOH 9:1 + 1 µL formic acid, m/z) [M+H]$^+$ calc. for C$_{16}$H$_{15}$NO$_2$, 254.1176; found 254.1170.

IR (KBr): ν = 572 cm^{-1} (w),814 cm^{-1} (w), 964 cm^{-1} (w), 1111 cm^{-1} (w), 1177 cm^{-1} (w), 1284 cm^{-1} (w), 1399 cm^{-1} (w), 1434 cm^{-1} (w), 1514 cm^{-1} (w), 1668 cm^{-1} (s), 2282 cm^{-1} (w), 2852 cm^{-1} (w), 2923 cm^{-1} (w), 3207 cm^{-1} (m), 3364 cm^{-1} (s), 3436 cm^{-1} (s)
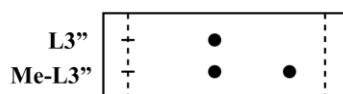

Figure 60. TLC analysis of the **L3"** (R_f = 0.44) and the obtained **Me-L3"** (R_f =0.82) (CH$_2$Cl$_2$/MeOH, 13:1)

5.3.15 Synthesis of the NHC-based MOF

The NHC-MOFs were synthesized as per literature[423] with slight modifications.

Describing **Table 18**, **Ent 3** as an example, in a headspace vial (10 mL), **L1** (120 mg, 0.35 mmol), Zn(NO$_3$)$_2$·6H$_2$O (104 mg, 0.35 mmol), and [Cu(CH$_3$CN)$_4$]PF$_6$ (65 mg, 0.175 mmol), were combined and dissolved in dry DMF (3 mL) in the glovebox. The vial was sealed, and the mixture was heated at 120 °C for 10 d. After 10 days, the mixture was cooled slowly (10 °C hr^{-1}) till room temperature, after which the precipitated powder was washed with fresh DMF and methanol, and then dried under vacuum to obtain the **NHC-MOF3** (Yield: 235 mg).

For **Ent 6** and **7**, the reaction was conducted in Teflon-lined autoclaves with procedure as described above for **Ent 3**.

IR (KBr, NHC-MOF3): ν = 484 cm^{-1} (w), 523 cm^{-1} (w), 584 cm^{-1} (w), 624 cm^{-1} (w), 696 cm^{-1} (w), 725 cm^{-1} (w), 750 cm^{-1} (w), 783 cm^{-1} (m), 844 cm^{-1} (w), 866 cm^{-1} (w), 951 cm^{-1} (w), 1017 cm^{-1} (w), 1072 cm^{-1} (w), 1184 cm^{-1} (w), 1258 cm^{-1} (m), 1383 cm^{-1} (s), 1553 cm^{-1} (s), 1622 cm^{-1} (s), 2362 cm^{-1} (w), 3091 cm^{-1} (m), 3429 cm^{-1} (m).

Table 18. Reaction conditions for the synthesis of the different NHC-MOFs.

Ent	NHC-MOF Code	L1		Zn(NO$_3$)$_2$ 6H$_2$O		[Cu(CH$_3$CN)$_4$]PF$_6$		DMF	Yield [mg]
		Moles [mmol]	Weight [mg]	Moles [mmol]	Weight [mg]	Moles [mmol]	Weight [mg]	Volume [mL]	
1	NHC-MOF1	0.580	200	0.580	173	0.290	108	5	157
2	NHC-MOF2	0.580	200	0.580	173	0.290	108	5	183
3	NHC-MOF3	0.350	120	0.350	104	0.175	65	3	235
4	NHC-MOF4	0.350	120	0.350	104	0.175	65	3	56
5	NHC-MOF5	0.350	120	0.350	104	0.175	65	3	67
6	NHC-MOFI[a]	0.300	100	0.300	87	0.145	54	5	68
7	NHC-MOFII[a]	0.580	200	0.580	173	0.290	108	5	70

[a]Synthesis of the **NHC-MOFI** and **NHC-MOFII** was conducted separately by research partners from the group of Prof. Dr. Harald Krautscheid at the Institute of Inorganic Chemistry, Universität Leipzig, who carried out the NHC-MOF preparation using Teflon-lined autoclaves (see **Chapter 7.2.13** for more details).

5.3.16 Identifying the Metal Contents *via* FAAS

For sample preparation, exactly weighed NHC-MOF powders were reduced to ashes at 550 °C for 20 h. The residues were taken up in 10 mL of 20 % nitric acid, transferred into a 100 mL volumetric flask

and filled up using double-distilled water. The resulting samples were directly injected in the AAS or if necessary, after dilution with 2 % nitric acid and quantitation was realized *via* external calibration.

Table 19. Atomic ratio of Zn and Cu in NHC-MOFs determined by FAAS.

Ent	NHC-MOF Code	Copper (Cu)		Zinc (Zn)		Cu:Zn Atomic Ratio
		Wt.%	Atomic Ratio	Wt.%	Atomic Ratio	
1	NHC-MOF1	3.75	0.13	11.75	0.39	0.33 : 1
2	NHC-MOF2	3.84	0.13	10.85	0.36	0.37 : 1
3	NHC-MOF3	4.66	0.16	8.97	0.30	0.53 : 1
4	NHC-MOF4	5.14	0.18	10.49	0.35	0.51 : 1
5	NHC-MOF5	2.12	0.07	8.97	0.30	0.24 : 1
6	NHC-MOFI[a]	2.80	0.10	9.20	0.31	0.31 : 1
7	NHC-MOFII[a]	2.40	0.08	10.50	0.35	0.24: 1

[a]Synthesis of the **NHC-MOFI** and **NHC-MOFII** was conducted separately by research partners from the group of Prof. Dr. Harald Krautscheid at the Institute of Inorganic Chemistry, Universität Leipzig, who carried out the NHC-MOF preparation using Teflon-lined autoclaves (see **Chapter 7.2.13** for more details).

5.3.17   Sonication Thermal Control

An ultrasonication reaction vessel was dried overnight in an oven at 120 °C and attached to the sonicator, followed by the addition of THF:MeOH (9.67:0.33, 10 mL). The reaction vessel was immersed in a beaker with ice cold water depending on the method of cooling. A single sonication cycle ran for 90 min so cooling was conducted *via* two methods, *1ce* cool, i.e., cooled at the very beginning, and *2ce* cool, i.e., cooled once at the beginning and once after 45 min. The average room temperature (RT) was 22 °C. Sonication was conducted in cycles with the following conditions: 5 s Pulse, 10 s Pause for 30 min (actual sonication time = 90 min) at amplitude of 30 %. After the end of a cycle, a digital thermometer was dipped into the solvent mixture to ascertain the solvent temperature. For our experiment, 10 such cycles were conducted each with *1ce* cooling and the *2ce* cooling and the temperature recorded.
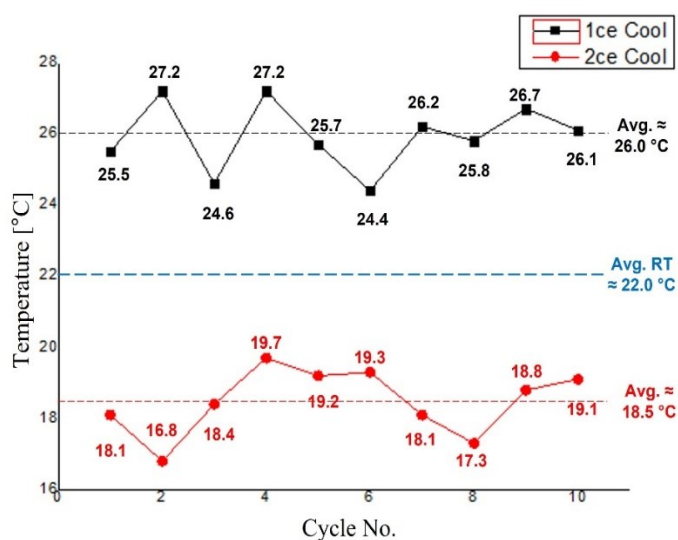

Figure 61. Control sonication conducted in the presence of solvent THF to ascertain temperature changes on multiple cycles of sonication.

5.3.18 Mechanochemical Activation of NHC-MOFs by Ultrasonication

5.3.18.1 ^1H NMR Investigations of Ultrasound-Induced Mechanochemical Activation

Table 20. Reaction conditions for the ultrasonication experiments conducted with different NHC-MOFs.

SonX	NHC-MOF		NaAsc		Phenylacetylene		Benzylazide		Son Cycles
	Code	Weight [mg]	Moles [mmol]	Weight [mg]	Moles [mmol]	Weight [mg]	Moles [mmol]	Weight [mg]	
Son1	NHC-MOF1	20	-	-	0.76	77	0.76	103	10
Son2	NHC-MOF1	20	-	-	0.76	77	0.76	103	10
Son3	NHC-MOF1	10	0.024	5	0.39	39	0.39	52	15
Son4	NHC-MOF3	20	-	-	0.76	77	0.76	103	20
Son5	NHC-MOFII[a]	10	-	-	0.39	39	0.39	52	20
Son6	NHC-MOF5	10	-	-	0.39	39	0.39	52	25

[a]Synthesis of **NHC-MOFII** was conducted separately by research partners from the group of Prof. Dr. Harald Krautscheid at the Institute of Inorganic Chemistry, Universität Leipzig, who carried out the NHC-MOF preparation using Teflon-lined autoclaves (see **Chapter 7.2.13** for more details).

An ultrasonication reaction vessel was dried overnight in an oven at 120 °C and attached to the sonicator. After 3x cycles of vacuum and flushing with N_2, the synthesized NHC-MOF (~10 wt.% of total weight of benzylazide (**10**) and phenyacetylene (**11**)) was added to the vessel in counterflow of N_2, followed by the addition of THF-d_8:MeOH (9.67:0.33, 10 mL). In the cases in which sodium ascorbate (NaAsc) was required, it was added at this point (3 eq. of Cu in NHC-MOF) in the counterflow of N_2. This mixture was then degassed with N_2 for 15 min to dispel any presence of O_2. Using an Eppendorf pipette, (**10**) and (**11**) (**Table 20**) were added to the flask under a counterflow of N_2 and the reaction vessel was then immersed in a beaker with ice cold water. Sonication was conducted in cycles with the following conditions: 5 s Pulse, 10 s Pause for 30 min (actual sonication time = 90 min) at amplitude of 30 %. With inclusion of a 45 min rest time, the total time of a single cycle of sonication was 135 min. For our experiment, up to 25 such cycles were conducted (**Table 20**) with ^1H NMR conducted at regular intermediate cycle. The ultrasonication experiment conducted used the *2ce cooling* system. The peak at 4.34 ppm (marked by the red box) belonging to the -CH_2- of the benzylazide was used as the reference and the percent conversion was calculated by utilizing the ratio of the integral of the reactant and the product peaks (5.58 ppm (green box) and 8.11 ppm (blue box)) (see **Appendix**).

For product: 1-benzyl-4-phenyl-1*H*-1,2,3-triazole (**12**):
^1H NMR (400 MHz, THF-d_8, δ): 8.11 (s, 1H), 5.58 (s, 2H).

5.3.18.2 ^1H NMR Investigations of Control Experiments

For control experiments, a two-necked flask attached to a reflux condenser was subjected to 3x cycles heating under vacuum and flushing with N_2. The peak at 4.34 ppm (marked by the red box) belonging to the -CH_2- of the benzylazide (**10**) was used as reference and the percent conversion was calculated by utilizing the ratio of the integral of the reactant and the product peaks (5.58 ppm (green box) and 8.11 ppm (blue box)) (see **Appendix**).

For product: 1-benzyl-4-phenyl-1*H*-1,2,3-triazole (**12**):

^{1}H NMR (400 MHz, THF-d_8, δ): 8.11 (s, 1H), 5.58 (s, 2H).

5.3.18.2.1 In the Presence of NHC-MOF

For controls in the presence of NHC-MOF, the synthesized NHC-MOF (10 wt.% of total weight of benzylazide (**10**) and phenylacetylene (**11**)) was added to the flask in counterflow of N$_2$ and was followed by the addition of THF-d_8:MeOH (9.67:0.33, 5mL). This was then degassed with N$_2$ for 15 min to dispel any presence of O$_2$. Using an Eppendorf pipette, (**10**) and (**11**) (**Table 21**) were added to the flask under the counterflow of N$_2$. The reactions were conducted at RT (SonX.Cont.RT) and at 60 °C (SonX.Cont.60C).

Table 21. Reaction conditions for the control experiments for the conducted ultrasonication experiments with different NHC-MOFs.

SonX	Control Code	NHC-MOF Weight [mg]	Phenylacetylene		Benzylazide		Time
			Moles [mmol]	Weight [mg]	Moles [mmol]	Weight [mg]	
Son1	Son1.Cont.60C	20	0.76	77	0.76	103	50 h
	Son1.Cont.RT						7d
Son4	Son4.Cont.60C	5	0.19	19	0.19	26	55 h
	Son4.Cont.RT						50 h
Son5	Son5.Cont.60C	10	0.39	39	0.39	52	50 h
	Son5.Cont.RT						65 h

5.3.18.2.2 In the Absence of Any NHC-MOF

For control experiment at 60 °C without any NHC-MOF, THF-d_8:MeOH (9.67:0.33, 5mL) was degassed with N$_2$ for 15 min to dispel any presence of O$_2$. Using an Eppendorf pipette, phenylacetylene (38.5 mg, 0.375 mmol) (**11**) and benzylazide (51 mg, 0.375 mmol) (**10**) were added to the flask under the counterflow of N$_2$. The reaction was then conducted at 60 °C and a sample was collected at 25 h (see **Figure A52D**).

5.4 Mechanochemically Active Thermoplastic Polyurethane (TPU) Systems

5.4.1 Calculation of GPC for TPU

GPC was performed in tetrahydrofuran (THF) with an external calibration of polystyrene (PS) standards with a molecular weight range from 1,050 to 115,000 g mol^{-1}. The prepared samples had a concentration of 1-5 mg (sample) mL^{-1} (THF). From the GPC, the M_n and PDI of the samples were found and the rest calculated as follows:

➤ Calculating M$_{hard/soft}$

$$M_{hard/soft} = (\chi_{soft}.M_{soft} + \chi_{hard}.M_{hard}) / (\chi_{soft} + \chi_{hard}) \qquad \text{eq. (5.1)}$$

where M$_{soft}$ = 3150.26 g mol^{-1}, M$_{hard}$ = 340.38 g mol^{-1} and $\chi_{soft/hard}$ is ratio of hard and soft segments, i.e., for TPU70, χ_{soft} = 0.3 and χ_{hard} = 0.7.

> Calculate Degree of Polymerization (DP)
>
> $M_{n(GPC)} = DP * M_{hard/soft}$ eq. (**5.2**)

> Calculate Conversion (p)
>
> $DP = 1 (1-p)^{-1}$, since [OH]=[NCO] (1:1)   eq. (**5.3**)

5.4.2 Development Stage 1

Bis(hydroxy)-telechelic poly(tetrahydrofuran) pTHF (M_n = 2900 g mol^{-1}) (**16**) was weight directly (**Table 22**) into a 100 mL two-necked round bottom flask equipped with a big egg-shaped magnetic stirrer. Subsequently, the flask was attached to a high vacuum line and heated to 50 °C with a water bath for at least 1 hour. A second two-necked round bottom flask was heated under vacuum and purged with N$_2$ three times, after which dry THF was collected in the flask from the SPS (Solvent Purification System). Likewise, two 10 mL Schlenk tubes equipped with magnetic stirrer (long cylindrical) were also purged with N$_2$. 4,4'-methylenebis(phenylisocyanate) (MDI) (**17**) (**Table 22**) was weighed directly into one Schlenk tube and was subjected subsequently to vacuum/N$_2$ cycle for at least three times (without heating). The MDI was then dissolved in 3 mL THF by stirring. In parallel, 1,4-butanediol (BDO) (**18**) (**Table 22**) was placed in the second Schlenk tube *via* Eppendorf pipette and subjected to three vacuum/N$_2$ cycles (without heating). The (**18**) was then dissolved in 1 mL THF by stirring. Once the components were ready, the flask containing (**16**) was removed from vacuum and placed under N$_2$ environment. The (**17**) from the Schlenk tube was added to the pTHF flask and stirred for 5 min. Afterwards, an additional portion of 15 mL dry THF was added carefully by rinsing on the glass wall (to avoid bubbles) and the mixture stirred for 15 min at RT. Subsequently, two drops of 1,8-diazabicyclo[5.4.0]undec-7-ene (DBU) were added and the reaction mixture was stirred at room temperature. After 15 min, (**18**) is added to the reaction flask. The mixture was then allowed to stir for another 15 min before pouring into a Petri dish (if the mixture is too viscous, additional THF was added). The Petri dish was covered by its top and stored for minimum 5 d.

Table 22. Reaction conditions for the synthesis of thermoplastic polyurethane (TPU) as per Development Stage 1 (DS1).

Ent	Soft/Hard (mol ratio)	pTHF		MDI		BDO		
		Moles (mmol)	Weight (mg)	Moles (mmol)	Weight (mg)	Moles (mmol)	Weight (mg)	Volume (μL)
O-TPU30	70:30	2.19	6400	3.13	784	0.94	85	83
O-TPU40	60:40	2.14	6208	3.57	893	1.43	129	126
O-TPU50	50:50	2.07	6000	4.14	1036	2.07	186	183
O-TPU60	40:60	1.97	5727	4.94	1236	2.96	267	263
O-TPU70	30:70	1.83	5315	6.11	1529	4.27	385	379

5.4.3 Kinetic Experiment

The kinetic experiment was conducted according to the procedure described in Development Stage 1 for O-TPU50 (see **Table 22**). It was divided into three synthesis stages (see **Table 23**) with each part consisting of 15 min of experimental time. Samples were collected thrice from every synthesis stage under the counterflow of N$_2$, placed in a vial and methanol was added to extinguish the reaction. The

vial was then kept overnight to ensure removal of the solvents before preparation of GPC samples in THF.

Table 23. Detailing of sample collection for understanding the kinetics of a O-TPU50 synthesis as per procedure of Development Stage 1 (DS1, **Chapter 5.4.2**).

Ent	TPU Synthesis Stage	Sample Collected	Time passed in the reaction [min]	Weight of Sample [mg]
1	Addition of 15 mL THF after addition of MDI (**17**) to pTHF (**16**)	K-TPU50-1	5[a]	5.58
2		K-TPU50-2	10	4.34
3		K-TPU50-3	15	4.67
4	Addition of DBU	K-TPU50-4	20	4.66
5		K-TPU50-5	25	4.88
6		K-TPU50-6	30	5.38
7	Addition of BDO (**18**)	K-TPU50-7	35	N/A
8		K-TPU50-8	40	4.90
9		K-TPU50-9	45	4.93

[a]The first sample collection occurs at the 5th minute, immediately after the addition of the 15 mL THF to the reaction mixture as the waiting time after addition of MDI (**17**) to the pTHF (**16**) flask is 5 min before the THF is added.

5.4.4 Development Stage 2

Before the synthesis of the thermoplastic polyurethane (TPU), multiple preparatory steps were required. A day before, bis(hydroxy)-telechelic poly(tetrahydrofuran) pTHF (**16**) (M_n = 2900 g mol^{-1}, **Table 24**) was heated to 50 °C with a water bath and dried using the high vacuum line for at least 24 h in a two-necked flask. Previous to the synthesis, the commercially obtained 1,4-butanediol (**18**) (BDO, b.p. = 230 °C)[440] was freshly distilled in the presence of CaH$_2$ at 110 °C and 0.1 mbar pressure. Two Schlenk tubes were prepared in parallel with multiple cycles of heating under vacuum and purging with N$_2$. In one of the tubes, 4,4'-methylenebis(phenylisocyanate) (MDI) (**17**) (**Table 24**) was added and subjected subsequently to vacuum (without heating) and N$_2$ cycle for at least three times before the addition of 3 mL dry THF and stirring to dissolve the (**17**). In the other tube, the freshly distilled BDO was placed with an Eppendorf pipette and was also subjected subsequently to vacuum (without heating) and N$_2$ cycle for at least three times before the addition of 1 mL dry THF and stirring. Now that all components were ready, the synthesis of TPU could be initiated. The flask containing the (**16**) was purged with N$_2$ and (**17**) was added to this by the means of a syringe. After 5 min of stirring, an additional portion of 15 mL dry THF was added carefully by rinsing on the glass wall (to avoid bubbles). This reaction mixture was further stirred for 15 min. Subsequently, three drops of 1,8-diazabicyclo[5.4.0]undec-7-ene (DBU) were added to the reaction mixture and stirred for further 15 min. To this reaction mixture, (**18**) was added. The reaction mixture was stirred further till the mixture turned viscous enough that the magnetic stirrer stopped rotating, before pouring into a Petri dish (if the mixture is to viscous, additional THF can be added). The Petri dish was covered and stored in the dark for a minimum of 5 d.

Table 24. Reaction conditions for the synthesis of thermoplastic polyurethane (TPU) as per procedure of Development Stage 2 (DS2).

Ent	Soft/Hard (mol ratio)	pTHF		MDI		BDO		
		Moles (mmol)	Weight (mg)	Moles (mmol)	Weight (mg)	Moles (mmol)	Weight (mg)	Volume (µL)
TPU30	70:30	2.19	6400	3.13	784	0.94	85	83
TPU40	60:40	2.14	6208	3.57	893	1.43	129	126
TPU50	50:50	2.07	6000	4.14	1036	2.07	186	183
TPU60	40:60	1.97	5727	4.94	1236	2.96	267	263
TPU70	30:70	1.83	5315	6.11	1529	4.27	385	379

5.4.5   Development Stage 3

Before the synthesis of the thermoplastic polyurethane (TPU), multiple preparatory steps were required. A day before, bis(hydroxy)-telechelic poly(tetrahydrofuran) pTHF (6.0 g, 2.06 mmol, M_n = 2900 g mol^{-1}) (**16**) was heated to 50 °C with a water bath and dried using the high vacuum line for at least 24 h in a two-necked flask. Previous to the synthesis, the commercially obtained 1,4-butanediol (**18**) (BDO, b.p. = 230 °C)[440] was freshly distilled in the presence of CaH_2 at 110 °C and 0.1 mbar pressure. Two Schlenk tubes were prepared in parallel with multiple cycles of heating under vacuum and purging with N_2. In one of the tubes, 4,4'-methylenebis(phenylisocyanate) (MDI) (**17**) (1036 mg, 4.14 mmol) was added and subjected subsequently to vacuum (without heating) and N_2 cycle for at least three times before the addition of 3 mL dry THF and stirring to dissolve the (**17**). In the other tube, the freshly distilled (**18**) was added along with 3-hydroxyphenylacetylene (**14**) (8.5 mg, 0.0723 mmol) and 8-azidonaphthalen-2-ol (**13**) (13.4 mg, 0.0723 mmol), and subjected subsequently to vacuum (without heating) and N_2 cycle for at least three times before the addition of 1 mL dry THF and stirring. Additionally, the synthesized **NHC-MOF3** was transferred from the inside of the glovebox to the outside in a headspace vial, to which 2 mL dry THF was added. Now that all components were ready, the synthesis of TPU could be initiated. The flask containing the (**16**) was purged with N_2 and (**17**) was added to this by the means of a syringe. After 5 min of stirring, an additional portion of 15 mL dry THF was added carefully by rinsing on the glass wall (to avoid bubbles). This reaction mixture was further stirred for 15 min. Subsequently, three drops of 1,8-diazabicyclo[5.4.0]undec-7-ene (DBU) were added to the reaction mixture and stirred for further 15 min. To this reaction mixture, the contents of the second Schlenk tube ((**13**), (**14**) and (**18**)) were added. After 7 min, the **NHC-MOF3** (6 mg, 4.66 % Cu in **NHC-MOF3**, 0.06 eq. of Cu) which was suspended in the THF by either of the three methods, i.e., stirring for 15 min, placed in an ultrasonic bath for 10 min or placed in an ultrasonic bath for 10 s (see **Table 25**), was added to the reaction mixture, which was stirred further till the mixture turns viscous enough that the magnetic stirrer stopped rotating, before pouring into a Petri dish (if the mixture is to viscous, additional THF can be added). The Petri dish was covered and stored in the dark for a minimum of 5 d.

Table 25. Detailed description of the TPU50 foils made according to the procedure of Development Stage 3 (DS3).

Ent	Entry Code (Long Version)	TPU50 Code (Short Version)	Description	Conducted Stretching Experiment Code
1	TPU50_Stir15min	TPU50_1	The TPU50 was made according to the procedure described in DS3 with the **NHC-MOF3** suspended in the THF inside a headspace vial by stirring for 15 min.	EXP1 EXP2
2	TPU50_USB10min	TPU50_2	The TPU50 was made according to the procedure described in DS3 with the **NHC-MOF3** suspended in the THF inside a headspace vial by placing in an ultrasonic bath for 10 min.	EXP3 EXP4
3	TPU50_USB10sec	TPU50_3	The TPU50 was made according to the procedure described in DS3 with the **NHC-MOF3** suspended in the THF inside a headspace vial by placing in an ultrasonic bath for 10 s.	EXP6

5.4.6 Synthesis of 8-Azidonaphthalen-2-ol (13)
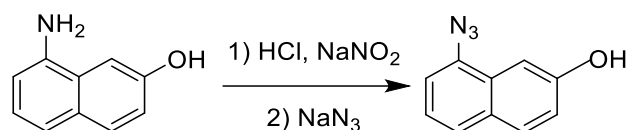
Scheme 33. The synthesis of 8-azidonaphthalen-2-ol (**13**).

The synthesis was conducted according to the described literature with slight modifications.[264]
To a suspension of 8-amino-2-naphthol (2.00 g, 12.5 mmol) in distilled water (70 mL), HCl (8 mL, 36 %) was added dropwise. The reaction mixture was then cooled and maintained at -5 °C till stated differently. A solution of $NaNO_2$ (1.30 g, 18.75 mmol) was prepared in ice-cold distilled water (10 mL), added dropwise, and the mixture was stirred for 30 min. To this, a solution of NaN_3 (1.21 g, 18.75 mmol) in ice cold water (15 mL) was added over a period of 40 min using a control syringe pump. The reaction mixture temperature was then raised to RT and stirred for a further 1 h. Afterwards, the solution was extracted with Et_2O and washed with water. The organic layers were dried *via* Na_2SO_4 and the solvent was evaporated under reduced pressure. After purification *via* flash chromatography on silica (n-hexane/ethyl acetate 5:1), the compound (1.33 g, 58 %) was obtained as a pale brownish-white solid.

^{1}H NMR (400 MHz, CDCl$_3$) δ 7.74 (d, J = 8.8 Hz, 1H), 7.57 (m, 1H), 7.39 (d, J = 2.6 Hz, 1H), 7.32 (dd, J = 8.2, 7.4 Hz, 1H), 7.22 (dd, J = 7.4, 1.0 Hz, 1H), 7.15 (dd, J = 8.8, 2.6 Hz, 1H), 5.11 (s, 1H).
^{13}C NMR (101 MHz, CDCl$_3$) δ 153.75, 134.94, 129.85, 127.54, 124.57, 123.34, 118.69, 114.51, 104.74, 77.32, 77.21, 77.00, 76.69.
ESI-TOF m/z: (negative mode, THF:MeOH 99:1, m/z) [M-H]$^-$ found 184.0543, simulated 184.0505 for $C_{10}H_7N_3O^-$.
IR (KBr) 521 (w), 556 (w), 668(w), 740 (w), 830 (m), 860 (w), 916 (w), 1013 (w), 1138 (w), 1176 (m), 1201 (w), 1235 (m), 1297 (s), 1355 (w), 1395 (w), 1467 (m), 1524 (w), 1595 (m), 1631 (w), 2124 (s), 2362 (w), 3310 (m)

5.4.7 Synthesis of 8-(4-(3-hydroxyphenyl)-1,2,3-triazol-1-yl)naphthalen-2-ol (15)
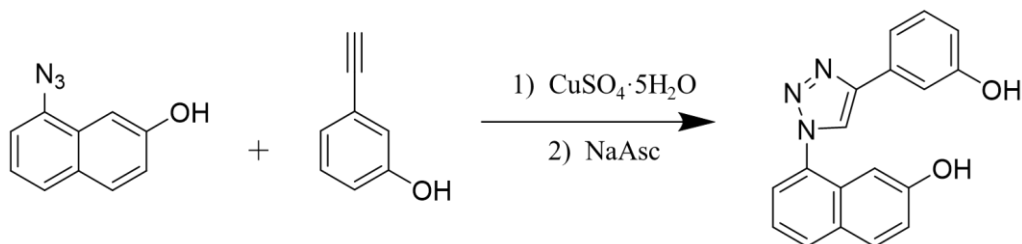
Scheme 34. The synthesis of 8-(4-(3-hydroxyphenyl)-1,2,3-triazol-1-yl)naphthalen-2-ol (**15**).

The synthesis was conducted according to the described literature with slight modifications.[264]
A stock solution of $CuSO_4 \cdot 5H_2O$ (54.0 µmol, 13.4 mg in 0.5 mL water) and a stock solution of sodium ascorbate (NaAsc) (80.0 µmol, 16.1 mg in 0.5 mL water) were added to a mixture of (**13**) (100.0 mg, 0.54 mmol) and (**14**) (67.1 mg, 0.54 mmol) in EtOH (4 mL), and the resultant solution was stirred overnight at RT. The reaction mixture was diluted with 15 mL water, extracted with $CHCl_3$ (3 x 10 mL), dried over Na_2SO_4, and the solvent evaporated under reduced pressure. After purification *via* column chromatography ($CHCl_3$:MeOH 20:1), (**15**) (121.0 mg, 0.4 mmol, 74 %) was obtained as a brownish-yellow solid.

^{1}H NMR (500 MHz, , DMSO-d_6) δ 10.02 (s, 1H), 9.59 (s, 1H), 9.00 (s, 1H), 8.05 (d, J = 8.3 Hz, 1H), 7.97 (d, J = 8.9 Hz, 1H), 7.67 (d, J = 6.1 Hz, 1H), 7.47 – 7.42 (m, 2H), 7.39 (d, J = 7.7 Hz, 1H), 7.28 (t, J = 7.8 Hz, 1H), 7.19 (d, J = 11.2 Hz, 1H), 6.79 (d, J = 6.8 Hz, 2H).
^{13}C NMR (126 MHz, , DMSO-d_6) δ 158.32, 157.56, 147.08, 132.09, 130.50, 128.92, 124.69, 124.47, 122.34, 120.29, 116.76, 115.66, 112.58, 103.54.
ESI-TOF m/z: (negative mode, THF:MeOH 99:1, m/z) [M-H]$^-$ found 302.0960, simulated 302.0924 for $C_{18}H_{13}N_3O_2$.
IR(KBr): 538 (w), 694 (m), 716 (m), 738 (m), 772 (m), 787 (m), 827 (s), 877 (m), 968 (w), 1047 (m), 1077 (w), 1189 (s), 1230 (s), 1247(s), 1266 (m), 1298 (s), 1381 (w), 1431 (m), 1452 (s), 1481 (s), 1522 (s), 1585 (s), 1623 (m), 2590 (m), 3066 (m), 3343 (m)

5.4.8 Mechanical Properties of TPU

5.4.8.1 Calculation of Young's (E) Modulus

The Young's moduli of the TPU foils were determined *via* extensional rotational rheology with oscillating stress-strain experiments. The experiment was conducted with TPU30, 50 and 70 with an applied strain ranging from 0.01 % to 5.00 %. The strain determined stress values which established elastic and plastic regions (see **Figure A62Ai** and **Bi**, and **Figure 48B**). The Young's moduli were calculated by using the slope of the linear regression in the low strain range from 0.01 % to 0.50 % (see **Figure A62Aii** and **Bii**, and **Figure 48C**).

Table 26. The calculated values of Young's (E) modulus of TPU30, 50 and 70.

Ent	TPU"X"	Young's (E) Modulus [MPa]
1	TPU30	0.002
2	TPU50	0.013
3	TPU70	0.033

5.4.8.2 Determination of Crystallinity (DSC analysis)

The crystallinity of the TPU foils was calculated by measuring the area under the curve of the peak of $T_{m,soft}$ (~23 °C) to obtain the $\Delta H_{m,soft}$. The crystallinity was calculated by using the formula:

$$\alpha = (\Delta H_{m,soft} / \Delta H_{m0}) \qquad \text{eq. (5.4)}$$

where, $\Delta H_{m0} = 172$ J g^{-1} for pTHF at 100 % crystallinity.[434]

Table 27. Melting enthalpy $\Delta H_{m,soft}$ and calculated crystallinity of TPU30-80 of Development Stages 1 (DS1) and 2 (DS2).

Ent	TPU"X"	Soft/Hard (mol ratio)	Development Stage 1 O-TPU"X"			Development Stage 2 TPU"X"		
			$T_{m,soft}$ [°C]	$\Delta H_{m,soft}$ [J g^{-1}]	α [%]	$T_{m,soft}$ [°C]	$\Delta H_{m,soft}$ [J g^{-1}]	α [%]
1	TPU30	70:30	25	53.04	31	26	41.23	24
2	TPU40	60:40	22	48.20	28	24	43.18	25
3	TPU50	50:50	27	54.00	31	22	37.38	22
4	TPU60	40:60	21	36.65	21	21	36.52	21
5	TPU70	30:70	23	55.08	32	19	26.97	16
6	TPU80	20:80	-	-	-	17	18.01	11

Table 28. Melting enthalpy $\Delta H_{m,soft}$ and calculated crystallinity of TPU50_1, 2 and 3 of Development Stage 3 (DS3).

Ent	TPU"X"	Soft/Hard (mol ratio)	$T_{m,soft}$ [°C]	$\Delta H_{m,soft}$ [J g^{-1}]	α [%]
1	TPU50_1	50:50	23	46.58	27
2	TPU50_2	50:50	22	42.75	25
3	TPU50-3	50:50	23	41.06	24

Table 29. Melting enthalpy $\Delta H_{m,soft}$ and calculated crystallinity of TPU50_1 and 3 before and after stretching experiment (SE).

Ent	TPU"X"	Soft/Hard (mol ratio)	SE Status	$T_{m,soft}$ [°C]	$\Delta H_{m,soft}$ [J g^{-1}]	α [%]
1	TPU50_2	50:50	Before SE	22	42.75	25
			After SE	21	43.14	25
2	TPU50_3	50:50	Before SE	23	41.06	24
			After SE	23	41.91	24

5.4.9 Mechanochemical activation of PU-Networks

5.4.9.1 *Stress experiments via Tensile Rheology*

To conduct the stress experiments, the obtained TPU films were cut into dumbbell shaped samples with hydraulic cutting press in accordance with DIN 53504 type 3a/ISO 37 type 3 with thicknesses 0.5-0.9 mm, of which the 0.7 or 0.5 mm samples were used for extensional oscillatory and rotational rheology experiments (henceforth called as stretching experiments (SE)) which were conducted on Anton Paar (Physica) MCR 101/SN 80753612 *via* Universal Extensional Fixture (UXF) at 25 °C. The selected samples were fixed in the UXF sample holder and subjected to oscillating stretching experiments. Based on previous experimentational knowledge, the strain rate was set at 0.5 Hz while the deformation was set at ε = 40 % to investigate the mechanochemical activation of the Cu(I) bis(NHC) within the synthesized **NHC-MOF3**, embedded in a TPU matrix. The points at which the sample holder clamped the sample were marked so as to have uniform clamping points in case the sample needed to be removed for any reason. A single cycle of measurement is divided into three segments: the stretching experiment lasting 60 min, heating at 50 °C for 30 min to initiate shape-memory and then recovering at 25 °C for 75 min.
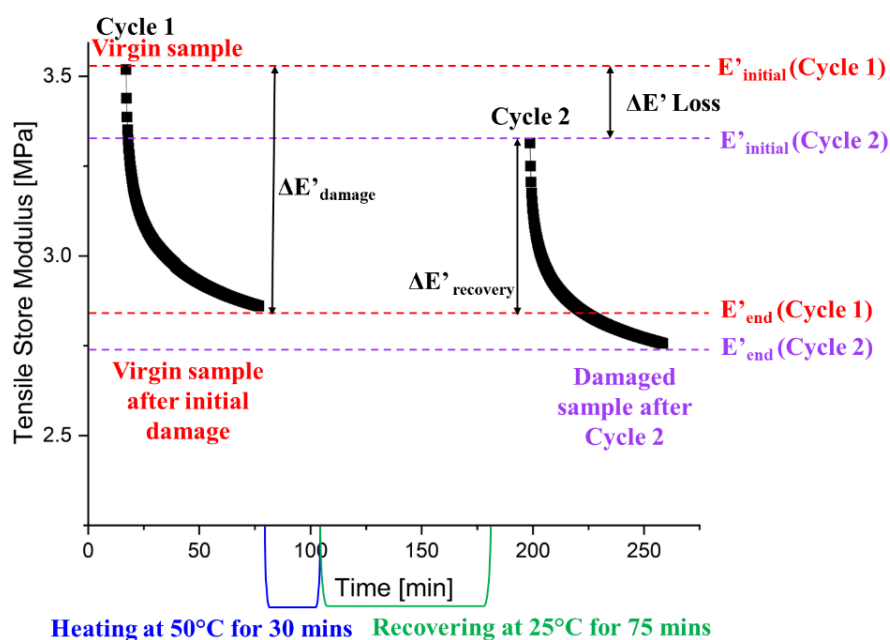
Scheme 35. A schematic concept describing the meaning of a cycle as mentioned. A typical single cycle consists of the stretching experiment lasting 60 min, heating at 50 °C for 30 min to initiate shape-memory and then recovery at 25 °C for 75 min. The scheme also exhibits the terms necessary to calculate the shape memory and recovery efficiency.

5.4.9.2 *Shape Memory and Recovery Efficiency*

The shape-memory and the recovery efficiency can be measured from such obtained measurements using the following formula:

Shape Memory Efficiency: How much of the initial value was reached after X^{th} cycle.

$$\eta_{classic} = \frac{E'_{initial} \ (X^{th} \ Cycle)}{E'_{initial} \ (Virgin)}$$

<div align="right">eq. (5.5)</div>

Recovery Efficiency: How much of the damage of the previous run was recovered.

$$\eta_{recovery} = \frac{E'_{initial}\ (X^{th}\ Cycle) - E'_{end}\ (X-1\ Cycle)}{E'_{initial}\ (X^{th}\ Cycle) - E'_{end}\ (X^{th}\ Cycle)}$$

eq. (5.6)

5.4.10 Fluorescence Measurements

5.4.10.1 Fluorescence Calibration
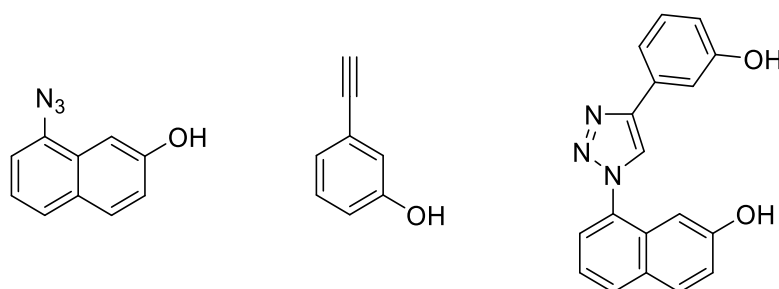
Figure 62. The components of the dye system: the precursors (**13**) and (**14**), and the "click" dye (**15**).

The fluorescence spectrometer's dye system calibration involved embedding the click dye in varying ratios in a TPU50 polyurethane matrix. To avoid potential internal quenching effects, the total concentration of (**13**) and (**14**) (in mmol) was kept constant at 10 µmol g^{-1} of TPU, where the total weight of TPU was ~7.23 g from its components (**16**), (**17**), and (**18**). A slightly modified synthetic procedure of DS3 was used to add the click dye into the same Schlenk flask as that of the dye precursors in different ratios corresponding to the amounts mentioned in **Table 30**. The resulting TPU50 foils were cut into dumbbell-shaped samples (20 x 4 x 0.5 mm) for fluorescence emission spectra measurement. The UV-vis and fluorescence measurements in solution were previously conducted and published.[264] Accordingly, the excitation wavelength of 377 nm was thus chosen, and an emission spectrum ranging from 390 nm to 650 nm was collected. Each measurement was performed at least three times per side. The voltage selected was 585 V.

In **Table 30**, **Ent 1**, only the dye precursors (**13**) and (**14**) were present at a concentration of 10 µmol g^{-1} of TPU, and none of the fluorescent dye (**15**) was present. Therefore, ideally, no fluorescence should have been observed. However, fluorescence was recorded at approximately 438 nm and was attributed to precursor (**13**) (**Figure 63A**). As the concentration of (**15**) varied (**Table 30**, **Ent 2-4**), increasing fluorescence at λ_{em} = 458 nm was observed (**Figure 63A**), which was attributed to the fluorescent dye (**15**). The fluorescence was plotted against the conversion, calculated based on the concentrations of dye, and linear fitting was performed (**Figure 63B**) to obtain a calibration equation (see **Equation 5.7**) for calculating the '*true*' conversion % of the mechanochemically triggered "click" reaction based on the measured fluorescence.

Although the calibration equation is based on samples of thickness 0.5 mm and is intended for use on similarly thick samples to obtain accurate conversion values, it is extended to other thicknesses (~0.7 mm) to quantify all samples uniformly and observe trends. In such cases, however, the conversion % was reported as '*estimated*' conversion % instead of '*true*' conversion %.

y = 5.77x + 36

eq. (5.7)

where y = fluorescence intensity measured and x = conversion % achieved.

Table 30. Reaction conditions for the TPU50 foils synthesized with varying concentrations of dye precursors (**13**) and (**14**) along with fluorescent dye (**15**) embedded within the TPU50 and used to conduct fluorescence test measurement with $\lambda_{ex} = 377$ nm to observe the subsequent emission spectra at $\lambda_{em} = 458$ nm for calibration experiments.

Ent	TPU50 Code	Conversion [%]	Moles (13) $n_{(13)}$ [µmol]	Mass (13) $m_{(13)}$ [mg]	Moles (14) $n_{(14)}$ [µmol]	Mass (14) $m_{(14)}$ [mg]	Moles (15) $n_{(15)}$ [µmol]	Mass (15) $m_{(15)}$ [mg]
1	TPU50_Ref0%	0	72.3	13.4	72.3	8.5	0.0	0.0
2	TPU50_Ref25%	25	54.0	10.0	54.0	6.4	18.0	5.5
3	TPU50_Ref50%	50	36.2	6.7	36.2	4.3	36.2	11.0
4	TPU50_Ref75%	75	18.0	3.3	18.0	2.1	54.0	16.3
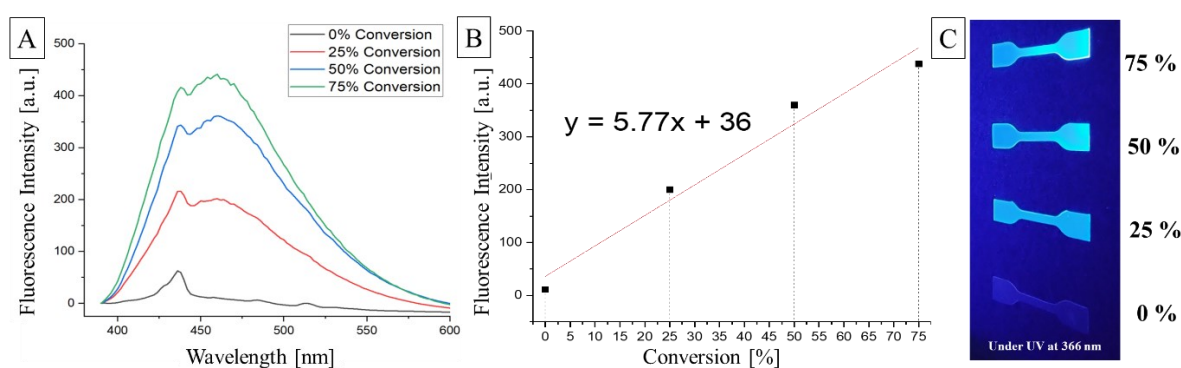
Figure 63. A) The fluorescence test measurement samples conducted with preparing TPU50 foils with different concentrations of (**13**), (**14**) and (**15**) without **NHC-MOF3** to measure the fluorescence emission behaviour with $\lambda_{ex} = 377$ nm over the range $\lambda_{em} = 390$-650 nm. **B**) The fluorescence intensities at $\lambda_{em} = 458$ nm were plotted against the conversion % to obtain a linear fit. **C**) The different TPU samples with different concentrations of the dye system as per **Table 30** under a UV lamp at 366 nm.

6 REFERENCES

[1] H.-W. Wanzlick, B. Lachmann, E. Schikora, "Chemie nucleophiler Carbene, VIII. Zur Bildung und Reaktivität des Bis-[1.3-diphenyl-imidazolidinylidens-(2)]", *Chemische Berichte* **1965**, *98*, 3170, https://doi.org/10.1002/cber.19650981012.

[2] H.-W. Wanzlick, H.-J. Schönherr, "Direct Synthesis of a Mercury Salt-Carbene Complex", *Angewandte Chemie International Edition in English* **1968**, *7*, 141, https://doi.org/10.1002/anie.196801412.

[3] K. Öfele, "1,3-Dimethyl-4-imidazolinyliden-(2)-pentacarbonylchrom ein neuer übergangsmetall-carben-komplex", *Journal of Organometallic Chemistry* **1968**, *12*, https://doi.org/10.1016/S0022-328X(00)88691-X.

[4] K. Öfele, "Pentacarbonyl(2,3-diphenylcyclopropenylidene)-chromium(0)", *Angewandte Chemie International Edition in English* **1968**, *7*, 950, https://doi.org/10.1002/anie.196809501.

[5] A. Igau, H. Grutzmacher, A. Baceiredo, G. Bertrand, "Analogous .alpha.,.alpha.'-bis-carbenoid, triply bonded species: synthesis of a stable .lambda.3-phosphino carbene-.lambda.5-phosphaacetylene", *Journal of the American Chemical Society* **1988**, *110*, 6463, https://doi.org/10.1021/ja00227a028.

[6] A. J. Arduengo, III, R. L. Harlow, M. Kline, "A stable crystalline carbene", *Journal of the American Chemical Society* **1991**, *113*, 361, https://doi.org/10.1021/ja00001a054.

[7] M. N. Hopkinson, C. Richter, M. Schedler, F. Glorius, "An overview of N-heterocyclic carbenes", *Nature* **2014**, *510*, 485, https://doi.org/10.1038/nature13384.

[8] D. Bourissou, O. Guerret, F. P. Gabbaï, G. Bertrand, "Stable Carbenes", *Chemical Reviews* **2000**, *100*, 39, https://doi.org/10.1021/cr940472u.

[9] P. de Frémont, N. Marion, S. P. Nolan, "Carbenes: Synthesis, properties, and organometallic chemistry", *Coordination Chemistry Reviews* **2009**, *253*, 862, https://doi.org/10.1016/j.ccr.2008.05.018.

[10] W. A. Herrmann, C. Köcher, "N-Heterocyclic Carbenes", *Angewandte Chemie International Edition in English* **1997**, *36*, 2162, https://doi.org/10.1002/anie.199721621.

[11] M. K. Denk, K. Hatano, M. Ma, "Nucleophilic carbenes and the wanzlick equilibrium: A reinvestigation", *Tetrahedron Letters* **1999**, *40*, 2057, https://doi.org/10.1016/S0040-4039(99)00164-1.

[12] R. Breslow, "On the Mechanism of Thiamine Action. IV.1 Evidence from Studies on Model Systems", *Journal of the American Chemical Society* **1958**, *80*, 3719, https://doi.org/10.1021/ja01547a064.

[13] A. Berkessel, S. Elfert, V. R. Yatham, J. M. Neudörfl, N. E. Schlörer, J. H. Teles, "Umpolung by N-heterocyclic carbenes: generation and reactivity of the elusive 2,2-diamino enols (Breslow intermediates)", *Angewandte Chemie International Edition* **2012**, *51*, 12370, https://doi.org/10.1002/anie.201205878.

[14] X. Bugaut, F. Glorius, "Organocatalytic umpolung: N-heterocyclic carbenes and beyond", *Chemical Society Reviews* **2012**, *41*, 3511, http://dx.doi.org/10.1039/C2CS15333E.

[15] M. N. Hopkinson, F. Glorius, "An Overview of NHCs", in *N-Heterocyclic Carbenes in Organocatalysis*, 2018, p. 1, https://doi.org/10.1002/9783527809042.ch1.

[16] D. J. N. a. S. P. Nolan, "N-Heterocyclic Carbenes", in *N-Heterocyclic Carbenes: Effective Tools for Organometallic Synthesis*, S.P. Nolan, Ed., Wiley-VCH, Germany, 2014, https://doi.org/10.1002/9783527671229.ch01.

[17] T. Dröge, F. Glorius, "The Measure of All Rings—N-Heterocyclic Carbenes", *Angewandte Chemie International Edition* **2010**, *49*, 6940, http://dx.doi.org/10.1002/anie.201001865.

[18] A. J. Arduengo, III, J. R. Goerlich, W. J. Marshall, "A stable diaminocarbene", *Journal of the American Chemical Society* **1995**, *117*, 11027, https://doi.org/10.1021/ja00149a034.

[19] C. Heinemann, T. Müller, Y. Apeloig, H. Schwarz, "On the Question of Stability, Conjugation, and "Aromaticity" in Imidazol-2-ylidenes and Their Silicon Analogs", *Journal of the American Chemical Society* **1996**, *118*, 2023, https://doi.org/10.1021/ja9523294.

[20] A. J. Arduengo, III, H. V. R. Dias, R. L. Harlow, M. Kline, "Electronic stabilization of nucleophilic carbenes", *Journal of the American Chemical Society* **1992**, *114*, 5530, https://doi.org/10.1021/ja00040a007.

[21] D. J. Nelson, S. P. Nolan, "Quantifying and understanding the electronic properties of N-heterocyclic carbenes", *Chemical Society Reviews* **2013**, *42*, 6723, http://dx.doi.org/10.1039/C3CS60146C.

[22] H. V. Huynh, "Electronic Properties of N-Heterocyclic Carbenes and Their Experimental Determination", *Chemical Reviews* **2018**, *118*, 9457, https://doi.org/10.1021/acs.chemrev.8b00067.

[23] C. A. Tolman, "Steric effects of phosphorus ligands in organometallic chemistry and homogeneous catalysis", *Chemical Reviews* **1977**, *77*, 313, https://doi.org/10.1021/cr60307a002.

[24] C. A. Tolman, "Electron donor-acceptor properties of phosphorus ligands. Substituent additivity", *Journal of the American Chemical Society* **1970**, *92*, 2953, https://doi.org/10.1021/ja00713a006.

[25] A. R. Chianese, X. Li, M. C. Janzen, J. W. Faller, R. H. Crabtree, "Rhodium and Iridium Complexes of N-Heterocyclic Carbenes via Transmetalation: Structure and Dynamics", *Organometallics* **2003**, *22*, 1663, https://doi.org/10.1021/om021029+.

[26] R. A. Kelly Iii, H. Clavier, S. Giudice, N. M. Scott, E. D. Stevens, J. Bordner, I. Samardjiev, C. D. Hoff, L. Cavallo, S. P. Nolan, "Determination of N-Heterocyclic Carbene (NHC) Steric and Electronic Parameters using the [(NHC)Ir(CO)2Cl] System", *Organometallics* **2008**, *27*, 202, https://doi.org/10.1021/om701001g.

[27] S. Wolf, H. Plenio, "Synthesis of (NHC)Rh(cod)Cl and (NHC)RhCl(CO)2 complexes – Translation of the Rh- into the Ir-scale for the electronic properties of NHC ligands", *Journal of Organometallic Chemistry* **2009**, *694*, 1487, https://doi.org/10.1016/j.jorganchem.2008.12.047.

[28] D. G. Gusev, "Donor Properties of a Series of Two-Electron Ligands", *Organometallics* **2009**, *28*, 763, https://doi.org/10.1021/om800933x.

[29] D. G. Gusev, "Electronic and Steric Parameters of 76 N-Heterocyclic Carbenes in Ni(CO)3(NHC)", *Organometallics* **2009**, *28*, 6458, https://doi.org/10.1021/om900654g.

[30] Q. Shi, R. J. Thatcher, J. Slattery, P. S. Sauari, A. C. Whitwood, P. C. McGowan, R. E. Douthwaite, "Synthesis, Coordination Chemistry and Bonding of Strong N-Donor Ligands Incorporating the 1H-Pyridin-(2E)-Ylidene (PYE) Motif", *Chemistry – A European Journal* **2009**, *15*, 11346, https://doi.org/10.1002/chem.200901382.

[31] R. Tonner, G. Frenking, "Tolman's Electronic Parameters for Divalent Carbon(0) Compounds", *Organometallics* **2009**, *28*, 3901, https://doi.org/10.1021/om900206w.

[32] A. C. Hillier, W. J. Sommer, B. S. Yong, J. L. Petersen, L. Cavallo, S. P. Nolan, "A Combined Experimental and Theoretical Study Examining the Binding of N-Heterocyclic Carbenes (NHC) to the Cp*RuCl (Cp* = η5-C5Me5) Moiety: Insight into Stereoelectronic Differences between Unsaturated and Saturated NHC Ligands", *Organometallics* **2003**, *22*, 4322, http://dx.doi.org/10.1021/om034016k.

[33] H. Clavier, S. P. Nolan, "Percent buried volume for phosphine and N-heterocyclic carbene ligands: steric properties in organometallic chemistry", *Chemical Communications* **2010**, *46*, 841, http://dx.doi.org/10.1039/B922984A.

[34] A. Gómez-Suárez, D. J. Nelson, S. P. Nolan, "Quantifying and understanding the steric properties of N-heterocyclic carbenes", *Chemical Communications* **2017**, *53*, 2650, http://dx.doi.org/10.1039/C7CC00255F.

[35] P. Bellotti, M. Koy, M. N. Hopkinson, F. Glorius, "Recent advances in the chemistry and applications of N-heterocyclic carbenes", *Nature Reviews Chemistry* **2021**, *5*, 711, https://doi.org/10.1038/s41570-021-00321-1.

[36] A. Poater, B. Cosenza, A. Correa, S. Giudice, F. Ragone, V. Scarano, L. Cavallo, "SambVca: A Web Application for the Calculation of the Buried Volume of N-Heterocyclic Carbene Ligands", *European Journal of Inorganic Chemistry* **2009**, *2009*, 1759, https://doi.org/10.1002/ejic.200801160.

[37] D. J. Cardin, B. Cetinkaya, M. F. Lappert, "Transition metal-carbene complexes", *Chemical Reviews* **1972**, *72*, 545, https://doi.org/10.1021/cr60279a006.

[38] P. D. Fremont, "Synthesis of Well-Defined N-Heterocyclic Carbene (NHC) Complexes of Late Transition Metals", in *Chemistry*, University of New Orleans, 2008, p. Ph.D./,

[39] L. P. Spencer, M. D. Fryzuk, "Synthesis and reactivity of zirconium and hafnium complexes incorporating chelating diamido-N-heterocyclic-carbene ligands", *Journal of Organometallic Chemistry* **2005**, *690*, 5788, https://doi.org/10.1016/j.jorganchem.2005.07.121.

[40] N. A. Jones, S. T. Liddle, C. Wilson, P. L. Arnold, "Titanium(III) Alkoxy-N-heterocyclic Carbenes and a Safe, Low-Cost Route to TiCl3(THF)3", *Organometallics* **2007**, *26*, 755, https://doi.org/10.1021/om060486d.

[41] L. P. Spencer, C. Beddie, M. B. Hall, M. D. Fryzuk, "Synthesis, Reactivity, and DFT Studies of Tantalum Complexes Incorporating Diamido-N-heterocyclic Carbene Ligands. Facile Endocyclic C–H Bond Activation", *Journal of the American Chemical Society* **2006**, *128*, 12531, https://doi.org/10.1021/ja063282x.

[42] S. P. Downing, S. C. Guadaño, D. Pugh, A. A. Danopoulos, R. M. Bellabarba, M. Hanton, D. Smith, R. P. Tooze, "Indenyl- and Fluorenyl-Functionalized N-Heterocyclic Carbene Complexes of Titanium, Zirconium, Vanadium, Chromium, and Yttrium", *Organometallics* **2007**, *26*, 3762, https://doi.org/10.1021/om700269u.

[43] M. Nonnenmacher, D. Kunz, F. Rominger, T. Oeser, "First examples of dipyrido[1,2-c:2',1'-e]imidazolin-7-ylidenes serving as NHC-ligands: Synthesis, properties and structural features of their chromium and tungsten pentacarbonyl complexes", *Journal of Organometallic Chemistry* **2005**, *690*, 5647, https://doi.org/10.1016/j.jorganchem.2005.07.033.

[44] F. Wu, V. K. Dioumaev, D. J. Szalda, J. Hanson, R. M. Bullock, "A Tungsten Complex with a Bidentate, Hemilabile N-Heterocyclic Carbene Ligand, Facile Displacement of the Weakly Bound W–(CC) Bond, and the Vulnerability of the NHC Ligand toward Catalyst Deactivation during Ketone Hydrogenation", *Organometallics* **2007**, *26*, 5079, https://doi.org/10.1021/om700694e.

[45] H. Braband, D. Przyrembel, U. Abram, "Phenylimidorhenium(V) Complexes with 1,3-Diethyl-4,5-dimethylimidazole-2- ylidene Ligands", *Zeitschrift für anorganische und allgemeine Chemie* **2006**, *632*, 779, https://doi.org/10.1002/zaac.200500409.

[46] E. Oehlke, T. Kückmann, U. Abram, "Silver(I) Complexes of 1,3-Dialkyl-4,5-dimethylimidazol-2-ylidenes and their Use as Precursors for the Synthesis of Rhenium(V) NHC Complexes", *Zeitschrift für anorganische und allgemeine Chemie* **2007**, *633*, 830, https://doi.org/10.1002/zaac.200700021.

[47] A. M. Maj, L. Delaude, A. Demonceau, A. F. Noels, "Synthesis of N-heterocyclic carbene precursors bearing biphenyl units and their use in ruthenium-catalyzed ring-opening metathesis polymerization", *Journal of Organometallic Chemistry* **2007**, *692*, 3048, https://doi.org/10.1016/j.jorganchem.2007.03.027.

[48] G. Occhipinti, H.-R. Bjørsvik, K. W. Törnroos, A. Fürstner, V. R. Jensen, "The First Imidazolium-Substituted Metal Alkylidene", *Organometallics* **2007**, *26*, 4383, https://doi.org/10.1021/om700590v.

[49] M. Bortenschlager, J. Schütz, D. von Preysing, O. Nuyken, W. A. Herrmann, R. Weberskirch, "Rhodium–NHC-complexes as potent catalysts in the hydroformylation of 1-octene", *Journal of Organometallic Chemistry* **2005**, *690*, 6233, https://doi.org/10.1016/j.jorganchem.2005.09.038.

[50] H. Someya, H. Ohmiya, H. Yorimitsu, K. Oshima, "N-Heterocyclic Carbene Ligands in Cobalt-Catalyzed Sequential Cyclization/Cross-Coupling Reactions of 6-Halo-1-hexene Derivatives with Grignard Reagents", *Organic Letters* **2007**, *9*, 1565, https://doi.org/10.1021/ol070392f.

[51] S. Fantasia, H. Jacobsen, L. Cavallo, S. P. Nolan, "Insertion of a N-Heterocyclic Carbene (NHC) into a Platinum–Olefin Bond", *Organometallics* **2007**, *26*, 3286, https://doi.org/10.1021/om700447u.

[52] S.-M. Lee, H.-J. Yoon, J.-H. Kim, W.-J. Chung, Y.-S. Lee, "Highly active organosilane-based N-heterocyclic carbene-palladium complex immobilized on silica particles for the Suzuki reaction", *Pure and Applied Chemistry* **2007**, *79*, 1553, https://doi.org/10.1351/pac200779091553.

[53] V. J. Catalano, M. A. Malwitz, A. O. Etogo, "Pyridine Substituted N-Heterocyclic Carbene Ligands as Supports for Au(I)–Ag(I) Interactions: Formation of a Chiral Coordination Polymer", *Inorganic Chemistry* **2004**, *43*, 5714, https://doi.org/10.1021/ic049604k.

[54] L. Ricard, F. Gagosz, "Synthesis and Reactivity of Air-Stable N-Heterocyclic Carbene Gold(I) Bis(trifluoromethanesulfonyl)imidate Complexes", *Organometallics* **2007**, *26*, 4704, https://doi.org/10.1021/om7006002.

[55] G. Anantharaman, K. Elango, "Synthesis and Characterization of NHC-Stabilized Zinc Aryloxide and Zinc Hydroxyaryloxide", *Organometallics* **2007**, *26*, 1089, https://doi.org/10.1021/om060867r.

[56] Q.-X. Liu, L.-N. Yin, J.-C. Feng, "New N-heterocyclic carbene silver(I) and mercury(II) 2-D supramolecular layers by the π–π stacking interactions", *Journal of Organometallic Chemistry* **2007**, *692*, 3655, https://doi.org/10.1016/j.jorganchem.2007.05.005.

[57] X. Hu, Y. Tang, P. Gantzel, K. Meyer, "Silver Complexes of a Novel Tripodal N-Heterocyclic Carbene Ligand: Evidence for Significant Metal–Carbene π-Interaction", *Organometallics* **2003**, *22*, 612, https://doi.org/10.1021/om020935j.

[58] D. Nemcsok, K. Wichmann, G. Frenking, "The Significance of π Interactions in Group 11 Complexes with N-Heterocyclic Carbenes", *Organometallics* **2004**, *23*, 3640, https://doi.org/10.1021/om049802j.

[59] S. Díez-González, S. P. Nolan, "Stereoelectronic parameters associated with N-heterocyclic carbene (NHC) ligands: A quest for understanding", *Coordination Chemistry Reviews* **2007**, *251*, 874, https://doi.org/10.1016/j.ccr.2006.10.004.

[60] M. Jalal, B. Hammouti, R. Touzani, A. Aouniti, I. Ozdemir, "Metal-NHC heterocycle complexes in catalysis and biological applications: Systematic review", *Materials Today: Proceedings* **2020**, *31*, S122, https://doi.org/10.1016/j.matpr.2020.06.398.

[61] S. T. Nguyen, L. K. Johnson, R. H. Grubbs, J. W. Ziller, "Ring-opening metathesis polymerization (ROMP) of norbornene by a Group VIII carbene complex in protic media", *Journal of the American Chemical Society* **1992**, *114*, 3974, https://doi.org/10.1021/ja00036a053.

[62] X. Bantreil, J. Broggi, S. P. Nolan, "N-Heterocyclic carbene containing complexes in catalysis", *Annual Reports Section "B" (Organic Chemistry)* **2009**, *105*, 232, http://dx.doi.org/10.1039/B822056P.

[63] M. Scholl, S. Ding, C. W. Lee, R. H. Grubbs, "Synthesis and Activity of a New Generation of Ruthenium-Based Olefin Metathesis Catalysts Coordinated with 1,3-Dimesityl-4,5-dihydroimidazol-2-ylidene Ligands", *Organic Letters* **1999**, *1*, 953, https://doi.org/10.1021/ol990909q.

[64] M. Scholl, T. M. Trnka, J. P. Morgan, R. H. Grubbs, "Increased ring closing metathesis activity of ruthenium-based olefin metathesis catalysts coordinated with imidazolin-2-ylidene ligands", *Tetrahedron Letters* **1999**, *40*, 2247, https://doi.org/10.1016/S0040-4039(99)00217-8.

[65] T. M. Trnka, R. H. Grubbs, "The Development of L2X2RuCHR Olefin Metathesis Catalysts: An Organometallic Success Story", *Accounts of Chemical Research* **2001**, *34*, 18, https://doi.org/10.1021/ar000114f.

[66] A. K. Chatterjee, R. H. Grubbs, "Synthesis of Trisubstituted Alkenes via Olefin Cross-Metathesis", *Organic Letters* **1999**, *1*, 1751, https://doi.org/10.1021/ol991023p.

[67] C. W. Bielawski, R. H. Grubbs, "Highly Efficient Ring-Opening Metathesis Polymerization (ROMP) Using New Ruthenium Catalysts Containing N-Heterocyclic Carbene Ligands", *Angewandte Chemie International Edition* **2000**, *39*, 2903, https://doi.org/10.1002/1521-3773(20000818)39:16<2903::AID-ANIE2903>3.0.CO;2-Q.

[68] C. W. Bielawski, D. Benitez, R. H. Grubbs, "An "Endless" Route to Cyclic Polymers", *Science* **2002**, *297*, 2041, https://doi.org/10.1126/science.1075401.

[69] S. Enthaler, R. Jackstell, B. Hagemann, K. Junge, G. Erre, M. Beller, "Efficient transfer hydrogenation of ketones in the presence of ruthenium N-heterocyclic carbene catalysts", *Journal of Organometallic Chemistry* **2006**, *691*, 4652, https://doi.org/10.1016/j.jorganchem.2006.07.013.

[70] N. Gürbüz, E. Ö. Özcan, İ. Özdemir, B. Çetinkaya, O. Şahin, O. Büyükgüngör, "Preparation of a series of Ru(ii) complexes with N-heterocyclic carbene ligands for the catalytic transfer hydrogenation of aromatic ketones", *Dalton Transactions* **2012**, *41*, 2330, http://dx.doi.org/10.1039/C1DT11203A.

[71] X.-Q. Guo, Y.-N. Wang, D. Wang, L.-H. Cai, Z.-X. Chen, X.-F. Hou, "Palladium, iridium and ruthenium complexes with acyclic imino-N-heterocyclic carbenes and their application in aqua-phase Suzuki–Miyaura cross-coupling reaction and transfer hydrogenation", *Dalton Transactions* **2012**, *41*, 14557, http://dx.doi.org/10.1039/C2DT31989F.

[72] A. Prades, M. Viciano, M. Sanaú, E. Peris, "Preparation of a Series of "Ru(p-cymene)" Complexes with Different N-Heterocyclic Carbene Ligands for the Catalytic β-Alkylation of Secondary Alcohols and Dimerization of Phenylacetylene", *Organometallics* **2008**, *27*, 4254, https://doi.org/10.1021/om800377m.

[73] I. Özdemir, S. Demir, B. Çetinkaya, C. Gourlaouen, F. Maseras, C. Bruneau, P. H. Dixneuf, "Direct Arylation of Arene C–H Bonds by Cooperative Action of NHCarbene–Ruthenium(II) Catalyst and Carbonate via Proton Abstraction Mechanism", *Journal of the American Chemical Society* **2008**, *130*, 1156, https://doi.org/10.1021/ja710276x.

[74] S. Yaşar, Ö. Doğan, I. Özdemir, B. Çetinkaya, "Ruthenium N-heterocyclic–carbene catalyzed diarylation of arene C⎯H bond", *Applied Organometallic Chemistry* **2008**, *22*, 314, https://doi.org/10.1002/aoc.1392.

[75] L. U. Nordstrøm, H. Vogt, R. Madsen, "Amide synthesis from alcohols and amines by the extrusion of dihydrogen", *Journal of the American Chemical Society* **2008**, *130*, 17672, https://doi.org/10.1021/ja808129p.

[76] S. C. Ghosh, S. Muthaiah, Y. Zhang, X. Xu, S. H. Hong, "Direct Amide Synthesis from Alcohols and Amines by Phosphine-Free Ruthenium Catalyst Systems", *Advanced Synthesis & Catalysis* **2009**, *351*, 2643, https://doi.org/10.1002/adsc.200900482.

[77] W.-Q. Wang, H. Cheng, Y. Yuan, Y.-Q. He, H.-J. Wang, Z.-Q. Wang, W. Sang, C. Chen, F. Verpoort, "Highly Efficient N-Heterocyclic Carbene/Ruthenium Catalytic Systems for the Acceptorless Dehydrogenation of Alcohols to Carboxylic Acids: Effects of Ancillary and Additional Ligands", *Catalysts* **2020**, *10*, 10, https://doi.org/10.3390/catal10010010.

[78] H. Türkmen, T. Pape, F. E. Hahn, B. Çetinkaya, "Annulated N-Heterocyclic Carbene Ligands Derived from 2-Methylaminopiperidine: Their Complexes and Catalytic Applications", *Organometallics* **2008**, *27*, 571, https://doi.org/10.1021/om701105y.

[79] H. Türkmen, T. Pape, F. E. Hahn, B. Çetinkaya, "Efficient Transfer Hydrogenation Using Iridium and Rhodium Complexes of Benzannulated N-Heterocyclic Carbenes", *European Journal of Inorganic Chemistry* **2008**, *2008*, 5418, https://doi.org/10.1002/ejic.200800715.

[80] J. D. Egbert, S. P. Nolan, "Tandem deuteration/hydrosilylation reactions catalyzed by a rhodium carbene complex under solvent-free conditions", *Chemical Communications* **2012**, *48*, 2794, http://dx.doi.org/10.1039/C2CC17196A.

[81] S. J. Geier, C. M. Vogels, J. A. Melanson, S. A. Westcott, "The transition metal-catalysed hydroboration reaction", *Chemical Society Reviews* **2022**, *51*, 8877, http://dx.doi.org/10.1039/D2CS00344A.

[82] J. M. Praetorius, C. M. Crudden, "N-Heterocyclic carbene complexes of rhodium: structure, stability and reactivity", *Dalton Transactions* **2008**, 4079, http://dx.doi.org/10.1039/B802114G.

[83] H. M. Lee, T. Jiang, E. D. Stevens, S. P. Nolan, "A Cationic Iridium Complex Bearing an Imidazol-2-ylidene Ligand as Alkene Hydrogenation Catalyst", *Organometallics* **2001**, *20*, 1255, https://doi.org/10.1021/om000990x.

[84] H. M. Lee, D. C. Smith, Z. He, E. D. Stevens, C. S. Yi, S. P. Nolan, "Catalytic Hydrogenation of Alkenes by the Ruthenium–Carbene Complex HRu(CO)Cl(PCy3)(IMes) (IMes = Bis(1,3-(2,4,6-trimethylphenyl)imidazol-2-ylidene)", *Organometallics* **2001**, *20*, 794, https://doi.org/10.1021/om000882a.

[85] D. Kremzow, G. Seidel, C. W. Lehmann, A. Fürstner, "Diaminocarbene- and Fischer-Carbene Complexes of Palladium and Nickel by Oxidative Insertion: Preparation, Structure, and Catalytic Activity", *Chemistry – A European Journal* **2005**, *11*, 1833, https://doi.org/10.1002/chem.200400928.

[86] E. A. B. Kantchev, C. J. O'Brien, M. G. Organ, "Palladium Complexes of N-Heterocyclic Carbenes as Catalysts for Cross-Coupling Reactions—A Synthetic Chemist's Perspective", *Angewandte Chemie International Edition* **2007**, *46*, 2768, https://doi.org/10.1002/anie.200601663.

[87] G. Altenhoff, S. Würtz, F. Glorius, "The first palladium-catalyzed Sonogashira coupling of unactivated secondary alkyl bromides", *Tetrahedron Letters* **2006**, *47*, 2925, https://doi.org/10.1016/j.tetlet.2006.02.111.

[88] Z. I. Dehimat, S. Yaşar, D. Tebbani, İ. Özdemir, "Sonogashira cross-coupling reaction catalyzed by N-heterocyclic carbene-Pd(II)-PPh3 complexes under copper free and aerobic conditions", *Inorganica Chimica Acta* **2018**, *469*, 325, https://doi.org/10.1016/j.ica.2017.09.048.

[89] J. Yang, J.-Z. Lu, T. Wang, Y.-Y. Zhao, G.-H. Zhu, "A series of (NHC)Pd(N^O)(OAc) complexes: synthesis, characterization and catalytic activities towards desulfinative Sonogashira coupling of arylsulfonyl hydrazides with arylalkynes", *Applied Organometallic Chemistry* **2020**, *34*, e5558, https://doi.org/10.1002/aoc.5558.

[90] G. A. Grasa, S. P. Nolan, "Palladium/Imidazolium Salt Catalyzed Coupling of Aryl Halides with Hypervalent Organostannates", *Organic Letters* **2001**, *3*, 119, https://doi.org/10.1021/ol006827f.

[91] N. Hadei, E. A. B. Kantchev, C. J. O'Brien, M. G. Organ, "Room-Temperature Negishi Cross-Coupling of Unactivated Alkyl Bromides with Alkyl Organozinc Reagents Utilizing a Pd/N-Heterocyclic Carbene Catalyst", *The Journal of Organic Chemistry* **2005**, *70*, 8503, https://doi.org/10.1021/jo051304c.

[92] W. A. Herrmann, C.-P. Reisinger, M. Spiegler, "Chelating N-heterocyclic carbene ligands in palladium-catalyzed heck-type reactions1N-Heterocyclic Carbenes, Part 17.-For the preceding communication of this series, see [3].1", *Journal of Organometallic Chemistry* **1998**, *557*, 93, https://doi.org/10.1016/S0022-328X(97)00736-5.

[93] C. Zhang, J. Huang, M. L. Trudell, S. P. Nolan, "ChemInform Abstract: Palladium—Imidazol-2-ylidene Complexes as Catalysts for Facile and Efficient Suzuki Cross-Coupling Reactions of Aryl Chlorides with Arylboronic Acids", *ChemInform* **1999**, *30*, https://doi.org/10.1002/chin.199939065.

[94] V. Karthik, I. A. Bhat, G. Anantharaman, "Backbone Thio-Functionalized Imidazol-2-ylidene–Metal Complexes: Synthesis, Structure, Electronic Properties, and Catalytic Activity", *Organometallics* **2013**, *32*, 7006, https://doi.org/10.1021/om400585b.

[95] W. A. Herrmann, M. Elison, J. Fischer, C. Köcher, G. R. J. Artus, "Metal Complexes of N-Heterocyclic Carbenes—A New Structural Principle for Catalysts in Homogeneous Catalysis", *Angewandte Chemie International Edition in English* **1995**, *34*, 2371, https://doi.org/10.1002/anie.199523711.

[96] N. Kaloğlu, M. Kaloğlu, M. N. Tahir, C. Arıcı, C. Bruneau, H. Doucet, P. H. Dixneuf, B. Çetinkaya, İ. Özdemir, "Synthesis of N-heterocyclic carbene-palladium-PEPPSI complexes and their catalytic activity in the direct C-H bond activation", *Journal of Organometallic Chemistry* **2018**, *867*, 404, https://doi.org/10.1016/j.jorganchem.2017.10.019.

[97] S. P. Nolan, "*N-Heterocyclic Carbenes: Effective Tools for Organometallic Synthesis*", Wiley-VCH, Germany, 2014, p. 568,

[98] A. J. Arduengo, III, H. V. R. Dias, J. C. Calabrese, F. Davidson, "Homoleptic carbene-silver(I) and carbene-copper(I) complexes", *Organometallics* **1993**, *12*, 3405, https://doi.org/10.1021/om00033a009.

[99] H. G. Raubenheimer, S. Cronje, P. J. Olivier, J. G. Toerien, P. H. van Rooyen, "Synthesis and Crystal Structure of a Monocarbene Complex of Copper", *Angewandte Chemie International Edition in English* **1994**, *33*, 672, https://doi.org/10.1002/anie.199406721.

[100] A. A. D. Tulloch, A. A. Danopoulos, S. Kleinhenz, M. E. Light, M. B. Hursthouse, G. Eastham, "Structural Diversity in Pyridine-N-Functionalized Carbene Copper(I) Complexes", *Organometallics* **2001**, *20*, 2027, http://dx.doi.org/10.1021/om010014t.

[101] W. S. Mahoney, D. M. Brestensky, J. M. Stryker, "Selective hydride-mediated conjugate reduction of .alpha.,.beta.-unsaturated carbonyl compounds using [(Ph3P)CuH]6", *Journal of the American Chemical Society* **1988**, *110*, 291, https://doi.org/10.1021/ja00209a048.

[102] H. Kaur, F. K. Zinn, E. D. Stevens, S. P. Nolan, "(NHC)CuI (NHC = N-Heterocyclic Carbene) Complexes as Efficient Catalysts for the Reduction of Carbonyl Compounds", *Organometallics* **2004**, *23*, 1157, https://doi.org/10.1021/om034285a.

[103] M. Meldal, C. W. Tornøe, "Peptidotriazoles: Copper(I)-Catalyzed 1,3-Dipolar Cycloadditions on Solid-Phase", in *Proceedings of the Second International and the Seventeenth American Peptide Symposium*, 2001263, https://doi.org/10.1007/978-94-010-0464-0_119.

[104] H. C. Kolb, M. G. Finn, K. B. Sharpless, "Click Chemistry: Diverse Chemical Function from a Few Good Reactions", *Angewandte Chemie International Edition* **2001**, *40*, 2004, http://dx.doi.org/10.1002/1521-3773(20010601)40:11<2004::AID-ANIE2004>3.0.CO;2-5.

[105] S. Díez-González, A. Correa, L. Cavallo, S. P. Nolan, "(NHC)Copper(I)-Catalyzed [3+2] Cycloaddition of Azides and Mono- or Disubstituted Alkynes", *Chemistry − A European Journal* **2006**, *12*, 7558, https://doi.org/10.1002/chem.200600961.

[106] S. Díez-González, S. P. Nolan, "[(NHC)₂Cu]X Complexes as Efficient Catalysts for Azide–Alkyne Click Chemistry at Low Catalyst Loadings", *Angewandte Chemie International Edition* **2008**, *47*, 8881, http://dx.doi.org/10.1002/anie.200803289.

[107] H. Lebel, M. Davi, S. Díez-González, S. P. Nolan, "Copper–Carbene Complexes as Catalysts in the Synthesis of Functionalized Styrenes and Aliphatic Alkenes", *The Journal of Organic Chemistry* **2007**, *72*, 144, https://doi.org/10.1021/jo061781a.

[108] H. Lebel, V. Paquet, "Rhodium-Catalyzed Methylenation of Aldehydes", *Journal of the American Chemical Society* **2004**, *126*, 320, https://doi.org/10.1021/ja038112o.

[109] M. R. Fructos, T. R. Belderrain, M. C. Nicasio, S. P. Nolan, H. Kaur, M. M. Díaz-Requejo, P. J. Pérez, "Complete Control of the Chemoselectivity in Catalytic Carbene Transfer Reactions from Ethyl Diazoacetate: An N-Heterocyclic Carbene−Cu System That Suppresses Diazo Coupling", *Journal of the American Chemical Society* **2004**, *126*, 10846, https://doi.org/10.1021/ja047284y.

[110] T. Ohishi, M. Nishiura, Z. Hou, "Carboxylation of Organoboronic Esters Catalyzed by N-Heterocyclic Carbene Copper(I) Complexes", *Angewandte Chemie International Edition* **2008**, *47*, 5792, https://doi.org/10.1002/anie.200801857.

[111] W. Wu, Z. Lin, H. Jiang, "Recent advances in the synthesis of cyclopropanes", *Organic & Biomolecular Chemistry* **2018**, *16*, 7315, http://dx.doi.org/10.1039/C8OB01187G.

[112] S. Chen, J. Ma, J. Wang, "Palladium-catalyzed cyclopropanation of electron-deficient olefins with aryldiazocarbonyl compounds", *Tetrahedron Letters* **2008**, *49*, 6781, https://doi.org/10.1016/j.tetlet.2008.09.024.

[113] G. Berthon-Gelloz, M. Marchant, B. F. Straub, I. E. Marko, "Palladium-Catalyzed Cyclopropanation of Alkenyl Silanes by Diazoalkanes: Evidence for a Pd0 Mechanism", *Chemistry − A European Journal* **2009**, *15*, 2923, https://doi.org/10.1002/chem.200802052.

[114] H. Wang, D. M. Guptill, A. V. Alvarez, D. G. Musaev, H. M. L. Davies, "Rhodium-catalyzed enantioselective cyclopropanation of electron deficient alkenes", *Chemical Science* **2013**, *4*, 2844, https://doi.org/10.1039/C3SC50425E.

[115] F. González-Bobes, M. D. B. Fenster, S. Kiau, L. Kolla, S. Kolotuchin, M. Soumeillant, "Rhodium-Catalyzed Cyclopropanation of Alkenes with Dimethyl Diazomalonate", *Advanced Synthesis & Catalysis* **2008**, *350*, 813, https://doi.org/10.1002/adsc.200800027.

[116] R. G. Salomon, J. K. Kochi, "Copper(I) catalysis in cyclopropanations with diazo compounds. Role of olefin coordination", *Journal of the American Chemical Society* **1973**, *95*, 3300, https://doi.org/10.1021/ja00791a038.

[117] W. Kirmse, "Copper Carbene Complexes: Advanced Catalysts, New Insights", *Angewandte Chemie International Edition* **2003**, *42*, 1088, https://doi.org/10.1002/anie.200390290.

[118] H. Lebel, J.-F. Marcoux, C. Molinaro, A. B. Charette, "Stereoselective Cyclopropanation Reactions", *Chemical Reviews* **2003**, *103*, 977, https://doi.org/10.1021/cr010007e.

[119] C. Deng, H.-K. Liu, Z.-B. Zheng, L. Wang, X. Yu, W. Zhang, Y. Tang, "Copper-Catalyzed Enantioselective Cyclopropanation of Internal Olefins with Diazomalonates", *Organic Letters* **2017**, *19*, 5717, https://doi.org/10.1021/acs.orglett.7b02694.

[120] G. A. B. Abdullin MI, Gazizova ER, Dokichev VA, Sultanova RM, Zaikov GE, Abzaldinov Kh. S. , "Cyclopropane derivatives of syndiotactic 1,2-polybutadiene", *Bulletin of Kazan Technological University* **2015**,

[121] J. Urbano, B. Korthals, M. M. Díaz-Requejo, P. J. Pérez, S. Mecking, "Catalytic cyclopropanation of polybutadienes", *Journal of Polymer Science Part A: Polymer Chemistry* **2010**, *48*, 4439, https://doi.org/10.1002/pola.24231.

[122] A. Caballero, M. M. Díaz-Requejo, T. R. Belderraín, M. C. Nicasio, S. Trofimenko, P. J. Pérez, "Highly Regioselective Functionalization of Aliphatic Carbon–Hydrogen Bonds with a Perbromohomoscorpionate Copper(I) Catalyst", *Journal of the American Chemical Society* **2003**, *125*, 1446, https://doi.org/10.1021/ja0291484.

[123] A. L. Rheingold, L. M. Liable-Sands, C. L. Incarvito, S. Trofimenko, "Novel scorpionate ligands devoid of C–H bonds: BpBr3 and TpBr3", *Journal of the Chemical Society, Dalton Transactions* **2002**, 2297, http://dx.doi.org/10.1039/B111568P.

[124] C. Martín, F. Molina, E. Alvarez, T. R. Belderrain, "Stable N-Heterocyclic Carbene (NHC)–Palladium(0) Complexes as Active Catalysts for Olefin Cyclopropanation Reactions with Ethyl Diazoacetate", *Chemistry – A European Journal* **2011**, *17*, 14885, https://doi.org/10.1002/chem.201102900.

[125] M. R. Fructos, J. Urbano, M. M. Díaz-Requejo, P. J. Pérez, "Evidencing an inner-sphere mechanism for NHC-Au(I)-catalyzed carbene-transfer reactions from ethyl diazoacetate", *Beilstein Journal of Organic Chemistry* **2015**, *11*, 2254, https://doi.org/10.3762/bjoc.11.245.

[126] M. R. Fructos, T. R. Belderrain, P. de Frémont, N. M. Scott, S. P. Nolan, M. M. Díaz-Requejo, P. J. Pérez, "A Gold Catalyst for Carbene-Transfer Reactions from Ethyl Diazoacetate", *Angewandte Chemie International Edition* **2005**, *44*, 5284, https://doi.org/10.1002/anie.200501056.

[127] R. E. Gawley, S. Narayan, "Stannyl cyclopropanes by diastereoselective cyclopropanations with (tributylstannyl)-diazoacetate esters catalyzed by Cu(i) N-heterocyclic carbene", *Chemical Communications* **2005**, 5109, http://dx.doi.org/10.1039/B509958G.

[128] S. Neumann, M. Biewend, S. Rana, W. H. Binder, "The CuAAC: Principles, Homogeneous and Heterogeneous Catalysts, and Novel Developments and Applications", *Macromolecular Rapid Communications* **2020**, *41*, 1900359, https://doi.org/10.1002/marc.201900359.

[129] W. H. Binder, R. Sachsenhofer, "'Click' Chemistry in Polymer and Materials Science", *Macromolecular Rapid Communications* **2007**, *28*, 15, http://dx.doi.org/10.1002/marc.200600625.

[130] W. H. Binder, R. Sachsenhofer, "'Click' Chemistry in Polymer and Material Science: An Update", *Macromolecular Rapid Communications* **2008**, *29*, 952, http://dx.doi.org/10.1002/marc.200800089.

[131] W. H. Binder, R. Sachenshofer, ""Click"-chemistry on supramolecular materials", in *Click Chemistry for Biotechnology and Materials Science*, J. Lahann, Ed., Wiley-Blackwell, 2009, p. 119, http://dx.doi.org/10.1002/9780470748862.ch7.

[132] M. Meldal, C. W. Tornøe, "Cu-Catalyzed Azide–Alkyne Cycloaddition", *Chemical Reviews* **2008**, *108*, 2952, http://dx.doi.org/10.1021/cr0783479.

[133] H. C. Kolb, K. B. Sharpless, "The growing impact of click chemistry on drug discovery", *Drug Discovery Today* **2003**, *8*, 1128, https://doi.org/10.1016/S1359-6446(03)02933-7.

[134] K. B. Sharpless, Z. P. Demko, "A Click Chemistry Approach to Tetrazoles by Huisgen 1,3-Dipolar Cycloaddition: Synthesis of 5-Sulfonyl Tetrazoles from Azides and Sulfonyl Cyanides", *Angewandte Chemie International Edition* **2002**, *41*, 2110, http://dx.doi.org/10.1002/1521-3773(20020617)41:12<2110::AID-ANIE2110>3.0.CO;2-7.

[135] R. Huisgen, "Kinetics and reaction mechanisms: selected examples from the experience of forty years", *Pure and Applied Chemistry* **1989**, *61*, 613, https://doi.org/10.1351/pac198961040613.

[136] R. Huisgen, "Cycloadditionen — Begriff, Einteilung und Kennzeichnung", *Angewandte Chemie* **1968**, *80*, 329, http://dx.doi.org/10.1002/ange.19680800902.

[137] R. Huisgen, "1.3-Dipolare Cycloadditionen Rückschau und Ausblick", *Angewandte Chemie* **1963**, *75*, 604, http://dx.doi.org/10.1002/ange.19630751304.

[138] W. G. Lewis, L. G. Green, F. Grynszpan, Z. Radić, P. R. Carlier, P. Taylor, M. G. Finn, K. B. Sharpless, "Click Chemistry In Situ: Acetylcholinesterase as a Reaction Vessel for the Selective Assembly of a Femtomolar Inhibitor from an Array of Building Blocks", *Angewandte Chemie International Edition* **2002**, *41*, 1053, https://doi.org/10.1002/1521-3773(20020315)41:6<1053::AID-ANIE1053>3.0.CO;2-4.

[139] G. Delaittre, N. K. Guimard, C. Barner-Kowollik, "Cycloadditions in Modern Polymer Chemistry", *Accounts of Chemical Research* **2015**, *48*, 1296, http://dx.doi.org/10.1021/acs.accounts.5b00075.

[140] V. V. Rostovtsev, L. G. Green, V. V. Fokin, K. B. Sharpless, "A Stepwise Huisgen Cycloaddition Process: Copper(I)-Catalyzed Regioselective "Ligation" of Azides and Terminal Alkynes", *Angewandte Chemie International Edition* **2002**, *41*, 2596, http://dx.doi.org/10.1002/1521-3773(20020715)41:14<2596::AID-ANIE2596>3.0.CO;2-4.

[141] M. van Dijk, D. T. S. Rijkers, R. M. J. Liskamp, C. F. van Nostrum, W. E. Hennink, "Synthesis and Applications of Biomedical and Pharmaceutical Polymers via Click Chemistry Methodologies", *Bioconjugate Chemistry* **2009**, *20*, 2001, http://dx.doi.org/10.1021/bc900087a.

[142] V. K. Tiwari, B. B. Mishra, K. B. Mishra, N. Mishra, A. S. Singh, X. Chen, "Cu-Catalyzed Click Reaction in Carbohydrate Chemistry", *Chemical Reviews* **2016**, *116*, 3086, http://dx.doi.org/10.1021/acs.chemrev.5b00408.

[143] S. Chassaing, V. Beneteau, P. Pale, "When CuAAC 'Click Chemistry' goes heterogeneous", *Catalysis Science & Technology* **2016**, *6*, 923, http://dx.doi.org/10.1039/C5CY01847A.

[144] P. Espeel, F. E. Du Prez, ""Click"-Inspired Chemistry in Macromolecular Science: Matching Recent Progress and User Expectations", *Macromolecules* **2015**, *48*, 2, http://dx.doi.org/10.1021/ma501386v.

[145] I. S. Park, M. S. Kwon, Y. Kim, J. S. Lee, J. Park, "Heterogeneous Copper Catalyst for the Cycloaddition of Azides and Alkynes without Additives under Ambient Conditions", *Organic Letters* **2008**, *10*, 497, http://dx.doi.org/10.1021/ol702790w.

[146] A. Pourjavadi, S. H. Hosseini, F. Matloubi Moghaddam, S. E. Ayati, "Copper loaded cross-linked poly(ionic liquid): robust heterogeneous catalyst in ppm amount", *RSC Advances* **2015**, *5*, 29609, http://dx.doi.org/10.1039/C5RA00127G.

[147] M. Biewend, "Synthesis and mechanochemical activation of copper(I)-bis(NHC) complexes with different architectures", in *Naturwissenschaftlichen Fakultät II*, Martin-Luther-Universität Halle-Wittenberg, Halle, 2021, p. PhD/164, http://dx.doi.org/10.25673/35746.

[148] M. Meldal, "Polymer "Clicking" by CuAAC Reactions", *Macromolecular Rapid Communications* **2008**, *29*, 1016, http://dx.doi.org/10.1002/marc.200800159.

[149] V. O. Rodionov, V. V. Fokin, M. G. Finn, "Mechanism of the Ligand-Free CuI-Catalyzed Azide–Alkyne Cycloaddition Reaction", *Angewandte Chemie International Edition* **2005**, *44*, 2210, https://doi.org/10.1002/anie.200461496.

[150] J. D. Egbert, C. S. J. Cazin, S. P. Nolan, "Copper N-heterocyclic carbene complexes in catalysis", *Catalysis Science & Technology* **2013**, *3*, 912, http://dx.doi.org/10.1039/C2CY20816D.

[151] S. Schoffelen, M. Meldal, "Alkyne-Azide Reactions", in *Modern Alkyne Chemistry*, Wiley-VCH Verlag GmbH & Co. KGaA, 2014, p. 113, http://dx.doi.org/10.1002/9783527677894.ch5.

[152] M. M. Sanne Schoffelen, "Catalytic Click Reactions", in *Applied Homogeneous Catalysis with Organometallic Compounds*, p. 1541, https://doi.org/10.1002/9783527651733.ch32.

[153] D. Döhler, P. Michael, W. H. Binder, "CuAAC-Based Click Chemistry in Self-Healing Polymers", *Accounts of Chemical Research* **2017**, *50*, 2610, http://dx.doi.org/10.1021/acs.accounts.7b00371.

[154] B. T. Worrell, J. A. Malik, V. V. Fokin, "Direct Evidence of a Dinuclear Copper Intermediate in Cu(I)-Catalyzed Azide-Alkyne Cycloadditions", *Science* **2013**, *340*, 457, https://doi.org/10.1126/science.1229506.

[155] L.-A. Schaper, S. J. Hock, W. A. Herrmann, F. E. Kühn, "Synthesis and Application of Water-Soluble NHC Transition-Metal Complexes", *Angewandte Chemie International Edition* **2013**, *52*, 270, http://dx.doi.org/10.1002/anie.201205119.

[156] S. Diez-Gonzalez, E. D. Stevens, S. P. Nolan, "A [(NHC)CuCl] complex as a latent Click catalyst", *Chemical Communications* **2008**, *0*, 4747, http://dx.doi.org/10.1039/B806806B.

[157] S. Diez-Gonzalez, E. C. Escudero-Adan, J. Benet-Buchholz, E. D. Stevens, A. M. Z. Slawin, S. P. Nolan, "[(NHC)CuX] complexes: Synthesis, characterization and catalytic activities in reduction reactions and Click Chemistry. On the advantage of using well-defined catalytic systems", *Dalton Transactions* **2010**, *39*, 7595, http://dx.doi.org/10.1039/C0DT00218F.

[158] T. Nakamura, T. Terashima, K. Ogata, S.-i. Fukuzawa, "Copper(I) 1,2,3-Triazol-5-ylidene Complexes as Efficient Catalysts for Click Reactions of Azides with Alkynes", *Organic Letters* **2011**, *13*, 620, http://dx.doi.org/10.1021/ol102858u.

[159] C. Nolte, P. Mayer, B. F. Straub, "Isolation of a Copper(I) Triazolide: A "Click" Intermediate", *Angewandte Chemie International Edition* **2007**, *46*, 2101, http://dx.doi.org/10.1002/anie.200604444.

[160] F. Lazreg, C. S. J. Cazin, "Copper(I)–N-Heterocyclic Carbene Complexes as Efficient Catalysts for the Synthesis of 1,4-Disubstituted 1,2,3-Sulfonyltriazoles in Air", *Organometallics* **2018**, *37*, 679, https://doi.org/10.1021/acs.organomet.7b00506.

[161] T. M. Horsley Downie, J. W. Hall, T. P. Collier Finn, D. J. Liptrot, J. P. Lowe, M. F. Mahon, C. L. McMullin, M. K. Whittlesey, "The first ring-expanded NHC–copper(i) phosphides as catalysts in the highly selective hydrophosphination of isocyanates", *Chemical Communications* **2020**, *56*, 13359, http://dx.doi.org/10.1039/D0CC05694D.

[162] M. Sharma, B. Adhikari, R. F. Awoyemi, A. M. Perkins, A. K. Duckworth, B. Donnadieu, D. O. Wipf, S. L. Stokes, J. P. Emerson, "Copper(II) NHC Catalyst for the Formation of Phenol from Arylboronic Acid", *Chemistry* **2022**, *4*, 560, https://doi.org/10.3390/chemistry4020040.

[163] Q. a. W. Dou, Tao and Jia, Duo and Hu, Yaoqiang and Liu, Zhiling and Zhang, Nina, "Ring Expansion of Oxetanes to 4-Substituted Furans with Nhc-Cu Catalysts", Tetrahedron Letters, 2023, http://dx.doi.org/10.2139/ssrn.4330270.

[164] J. D. Cope, P. E. Sheridan, C. J. Galloway, R. F. Awoyemi, S. L. Stokes, J. P. Emerson, "Synthesis and Characterization of a Tetradentate, N-Heterocyclic Carbene Copper(II) Complex and Its Use as a Chan–Evans–Lam Coupling Catalyst", *Organometallics* **2020**, *39*, 4457, https://doi.org/10.1021/acs.organomet.0c00552.

[165] B. M. Zimmermann, T. T. Ngoc, D.-I. Tzaras, T. Kaicharla, J. F. Teichert, "A Bifunctional Copper Catalyst Enables Ester Reduction with H2: Expanding the Reactivity Space of Nucleophilic Copper Hydrides", *Journal of the American Chemical Society* **2021**, *143*, 16865, https://doi.org/10.1021/jacs.1c09626.

[166] M. M. Caruso, D. A. Davis, Q. Shen, S. A. Odom, N. R. Sottos, S. R. White, J. S. Moore, "Mechanically-Induced Chemical Changes in Polymeric Materials", *Chemical Reviews* **2009**, *109*, 5755, http://dx.doi.org/10.1021/cr9001353.

[167] J. Li, C. Nagamani, J. S. Moore, "Polymer Mechanochemistry: From Destructive to Productive", *Accounts of Chemical Research* **2015**, *48*, 2181, http://dx.doi.org/10.1021/acs.accounts.5b00184.

[168] R. Groote, R. T. M. Jakobs, R. P. Sijbesma, "Mechanocatalysis: forcing latent catalysts into action", *Polymer Chemistry* **2013**, *4*, 4846, http://dx.doi.org/10.1039/C3PY00071K.

[169] Y. Chen, G. Mellot, D. van Luijk, C. Creton, R. P. Sijbesma, "Mechanochemical tools for polymer materials", *Chemical Society Reviews* **2021**, *50*, 4100, http://dx.doi.org/10.1039/D0CS00940G.

[170] G. Kaupp, "Mechanochemistry: the varied applications of mechanical bond-breaking", *CrystEngComm* **2009**, *11*, 388, http://dx.doi.org/10.1039/B810822F.

[171] G. Kaupp, "Waste-free synthesis and production all across chemistry with the benefit of self-assembled crystal packings", *The Journal of Physical Organic Chemistry* **2008**, *21*, 630, https://doi.org/10.1002/poc.1340.

[172] H. Staudinger, W. Heuer, "Über hochpolymere Verbindungen, 93. Mitteil.: Über das Zerreißen der Faden-Moleküle des Poly-styrols", *Berichte der deutschen chemischen Gesellschaft (A and B Series)* **1934**, *67*, 1159, http://dx.doi.org/10.1002/cber.19340670708.

[173] M. M. Caruso, D. A. Davis, Q. Shen, S. A. Odom, N. R. Sottos, S. R. White, J. S. Moore, "Mechanically-Induced Chemical Changes in Polymeric Materials", *Chem. Rev.* **2009**, *109*, 5755, http://dx.doi.org/10.1021/cr9001353.

[174] C. E. Diesendruck, J. S. Moore, "Mechanophores for Self-Healing Applications", in *Self-Healing Polymers*, 2013, p. 193, https://doi.org/10.1002/9783527670185.ch8.

[175] N. R. Sottos, "Flex, release and repeat", *Nature Chemistry* **2014**, *6*, 381, https://doi.org/10.1038/nchem.1927.

[176] Y. Chen, A. J. H. Spiering, S. Karthikeyan, G. W. M. Peters, E. W. Meijer, R. P. Sijbesma, "Mechanically induced chemiluminescence from polymers incorporating a 1,2-dioxetane unit in the main chain", *Nature Chemistry* **2012**, *4*, 559, https://doi.org/10.1038/nchem.1358.

[177] J. M. Clough, A. Balan, R. P. Sijbesma, "Mechanochemical Reactions Reporting and Repairing Bond Scission in Polymers", in *Topics in Current Chemistry*, R. Boulatov, Ed., Springer International Publishing, Cham, 2015, p. 209, https://doi.org/10.1007/128_2015_641.

[178] J. M. J. Paulusse, R. P. Sijbesma, "Ultrasound in polymer chemistry: Revival of an established technique", *Journal of Polymer Science Part A: Polymer Chemistry* **2006**, *44*, 5445, https://doi.org/10.1002/pola.21646.

[179] M. T. Ong, J. Leiding, H. Tao, A. M. Virshup, T. J. Martínez, "First Principles Dynamics and Minimum Energy Pathways for Mechanochemical Ring Opening of Cyclobutene", *Journal of the American Chemical Society* **2009**, *131*, 6377, http://dx.doi.org/10.1021/ja8095834.

[180] M. K. Beyer, "The mechanical strength of a covalent bond calculated by density functional theory", *The Journal of Chemical Physics* **2000**, *112*, 7307, https://doi.org/10.1063/1.481330.

[181] J. Ribas-Arino, D. Marx, "Covalent Mechanochemistry: Theoretical Concepts and Computational Tools with Applications to Molecular Nanomechanics", *Chemical Reviews* **2012**, *112*, 5412, http://dx.doi.org/10.1021/cr200399q.

[182] M. K. Beyer, H. Clausen-Schaumann, "Mechanochemistry: The Mechanical Activation of Covalent Bonds", *Chemical Reviews* **2005**, *105*, 2921, http://dx.doi.org/10.1021/cr030697h.

[183] J. N. Brantley, K. M. Wiggins, C. W. Bielawski, "Polymer mechanochemistry: the design and study of mechanophores", *Polymer International* **2013**, *62*, 2, http://dx.doi.org/10.1002/pi.4350.

[184] H. M. Klukovich, T. B. Kouznetsova, Z. S. Kean, J. M. Lenhardt, S. L. Craig, "A backbone lever-arm effect enhances polymer mechanochemistry", *Nature Chemistry* **2013**, *5*, 110, http://dx.doi.org/10.1038/nchem.1540.

[185] J. Wang, T. B. Kouznetsova, Z. S. Kean, L. Fan, B. D. Mar, T. J. Martínez, S. L. Craig, "A Remote Stereochemical Lever Arm Effect in Polymer Mechanochemistry", *Journal of the American Chemical Society* **2014**, *136*, 15162, http://dx.doi.org/10.1021/ja509585g.

[186] P. Michael, "Synthesis and characterization of polymer based Cu(I)-mechanocatalysts", in *Naturwissenschaftlichen Fakultät II*, Martin Luther University, Halle-Wittenberg, Halle (Saale), 2016, p. Doktorgrades der Naturwissenschaften (Dr. rer. nat.)/167, http://dx.doi.org/10.25673/1872.

[187] B. A. Beiermann, S. L. B. Kramer, J. S. Moore, S. R. White, N. R. Sottos, "Role of Mechanophore Orientation in Mechanochemical Reactions", *ACS Macro Letters* **2012**, *1*, 163, https://doi.org/10.1021/mz2000847.

[188] S. L. Potisek, D. A. Davis, N. R. Sottos, S. R. White, J. S. Moore, "Mechanophore-Linked Addition Polymers", *Journal of the American Chemical Society* **2007**, *129*, 13808, https://doi.org/10.1021/ja076189x.

[189] D. A. Davis, A. Hamilton, J. Yang, L. D. Cremar, D. Van Gough, S. L. Potisek, M. T. Ong, P. V. Braun, T. J. Martínez, S. R. White, J. S. Moore, N. R. Sottos, "Force-induced activation of covalent bonds in mechanoresponsive polymeric materials", *Nature* **2009**, *459*, 68, https://doi.org/10.1038/nature07970.

[190] C. M. Kingsbury, P. A. May, D. A. Davis, S. R. White, J. S. Moore, N. R. Sottos, "Shear activation of mechanophore-crosslinked polymers", *Journal of Materials Chemistry* **2011**, *21*, 8381, http://dx.doi.org/10.1039/C0JM04015K

[191] Y.-K. Song, K.-H. Lee, W.-S. Hong, S.-Y. Cho, H.-C. Yu, C.-M. Chung, "Fluorescence sensing of microcracks based on cycloreversion of a dimeric anthracene moiety", *Journal of Materials Chemistry* **2012**, *22*, 1380, http://dx.doi.org/10.1039/C1JM13709C.

[192] R. Göstl, R. P. Sijbesma, "π-extended anthracenes as sensitive probes for mechanical stress", *Chemical Science* **2016**, *7*, 370, http://dx.doi.org/10.1039/C5SC03297K.

[193] D. C. Church, G. I. Peterson, A. J. Boydston, "Comparison of Mechanochemical Chain Scission Rates for Linear versus Three-Arm Star Polymers in Strong Acoustic Fields", *ACS Macro Letters* **2014**, *3*, 648, http://dx.doi.org/10.1021/mz5003068.

[194] Z. S. Kean, G. R. Gossweiler, T. B. Kouznetsova, G. B. Hewage, S. L. Craig, "A Coumarin Dimer Probe of Mechanochemical Scission Efficiency in the Sonochemical Activation of Chain-Centered Mechanophore Polymers", *Chemical Communications* **2015**, *51*, 9157, http://dx.doi.org/10.1039/C5CC01836F.

[195] L. Wang, W. Zhou, Q. Tang, H. Yang, Q. Zhou, X. Zhang, "Rhodamine-Functionalized Mechanochromic and Mechanofluorescent Hydrogels with Enhanced Mechanoresponsive Sensitivity", *Polymers* **2018**, *10*, 994, https://doi.org/10.3390/polym10090994.

[196] L.-J. Wang, K.-X. Yang, Q. Zhou, H.-Y. Yang, J.-Q. He, X.-Y. Zhang, "Rhodamine Mechanophore Functionalized Mechanochromic Double Network Hydrogels with High Sensitivity to Stress", *Chinese Journal of Polymer Science* **2019**, https://doi.org/10.1007/s10118-019-2293-1.

[197] Z. Ma, Y. Ji, Y. Lan, G.-C. Kuang, X. Jia, "Two novel rhodamine-based molecules with different mechanochromic and photochromic properties in solid state", *Journal of Materials Chemistry C* **2018**, *6*, 2270, http://dx.doi.org/10.1039/C8TC00145F.

[198] J. M. Lenhardt, A. L. Black, S. L. Craig, "gem-Dichlorocyclopropanes as Abundant and Efficient Mechanophores in Polybutadiene Copolymers under Mechanical Stress", *Journal of the American Chemical Society* **2009**, *131*, 10818, http://dx.doi.org/10.1021/ja9036548.

[199] A. L. B. Ramirez, Z. S. Kean, J. A. Orlicki, M. Champhekar, S. M. Elsakr, W. E. Krause, S. L. Craig, "Mechanochemical strengthening of a synthetic polymer in response to typically destructive shear forces", *Nature Chemistry* **2013**, *5*, 757, https://doi.org/10.1038/nchem.1720.

[200] Y. Chen, A. J. H. Spiering, KarthikeyanS, G. W. M. Peters, E. W. Meijer, R. P. Sijbesma, "Mechanically induced chemiluminescence from polymers incorporating a 1,2-dioxetane unit in the main chain", *Nature Chemistry* **2012**, *4*, 559, http://dx.doi.org/10.1038/nchem.1358.

[201] N. J. Turro, P. Lechtken, N. E. Schore, G. Schuster, H. C. Steinmetzer, A. Yekta, "Tetramethyl-1,2-dioxetane. Experiments in chemiexcitation, chemiluminescence, photochemistry, chemical dynamics, and spectroscopy", *Accounts of Chemical Research* **1974**, *7*, 97, https://doi.org/10.1021/ar50076a001.

[202] G. B. Schuster, N. J. Turro, H. C. Steinmetzer, A. P. Schaap, G. Faler, W. Adam, J. C. Liu, "Adamantylideneadamantane-1,2-dioxetane. Chemiluminescence and decomposition kinetics of an unusually stable 1,2-dioxetane", *Journal of the American Chemical Society* **1975**, *97*, 7110, https://doi.org/10.1021/ja00857a024.

[203] Y. Sagara, M. Karman, E. Verde-Sesto, K. Matsuo, Y. Kim, N. Tamaoki, C. Weder, "Rotaxanes as Mechanochromic Fluorescent Force Transducers in Polymers", *Journal of the American Chemical Society* **2018**, *140*, 1584, https://doi.org/10.1021/jacs.7b12405.

[204] C. K. Lee, C. E. Diesendruck, E. Lu, A. N. Pickett, P. A. May, J. S. Moore, P. V. Braun, "Solvent Swelling Activation of a Mechanophore in a Polymer Network", *Macromolecules* **2014**, *47*, 2690, https://doi.org/10.1021/ma500195h.

[205] J. M. Clough, J. van der Gucht, R. P. Sijbesma, "Mechanoluminescent Imaging of Osmotic Stress-Induced Damage in a Glassy Polymer Network", *Macromolecules* **2017**, *50*, 2043, http://dx.doi.org/10.1021/acs.macromol.6b02540.

[206] V. Zysman, T. Q. Nguyen, H.-H. Kausch, "Degradation on freezing dilute polystyrene solutions in p-xylene", *Journal of Polymer Science Part B: Polymer Physics* **1994**, *32*, 1257, http://dx.doi.org/10.1002/polb.1994.090320713.

[207] S. Wang, X. Yan, J. Ding, M. Liu, R. Cheng, C. Wu, R. Qian, "On the cryogenic "degradation" of polystyrene in dilute solution", *Journal of Macromolecular Science, Part B* **1997**, *36*, 187, https://doi.org/10.1080/00222349708220424.

[208] K. Imato, A. Irie, T. Kosuge, T. Ohishi, M. Nishihara, A. Takahara, H. Otsuka, "Mechanophores with a Reversible Radical System and Freezing-Induced Mechanochemistry in Polymer Solutions and Gels", *Angewandte Chemie International Edition* **2015**, *54*, 6168, http://dx.doi.org/10.1002/anie.201412413.

[209] K. M. Wiggins, J. N. Brantley, C. W. Bielawski, "Methods for activating and characterizing mechanically responsive polymers", *Chemical Society Reviews* **2013**, *42*, 7130, http://dx.doi.org/10.1039/C3CS35493H.

[210] A. F. Horn, E. W. Merrill, "Midpoint scission of macromolecules in dilute solution in turbulent flow", *Nature* **1984**, *312*, 140, http://dx.doi.org/10.1038/312140a0.

[211] G. J. Price, "The use of ultrasound for the controlled degradation of polymer solutions", *Advances in Sonochemistry* **1990**, *1*, 231,

[212] K. S. Suslick, "Sonochemistry", in *Kirk-Othmer Encyclopedia of Chemical Technology*, 4th edition, Kirk-Othmer, Ed., J. Wiley & Sons: New York, 1998, p. 517, https://doi.org/10.1002/0471238961.1915141519211912.a01.

[213] K. S. Suslick, "Mechanochemistry and sonochemistry: concluding remarks", *Faraday Discussions* **2014**, *170*, 411, http://dx.doi.org/10.1039/C4FD00148F.

[214] J. Kida, K. Imato, R. Goseki, D. Aoki, M. Morimoto, H. Otsuka, "The photoregulation of a mechanochemical polymer scission", *Nature Communications* **2018**, *9*, 3504, https://doi.org/10.1038/s41467-018-05996-7.

[215] G. Cravotto, E. C. Gaudino, P. Cintas, "On the mechanochemical activation by ultrasound", *Chemical Society Reviews* **2013**, *42*, 7521, http://dx.doi.org/10.1039/C2CS35456J.

[216] M. W. A. Kuijpers, P. D. Iedema, M. F. Kemmere, J. T. F. Keurentjes, "The mechanism of cavitation-induced polymer scission; experimental and computational verification", *Polymer* **2004**, *45*, 6461, http://dx.doi.org/10.1016/j.polymer.2004.06.051.

[217] R. Küng, R. Göstl, B. M. Schmidt, "Release of Molecular Cargo from Polymer Systems by Mechanochemistry", *Chemistry – A European Journal* **2022**, *28*, e202103860, https://doi.org/10.1002/chem.202103860.

[218] L. Tu, Z. Liao, Z. Luo, Y.-L. Wu, A. Herrmann, S. Huo, "Ultrasound-controlled drug release and drug activation for cancer therapy", *Exploration* **2021**, *1*, 20210023, https://doi.org/10.1002/EXP.20210023.

[219] R. Groote, "Mechanochemical activation of latent N-heterocyclic carbene catalysts", Technische Universiteit Eindhoven, Eindhoven, 2013, p. PhD/, https://doi.org/10.6100/IR747611.

[220] K. S. Suslick, G. J. Price, "Application of ultrasound to materials chemistry", *Annual Review of Materials Science* **1999**, *29*, 295, https://doi.org/10.1146/annurev.matsci.29.1.295.

[221] T. J. M. a. J. P. Lorimer, "*Applied Sonochemistry: Uses of Power Ultrasound in Chemistry and Processing*", 2002, https://doi.org/10.1002/352760054X.

[222] M. M. v. Iersel, "Sensible Sonochemistry", in *Chemical Engineering and Chemistry*, Technische Universiteit Eindhoven, Eindhoven, 2008, p. PhD/, https://doi.org/10.6100/IR638503.

[223] M. Okkuama, T. Hirose, "Mechanics of ultrasonic degradation of linear high polymer and ultrasonic cavitation", *Journal of Applied Polymer Science* **1963**, *7*, 591, https://doi.org/10.1002/app.1963.070070216.

[224] H. Oka, K. Imato, T. Sato, T. Ohishi, R. Goseki, H. Otsuka, "Enhancing Mechanochemical Activation in the Bulk State by Designing Polymer Architectures", *ACS Macro Letters* **2016**, *5*, 1124, http://dx.doi.org/10.1021/acsmacrolett.6b00529.

[225] K. Imato, H. Otsuka, "Reorganizable and stimuli-responsive polymers based on dynamic carbon–carbon linkages in diarylbibenzofuranones", *Polymer* **2018**, *137*, 395, https://doi.org/10.1016/j.polymer.2018.01.038.

[226] L. Rinaldi, K. Martina, F. Baricco, L. Rotolo, G. Cravotto, "Solvent-Free Copper-Catalyzed Azide-Alkyne Cycloaddition under Mechanochemical Activation", *Molecules* **2015**, *20*, 2837, https://doi.org/10.3390/molecules20022837.

[227] W. Liu, Y. Cao, W. Wang, D. Gong, T. Cao, J. Qian, K. Iqbal, W. Qin, H. Guo, "Mechanochromic luminescent covalent organic frameworks for highly selective hydroxyl radical detection", *Chemical Communications* **2019**, *55*, 167, http://dx.doi.org/10.1039/C8CC07783E.

[228] B. A. Beiermann, D. A. Davis, S. L. B. Kramer, J. S. Moore, N. R. Sottos, S. R. White, "Environmental effects on mechanochemical activation of spiropyran in linear PMMA", *Journal of Materials Chemistry* **2011**, *21*, 8443, http://dx.doi.org/10.1039/C0JM03967E.

[229] B. A. Beiermann, S. L. B. Kramer, P. A. May, J. S. Moore, S. R. White, N. R. Sottos, "The Effect of Polymer Chain Alignment and Relaxation on Force-Induced Chemical Reactions in an Elastomer", *Advanced Functional Materials* **2014**, *24*, 1529, http://dx.doi.org/10.1002/adfm.201302341.

[230] T. A. Kim, M. J. Robb, J. S. Moore, S. R. White, N. R. Sottos, "Mechanical Reactivity of Two Different Spiropyran Mechanophores in Polydimethylsiloxane", *Macromolecules* **2018**, *51*, 9177, https://doi.org/10.1021/acs.macromol.8b01919.

[231] P. Michael, W. H. Binder, "A Mechanochemically Triggered "Click" Catalyst", *Angewandte Chemie International Edition* **2015**, *54*, 13918, https://doi.org/10.1002/anie.201505678.

[232] G. Kister, M. Moniruzzaman, M. Khan, S. Debnath, "Mechanophore-linked hydroxyl-terminated polybutadiene for the remote detection and quantification of mechanical stress", *Dyes and Pigments* **2019**, *162*, 309, https://doi.org/10.1016/j.dyepig.2018.10.036.

[233] J. M. Lenhardt, A. L. Black, B. A. Beiermann, B. D. Steinberg, F. Rahman, T. Samborski, J. Elsakr, J. S. Moore, N. R. Sottos, S. L. Craig, "Characterizing the mechanochemically active domains in gem-dihalocyclopropanated polybutadiene under compression and tension", *Journal of Materials Chemistry* **2011**, *21*, 8454, http://dx.doi.org/10.1039/C0JM04117C.

[234] M. Biewend, S. Neumann, P. Michael, W. H. Binder, "Synthesis of polymer-linked copper(i) bis(N-heterocyclic carbene) complexes of linear and chain extended architecture", *Polymer Chemistry* **2019**, *10*, 1078, http://dx.doi.org/10.1039/C8PY01751D.

[235] R. T. M. Jakobs, S. Ma, R. P. Sijbesma, "Mechanocatalytic Polymerization and Cross-Linking in a Polymeric Matrix", *ACS Macro Letters* **2013**, *2*, 613, http://dx.doi.org/10.1021/mz400201c.

[236] G. R. Gossweiler, G. B. Hewage, G. Soriano, Q. Wang, G. W. Welshofer, X. Zhao, S. L. Craig, "Mechanochemical Activation of Covalent Bonds in Polymers with Full and Repeatable Macroscopic Shape Recovery", *ACS Macro Letters* **2014**, *3*, 216, http://dx.doi.org/10.1021/mz500031q.

[237] C. L. Brown, M. H. Barbee, J. H. Ko, H. D. Maynard, S. L. Craig, "Writing Without Ink: A Mechanically and Photochemically Responsive PDMS Polymer for Science Outreach", *Journal of Chemical Education* **2017**, *94*, 1752, http://dx.doi.org/10.1021/acs.jchemed.6b00806.

[238] Y. Chen, H. Zhang, X. Fang, Y. Lin, Y. Xu, W. Weng, "Mechanical Activation of Mechanophore Enhanced by Strong Hydrogen Bonding Interactions", *ACS Macro Letters* **2014**, *3*, 141, http://dx.doi.org/10.1021/mz400600r.

[239] X. Fang, H. Zhang, Y. Chen, Y. Lin, Y. Xu, W. Weng, "Biomimetic Modular Polymer with Tough and Stress Sensing Properties", *Macromolecules* **2013**, *46*, 6566, https://doi.org/10.1021/ma4014862.

[240] G. Hong, H. Zhang, Y. Lin, Y. Chen, Y. Xu, W. Weng, H. Xia, "Mechanoresponsive Healable Metallosupramolecular Polymers", *Macromolecules* **2013**, *46*, 8649, https://doi.org/10.1021/ma4017532.

[241] H. Zhang, Y. Chen, Y. Lin, X. Fang, Y. Xu, Y. Ruan, W. Weng, "Spiropyran as a Mechanochromic Probe in Dual Cross-Linked Elastomers", *Macromolecules* **2014**, *47*, 6783, http://dx.doi.org/10.1021/ma500760p.

[242] J. M. J. Paulusse, R. P. Sijbesma, "Reversible Mechanochemistry of a Pd[II] Coordination Polymer", *Angewandte Chemie International Edition* **2004**, *43*, 4460, http://dx.doi.org/10.1002/anie.200460040.

[243] J. M. J. Paulusse, J. P. J. Huijbers, R. P. Sijbesma, "Reversible, High Molecular Weight Palladium and Platinum Coordination Polymers Based on Phosphorus Ligands", *Macromolecules* **2005**, *38*, 6290, https://doi.org/10.1021/ma050561g.

[244] J. M. J. Paulusse, J. P. J. Huijbers, R. P. Sijbesma, "Quantification of Ultrasound-Induced Chain Scission in Pd[II]–Phosphine Coordination Polymers", *Chemistry – A European Journal* **2006**, *12*, 4928, http://dx.doi.org/10.1002/chem.200600120.

[245] S. Funtan, "Synthesis of biomimetic elastin-like polypeptides as molecular springs for the activation of Cu(I) bis(NHC) mechanocatalysts", in *Naturwissenschaftlichen Fakultät II*, Martin-Luther-Universität Halle-Wittenberg, Germany, 2020, p. Dr. rer. nat./178, http://dx.doi.org/10.25673/35198.

[246] J. M. J. Paulusse, R. P. Sijbesma, "Selectivity of mechanochemical chain scission in mixed palladium(ii) and platinum(ii) coordination polymers", *Chemical Communications* **2008**, 4416, http://dx.doi.org/10.1039/B806978F.

[247] M. Di Giannantonio, M. A. Ayer, E. Verde-Sesto, M. Lattuada, C. Weder, K. M. Fromm, "Triggered Metal Ion Release and Oxidation: Ferrocene as a Mechanophore in Polymers", *Angewandte Chemie International Edition* **2018**, *57*, 11445, https://doi.org/10.1002/anie.201803524.

[248] Y. Sha, Y. Zhang, E. Xu, Z. Wang, T. Zhu, S. L. Craig, C. Tang, "Quantitative and Mechanistic Mechanochemistry in Ferrocene Dissociation", *ACS Macro Letters* **2018**, *7*, 1174, https://doi.org/10.1021/acsmacrolett.8b00625.

[249] S. Karthikeyan, S. L. Potisek, A. Piermattei, R. P. Sijbesma, "Highly Efficient Mechanochemical Scission of Silver-Carbene Coordination Polymers", *Journal of the American Chemical Society* **2008**, *130*, 14968, https://doi.org/10.1021/ja806887k.

[250] R. Groote, B. M. Szyja, E. A. Pidko, E. J. M. Hensen, R. P. Sijbesma, "Unfolding and Mechanochemical Scission of Supramolecular Polymers Containing a Metal–Ligand Coordination Bond", *Macromolecules* **2011**, *44*, 9187, https://doi.org/10.1021/ma201722e.

[251] J. Rooze, R. Groote, R. T. M. Jakobs, R. P. Sijbesma, M. M. van Iersel, E. V. Rebrov, J. C. Schouten, J. T. F. Keurentjes, "Mechanism of Ultrasound Scission of a Silver–Carbene Coordination Polymer", *The Journal of physical Chemistry B* **2011**, *115*, 11038, https://doi.org/10.1021/jp203780a.

[252] A. Piermattei, S. Karthikeyan, R. P. Sijbesma, "Activating catalysts with mechanical force", *Nature Chemistry* **2009**, *1*, 133, https://doi.org/10.1038/nchem.167.

[253] R. Groote, L. van Haandel, R. P. Sijbesma, "The effect of molecular weight and catalyst concentration on catalytic activity in mechanochemically activated transesterification using silver(I)-N-heterocyclic carbene latent catalysts", *Journal of Polymer Science Part A: Polymer Chemistry* **2012**, *50*, 4929, http://dx.doi.org/10.1002/pola.26323.

[254] J.-L. Do, C. Mottillo, D. Tan, V. Štrukil, T. Friščić, "Mechanochemical Ruthenium-Catalyzed Olefin Metathesis", *Journal of The American Chemical Society* **2015**, *137*, 2476, https://doi.org/10.1021/jacs.5b00151.

[255] R. T. M. Jakobs, R. P. Sijbesma, "Mechanical Activation of a Latent Olefin Metathesis Catalyst and Persistence of its Active Species in ROMP", *Organometallics* **2012**, *31*, 2476, https://doi.org/10.1021/om300161z.

[256] R. Groote, R. T. M. Jakobs, R. P. Sijbesma, "Performance of Mechanochemically Activated Catalysts Is Enhanced by Suppression of the Thermal Effects of Ultrasound", *ACS Macro Letters* **2012**, *1*, 1012, http://dx.doi.org/10.1021/mz3002512.

[257] P. Michael, W. H. Binder, "A Mechanochemically Triggered "Click" Catalyst", *Angew. Chem. Int. Ed.* **2015**, *54*, 13918, https://onlinelibrary.wiley.com/doi/abs/10.1002/anie.201505678.

[258] P. Michael, S. K. Sheidaee Mehr, W. H. Binder, "Synthesis and characterization of polymer linked copper(I) bis(N-heterocyclic carbene) mechanocatalysts", *Journal of Polymer Science Part A: Polymer Chemistry* **2017**, *55*, 3893, https://doi.org/10.1002/pola.28775.

[259] S. Funtan, P. Michael, W. H. Binder, "Synthesis and Mechanochemical Activity of Peptide-Based Cu(I) Bis(N-heterocyclic carbene) Complexes", *Biomimetics* **2019**, *4*, 24, https://doi.org/10.3390/biomimetics4010024.

[260] S. Funtan, A. Funtan, R. Paschke, W. Binder, "Biomimetic Elastin-Like Polypeptides as Materials for the Activation of Mechanophoric Catalysts", *Organic Materials* **2020**, *02*, 116, http://dx.doi.org/10.1055/s-0040-1702149.

[261] C. Le Droumaguet, C. Wang, Q. Wang, "Fluorogenic click reaction", *Chemical Society Reviews* **2010**, *39*, 1233, http://dx.doi.org/10.1039/B901975H

[262] H. Hu, Z. Ma, X. Jia, "Reaction Cascades in Polymer Mechanochemistry", *Materials Chemistry Frontiers* **2020**, *4*, 3115, http://dx.doi.org/10.1039/D0QM00435A.

[263] M. Biewend, S. Neumann, P. Michael, W. H. Binder, "Synthesis of polymer-linked copper(i) bis(N-heterocyclic carbene) complexes of linear and chain extended architecture", *Polym. Chem.* **2019**, *10*, 1078, http://dx.doi.org/10.1039/C8PY01751D.

[264] M. Biewend, P. Michael, W. H. Binder, "Detection of stress in polymers: mechanochemical activation of CuAAC click reactions in poly(urethane) networks", *Soft Matter* **2020**, *16*, 1137, http://dx.doi.org/10.1039/C9SM02185J.

[265] P. Michael, M. Biewend, W. H. Binder, "Mechanochemical Activation of Fluorogenic CuAAC "Click" Reactions for Stress-Sensing Applications", *Macromol. Rapid Comm.* **2018**, *39*, 1800376, https://doi.org/10.1002/marc.201800376.

[266] C. I. Ezugwu, N. A. Kabir, M. Yusubov, F. Verpoort, "Metal–organic frameworks containing N-heterocyclic carbenes and their precursors", *Coordination Chemistry Reviews* **2016**, *307*, 188, https://doi.org/10.1016/j.ccr.2015.06.012.

[267] S. Chaemchuen, N. A. Kabir, K. Zhou, F. Verpoort, "Metal-organic frameworks for upgrading biogas via CO2 adsorption to biogas green energy", *Chemical Society Reviews* **2013**, *42*, 9304, http://dx.doi.org/10.1039/C3CS60244C.

[268] H. Li, M. Eddaoudi, M. O'Keeffe, O. M. Yaghi, "Design and synthesis of an exceptionally stable and highly porous metal-organic framework", *Nature* **1999**, *402*, 276, https://doi.org/10.1038/46248.

[269] S. S.-Y. Chui, S. M.-F. Lo, J. P. H. Charmant, A. G. Orpen, I. D. Williams, "A Chemically Functionalizable Nanoporous Material [Cu3(TMA)2(H2O)3]n", *Science* **1999**, *283*, 1148, http://dx.doi.org/10.1126/science.283.5405.1148.

[270] J. Lee, O. K. Farha, J. Roberts, K. A. Scheidt, S. T. Nguyen, J. T. Hupp, "Metal-organic framework materials as catalysts", *Chemical Society Reviews* **2009**, *38*, 1450, http://dx.doi.org/10.1039/B807080F.

[271] J. Liu, L. Chen, H. Cui, J. Zhang, L. Zhang, C.-Y. Su, "Applications of metal-organic frameworks in heterogeneous supramolecular catalysis", *Chemical Society Reviews* **2014**, *43*, 6011, http://dx.doi.org/10.1039/C4CS00094C.

[272] Y. Jiang, J. Huang, M. Hunger, M. Maciejewski, A. Baiker, "Comparative studies on the catalytic activity and structure of a Cu-MOF and its precursor for alcoholysis of cyclohexene oxide", *Catalysis Science & Technology* **2015**, *5*, 897, http://dx.doi.org/10.1039/C4CY00916A.

[273] M. Opanasenko, "Catalytic behavior of metal-organic frameworks and zeolites: Rationalization and comparative analysis", *Catalysis Today* **2015**, *243*, 2, https://doi.org/10.1016/j.cattod.2014.06.040.

[274] J. R. L. Hong-Cai Zhou, and Omar M. Yaghi, "Introduction to Metal–Organic Frameworks", *Chemical Reviews* **2012**, *112*, 673, https://doi.org/10.1021/cr300014x.

[275] B. F. Hoskins, R. Robson, "Design and construction of a new class of scaffolding-like materials comprising infinite polymeric frameworks of 3D-linked molecular rods. A reappraisal of the zinc cyanide and cadmium cyanide structures and the synthesis and structure of the diamond-related frameworks [N(CH3)4][CuIZnII(CN)4] and CuI[4,4',4'',4'''-tetracyanotetraphenylmethane]BF4.xC6H5NO2", *Journal of the American Chemical Society* **1990**, *112*, 1546, https://doi.org/10.1021/ja00160a038.

[276] W. Lu, Z. Wei, Z.-Y. Gu, T.-F. Liu, J. Park, J. Park, J. Tian, M. Zhang, Q. Zhang, T. Gentle Iii, M. Bosch, H.-C. Zhou, "Tuning the structure and function of metal–organic frameworks via linker design", *Chemical Society Reviews* **2014**, *43*, 5561, http://dx.doi.org/10.1039/C4CS00003J.

[277] S. R. Caskey, A. G. Wong-Foy, A. J. Matzger, "Dramatic Tuning of Carbon Dioxide Uptake via Metal Substitution in a Coordination Polymer with Cylindrical Pores", *Journal of the American Chemical Society* **2008**, *130*, 10870, https://doi.org/10.1021/ja8036096.

[278] H. Deng, S. Grunder, K. E. Cordova, C. Valente, H. Furukawa, M. Hmadeh, F. Gándara, A. C. Whalley, Z. Liu, S. Asahina, H. Kazumori, M. O'Keeffe, O. Terasaki, J. F. Stoddart, O. M. Yaghi, "Large-Pore Apertures in a Series of Metal-Organic Frameworks", *Science* **2012**, *336*, 1018, https://doi.org/10.1126/science.1220131.

[279] W. Morris, C. J. Doonan, H. Furukawa, R. Banerjee, O. M. Yaghi, "Crystals as Molecules: Postsynthesis Covalent Functionalization of Zeolitic Imidazolate Frameworks", *Journal of the American Chemical Society* **2008**, *130*, 12626, https://doi.org/10.1021/ja805222x.

[280] Y. Pan, X. Yu, "Preparation of Zeolitic Imidazolate Framework-91 and its modeling for pervaporation separation of water/ethanol mixtures", *Separation and Purification Technology* **2020**, *237*, 116330, https://doi.org/10.1016/j.seppur.2019.116330.

[281] M. Usman, M. Y. Khan, T. Anjum, A. L. Khan, B. Hoque, A. Helal, A. S. Hakeem, B. A. Al-Maythalony, "Controlled Covalent Functionalization of ZIF-90 for Selective CO2 Capture & Separation", *Membranes* **2022**, *12*, 1055, https://doi.org/10.3390/membranes12111055.

[282] J. C. Tan, T. D. Bennett, A. K. Cheetham, "Chemical structure, network topology, and porosity effects on the mechanical properties of Zeolitic Imidazolate Frameworks", *Proceedings of the National Academy of Sciences USA* **2010**, *107*, 9938, https://doi.org/10.1073/pnas.1003205107.

[283] J. C. Tan, A. K. Cheetham, "Mechanical properties of hybrid inorganic–organic framework materials: establishing fundamental structure–property relationships", *Chemical Society Reviews* **2011**, *40*, 1059, http://dx.doi.org/10.1039/C0CS00163E.

[284] S. S. Han, W. A. Goddard, "Metal−Organic Frameworks Provide Large Negative Thermal Expansion Behavior", *The Journal of Physical Chemistry C* **2007**, *111*, 15185, https://doi.org/10.1021/jp075389s.

[285] J. Kaur, G. Kaur, "Review on Flexible Metal-Organic Frameworks", *ChemistrySelect* **2021**, *6*, 8227, https://doi.org/10.1002/slct.202101524.

[286] K. S. Suslick, "Sonocatalysis", in *Handbook of Heterogeneous Catalysis*, G.K. Ertl, H.; Weitkamp, J., Ed., Wiley-VCH: Weinheim, 1997, https://doi.org/10.1002/9783527619474.ch8.

[287] X. Wang, H. Zhang, Z. Yang, C. Zhang, S. Liu, "Ultrasound-treated metal-organic framework with efficient electrocatalytic oxygen evolution activity", *Ultrasonics Sonochemistry* **2019**, *59*, 104714, https://doi.org/10.1016/j.ultsonch.2019.104714.

[288] P.-Z. Li, Y. Maeda, Q. Xu, "Top-down fabrication of crystalline metal–organic framework nanosheets", *Chemical Communications* **2011**, *47*, 8436, http://dx.doi.org/10.1039/C1CC12510A.

[289] Y.-z. Li, Z.-h. Fu, G. Xu, "Metal-organic framework nanosheets: Preparation and applications", *Coordination Chemistry Reviews* **2019**, *388*, 79, https://doi.org/10.1016/j.ccr.2019.02.033.

[290] P. Amo-Ochoa, L. Welte, R. González-Prieto, P. J. Sanz Miguel, C. J. Gómez-García, E. Mateo-Martí, S. Delgado, J. Gómez-Herrero, F. Zamora, "Single layers of a multifunctional laminar Cu(i,ii) coordination polymer", *Chemical Communications* **2010**, *46*, 3262, http://dx.doi.org/10.1039/B919647A.

[291] C. Hermosa, B. R. Horrocks, J. I. Martínez, F. Liscio, J. Gómez-Herrero, F. Zamora, "Mechanical and optical properties of ultralarge flakes of a metal–organic framework with molecular thickness", *Chemical Science* **2015**, *6*, 2553, http://dx.doi.org/10.1039/C4SC03115F.

[292] C. Martí-Gastaldo, J. E. Warren, K. C. Stylianou, N. L. O. Flack, M. J. Rosseinsky, "Enhanced Stability in Rigid Peptide-Based Porous Materials", *Angewandte Chemie International Edition* **2012**, *51*, 11044, https://doi.org/10.1002/anie.201203929.

[293] A. Kondo, C. C. Tiew, F. Moriguchi, K. Maeda, "Fabrication of metal–organic framework nanosheets and nanorolls with N-donor type bridging ligands", *Dalton Transactions* **2013**, *42*, 15267, http://dx.doi.org/10.1039/C3DT52130C.

[294] J.-C. Tan, P. J. Saines, E. G. Bithell, A. K. Cheetham, "Hybrid Nanosheets of an Inorganic–Organic Framework Material: Facile Synthesis, Structure, and Elastic Properties", *ACS Nano* **2012**, *6*, 615, https://doi.org/10.1021/nn204054k.

[295] P. J. Beldon, S. Tominaka, P. Singh, T. Saha Dasgupta, E. G. Bithell, A. K. Cheetham, "Layered structures and nanosheets of pyrimidinethiolate coordination polymers", *Chemical Communications* **2014**, *50*, 3955, http://dx.doi.org/10.1039/C4CC00771A.

[296] P. J. Saines, J.-C. Tan, H. H. M. Yeung, P. T. Barton, A. K. Cheetham, "Layered inorganic–organic frameworks based on the 2,2-dimethylsuccinate ligand: structural diversity and its effect on nanosheet exfoliation and magnetic properties", *Dalton Transactions* **2012**, *41*, 8585, http://dx.doi.org/10.1039/C2DT30648D.

[297] J. A. Foster, S. Henke, A. Schneemann, R. A. Fischer, A. K. Cheetham, "Liquid exfoliation of alkyl-ether functionalised layered metal–organic frameworks to nanosheets", *Chemical Communications* **2016**, *52*, 10474, http://dx.doi.org/10.1039/C6CC05154E.

[298] G. Lamming, O. El-Zubir, J. Kolokotroni, C. McGurk, P. G. Waddell, M. R. Probert, A. Houlton, "Two-Dimensional Frameworks Based on Ag(I)–N Bond Formation: Single Crystal to Single Molecular Sheet Transformation", *Inorganic Chemistry* **2016**, *55*, 9644, https://doi.org/10.1021/acs.inorgchem.6b01365.

[299] P. Chandrasekhar, A. Mukhopadhyay, G. Savitha, J. N. Moorthy, "Orthogonal self-assembly of a trigonal triptycene triacid: signaling of exfoliation of porous 2D metal–organic layers by fluorescence and selective CO2 capture by the hydrogen-bonded MOF", *Journal of Materials Chemistry A* **2017**, *5*, 5402, http://dx.doi.org/10.1039/C6TA11110F.

[300] M. J. Cliffe, E. Castillo-Martínez, Y. Wu, J. Lee, A. C. Forse, F. C. N. Firth, P. Z. Moghadam, D. Fairen-Jimenez, M. W. Gaultois, J. A. Hill, O. V. Magdysyuk, B. Slater, A. L. Goodwin, C. P. Grey, "Metal–Organic Nanosheets Formed via Defect-Mediated Transformation of a Hafnium Metal–Organic Framework", *Journal of the American Chemical Society* **2017**, *139*, 5397, https://doi.org/10.1021/jacs.7b00106.

[301] L. Cao, C. Wang, "Metal–Organic Layers for Electrocatalysis and Photocatalysis", *ACS Central Science* **2020**, *6*, 2149, https://doi.org/10.1021/acscentsci.0c01150.

[302] J. B. Lefton, K. B. Pekar, U. Haris, M. E. Zick, P. J. Milner, A. R. Lippert, L. Pejov, T. Runčevski, "Defect formation and amorphization of Zn-MOF-74 crystals by post-synthetic interactions with bidentate adsorbates", *Journal of Materials Chemistry A* **2021**, *9*, 19698, http://dx.doi.org/10.1039/D0TA10613E.

[303] T. D. Bennett, A. K. Cheetham, "Amorphous Metal–Organic Frameworks", *Accounts of Chemical Research* **2014**, *47*, 1555, https://doi.org/10.1021/ar5000314.

[304] K. W. Chapman, G. J. Halder, P. J. Chupas, "Pressure-Induced Amorphization and Porosity Modification in a Metal–Organic Framework", *Journal of the American Chemical Society* **2009**, *131*, 17546, https://doi.org/10.1021/ja908415z.

[305] Y. H. Hu, L. Zhang, "Amorphization of metal-organic framework MOF-5 at unusually low applied pressure", *Physical Review B* **2010**, *81*, 174103, https://doi.org/10.1103/PhysRevB.81.174103.

[306] V. V. Boldyrev, "Mechanochemistry and Mechanical Activation", *Materials Science Forum* **1996**, *225-227*, 511, https://doi.org/10.4028/www.scientific.net/MSF.225-227.511.

[307] P. Baláž, "*Mechanochemistry in Nanoscience and Minerals Engineering"*, 1 edition, Springer Berlin, Heidelberg, Germany, 2008, p. 413, https://doi.org/10.1007/978-3-540-74855-7.

[308] Y.-R. Miao, K. S. Suslick, "Chapter Nine - Mechanochemical Reactions of Metal-Organic Frameworks", in *Advances in Inorganic Chemistry*, R. van Eldik and R. Puchta, Eds., Academic Press, 2018, p. 403, https://doi.org/10.1016/bs.adioch.2017.11.001.

[309] Z. Su, Y.-R. Miao, G. Zhang, J. T. Miller, K. S. Suslick, "Bond breakage under pressure in a metal organic framework", *Chemical Science* **2017**, *8*, 8004, http://dx.doi.org/10.1039/C7SC03786D.

[310] Z. Su, W. L. Shaw, Y.-R. Miao, S. You, D. D. Dlott, K. S. Suslick, "Shock Wave Chemistry in a Metal–Organic Framework", *Journal of the American Chemical Society* **2017**, *139*, 4619, https://doi.org/10.1021/jacs.6b12956.

[311] C. Wang, D. Ikhlef, S. Kahlal, J.-Y. Saillard, D. Astruc, "Metal-catalyzed azide-alkyne "click" reactions: Mechanistic overview and recent trends", *Coordination Chemistry Reviews* **2016**, *316*, 1, https://doi.org/10.1016/j.ccr.2016.02.010.

[312] P. Li, S. Regati, H. Huang, H. D. Arman, J. C. G. Zhao, B. Chen, "A metal–organic framework as a highly efficient and reusable catalyst for the solvent-free 1,3-dipolar cycloaddition of organic azides to alkynes", *Inorganic Chemistry Frontiers* **2015**, *2*, 42, http://dx.doi.org/10.1039/C4QI00148F.

[313] X. Guo, L. Zeng, Z. Wang, T. Zhang, C. He, C. Duan, "Photocatalytic copper-catalyzed azide–alkyne cycloaddition click reaction with Cu(ii) coordination polymer", *RSC Advances* **2017**, *7*, 52907, http://dx.doi.org/10.1039/C7RA10207K.

[314] F. Wang, Y. Zhang, Z. Liu, Z. Du, L. Zhang, J. Ren, X. Qu, "A Biocompatible Heterogeneous MOF–Cu Catalyst for In Vivo Drug Synthesis in Targeted Subcellular Organelles", *Angewandte Chemie International Edition* **2019**, *58*, 6987, https://doi.org/10.1002/anie.201901760.

[315] G. Tuci, A. Rossin, X. Xu, M. Ranocchiari, J. A. van Bokhoven, L. Luconi, I. Manet, M. Melucci, G. Giambastiani, ""Click" on MOFs: A Versatile Tool for the Multimodal Derivatization of N3-Decorated Metal Organic Frameworks", *Chemistry of Materials* **2013**, *25*, 2297, https://doi.org/10.1021/cm400899a.

[316] Q. Fu, K. Xie, S. Tan, J. M. Ren, Q. Zhao, P. A. Webley, G. G. Qiao, "The use of reduced copper metal-organic frameworks to facilitate CuAAC click chemistry", *Chemical Communications* **2016**, *52*, 12226, http://dx.doi.org/10.1039/C6CC06890A.

[317] U. Fluch, B. D. McCarthy, S. Ott, "Post synthetic exchange enables orthogonal click chemistry in a metal organic framework", *Dalton Transactions* **2019**, *48*, 45, http://dx.doi.org/10.1039/C8DT04563A.

[318] I. Luz, F. X. Llabrés i Xamena, A. Corma, "Bridging homogeneous and heterogeneous catalysis with MOFs: "Click" reactions with Cu-MOF catalysts", *Journal of Catalysis* **2010**, *276*, 134, https://doi.org/10.1016/j.jcat.2010.09.010.

[319] J. Fonseca, T. Gong, L. Jiao, H.-L. Jiang, "Metal–organic frameworks (MOFs) beyond crystallinity: amorphous MOFs, MOF liquids and MOF glasses", *Journal of Materials Chemistry A* **2021**, *9*, 10562, http://dx.doi.org/10.1039/D1TA01043C.

[320] A. U. Czaja, N. Trukhan, U. Müller, "Industrial applications of metal–organic frameworks", *Chemical Society Reviews* **2009**, *38*, 1284, http://dx.doi.org/10.1039/B804680H.

[321] P. Z. Moghadam, A. Li, S. B. Wiggin, A. Tao, A. G. P. Maloney, P. A. Wood, S. C. Ward, D. Fairen-Jimenez, "Development of a Cambridge Structural Database Subset: A Collection of Metal–Organic Frameworks for Past, Present, and Future", *Chemistry of Materials* **2017**, *29*, 2618, https://doi.org/10.1021/acs.chemmater.7b00441.

[322] K. Oisaki, Q. Li, H. Furukawa, A. U. Czaja, O. M. Yaghi, "A Metal–Organic Framework with Covalently Bound Organometallic Complexes", *Journal of the American Chemical Society* **2010**, *132*, 9262, http://dx.doi.org/10.1021/ja103016y.

[323] S. Wang, Q. Yang, J. Zhang, X. Zhang, C. Zhao, L. Jiang, C.-Y. Su, "Two-Dimensional Charge-Separated Metal–Organic Framework for Hysteretic and Modulated Sorption", *Inorganic Chemistry* **2013**, *52*, 4198, http://dx.doi.org/10.1021/ic301781n.

[324] R. T. Yang, "Sorbents for Applications", in *Adsorbents: Fundamentals and Applications*, John Wiley & Sons, inc., 2003, p. 280, https://doi.org/10.1002/047144409X.ch10.

[325] S. A. Moggach, T. D. Bennett, A. K. Cheetham, "The Effect of Pressure on ZIF-8: Increasing Pore Size with Pressure and the Formation of a High-Pressure Phase at 1.47 GPa", *Angewandte Chemie International Edition* **2009**, *48*, 7087, https://doi.org/10.1002/anie.200902643.

[326] Y. Peng, Y. Li, Y. Ban, H. Jin, W. Jiao, X. Liu, W. Yang, "Metal-organic framework nanosheets as building blocks for molecular sieving membranes", *Science* **2014**, *346*, 1356, https://doi.org/10.1126/science.1254227.

[327] P. Kanoo, A. C. Ghosh, S. T. Cyriac, T. K. Maji, "A Metal–Organic Framework with Highly Polar Pore Surfaces: Selective CO2 Adsorption and Guest-Dependent On/Off Emission Properties", *Chemistry – A European Journal* **2012**, *18*, 237, https://doi.org/10.1002/chem.201101183.

[328] M. Dincă, J. R. Long, "Strong H2 Binding and Selective Gas Adsorption within the Microporous Coordination Solid Mg3(O2C-C10H6-CO2)3", *Journal of the American Chemical Society* **2005**, *127*, 9376, https://doi.org/10.1021/ja0523082.

[329] A. Hazra, P. Kanoo, T. K. Maji, "High heat of hydrogen adsorption and guest-responsive magnetic modulation in a 3D porous pillared-layer coordination framework", *Chemical Communications* **2011**, *47*, 538, http://dx.doi.org/10.1039/C0CC02490B.

[330] J. Y. Lee, J. M. Roberts, O. K. Farha, A. A. Sarjeant, K. A. Scheidt, J. T. Hupp, "Synthesis and Gas Sorption Properties of a Metal-Azolium Framework (MAF) Material", *Inorganic Chemistry* **2009**, *48*, 9971, http://dx.doi.org/10.1021/ic901174p.

[331] M. B. Lalonde, O. K. Farha, K. A. Scheidt, J. T. Hupp, "N-Heterocyclic Carbene-Like Catalysis by a Metal–Organic Framework Material", *ACS Catalysis* **2012**, *2*, 1550, https://doi.org/10.1021/cs300260f.

[332] C. E. Willans, S. French, L. J. Barbour, J.-A. Gertenbach, P. C. Junk, G. O. Lloyd, J. W. Steed, "A catenated imidazole-based coordination polymer exhibiting significant CO2 sorption at low pressure", *Dalton Transactions* **2009**, 6480, http://dx.doi.org/10.1039/B911265K.

[333] C. E. Willans, S. French, K. M. Anderson, L. J. Barbour, J.-A. Gertenbach, G. O. Lloyd, R. J. Dyer, P. C. Junk, J. W. Steed, "Tripodal imidazole frameworks: Reversible vapour sorption both with and without significant structural changes", *Dalton Transactions* **2011**, *40*, 573, http://dx.doi.org/10.1039/C0DT01011A.

[334] E. M. Phillips, M. Riedrich, K. A. Scheidt, "N-Heterocyclic Carbene-Catalyzed Conjugate Additions of Alcohols", *Journal of the American Chemical Society* **2010**, *132*, 13179, https://doi.org/10.1021/ja1061196.

[335] G.-Q. Kong, X. Xu, C. Zou, C.-D. Wu, "Two metal–organic frameworks based on a double azolium derivative: post-modification and catalytic activity", *Chemical Communications* **2011**, *47*, 11005, http://dx.doi.org/10.1039/C1CC14393J.

[336] O. M. Yaghi, Kalmutzki, M.J. and Diercks, C.S., "Emergence of Metal-Organic Frameworks", in *Introduction to Reticular Chemistry*, M.J.K.a.C.S.D. O.M. Yaghi, Ed., 2019, p. 1, https://doi.org/10.1002/9783527821099.ch1.

[337] H.-J. Lee, H. Kwon, J. Sim, D. Song, Y. Kim, J. Kim, K. Kim, E. Lee, "Synthetic control of coincidental formation of an N-heterocyclic carbene-copper(i) complex and imidazolium cations within metal-organic frameworks", *CrystEngComm* **2017**, *19*, 1528, http://dx.doi.org/10.1039/C7CE00078B.

[338] A. Burgun, R. S. Crees, M. L. Cole, C. J. Doonan, C. J. Sumby, "A 3-D diamondoid MOF catalyst based on in situ generated [Cu(L)2] N-heterocyclic carbene (NHC) linkers: hydroboration of CO2", *Chemical Communications* **2014**, *50*, 11760, http://dx.doi.org/10.1039/C4CC04761C.

[339] R. S. Crees, M. L. Cole, L. R. Hanton, C. J. Sumby, "Synthesis of a Zinc(II) Imidazolium Dicarboxylate Ligand Metal–Organic Framework (MOF): a Potential Precursor to MOF-Tethered N-Heterocyclic Carbene Compounds", *Inorganic Chemistry* **2010**, *49*, 1712, http://dx.doi.org/10.1021/ic9021118.

[340] S. Sen, N. N. Nair, T. Yamada, H. Kitagawa, P. K. Bharadwaj, "High Proton Conductivity by a Metal–Organic Framework Incorporating Zn8O Clusters with Aligned Imidazolium Groups Decorating the Channels", *Journal of the American Chemical Society* **2012**, *134*, 19432, http://dx.doi.org/10.1021/ja3076378.

[341] J. Chun, I. Gu Jung, H. Kim, M. Park, M. S. Lah, S. Uk Son, "Concomitant Formation of N-Heterocyclic Carbene-Copper Complexes within a Supramolecular Network in the Self-Assembly of Imidazolium Dicarboxylate with Metal Ions", *Inorganic Chemistry* **2009**, *48*, 6353, https://doi.org/10.1021/ic900846s.

[342] R. Shintani, K. Nozaki, "Copper-Catalyzed Hydroboration of Carbon Dioxide", *Organometallics* **2013**, *32*, 2459, https://doi.org/10.1021/om400175h.

[343] O. Bayer, "Das Di-Isocyanat-Polyadditionsverfahren (Polyurethane)", *Angewandte Chemie* **2006**, *59*, 257, https://doi.org/10.1002/ange.19470590901.

[344] J. O. Akindoyo, M. D. H. Beg, S. Ghazali, M. R. Islam, N. Jeyaratnam, A. R. Yuvaraj, "Polyurethane types, synthesis and applications – a review", *RSC Advances* **2016**, *6*, 114453, https://doi.org/10.1039/c6ra14525f.

[345] L. Jiang, Z. Ren, W. Zhao, W. Liu, H. Liu, C. Zhu, "Synthesis and structure/properties characterizations of four polyurethane model hard segments", *Royal Society Open Science* **2018**, *5*, 180536, https://doi.org/10.1098/rsos.180536.

[346] E. a. Z. Shamin, Fahmina, "Polyurethane : An Introduction", 2018, http://dx.doi.org/10.5772/51663.

[347] L. Cuvé, J.-P. Pascault, G. Boiteux, "Synthesis and properties of polyurethanes based on polyolefin: 2. Semicrystalline segmented polyurethanes prepared under heterogeneous or homogeneous synthesis conditions", *Polymer* **1992**, *33*, 3957, https://doi.org/10.1016/0032-3861(92)90389-E.

[348] L. Rueda-Larraz, B. F. d'Arlas, A. Tercjak, A. Ribes, I. Mondragon, A. Eceiza, "Synthesis and microstructure–mechanical property relationships of segmented polyurethanes based on a PCL–

PTHF–PCL block copolymer as soft segment", *European Polymer Journal* **2009**, *45*, 2096, https://doi.org/10.1016/j.eurpolymj.2009.03.013.

[349] I. Yilgör, E. Yilgör, G. L. Wilkes, "Critical parameters in designing segmented polyurethanes and their effect on morphology and properties: A comprehensive review", *Polymer* **2015**, *58*, A1, https://doi.org/10.1016/j.polymer.2014.12.014.

[350] S. Shetranjiwalla, S. Li, L. Bouzidi, S.-S. Narine, "Impact of Polymerization Protocol on Structure-Property Relationships of Entirely Lipid-Derived Poly(ester urethane)s", *Journal of Renewable Materials* **2017**, *5*, 333, https://doi.org/10.7569/JRM.2017.634102.

[351] W. Wang, H. Chen, Q. Dai, D. Zhao, Y. Zhou, L. Wang, D. Zeng, "Thermally healable PTMG-based polyurethane elastomer with robust mechanical properties and high healing efficiency", *Smart Materials and Structures* **2019**, *28*, 015008, https://dx.doi.org/10.1088/1361-665X/aaebc8.

[352] S.-H. Kang, D.-C. Ku, J.-H. Lim, Y.-K. Yang, N.-S. Kwak, T.-S. Hwang, "Characterization for pyrolysis of thermoplastic polyurethane by thermal analyses", *Macromolecular Research* **2005**, *13*, 212, https://doi.org/10.1007/BF03219054.

[353] U. Ojha, P. Kulkarni, R. Faust, "Syntheses and characterization of novel biostable polyisobutylene based thermoplastic polyurethanes", *Polymer* **2009**, *50*, 3448, https://doi.org/10.1016/j.polymer.2009.05.025.

[354] A. Saralegi, L. Rueda, B. Fernández-d'Arlas, I. Mondragon, A. Eceiza, M. A. Corcuera, "Thermoplastic polyurethanes from renewable resources: effect of soft segment chemical structure and molecular weight on morphology and final properties", *Polymer International* **2013**, *62*, 106, https://doi.org/10.1002/pi.4330.

[355] D. B. Klinedinst, I. Yilgör, E. Yilgör, M. Zhang, G. L. Wilkes, "The effect of varying soft and hard segment length on the structure–property relationships of segmented polyurethanes based on a linear symmetric diisocyanate, 1,4-butanediol and PTMO soft segments", *Polymer* **2012**, *53*, 5358, https://doi.org/10.1016/j.polymer.2012.08.005.

[356] F. Jokari-Sheshdeh, "Thermoplastic polyurethanes. Domain morphology evolution under mechanical and thermal load as a function of composition", in *Department of Chemistry*, University of Hamburg, Hamburg, 2017, p. Dr. rer. nat./,

[357] J. Datta, P. Kasprzyk, "Thermoplastic polyurethanes derived from petrochemical or renewable resources: A comprehensive review", *Polymer Engineering & Science* **2018**, *58*, E14, https://doi.org/10.1002/pen.24633.

[358] C. Nedolisa, "Designing High Hard Block Content Thermoplastic Polyurethane (TPU) Resins for Composite Applications", in *Department of Materials*, The University of Manchester, England, 2015, p. Ph.D./,

[359] S. Oprea, "Effect of structure on the thermal stability of crosslinked poly(ester-urethane)", *Polimery* **2009**, *54*, 120, https://doi.org/10.14314/polimery.2009.120.

[360] C.-s. Wang, D. J. Kenney, "Effect of Hard Segments on Morphology and Properties of Thermoplastic Polyurethanes", *Journal of Elastomers and Plastics* **1995**, *27*, 182 https://doi.org/10.1177/009524439502700207.

[361] M. V. Pandya, D. D. Deshpande, D. G. Hundiwale, "Thermal behavior of cast polyurethane elastomers", *Journal of Applied Polymer Science* **1988**, *35*, 1803, https://doi.org/10.1002/app.1988.070350708.

[362] C. Prisacariu, "*Polyurethane Elastomers - From Morphology to Mechanical Aspects*", Springer Vienna, Austria, 2011, https://doi.org/10.1007/978-3-7091-0514-6.

[363] C. P. Buckley, C. Prisacariu, C. Martin, "Elasticity and inelasticity of thermoplastic polyurethane elastomers: Sensitivity to chemical and physical structure", *Polymer* **2010**, *51*, 3213, https://doi.org/10.1016/j.polymer.2010.04.069.

[364] P. Ping, W. Wang, X. Chen, X. Jing, "The influence of hard-segments on two-phase structure and shape memory properties of PCL-based segmented polyurethanes", *Journal of Polymer Science Part B: Polymer Physics* **2007**, *45*, 557, https://doi.org/10.1002/polb.20974.

[365] K. Nakamae, T. Nishino, S. Asaoka, Sudaryanto, "Microphase separation and surface properties of segmented polyurethane—Effect of hard segment content", *International Journal of Adhesion and Adhesives* **1996**, *16*, 233, https://doi.org/10.1016/S0143-7496(96)00009-7.

[366] J. T. Koberstein, A. F. Galambos, L. M. Leung, "Compression-molded polyurethane block copolymers. 1. Microdomain morphology and thermomechanical properties", *Macromolecules* **1992**, *25*, 6195, https://doi.org/10.1021/ma00049a017.

[367] H. Huang, H. Pang, J. Huang, P. Yu, J. Li, M. Lu, B. Liao, "Influence of hard segment content and soft segment length on the microphase structure and mechanical performance of polyurethane-based polymer concrete", *Construction and Building Materials* **2021**, *284*, 122388, https://doi.org/10.1016/j.conbuildmat.2021.122388.

[368] K. S. Kang, C. Jee, J.-H. Bae, H. J. Jung, B. J. Kim, P. Huh, "Effect of soft/hard segments in poly (tetramethylene glycol)-Polyurethane for water barrier film", *Progress in Organic Coatings* **2018**, *123*, 238, https://doi.org/10.1016/j.porgcoat.2018.04.014.

[369] M. Behl, A. Lendlein, "Shape-memory polymers", *Materials Today* **2007**, *10*, 20, https://doi.org/10.1016/s1369-7021(07)70047-0.

[370] H. Meng, J. Hu, "A Brief Review of Stimulus-active Polymers Responsive to Thermal, Light, Magnetic, Electric, and Water/Solvent Stimuli", *Journal of Intelligent Material Systems and Structures* **2010**, *21*, 859, https://doi.org/10.1177/1045389x10369718.

[371] Q. Meng, J. Hu, "A review of shape memory polymer composites and blends", *Composites Part A: Applied Science and Manufacturing* **2009**, *40*, 1661, https://doi.org/10.1016/j.compositesa.2009.08.011.

[372] J. Kunzelman, T. Chung, P. T. Mather, C. Weder, "Shape memory polymers with built-in threshold temperature sensors", *Journal of Materials Chemistry* **2008**, *18*, 1082, http://dx.doi.org/10.1039/B718445J.

[373] T. Xie, "Tunable polymer multi-shape memory effect", *Nature* **2010**, *464*, 267, https://doi.org/10.1038/nature08863.

[374] S. Thakur, J. Hu, "Polyurethane: A Shape Memory Polymer (SMP)", in *Aspects of Polyurethanes*, Y. Faris, Ed., IntechOpen, Rijeka, 2017, p. Ch. 3, https://doi.org/10.5772/intechopen.69992.

[375] H. M. Jeong, B. K. Ahn, B. K. Kim, "Miscibility and shape memory effect of thermoplastic polyurethane blends with phenoxy resin", *European Polymer Journal* **2001**, *37*, 2245, https://doi.org/10.1016/S0014-3057(01)00123-9.

[376] G. Barot, I. J. Rao, "Constitutive modeling of the mechanics associated with crystallizable shape memory polymers", *Zeitschrift für angewandte Mathematik und Physik ZAMP* **2006**, *57*, 652, https://doi.org/10.1007/s00033-005-0009-6.

[377] "*Shape-Memory Polymers and Multifunctional Composites*", 1st edition, CRC Press, Boca Raton, 2010, https://doi.org/10.1201/9781420090208.

[378] W. M. Huang, Z. Ding, C. C. Wang, J. Wei, Y. Zhao, H. Purnawali, "Shape memory materials", *Materials Today* **2010**, *13*, 54, https://doi.org/10.1016/S1369-7021(10)70128-0.

[379] A. Metcalfe, A. C. Desfaits, I. Salazkin, L. Yahia, W. M. Sokolowski, J. Raymond, "Cold hibernated elastic memory foams for endovascular interventions", *Biomaterials* **2003**, *24*, 491, https://doi.org/10.1016/s0142-9612(02)00362-9.

[380] M. Ahmad, B. Xu, H. Purnawali, Y. Fu, W. Huang, M. Miraftab, J. Luo, "High Performance Shape Memory Polyurethane Synthesized with High Molecular Weight Polyol as the Soft Segment", *Applied Sciences* **2012**, *2*, 535, https://doi.org/10.3390/app2020535.

[381] Y. Q. Fu, W. M. Huang, J. K. Luo, H. Lu, "9 - Polyurethane shape-memory polymers for biomedical applications", in *Shape Memory Polymers for Biomedical Applications*, L.H. Yahia, Ed., Woodhead Publishing, 2015, p. 167, https://doi.org/10.1016/B978-0-85709-698-2.00009-X.

[382] C. Prisacariu, "Perspectives. Novel crosslinked polyurethanes as shape-memory materials", in *Polyurethane Elastomers - From Morphology to Mechanical Aspects*, 2011, https://doi.org/10.1007/978-3-7091-0514-6.

[383] C. Prisacariu, E. Scortanu, S. Coseri, B. Agapie, "Characterization of Shape-Memory Trifunctionally Cross-Linked Polyurethanes, with Varying Hard and Soft Segments", *International Journal of Polymer Analysis and Characterization* **2013**, *18*, 154, https://doi.org/10.1080/1023666x.2013.748128.

[384] S. Mondal, "Temperature responsive shape memory polyurethanes", *Polymer-Plastics Technology and Materials* **2021**, *60*, 1491, https://doi.org/10.1080/25740881.2021.1906903.

[385] A. Lendlein, R. Langer, "Biodegradable, Elastic Shape-Memory Polymers for Potential Biomedical Applications", *Science* **2002**, *296*, 1673, https://doi.org/10.1126/science.1066102.

[386] A. Lendlein, S. Kelch, "Shape-Memory Polymers", *Angewandte Chemie International Edition* **2002**, *41*, 2034, https://doi.org/10.1002/1521-3773(20020617)41:12<2034::AID-ANIE2034>3.0.CO;2-M.

[387] J. L. Hu, F. L. Ji, Y. W. Wong, "Dependency of the shape memory properties of a polyurethane upon thermomechanical cyclic conditions", *Polymer International* **2005**, *54*, 600, https://doi.org/10.1002/pi.1745.

[388] J. Diani, Y. Liu, K. Gall, "Finite strain 3D thermoviscoelastic constitutive model for shape memory polymers", *Polymer Engineering & Science* **2006**, *46*, 486, https://doi.org/10.1002/pen.20497.

[389] Y. Liu, K. Gall, M. L. Dunn, A. R. Greenberg, J. Diani, "Thermomechanics of shape memory polymers: Uniaxial experiments and constitutive modeling", *International Journal of Plasticity* **2006**, *22*, 279, https://doi.org/10.1016/j.ijplas.2005.03.004.

[390] A. Bhattacharyya, H. Tobushi, "Analysis of the isothermal mechanical response of a shape memory polymer rheological model", *Polymer Engineering & Science* **2000**, *40*, 2498, https://doi.org/10.1002/pen.11381.

[391] Y.-M. Ha, H. C. Seo, Y.-O. Kim, M.-S. Khil, J. W. Cho, J.-S. Lee, Y. C. Jung, "Effects of Hard Segment of Polyurethane with Disulfide Bonds on Shape Memory and Self-Healing Ability", *Macromolecular Research* **2020**, *28*, 234, https://doi.org/10.1007/s13233-020-8027-y.

[392] B. C. Chun, M. H. Chong, Y.-C. Chung, "Effect of glycerol cross-linking and hard segment content on the shape memory property of polyurethane block copolymer", *Journal of Materials Science* **2007**, *42*, 6524, https://doi.org/10.1007/s10853-007-1568-z.

[393] B. S. Lee, B. C. Chun, Y.-C. Chung, K. I. Sul, J. W. Cho, "Structure and Thermomechanical Properties of Polyurethane Block Copolymers with Shape Memory Effect", *Macromolecules* **2001**, *34*, 6431, https://doi.org/10.1021/ma001842l.

[394] T. Wang, N. Zhang, J. Dai, Z. Li, W. Bai, R. Bai, "Novel Reversible Mechanochromic Elastomer with High Sensitivity: Bond Scission and Bending-Induced Multicolor Switching", *ACS Applied Materials & Interfaces* **2017**, *9*, 11874, https://doi.org/10.1021/acsami.7b00176.

[395] Y. Sagara, M. Karman, A. Seki, M. Pannipara, N. Tamaoki, C. Weder, "Rotaxane-Based Mechanophores Enable Polymers with Mechanically Switchable White Photoluminescence", *ACS Central Science* **2019**, *5*, 874, https://doi.org/10.1021/acscentsci.9b00173.

[396] K. Imato, T. Kanehara, T. Ohishi, M. Nishihara, H. Yajima, M. Ito, A. Takahara, H. Otsuka, "Mechanochromic Dynamic Covalent Elastomers: Quantitative Stress Evaluation and Autonomous Recovery", *ACS Macro Letters* **2015**, *4*, 1307, https://doi.org/10.1021/acsmacrolett.5b00717.

[397] G. A. Filonenko, J. R. Khusnutdinova, "Dynamic Phosphorescent Probe for Facile and Reversible Stress Sensing", *Advanced Materials* **2017**, *29*, 1700563, https://doi.org/10.1002/adma.201700563.

[398] C. K. Lee, D. A. Davis, S. R. White, J. S. Moore, N. R. Sottos, P. V. Braun, "Force-Induced Redistribution of a Chemical Equilibrium", *Journal of the American Chemical Society* **2010**, *132*, 16107, https://doi.org/10.1021/ja106332g.

[399] H. Zhang, F. Gao, X. Cao, Y. Li, Y. Xu, W. Weng, R. Boulatov, "Mechanochromism and Mechanical-Force-Triggered Cross-Linking from a Single Reactive Moiety Incorporated into Polymer Chains", *Angewandte Chemie International Edition* **2016**, *55*, 3040, https://doi.org/10.1002/anie.201510171.

[400] M. P. Doyle, "Catalytic methods for metal carbene transformations", *Chemical Reviews* **1986**, *86*, 919, https://doi.org/10.1021/cr00075a013.

[401] A.-H. Li, L.-X. Dai, V. K. Aggarwal, "Asymmetric Ylide Reactions: Epoxidation, Cyclopropanation, Aziridination, Olefination, and Rearrangement", *Chemical Reviews* **1997**, *97*, 2341, https://doi.org/10.1021/cr960411r.

[402] Y.-R. Miao, Z. Su, K. S. Suslick, "Energy Storage during Compression of Metal–Organic Frameworks", *Journal of the American Chemical Society* **2017**, *139*, 4667, https://doi.org/10.1021/jacs.7b01593.

[403] Q. Wei, H. W. Xu, X. H. Yu, T. Shimada, M. S. Rearick, D. D. Hickmott, Y. S. Zhao, S. N. Luo, "Shock resistance of metal-organic framework Cu-1,3,5-benzenetricarboxylate with and without ferrocene inclusion", *Journal of Applied Physics* **2011**, *110*, 056102, https://doi.org/10.1063/1.3631104.

[404] C. Hermosa, B. R. Horrocks, J. I. Martínez, F. Liscio, J. Gómez-Herrero, F. Zamora, "Mechanical and optical properties of ultralarge flakes of a metal–organic framework with molecular thickness", *Chem. Sci.* **2015**, *6*, 2553, http://dx.doi.org/10.1039/C4SC03115F.

[405] M. J. Cliffe, E. Castillo-Martínez, Y. Wu, J. Lee, A. C. Forse, F. C. N. Firth, P. Z. Moghadam, D. Fairen-Jimenez, M. W. Gaultois, J. A. Hill, O. V. Magdysyuk, B. Slater, A. L. Goodwin, C. P. Grey, "Metal–Organic Nanosheets Formed via Defect-Mediated Transformation of a Hafnium Metal–Organic Framework", *J. Am. Chem. Soc.* **2017**, *139*, 5397, https://doi.org/10.1021/jacs.7b00106.

[406] A. Kondo, C. C. Tiew, F. Moriguchi, K. Maeda, "Fabrication of metal–organic framework nanosheets and nanorolls with N-donor type bridging ligands", *Dalton Trans.* **2013**, *42*, 15267, http://dx.doi.org/10.1039/C3DT52130C.

[407] K. S. Shinde, P. Michael, M. Rössle, S. Thiele, W. H. Binder, "Cyclopropanation of poly(isoprene) using NHC-Cu(I) catalysts: Introducing carboxylates", *Journal of Polymer Science* **2020**, *58*, 2864, https://doi.org/10.1002/pol.20200404.

[408] P. J. Dyson, P. G. Jessop, "Solvent effects in catalysis: rational improvements of catalysts via manipulation of solvent interactions", *Catalysis Science & Technology* **2016**, *6*, 3302, http://dx.doi.org/10.1039/C5CY02197A.

[409] C. Özen, N. Ş. Tüzün, "A DFT Study on the Mechanism of Cyclopropanation via Cu(acac)2-Catalyzed Diazo Ester Decomposition", *Organometallics* **2008**, *27*, 4600, https://doi.org/10.1021/om800094k.

[410] B. Angulo, C. I. Herrerías, Z. Hormigón, J. A. Mayoral, L. Salvatella, "Copper-catalyzed cyclopropanation reaction of but-2-ene", *Journal of Molecular Modeling* **2018**, *24*, 195, https://doi.org/10.1007/s00894-018-3737-1.

[411] J. M. Fraile, J. I. García, V. Martínez-Merino, J. A. Mayoral, L. Salvatella, "Theoretical (DFT) Insights into the Mechanism of Copper-Catalyzed Cyclopropanation Reactions. Implications for Enantioselective Catalysis", *Journal of the American Chemical Society* **2001**, *123*, 7616, https://doi.org/10.1021/ja003695c.

[412] M. Besora, A. A. C. Braga, W. M. C. Sameera, J. Urbano, M. R. Fructos, P. J. Pérez, F. Maseras, "A computational view on the reactions of hydrocarbons with coinage metal complexes", *Journal of Organometallic Chemistry* **2015**, *784*, 2, https://doi.org/10.1016/j.jorganchem.2014.10.009.

[413] M. M. Díaz-Requejo, M. C. Nicasio, P. J. Pérez, "BpCu-Catalyzed Cyclopropanation of Olefins: A Simple System That Operates under Homogeneous and Heterogeneous Conditions (Bp = Dihydridobis(pyrazolyl)borate)", *Organometallics* **1998**, *17*, 3051, https://doi.org/10.1021/om980061u.

[414] M. M. Díaz-Requejo, T. R. Belderrain, M. C. Nicasio, F. Prieto, P. J. Pérez, "Kinetics of the BpCu-Catalyzed Carbene Transfer Reaction (Bp = Dihydridobis(1-pyrazolyl)borate). Is a 14-Electron Species the Real Catalyst for the General Copper-Mediated Olefin Cyclopropanation?", *Organometallics* **1999**, *18*, 2601, https://doi.org/10.1021/om990270u.

[415] P.-F. Larsson, P.-O. Norrby, S. Woodward, "Mechanistic Aspects of Copper-Catalyzed Reactions", in *Copper-Catalyzed Asymmetric Synthesis*, N.K. Alexandre Alexakis, Simon Woodward, Ed., Wiley-VCH Verlag GmbH & Co. KGaA, 2014, p. 325, https://doi.org/10.1002/9783527664573.ch12.

[416] M. M. Díaz-Requejo, P. J. Pérez, "Copper, silver and gold-based catalysts for carbene addition or insertion reactions", *Journal of Organometallic Chemistry* **2005**, *690*, 5441, https://doi.org/10.1016/j.jorganchem.2005.07.092.

[417] I. S. Lishanskii, V. A. Tsitokhtsev, "The addition of carbalkoxycarbenes to conjugated diene polymers", *Polymer Science U.S.S.R.* **1968**, *10*, 1008, https://doi.org/10.1016/0032-3950(68)90179-2.

[418] B. Li, M. Berliner, R. Buzon, C. K. F. Chiu, S. T. Colgan, T. Kaneko, N. Keene, W. Kissel, T. Le, K. R. Leeman, B. Marquez, R. Morris, L. Newell, S. Wunderwald, M. Witt, J. Weaver, Z. Zhang, Z. Zhang, "Aqueous Phosphoric Acid as a Mild Reagent for Deprotection of tert-Butyl Carbamates, Esters, and Ethers", *Journal of Organometallic Chemistry* **2006**, *71*, 9045, https://doi.org/10.1021/jo061377b.

[419] A. C. Greene, J. Zhu, D. J. Pochan, X. Jia, K. L. Kiick, "Poly(acrylic acid-b-styrene) Amphiphilic Multiblock Copolymers as Building Blocks for the Assembly of Discrete Nanoparticles", *Macromolecules* **2011**, *44*, 1942, https://doi.org/10.1021/ma102869y.

[420] L. Chen, T. Jiang, J. Lin, C. Cai, "Toroid Formation through Self-Assembly of Graft Copolymer and Homopolymer Mixtures: Experimental Studies and Dissipative Particle Dynamics Simulations", *Langmuir* **2013**, *29*, 8417, https://doi.org/10.1021/la401553a.

[421] K. A. Davis, K. Matyjaszewski, "Atom Transfer Radical Polymerization of tert-Butyl Acrylate and Preparation of Block Copolymers", *Macromolecules* **2000**, *33*, 4039, https://doi.org/10.1021/ma991826s.

[422] K. S. Shinde, P. Michael, D. Fuhrmann, W. H. Binder, "A Mechanochemically Active Metal-Organic Framework (MOF) Based on Cu-Bis-NHC-Linkers: Synthesis and Mechano-Catalytic Activation", *Macromolecular Chemistry and Physics* **2023**, *224*, 2200207, https://doi.org/10.1002/macp.202200207.

[423] A. Burgun, R. S. Crees, M. L. Cole, C. J. Doonan, C. J. Sumby, "A 3-D diamondoid MOF catalyst based on in situ generated [Cu(L)2] N-heterocyclic carbene (NHC) linkers: hydroboration of CO2", *Chem. Commun.* **2014**, *50*, 11760, http://dx.doi.org/10.1039/C4CC04761C.

[424] O. Karagiaridi, Bury, Wojciech, Sarjeant, Amy A., Hupp, Joseph T., Farha, Omar K., "Synthesis and Characterization of Functionalized Metal-organic Frameworks", *JoVE* **2014**, e52094, https://dx.doi.org/10.3791/52094.

[425] S. E. H. L. B. Boström, F. Heck, C. Koschnick, A. J. Jones, M. J. Cliffe, R. Al Natour, M. Bonneau, V. Guillerm, O. Shekhah, M. Eddaoudi, J. Lopez-Cabrelles, S. Furukawa, M. Romero-Angel, C. Martí-Gastaldo, M. Yan, A. J. Morris, I. Romero-Muñiz, Y. Xiong, A. E. Platero-Prats, J. Roth, W. L. Queen, K. S. Mertin, D. E. Schier, N. R. Champness, H. H. Yeung, B. V. Lotsch, "How reproducible is the synthesis of Zr--porphyrin metal--organic frameworks? An interlaboratory study.", *Advanced Materials* **2024**, https://doi.org/10.1002/adma.202304832.

[426] R. Han, K. S. Walton, D. S. Sholl, "Does Chemical Engineering Research Have a Reproducibility Problem?", *Annual Review of Chemical and Biomolecular Engineering* **2019**, *10*, 43, https://doi.org/10.1146/annurev-chembioeng-060718-030323.

[427] A. De, M. Maliuta, I. Senkovska, S. Kaskel, "The Dilemma of Reproducibility of Gating Isotherms for Flexible MOFs", *Langmuir* **2022**, *38*, 14073, https://doi.org/10.1021/acs.langmuir.2c01999.

[428] J. Park, J. D. Howe, D. S. Sholl, "How Reproducible Are Isotherm Measurements in Metal–Organic Frameworks?", *Chemistry of Materials* **2017**, *29*, 10487, https://doi.org/10.1021/acs.chemmater.7b04287.

[429] S. Kitagawa, K. Uemura, "Dynamic porous properties of coordination polymers inspired by hydrogen bonds", *Chemical Society Reviews* **2005**, *34*, 109, http://dx.doi.org/10.1039/B313997M.

[430] S. Horike, S. Shimomura, S. Kitagawa, "Soft porous crystals", *Nature Chemistry* **2009**, *1*, 695, https://doi.org/10.1038/nchem.444.

[431] G. Cravotto, E. C. Gaudino, P. Cintas, "On the mechanochemical activation by ultrasound", *Chem. Soc. Rev.* **2013**, *42*, 7521, http://dx.doi.org/10.1039/C2CS35456J.

[432] K. S. Shinde, P. Michael, W. H. Binder, "Mechanochemical Activation of a Metal–Organic Framework Embedded within a Thermoplastic Polyurethane Matrix: Probing Fluorogenic Stress-

Sensing", *Macromolecular Chemistry and Physics* **2023**, *224*, 2300297, https://doi.org/10.1002/macp.202300297.

[433] K. Imato, T. Kanehara, S. Nojima, T. Ohishi, Y. Higaki, A. Takahara, H. Otsuka, "Repeatable mechanochemical activation of dynamic covalent bonds in thermoplastic elastomers", *Chemical Communications* **2016**, *52*, 10482, http://dx.doi.org/10.1039/C6CC04767J.

[434] S. Yoshida, H. Suga, S. Seki, "Thermodynamic Studies of Solid Polyethers. III. Poly(tetrahydrofuran), −[−(CH2)4O−]−n", *Polymer Journal* **1973**, *5*, 25, https://doi.org/10.1295/polymj.5.25.

[435] A. Elidrissi, O. Krim, S. Ousslimane, "Effect of sequence concentrations on segmented polyurethanes properties", *Pigment & Resin Technology* **2008**, *37*, 73, https://doi.org/10.1108/03699420810860419.

[436] P. Kong, S. Drechsler, S. Balog, S. Schrettl, C. Weder, A. F. M. Kilbinger, "Synthesis and properties of poly(norbornene)s with lateral aramid groups", *Polymer Chemistry* **2019**, *10*, 2057, http://dx.doi.org/10.1039/C9PY00187E.

[437] S. Gowda, C. Gowda, "Zinc/Hydrazine: A Low Cost-Facile System for the Reduction of Nitro Compounds", *ChemInform* **2003**, *34*, https://doi.org/10.1002/chin.200313048.

[438] A. Kumar, S. Tateyama, K. Yasaki, M. A. Ali, N. Takaya, R. Singh, T. Kaneko, "Ultrahigh performance bio-based polyimides from 4,4'-diaminostilbene", *Polymer* **2016**, *83*, 182, https://doi.org/10.1016/j.polymer.2015.12.008.

[439] A. Kanaya, Y. Takashima, A. Harada, "Double-Threaded Dimer and Supramolecular Oligomer Formed by Stilbene Modified Cyclodextrin: Effect of Acyl Migration and Photostimuli", *The Journal of Organic Chemistry* **2011**, *76*, 492, https://doi.org/10.1021/jo101936t.

[440] "*CRC Handbook of Chemistry and Physics (95th ed.)*", CRC Press, Boca Raton, 2014, https://doi.org/10.1201/b17118.

[441] İ. Gulcin, "Antioxidants and antioxidant methods: an updated overview", *Archives of Toxicology* **2020**, *94*, 651, https://doi.org/10.1007/s00204-020-02689-3.

[442] F. Himo, T. Lovell, R. Hilgraf, V. V. Rostovtsev, L. Noodleman, K. B. Sharpless, V. V. Fokin, "Copper(I)-Catalyzed Synthesis of Azoles. DFT Study Predicts Unprecedented Reactivity and Intermediates", *Journal of the American Chemical Society* **2005**, *127*, 210, https://doi.org/10.1021/ja0471525.

[443] J. Shen, P. T. Griffiths, S. J. Campbell, B. Utinger, M. Kalberer, S. E. Paulson, "Ascorbate oxidation by iron, copper and reactive oxygen species: review, model development, and derivation of key rate constants", *Scientific Reports* **2021**, *11*, 7417, https://doi.org/10.1038/s41598-021-86477-8.

[444] M. B. Davies, "Reactions of L-ascorbic acid with transition metal complexes", *Polyhedron* **1992**, *11*, 285, https://doi.org/10.1016/S0277-5387(00)83175-7.

[445] P. Hasin, Y. Wu, "Sonochemical synthesis of copper hydride (CuH)", *Chemical Communications* **2012**, *48*, 1302, http://dx.doi.org/10.1039/C2CC15741A.

[446] Y. Wang, D. Zhao, H. Ji, G. Liu, C. Chen, W. Ma, H. Zhu, J. Zhao, "Sonochemical Hydrogen Production Efficiently Catalyzed by Au/TiO2", *The Journal of Physical Chemistry C* **2010**, *114*, 17728, https://doi.org/10.1021/jp105691v.

7 APPENDIX

7.1 Cu(I) NHCs as Catalysts for Cyclopropanation

7.1.1 Kinetic Studies of the Cyclopropanation of PI
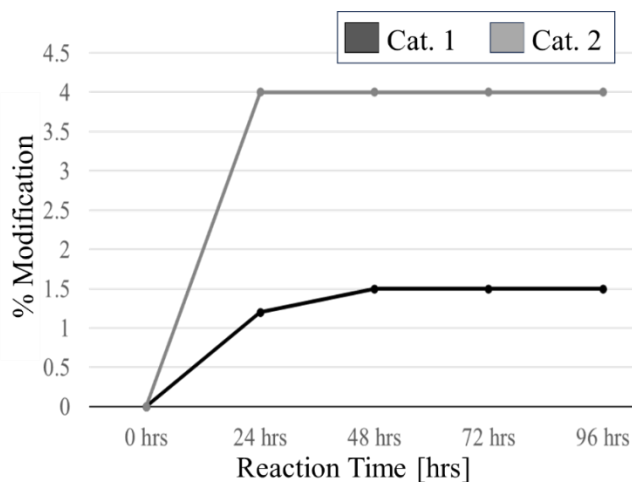
Figure A1. Kinetic approach to study the active reaction times. The solid content (wt.%) of PI **(3)** is 20 wt.% and the Cat:PI:EDA per double bond ratio is 0.05:1:2 with cyclohexane as the solvent.

Table A1. Time-dependent kinetic investigations of the cyclopropanation of PI.

Ent	Solvent	Solid Content	Variables	% Modification[a]	
				Cat. 1	Cat. 2
6	Cyclohexane	20 wt.%	i) 0 h	0	0
			ii) 24 h	1.2	4.0
			(iii) 48 h	1.5	4.0
			(iv) 72 h	1.5	4.0
			(v) 96 h	1.5	4.0

[a]Calculated according to the ratio of the signals at the peaks at 5.10 ppm and 4.80-4.63 ppm belonging to 1,4- and 3,4-poly(isoprene) respectively as well as the new peak after modification at 4.10 ppm belonging to the methylene protons of the -$CO_2CH_2CH_3$ moiety of the cyclopropane appearing in ^{1}H NMR spectroscopy (for details see **Chapter 5.2.2**).

7.1.2 Investigation Into the Limited % Modification
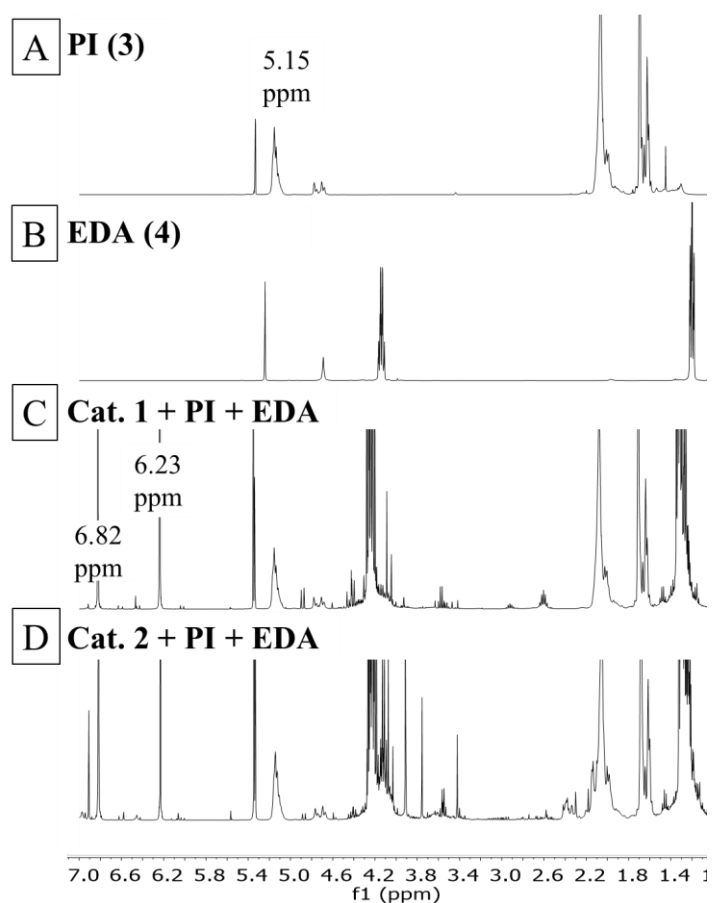
Figure A2. NMR spectra for EDA (**4**) in the presence of **A**) PI (**3**), **C**) Cat. **1** + PI and **D**) Cat. **2** + PI. The spectrum **B**) is of EDA. All NMR are measured in the solvent DCM-d_2.

7.1.3 Rheology Experiments
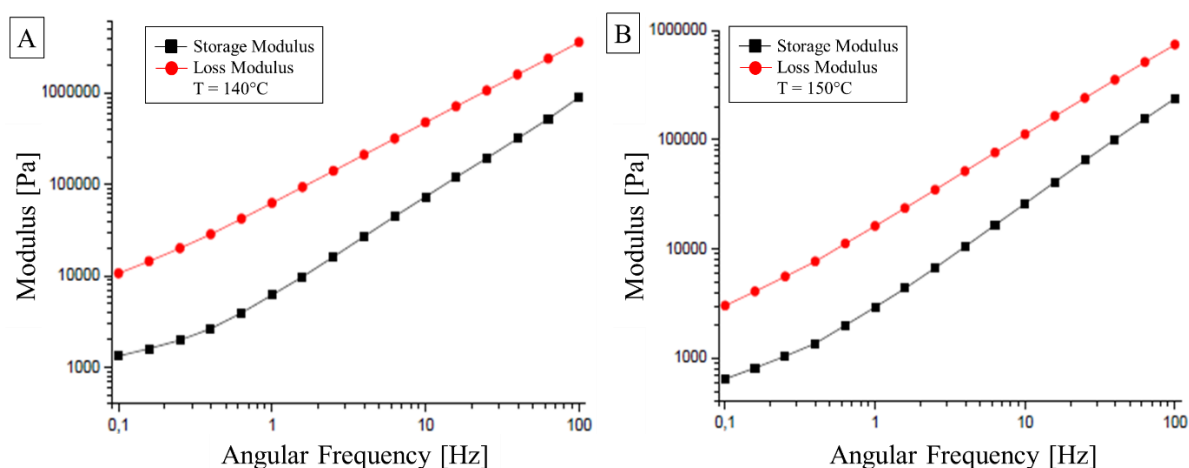
Figure A3. Frequency sweep of the deprotected sample (**9***) at different temperatures.

Table A2. Frequency vs. loss factor tan(δ) for virgin, 5 % modified and 5 % deprotected PIs.

Ent	Frequency (rad/s)	Loss Factor (tan(δ))			
		Virgin PI (3000 g mol^{-1})	Virgin PI (150,000 g mol^{-1})	5 % modified PI	Deprotected PI
1	100	20000	0.163	0.729	4.004
2	63.1	20000	0.177	3.158	4.544
3	39.8	20000	0.199	3.612	5.021
4	25.1	20000	0.227	6.108	5.477
5	15.8	20000	0.26	6.682	5.958
6	10	20000	0.3	11.086	6.487
7	6.31	20000	0.35	9.01	7.103
8	3.98	20000	0.417	6.289	7.845
9	2.51	20000	0.508	7.551	8.67
10	1.58	20000	0.639	6.85	9.535
11	1	20000	0.834	5.709	10.117
12	0.631	20000	1.125	3.394	10.687
13	0.398	20000	1.56	2.135	10.752
14	0.251	2.329	2.202	1.54	10.085
15	0.158	1.731	3.113	1.068	9.039
16	0.1	1.328	4.329	0.703	8.015

7.2   Cu(I) NHCs as Mechanocatalysts within Metal-Organic Frameworks (MOFs)

7.2.1   Characterization of *N,N′*-Bis(4-carboxyphenyl)ethylenediimine (**L1'**)
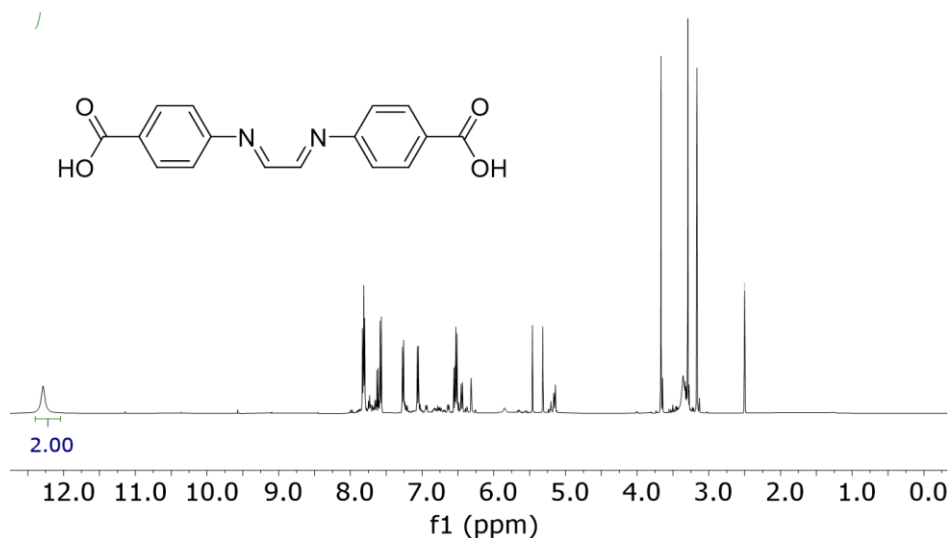
Figure A4. ^{1}H NMR spectrum of **L1'** in DMSO-d_6.
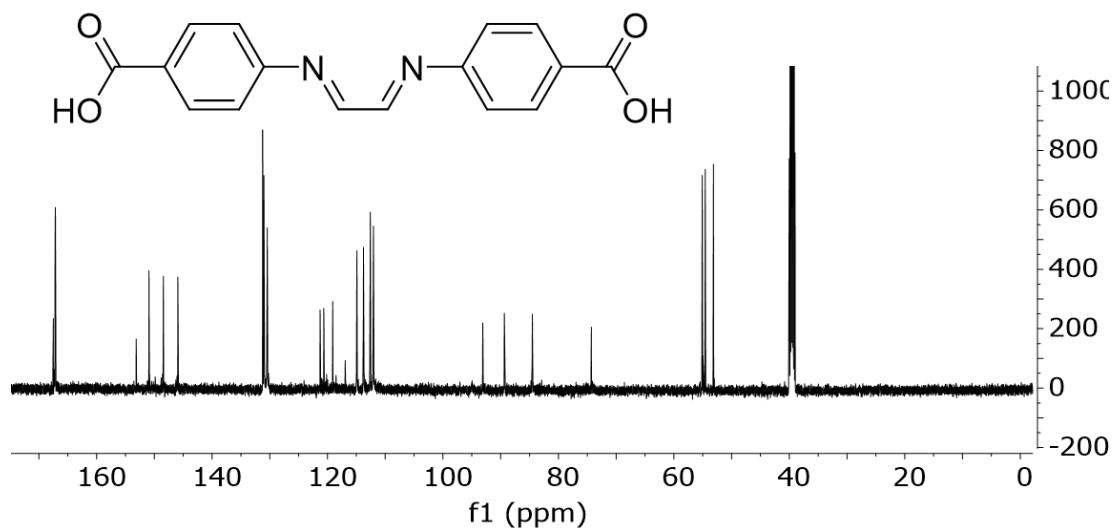
Figure A5. ^{13}C NMR spectrum of **L1'** in DMSO-d_6.

7.2.2   Characterization of 1,3-Bis(4-carboxyphenyl)imidazolium chloride (**L1**)
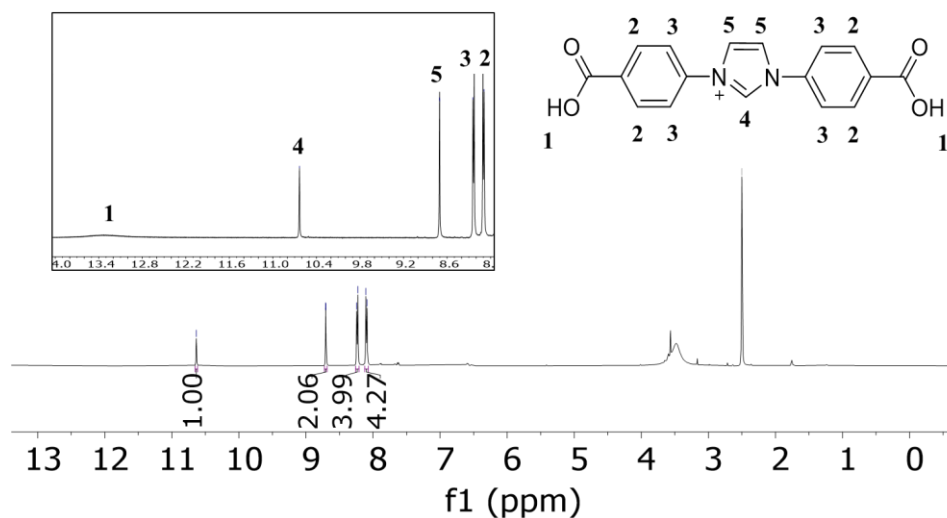
Figure A6. ^{1}H NMR spectrum of **L1** in DMSO-d_6.
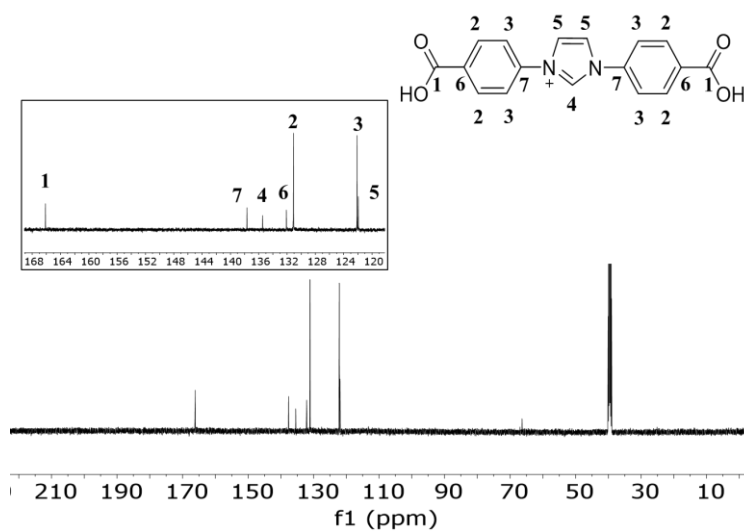
Figure A7. ^{13}C NMR spectrum of **L1** in DMSO-d_6.
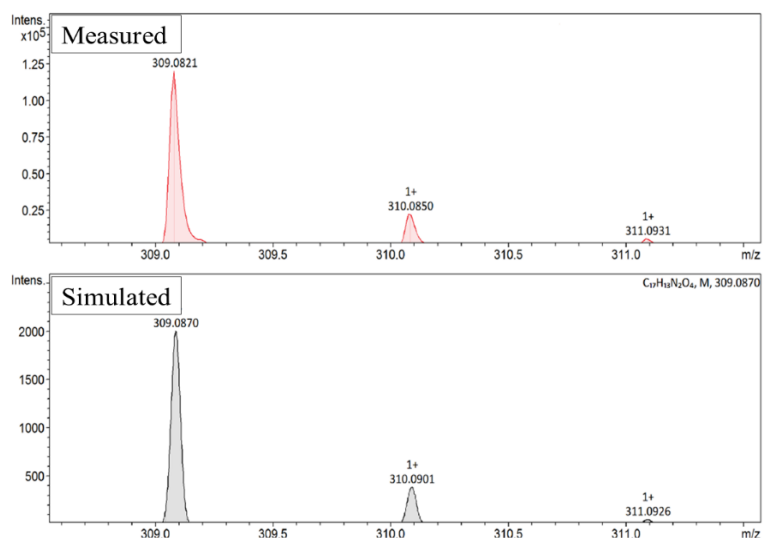
Figure A8. ESI-ToF MS spectrum of **L1**.
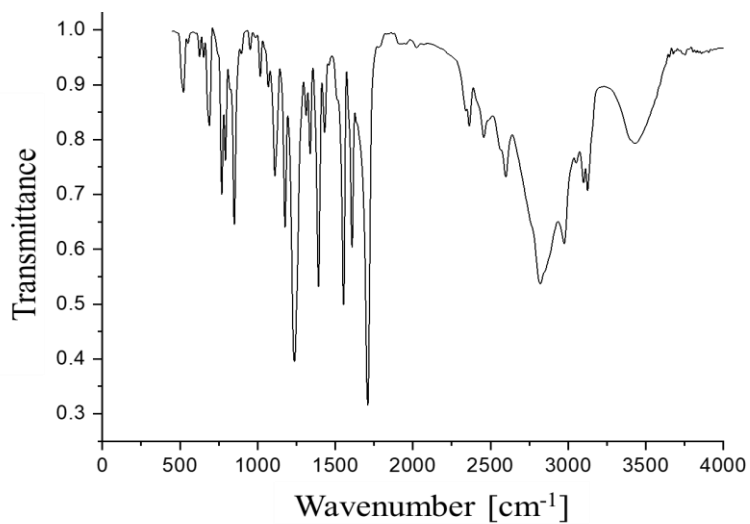
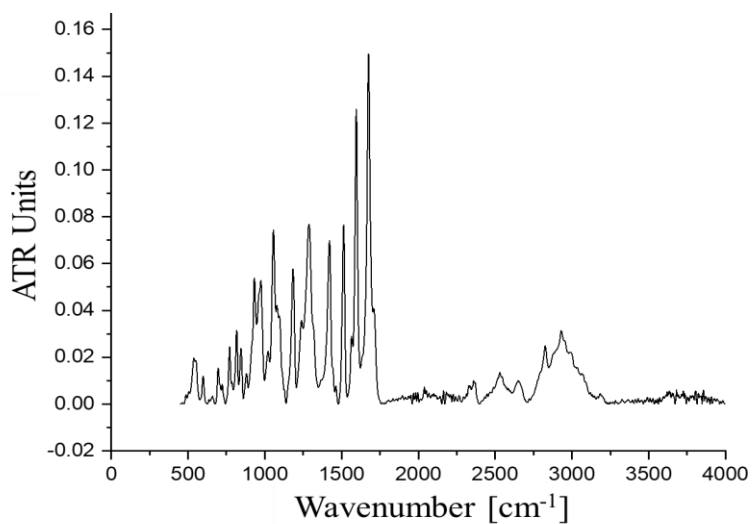**Figure A9.** IR(KBr) spectrum of **L1**.

7.2.3 Characterization of Methyl 4-aminobenzoate (**Me-L1"**)
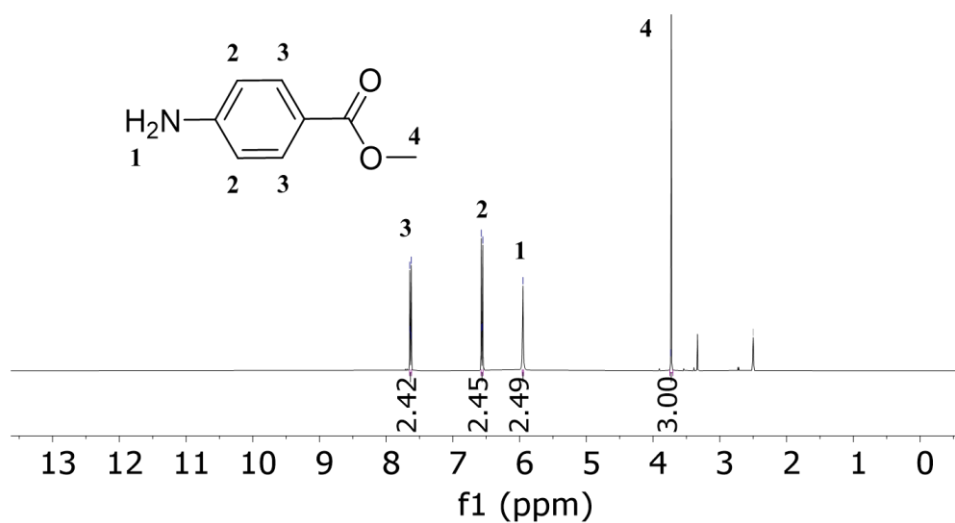
Figure A10. ^{1}H NMR spectrum of **Me-L1"** in DMSO-d_6.
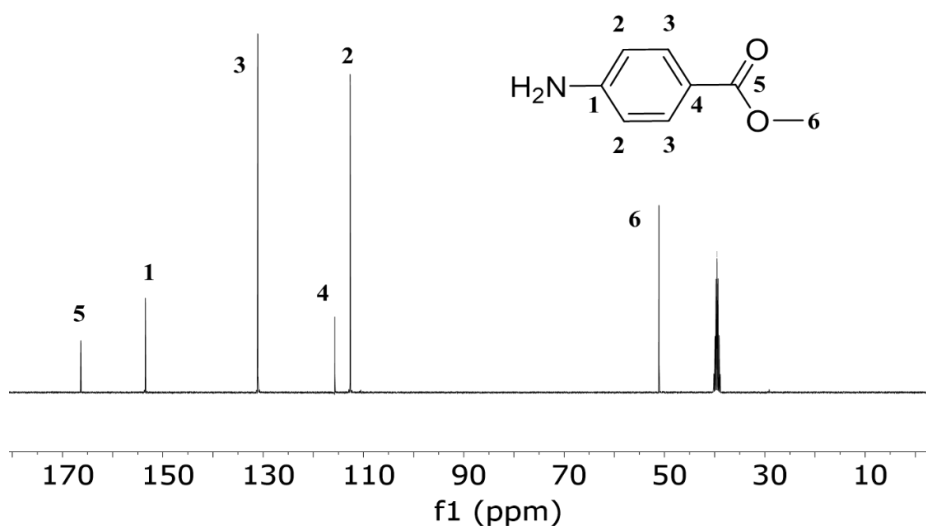
Figure A11. ^{13}C NMR spectrum of **Me-L1"** in DMSO-d_6.
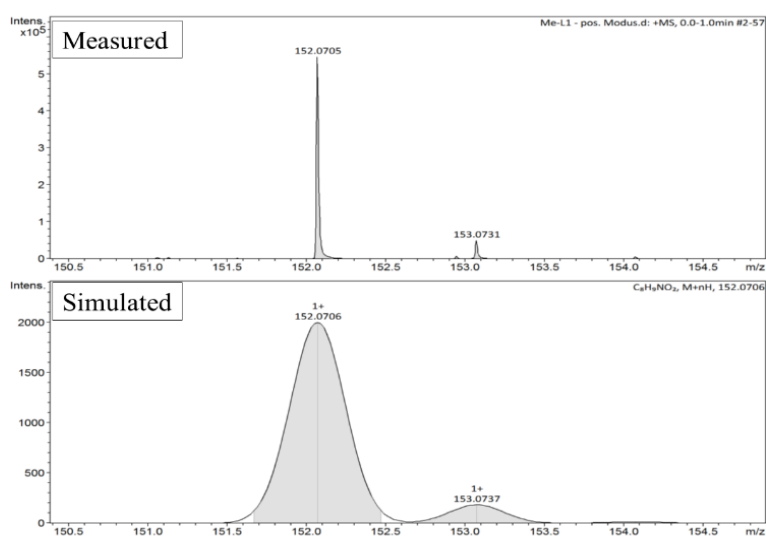
Figure A12. ESI-ToF MS spectrum of **Me-L1"**.
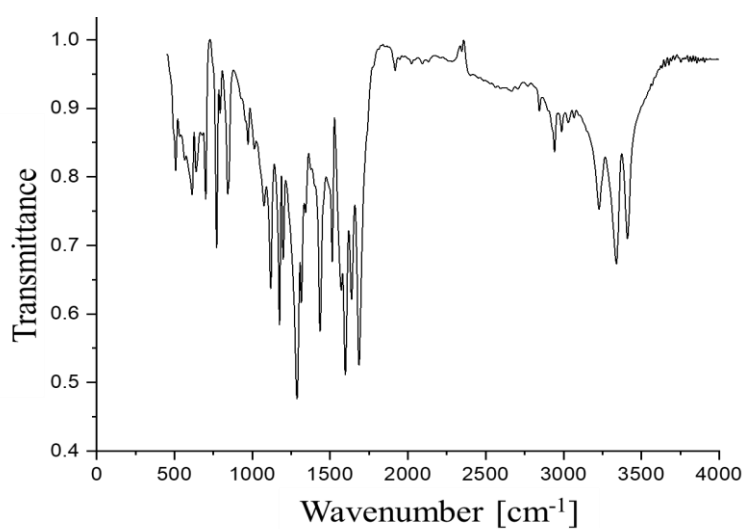
Figure A13. IR(KBr) spectrum of **Me-L1"**.

7.2.4 Characterization of 1,3-Bis(4-(methoxycarbonyl)phenyl)-1H-imidazol-3-ium chloride (**Me-L1**)
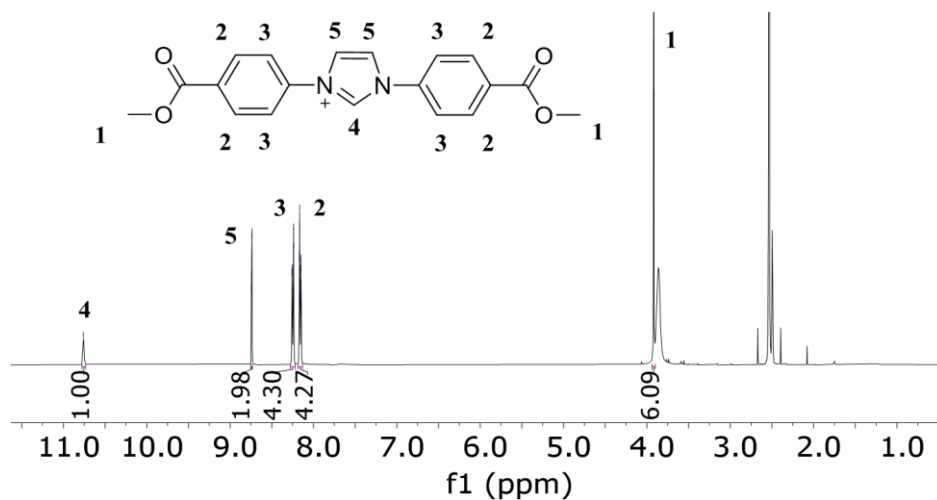
Figure A14. ^{1}H NMR spectrum of **Me-L1** in DMSO-d_6.
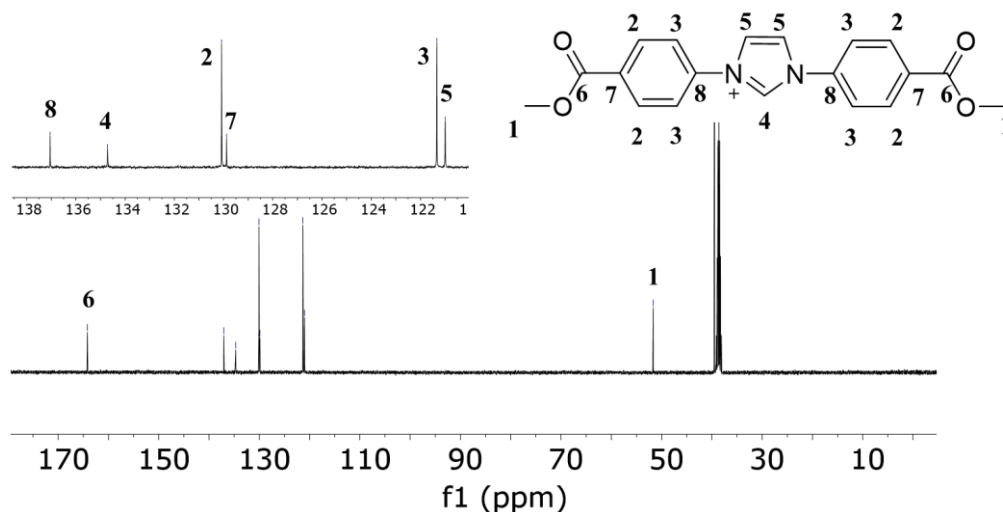
Figure A15. ^{13}C NMR spectrum of **Me-L1** in DMSO-d_6.
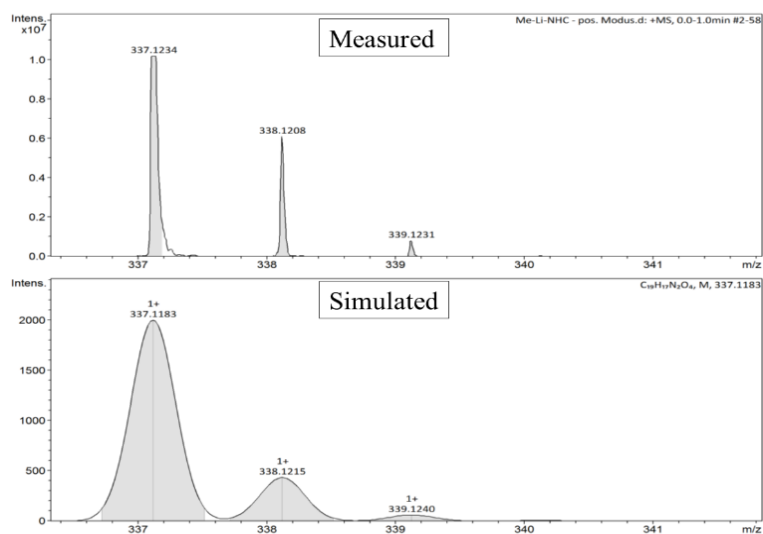
Figure A16. ESI-ToF MS spectrum of **Me-L1**.
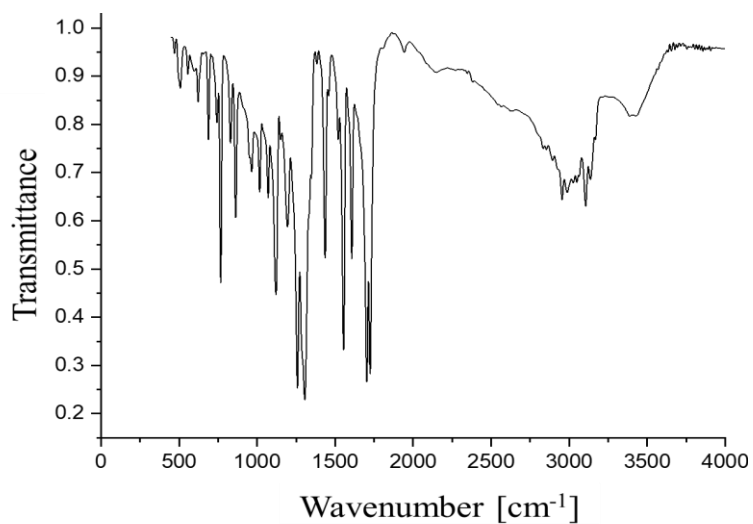
Figure A17. IR(KBr) spectrum of **Me-L1**.

7.2.5   Characterization   of   (2E,2'E)-3,3'-((((1E,2E)-ethane-1,2-diylidene)   bis(azaneylylidene))
bis(4,1-phenylene))diacrylic acid (**L2'**)
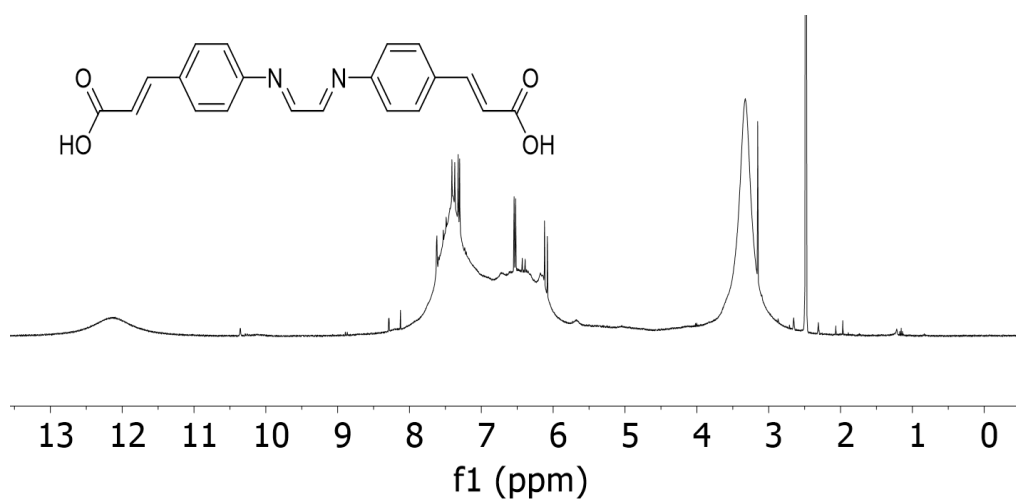
Figure A18. ^{1}H NMR spectrum of **L2'** in DMSO-d_6.
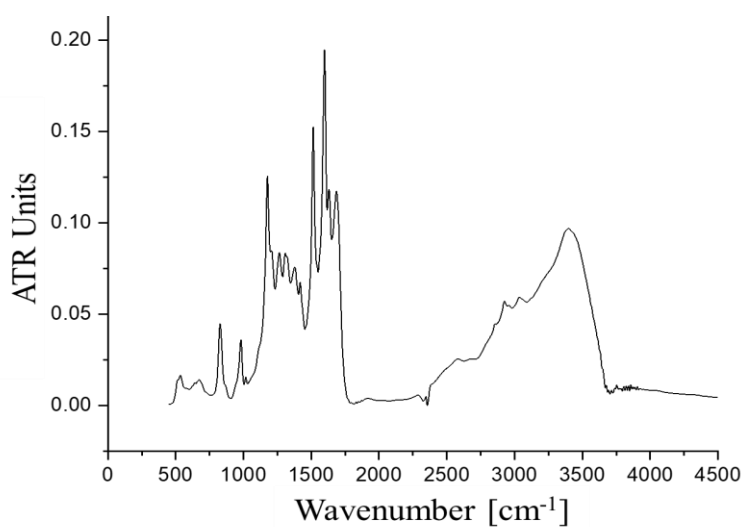
Figure A19. IR(ATR) spectrum of **L2'**.

7.2.6   Characterization of 1,3-Bis(4-((E)-2-carboxyvinyl)phenyl)-1H-imidazol-3-ium chloride (**L2**)
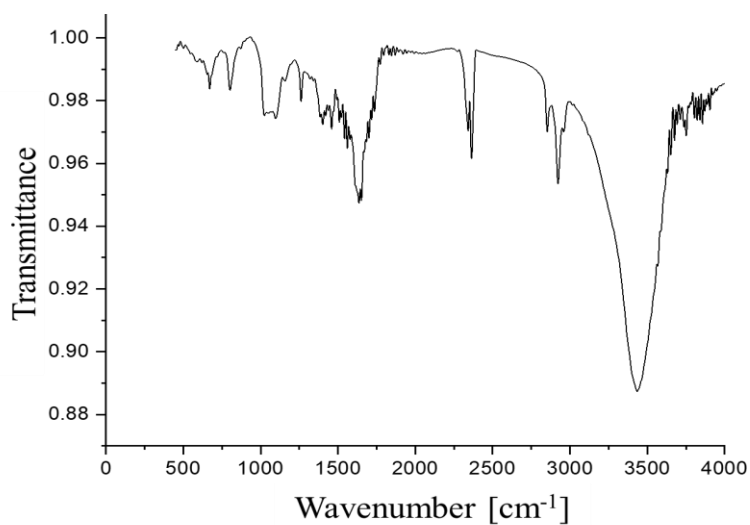
Figure A20. IR(KBr) spectrum of **L2**.

7.2.7   Characterization of Methyl (E)-3-(4-aminophenyl)acrylate (**Me-L2”**)
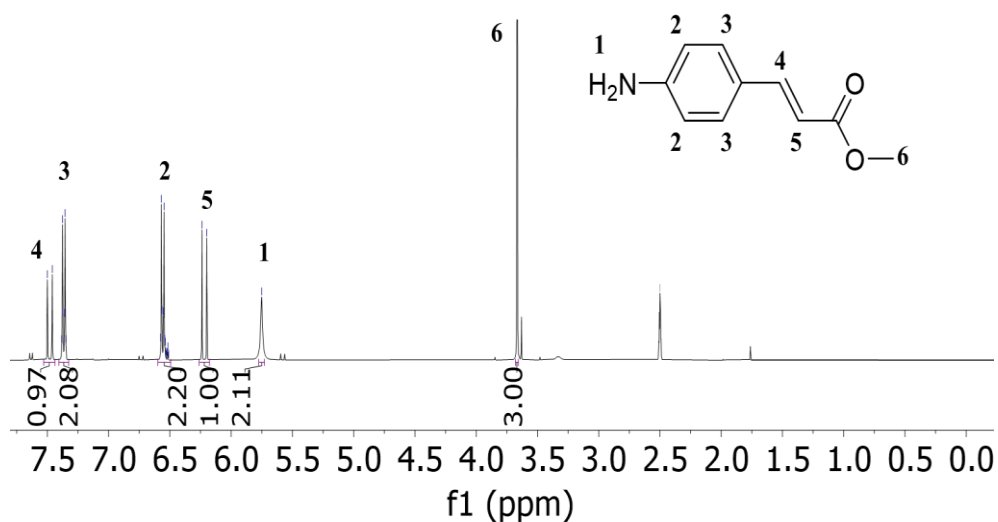
Figure A21. ¹H NMR spectrum of **Me-L2”** in DMSO-d_6.
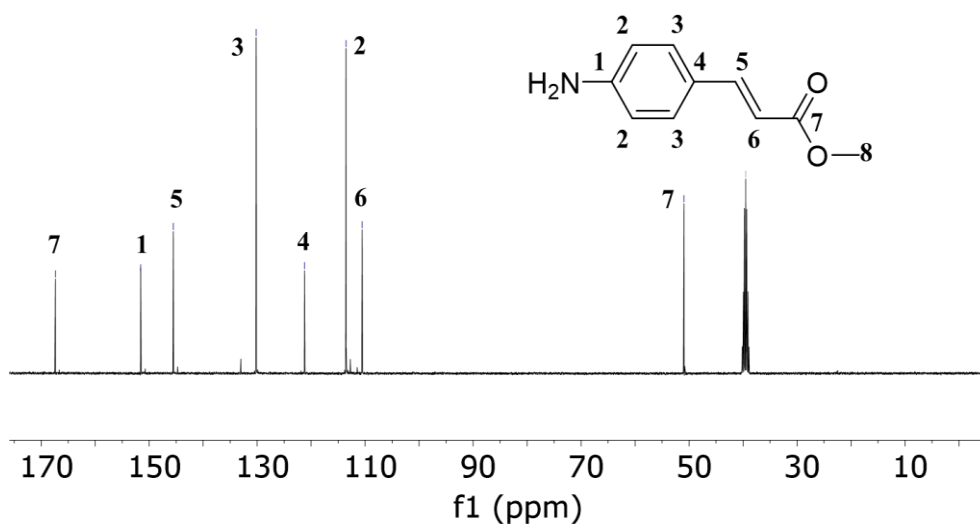
Figure A22. ^{13}C NMR spectrum of **Me-L2"** in DMSO-d_6.
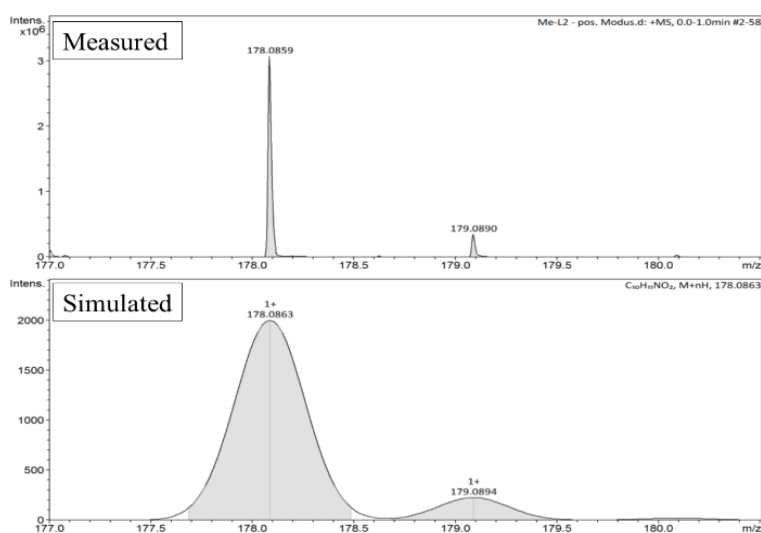
Figure A23. ESI-ToF MS spectrum of **Me-L2"**.
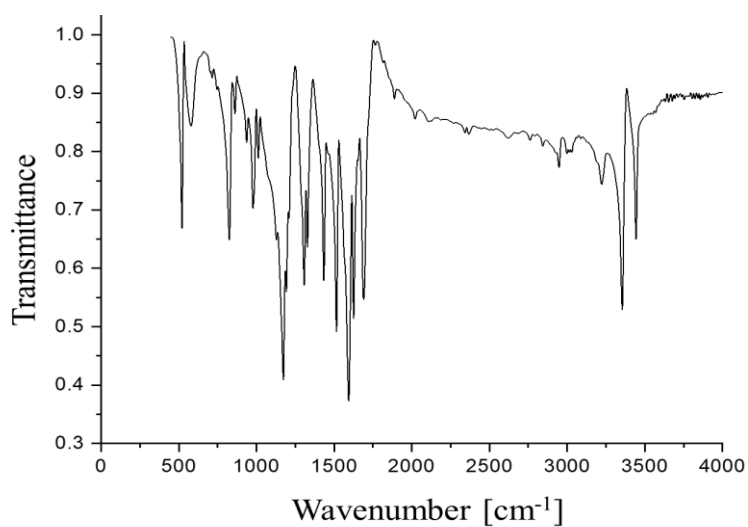
Figure A24. IR(KBr) spectrum of **Me-L2"**.

Characterization of Dimethyl 3,3'-((((1E,2E)-ethane-1,2-diylidene) bis(azaneylylidene)) bis(4,1-phenylene))(2E,2'E)-diacrylate (**Me-L2'**)
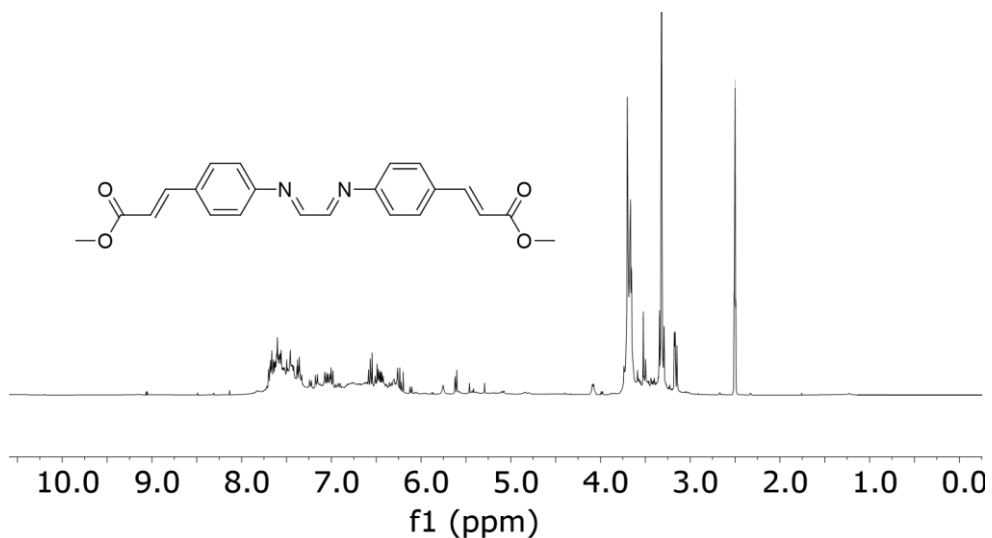
Figure A25. ^{1}H NMR spectrum of **Me-L2'** in DMSO-d_6.
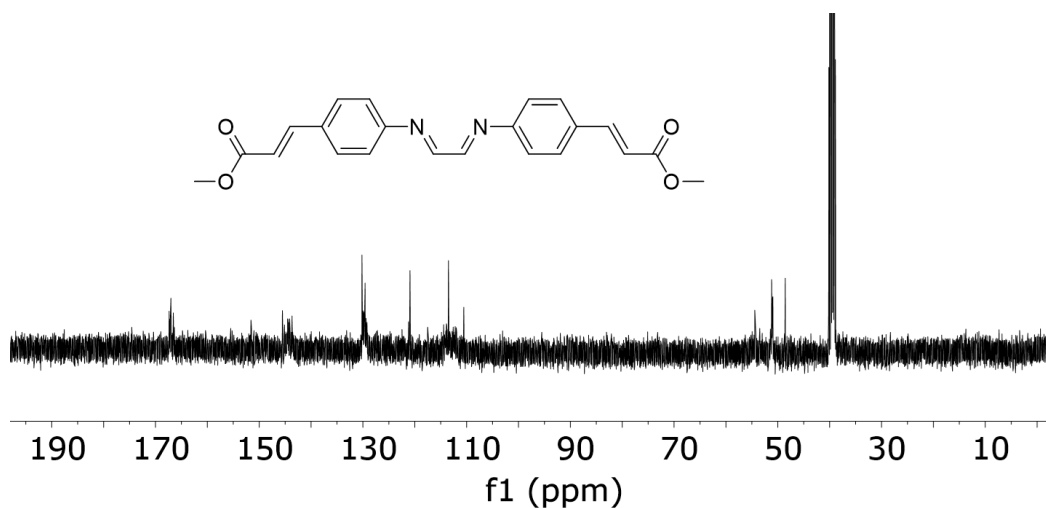
Figure A26. ^{13}C NMR spectrum of **Me-L2'** in DMSO-d_6.
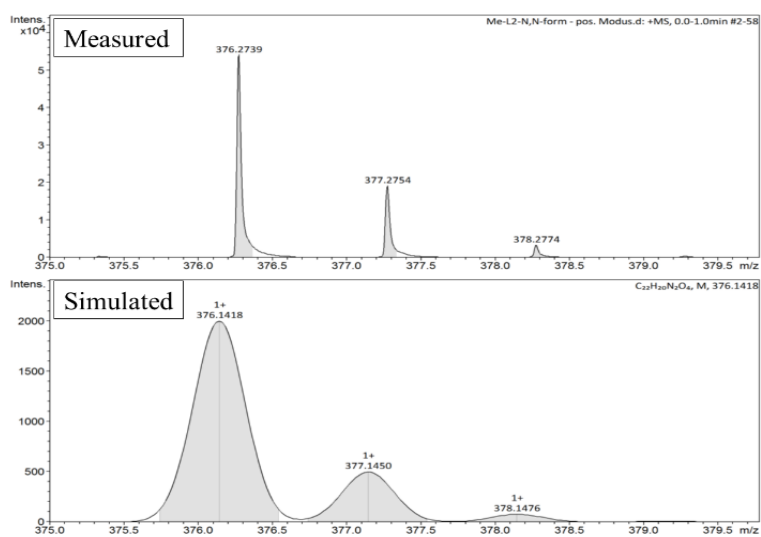
Figure A27. ESI-ToF MS spectrum of **Me-L2'**.
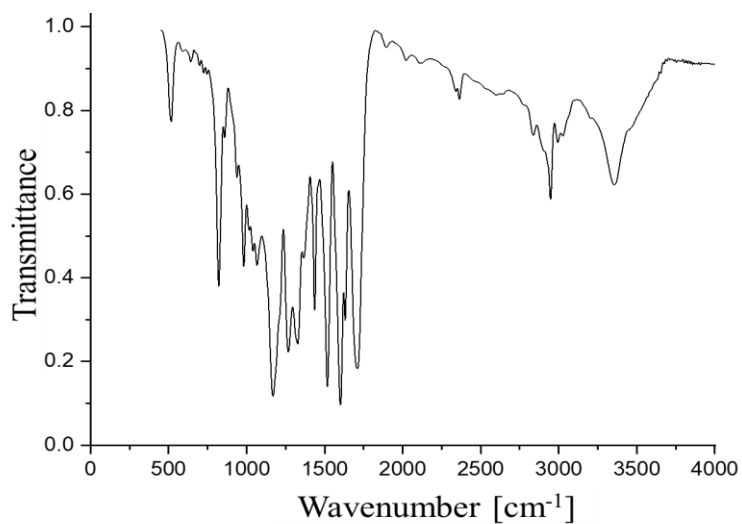
Figure A28. IR(KBr) spectrum of **Me-L2'**.

7.2.9 Characterization of 1,3-Bis(4-((E)-3-methoxy-3-oxoprop-1-en-1-yl)phenyl)-1H-imidazol-3-ium chloride (**Me-L2**)
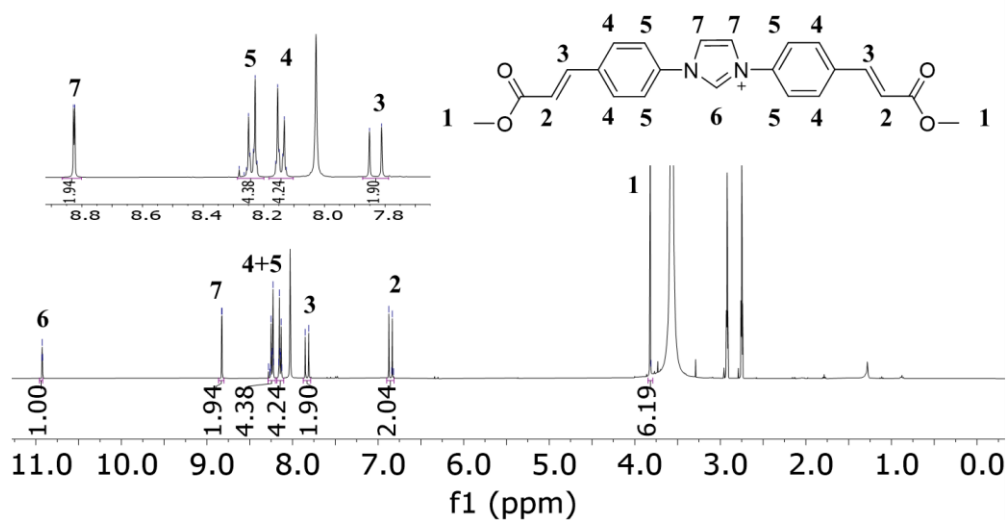
Figure A29. ^{1}H NMR spectrum of **Me-L2** in DMF-d_7.
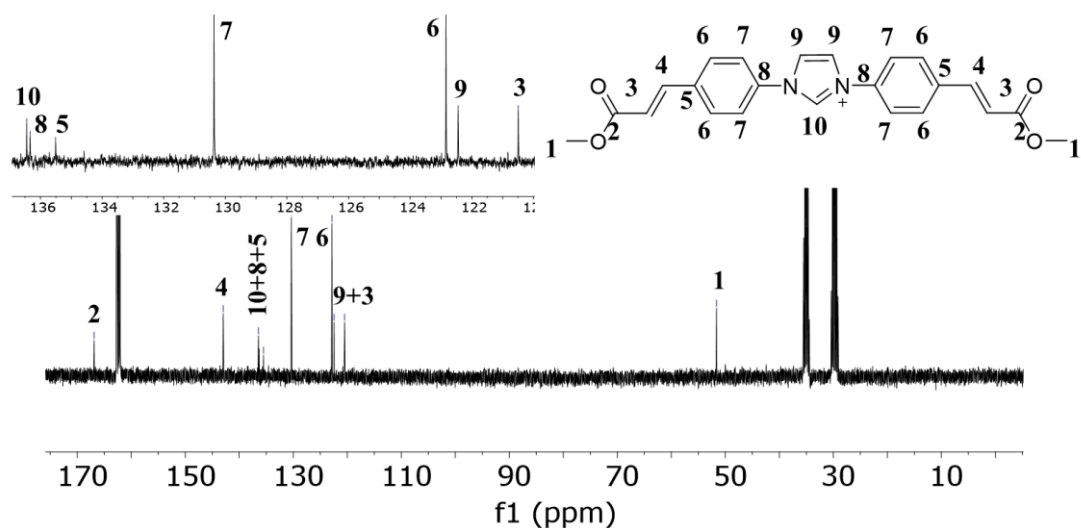
Figure A30. ^{13}C NMR spectrum of **Me-L2** in DMF-d_7.
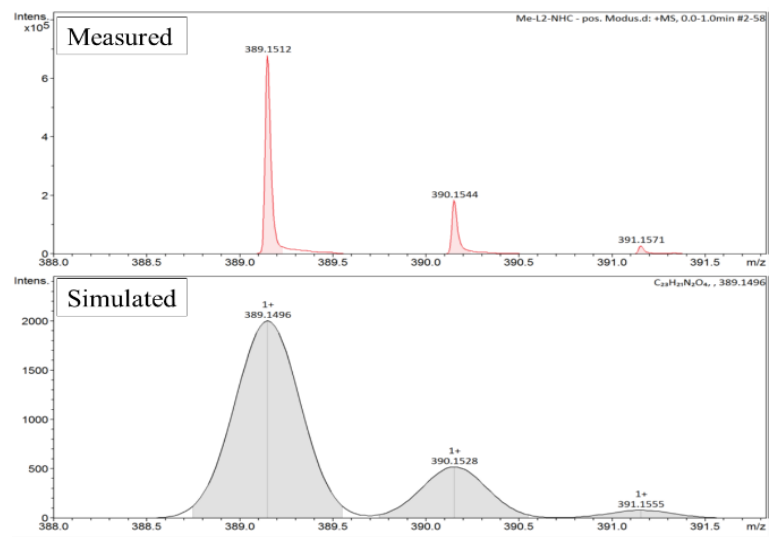
Figure A31. ESI-ToF MS spectrum of **Me-L2**.
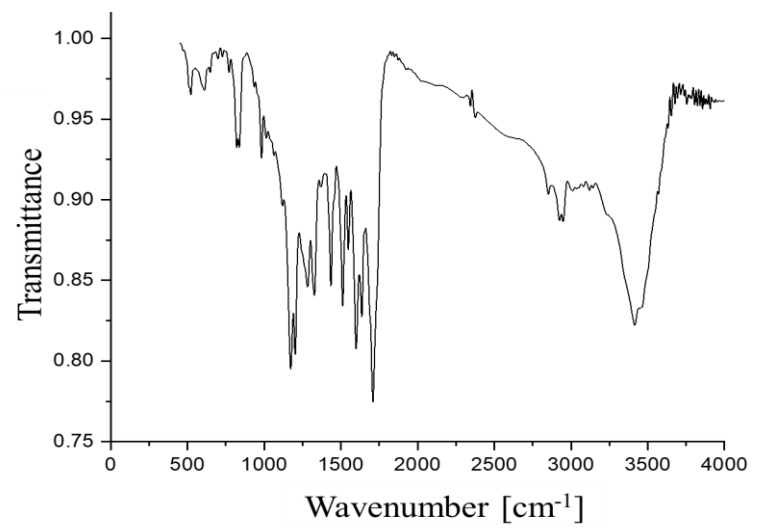
Figure A32. IR(KBr) spectrum of **Me-L2**.

7.2.10 Characterization of 4-(4'-Aminostilbene) Carboxylic Acid. (**L3"**)
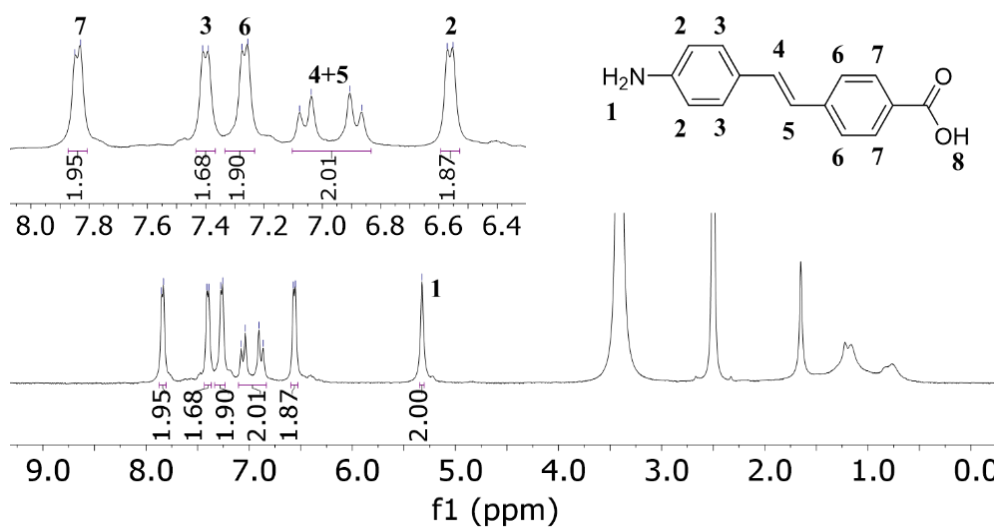
Figure A33. ^{1}H NMR spectrum of **L3"** in DMSO-d_6.
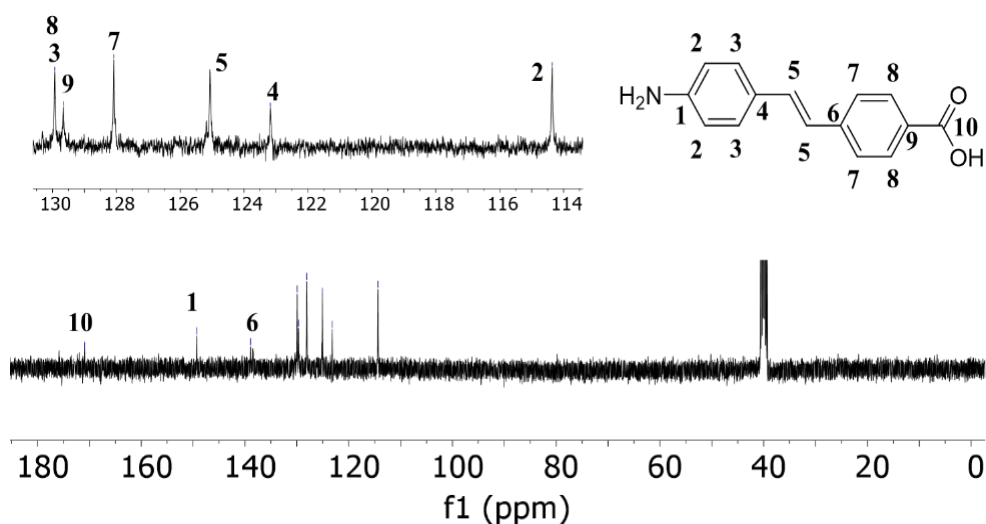
Figure A34. ^{13}C NMR spectrum of **L3"** in DMSO-d_6.
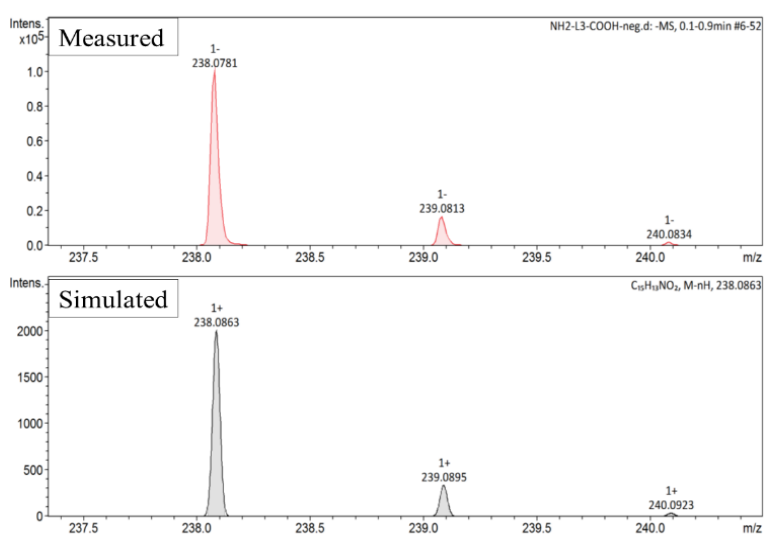
Figure A35. ESI-ToF MS spectrum of **L3"**.
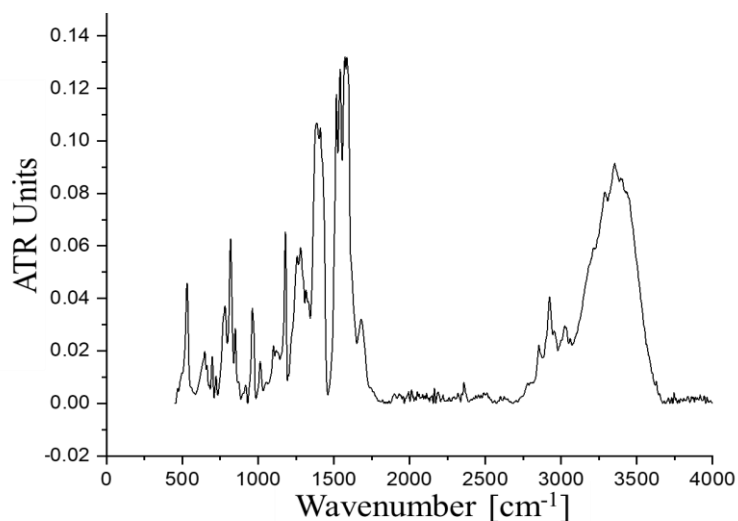
Figure A36. IR(ATR) spectrum of **L3"**.

7.2.11 Characterization of 4,4'-((1E,1'E)-(((((1E,2E)-ethane-1,2-diylidene) bis(azaneylylidene)) bis(4,1-phenylene))bis(ethene-2,1-diyl))dibenzoic acid (**L3'**)
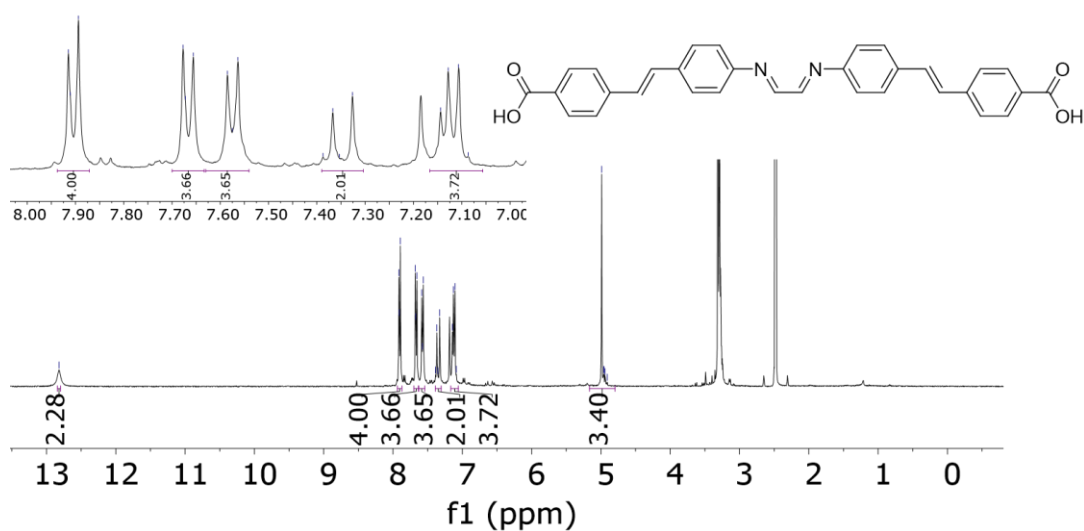
Figure A37. ^{1}H NMR spectrum of **L3'** in DMSO-d_6.
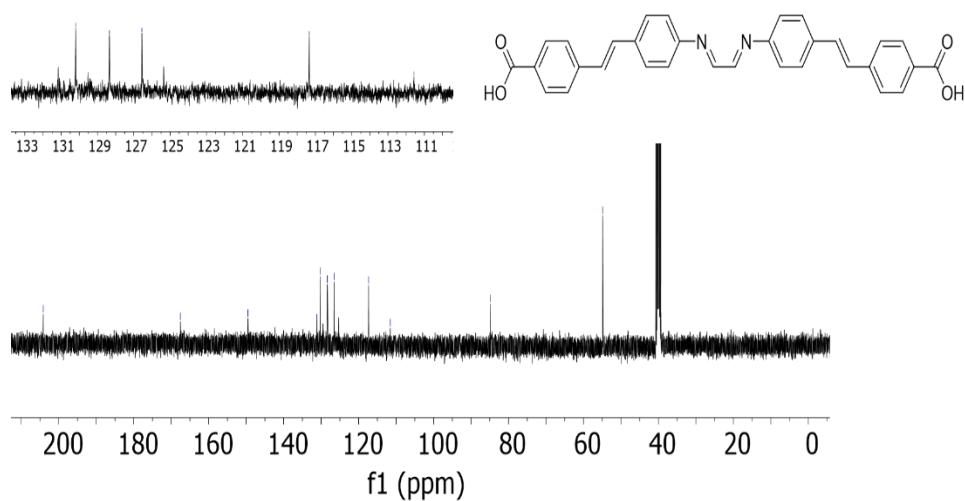
Figure A38. ^{13}C NMR spectrum of **L3'** in DMSO-d_6.

Figure A39. IR(ATR) spectrum of **L3'**.

7.2.12 Characterization of Methyl (E)-4-(4-aminostyryl)benzoate (**Me-L3"**)
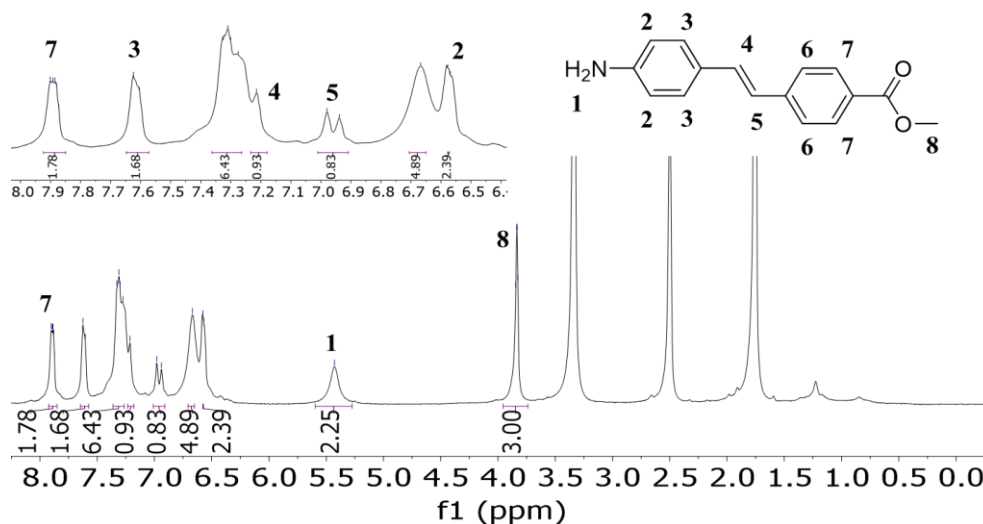
Figure A40. ¹H NMR spectrum of **Me-L3"** in DMSO-d_6.
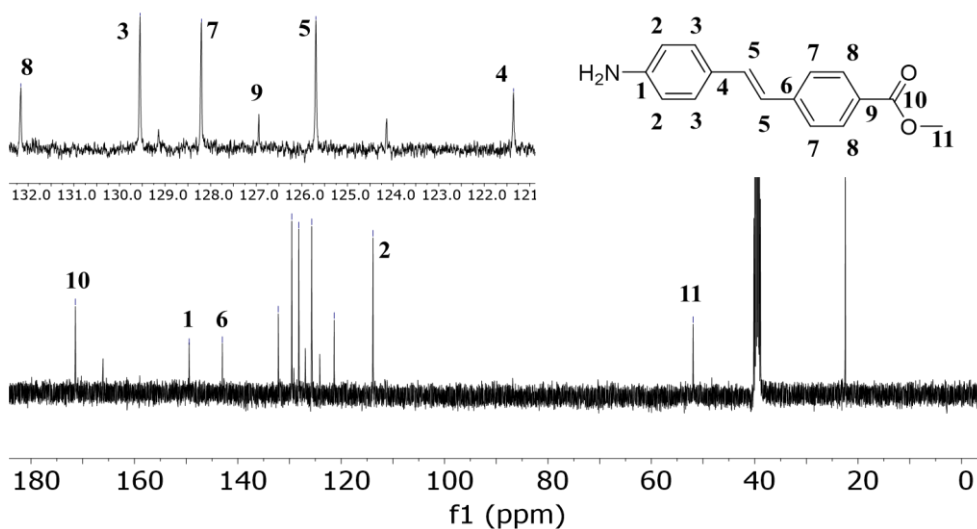
Figure A41. ¹³C NMR spectrum of **Me-L3"** in DMSO-d_6.
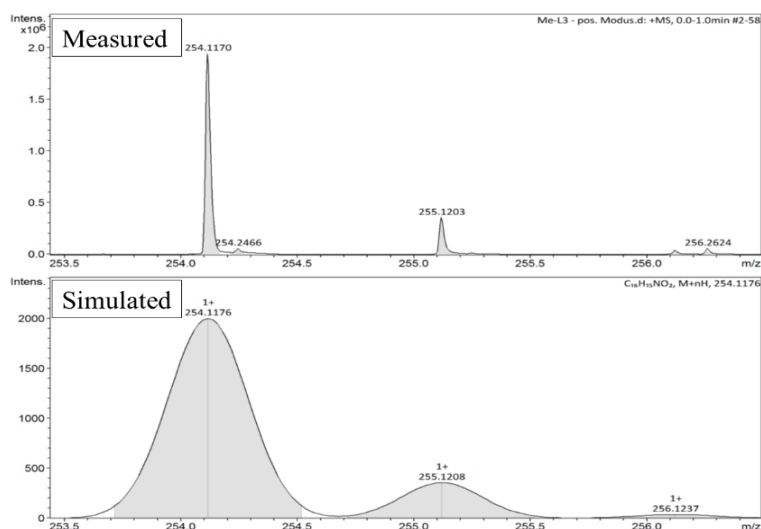
Figure A42. ESI-ToF MS spectrum of **Me-L3"**.
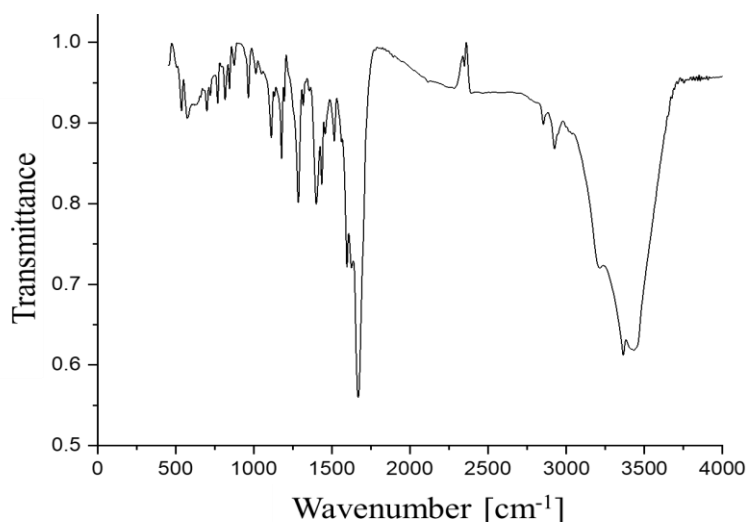
Figure A43. IR(KBr) spectrum of **Me-L3"**.

7.2.13 Synthesis of NHC-MOFI and II

The synthesis of **NHC-MOFI** and **NHC-MOFII** were conducted separately by research partners from the group of Prof. Dr. Harald Krautscheid at the Institute of Inorganic Chemistry, Universität Leipzig, who carried out the NHC-MOF preparation using Teflon lined autoclaves. The autoclaves were filled with the components as described in **Table 18**, **Ent 6** and **7**. The information given further was provided by the working group of Prof. Dr. Krautscheid (slightly modified for better understanding):

The products seem to be the same in all the reactions (visually). The products obtained were crystalline while the solution was a deep green in colour. It means copper(II) was formed during this reaction instead of copper(I). After washing the crystals with DMF and methanol, greenish-brown product was obtained. The crystals were in the form of thin plates which stuck together. Single crystal structure analysis was attempted unsuccessfully but the unit cell parameters were obtained as hexagonal primitive, a = 17.06, b = 17.06, c = 11.9 (90°, 90°, 120°). This was not the same as per the unit cell published in the referenced literature.[338] It was also not found in the Cambridge Structural Database (CSD), so it seems to be an unknown structure.

7.2.14   Characterization by IR
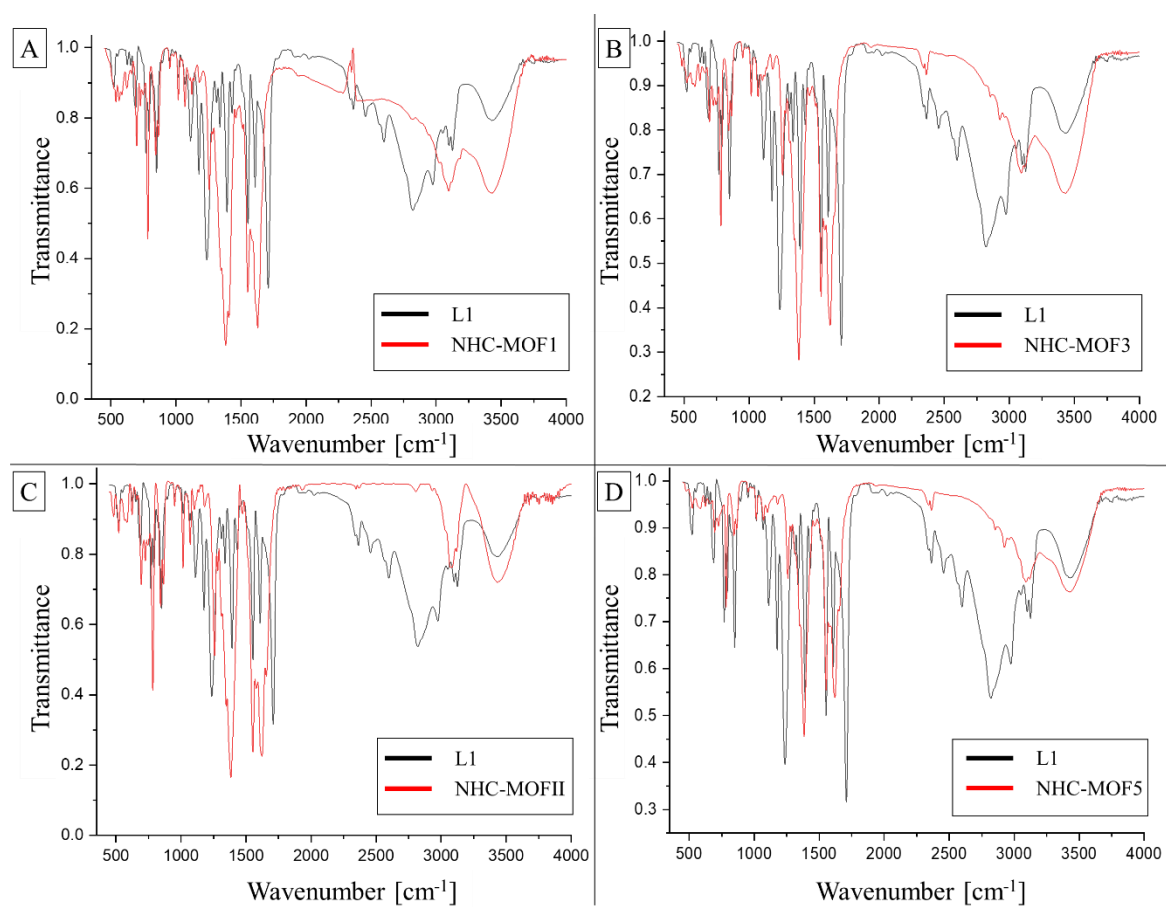
Figure A44. Individual IR(KBr) spectrum of **A) NHC-MOF1**, **B) NHC-MOF3**, **C) NHC-MOFII** and **D**) **NHC-MOF5**.

7.2.15 Characterization by TGA
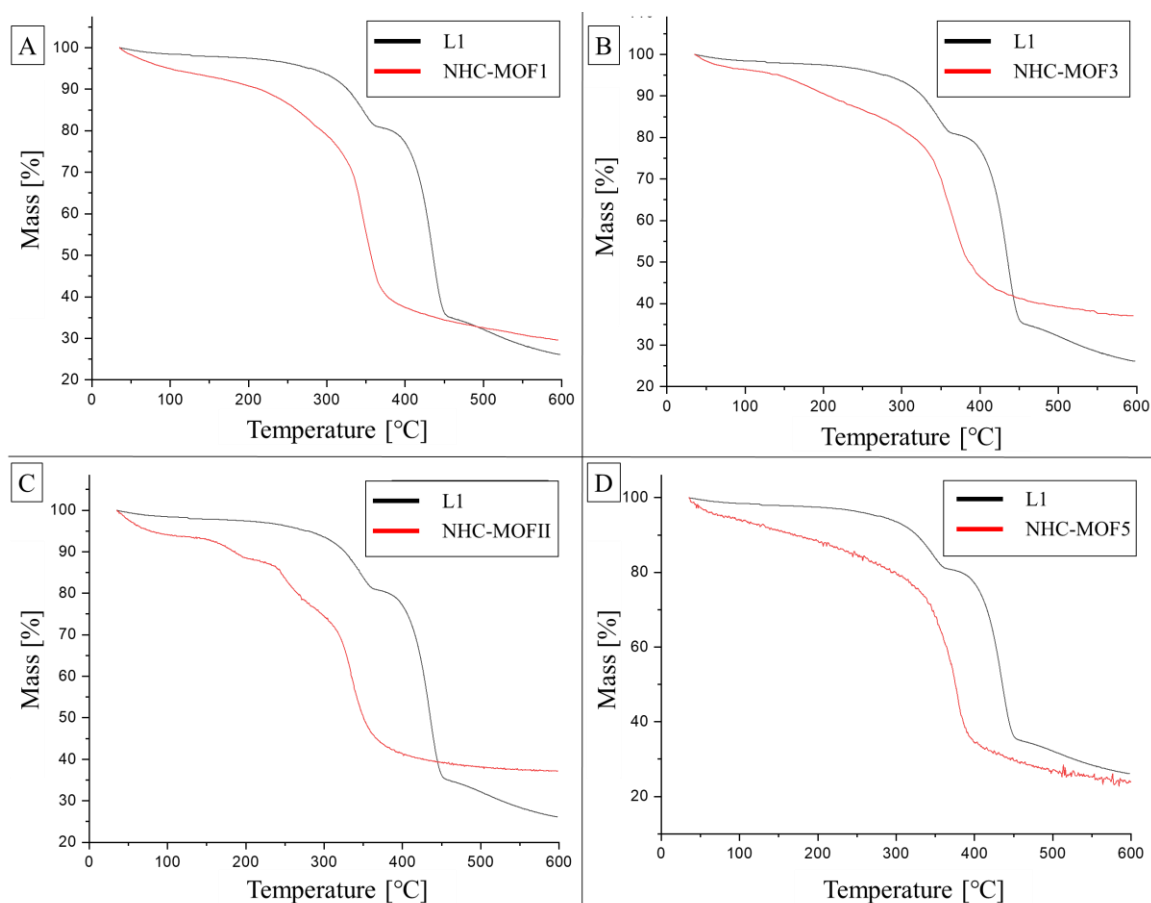
Figure A45. Individual TGA of **A) NHC-MOF1**, **B) NHC-MOF3**, **C) NHC-MOFII** and **D) NHC-MOF5**.
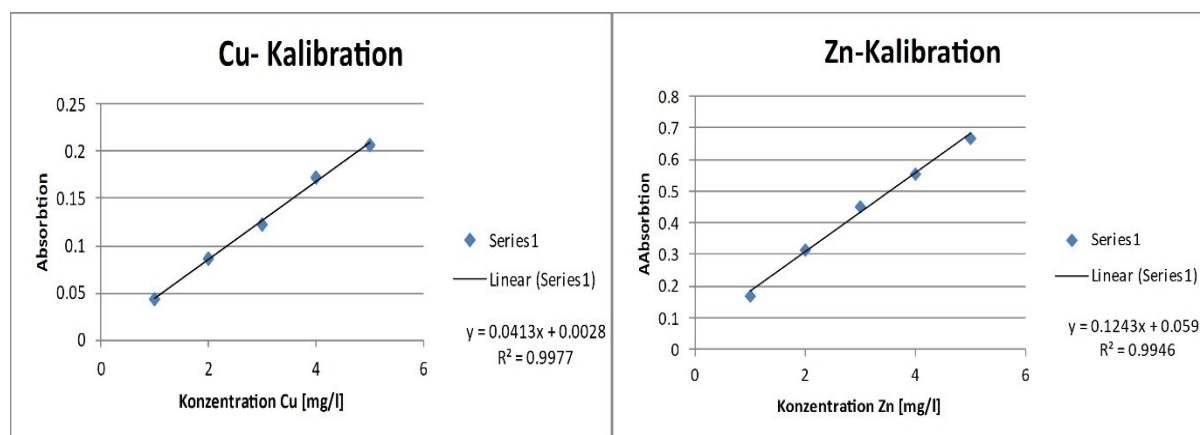
7.2.16 Calibration for FAAS

Figure A46. Calibration for linear fitting for Cu and Zn for the measurement of FAAS of (**NHC-MOF3**). The correlation coefficient, R^2, was 0.9977 and 0.9946, while the relative standard deviation, % RSD, was 1.1 % and 1.6 % for Cu and Zn respectively.

7.2.17 Investigations of Ultrasound-Induced Mechanochemical Activation

7.2.17.1 ^{1}H NMR Investigations of NHC-MOF1
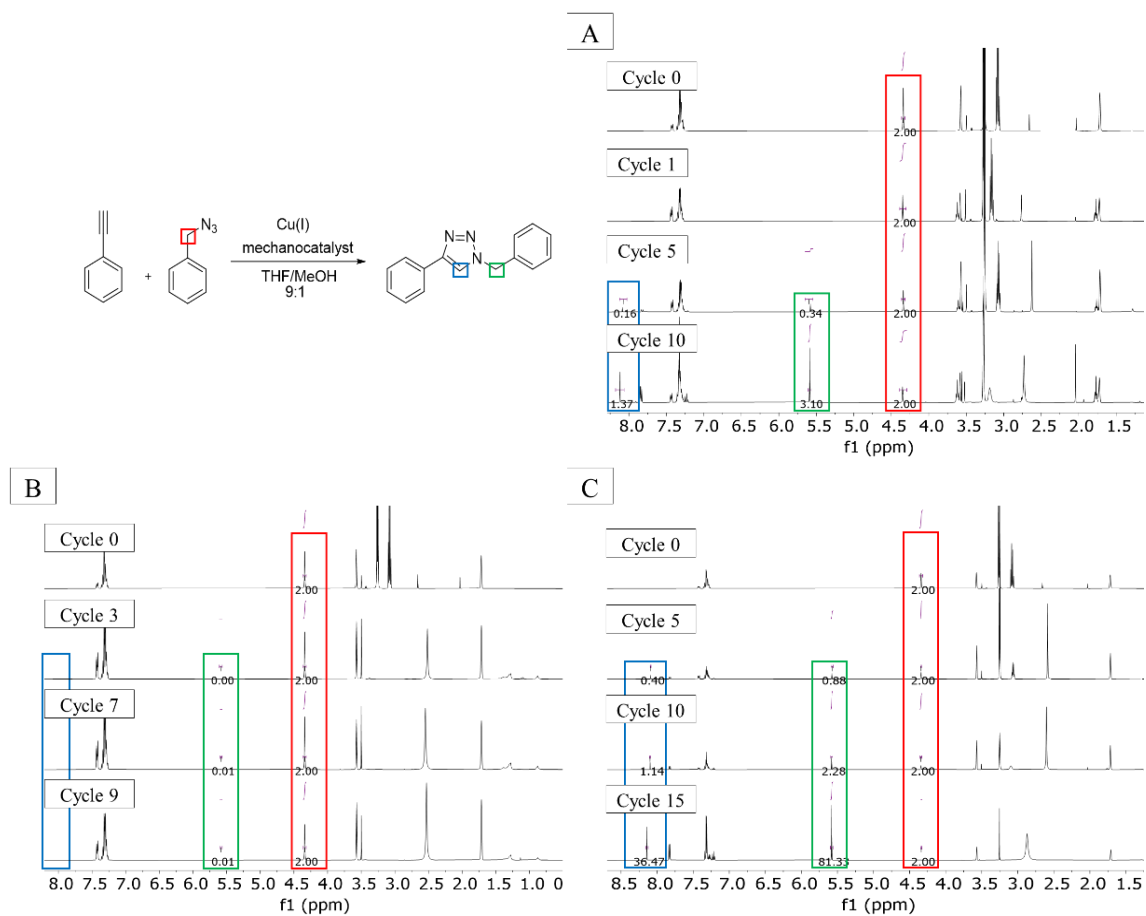
Figure A47. Monitoring of the coupled catalytic CuAAC of benzylazide (**10**) and phenylacetylene (**11**) to form 1-benzyl-4-phenyl-1*H*-1,2,3-triazole (**12**) due to the mechanochemical activation of **NHC-MOF1** by ultrasound with selected NMR spectra of **A**) Son1 at Cycles 0, 1, 5 and 10, **B**) Son2 at Cycles 0, 3, 7 and 9, and **C**) Son3 at Cycles 0, 5, 10 and 15.

7.2.17.2 PXRD of NHC-MOF1 Before and After Sonication
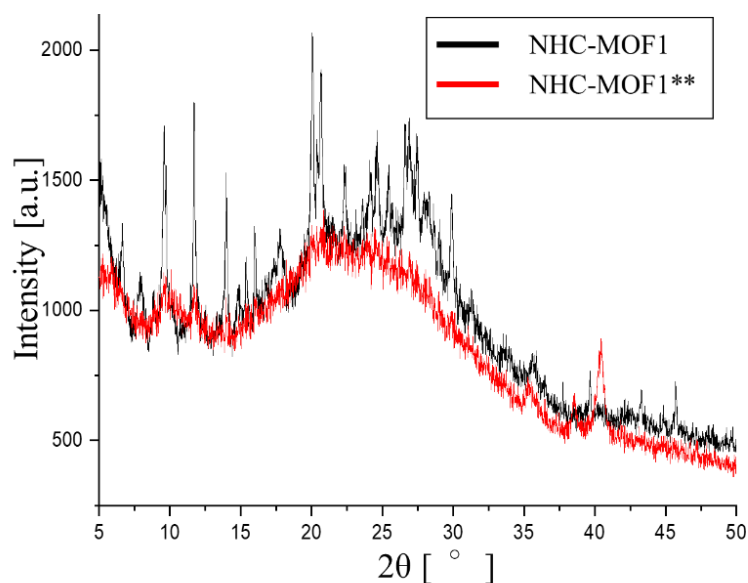
Figure A48. PXRD patterns (Cu-K$_{\alpha 1}$ radiation, $\lambda = 154.060$ pm) of the native **NHC-MOF1** as well as the NHC-MOF after sonication (**NHC-MOF1****).

The initial PXRD analysis of **NHC-MOF1** revealed both crystalline peaks and amorphous regions (see **Figure A48**). However, after subjecting the reaction mixture to 20 cycles of sonication (Son1) and collecting the resulting NHC-MOF powder, a new measurement was taken. The absence of the previously observed crystalline peaks indicated that the sonication had successfully disrupted the crystal structure, supporting the hypothesis presented in **Chapter 2**, resulting in the formation of new surfaces of the **NHC-MOF1** and making it suitable for conducting mechanophoric reactions.

7.2.17.3 The "Copper(II)/Ascorbate" System
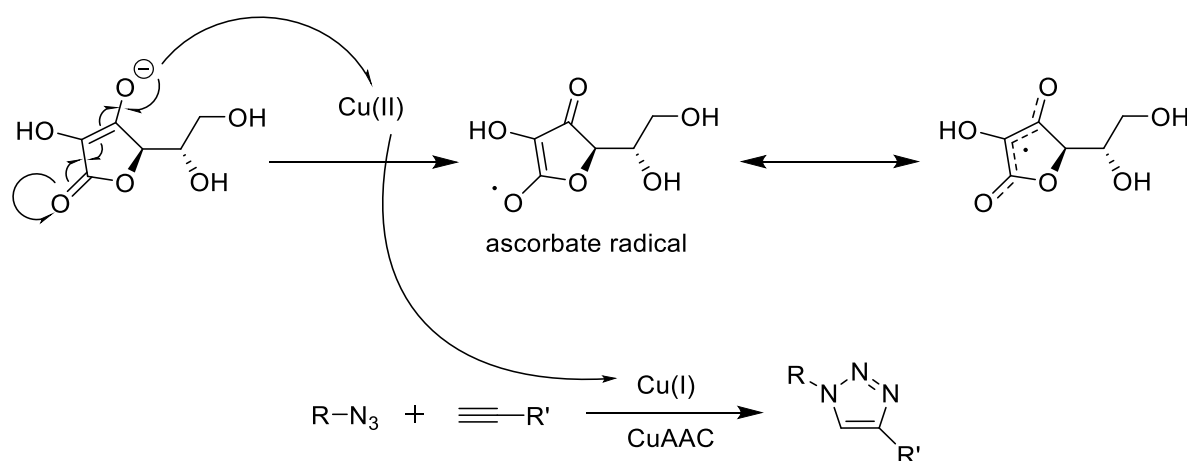
Scheme A1. The synthesis of a 1,2,3-triazole compound by CuAAC while using a copper(II)/ascorbate system. Adapted from literature.[441]

In a CuAAC (copper-catalysed azide-alkyne cycloaddition) reaction, the "copper(II)/ascorbate system" is widely used in which the active catalyst for CuAAC, i.e., Cu(I), is generated *in situ* from Cu(II) salts by using sodium ascorbate as a reducing agent.[442] The reduction reaction occurs *via* electron transfer from a sodium ascorbate to Cu(II), reducing the Cu(II) to Cu(I) and oxidizing the sodium ascorbate in

the process. This conversion from Cu(II) to Cu(I) is essential for the CuAAC reaction to occur, as Cu(I) serves as a critical intermediate in the cycloaddition step that results in the formation of the triazole product (see **Scheme A1**).[443, 444]
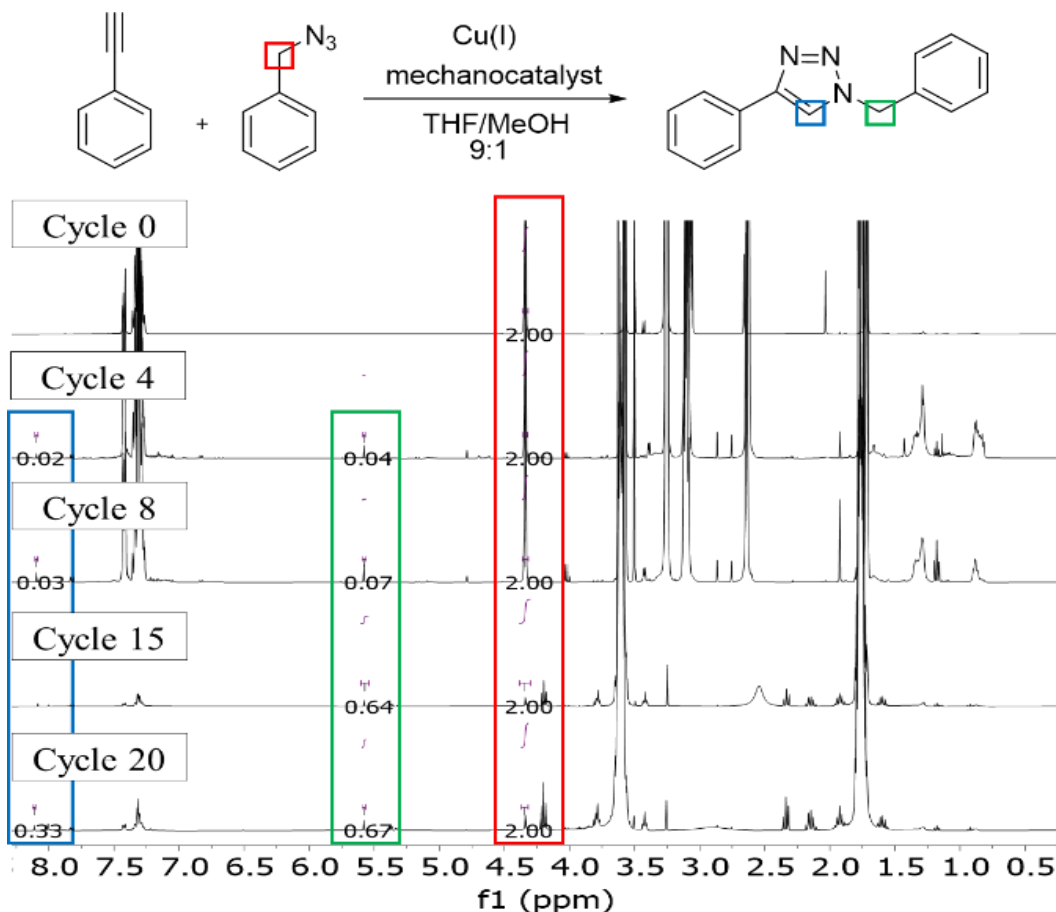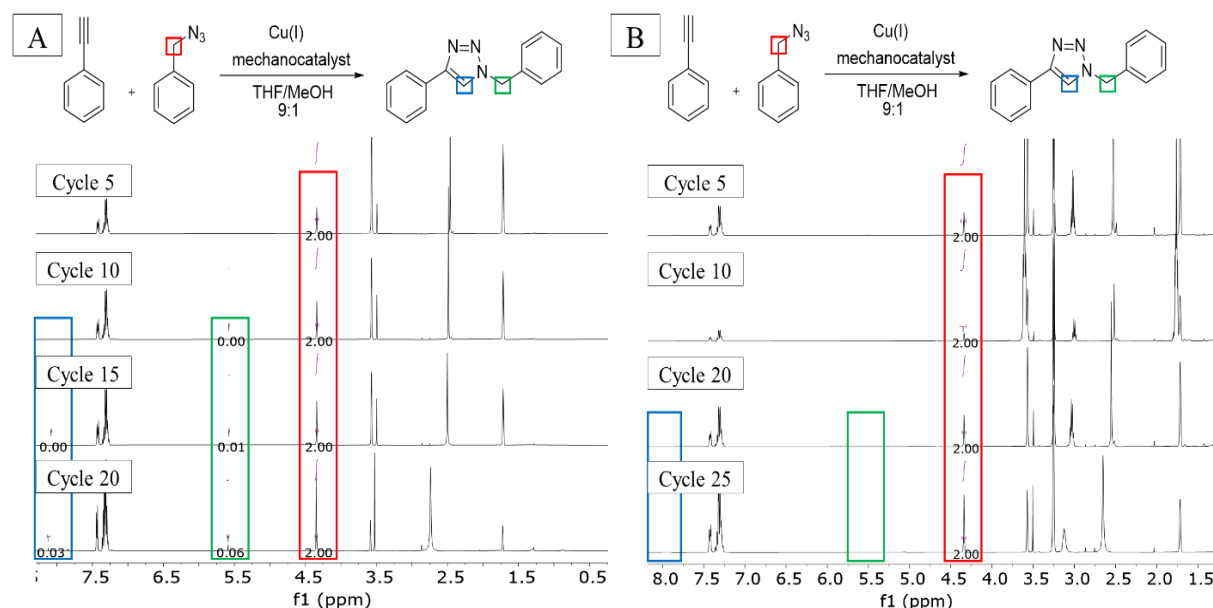
7.2.17.4 ¹H NMR Investigations of NHC-MOF3

Figure A49. Monitoring of the coupled catalytic CuAAC of benzylazide (**10**) and phenylacetylene (**11**) to form 1-benzyl-4-phenyl-1*H*-1,2,3-triazole (**12**) due to the mechanochemical activation of **NHC-MOF3** by ultrasound with selected NMR spectra of Son4 at Cycles 0, 4, 8, 15 and 20.

7.2.17.5 ¹H NMR Investigations of NHC-MOFII and NHC-MOF5

Figure A50. Monitoring of the coupled catalytic CuAAC of benzylazide (**10**) and phenylacetylene (**11**) to form 1-benzyl-4-phenyl-1*H*-1,2,3-triazole (**12**) due to the mechanochemical activation by ultrasound with selected NMR spectra of **A) NHC-MOFII** in Son5 at Cycles 5, 10, 15 and 20, and **B) NHC-MOF5** in Son6 at Cycles 5, 10, 20 and 25.
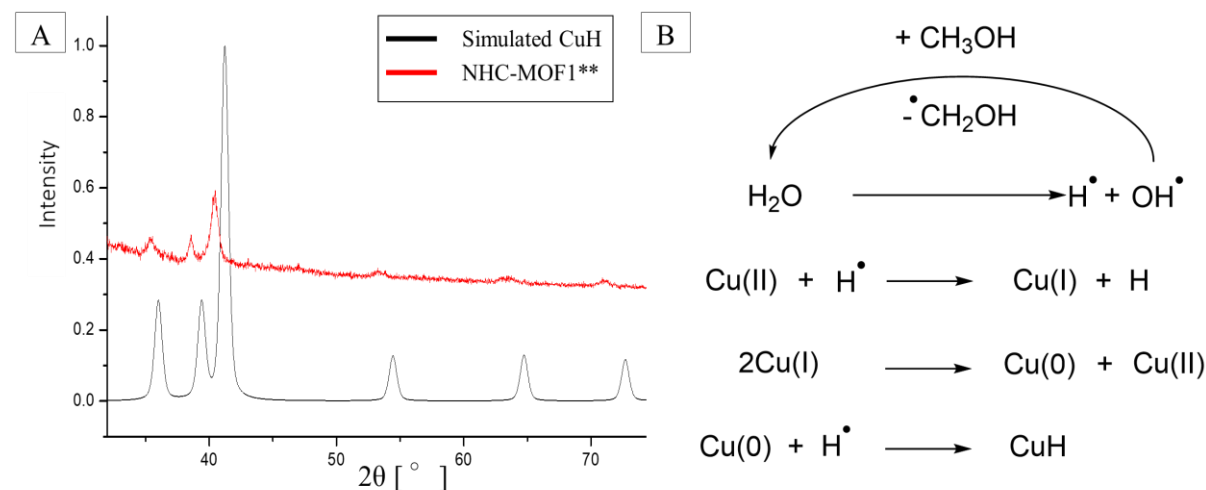
7.2.17.6 PXRD of NHC-MOF3 After Sonication

Figure A51. A) a close-up comparison of the additional peaks observed in PXRD after sonication of **NHC-MOF3** in Son4 to that of simulated peaks of CuH. **B)** A schematic presentation of the possible reaction pathway to the formation of the observed CuH.

PXRD measurements before and after sonication were conducted to probe the structure of the MOF. On sonication, multiple new peaks were seen at higher 2theta (2θ) values in the sonicated **NHC-MOF3** (**NHC-MOF3****) which are also not visible in the case of the MOF that underwent thermal control at 60 °C (**Figure 44**). The PXRD measurements were conducted by using the capillary method where the samples are inserted into capillaries to measure and hence, there should be no influence from the sample holder. The multiple new PXRD peaks at higher 2theta (2θ) were investigated and attributed to the

formation of copper(I) hydride (CuH) (**Figure A51A**), a phenomenon which has been observed previously to obtain the metal hydride by sonochemistry as per the reaction pathway stated in **Figure A51B**,[445] albeit the doubtful stability of CuH. This possibly occurred due to the release of copper by the destruction of the MOF by many continuous cycles of sonication. The presence of methanol in the THF-d_8/MeOH solvent mix for sonication further promotes the formation of CuH as the highly volatile MeOH can enter the cavitation bubbles during sonication and scavenge ˙OH radicals while also generating additional hydrogen species (radicals or molecules) due to the thermal reforming of the MeOH.[446] Either way, the yield of CuH would increase.

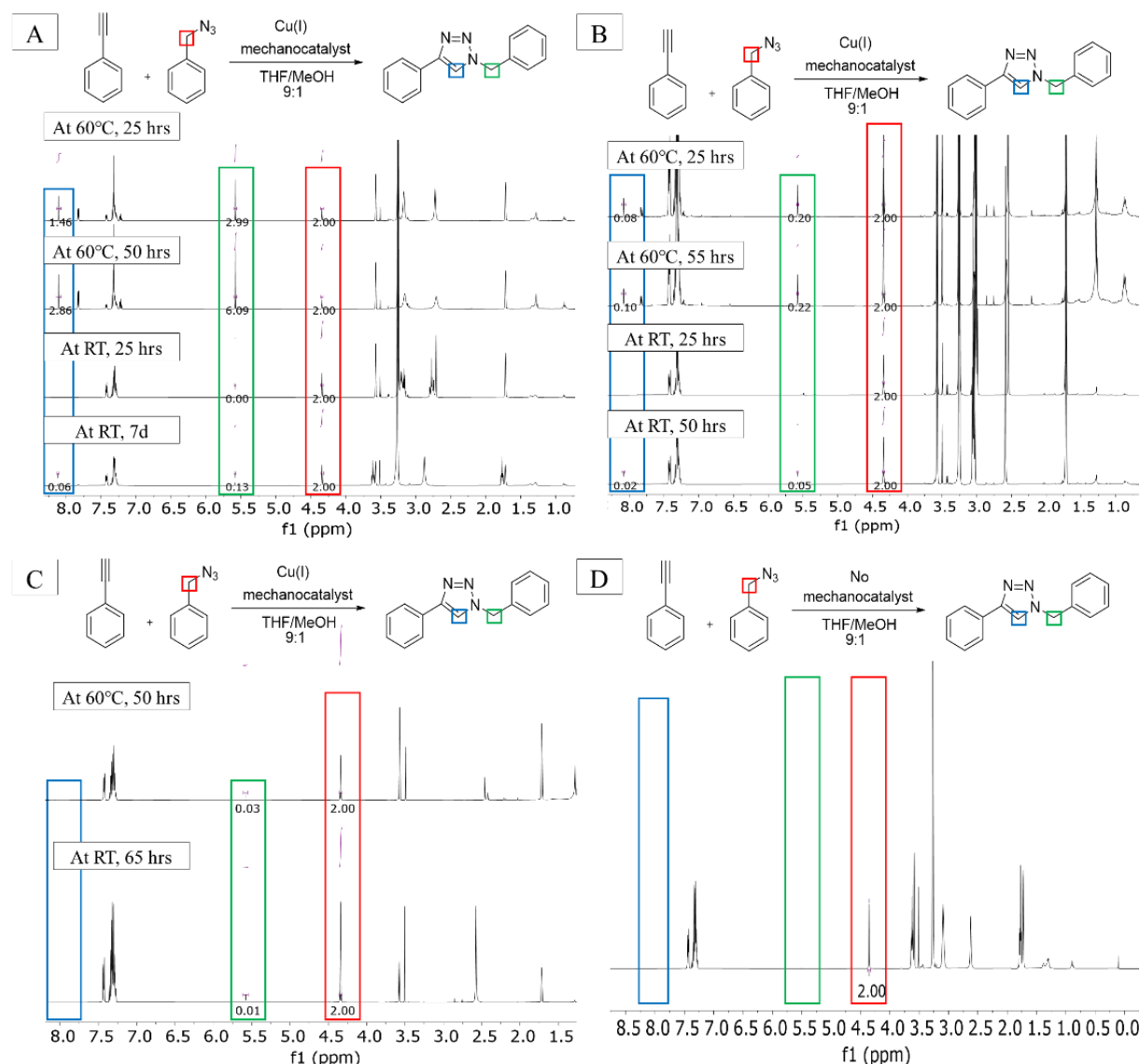### 7.2.18 ^{1}H NMR Investigations of Control Experiments

Figure A52. Monitoring of the coupled catalytic CuAAC of benzylazide (**10**) and phenylacetylene (**11**) to form 1-benzyl-4-phenyl-1H-1,2,3-triazole (**12**) as part of control experiments conducted at room temperature (RT) and 60 °C of **A**) Son1.Cont., **B**) Son4.Cont. and **C**) Son5.Cont. **D**) is the control conducted with no NHC-MOF catalyst at 60 °C.

7.3 Mechanochemically Active Thermoplastic Polyurethane (TPU) Systems

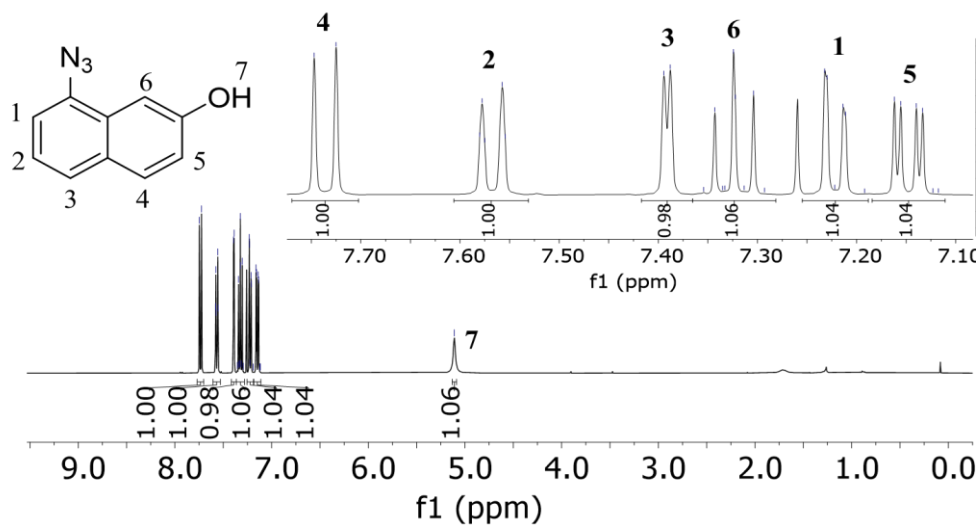### 7.3.1 Synthesis of 8-Azidonaphthalen-2-ol (13)
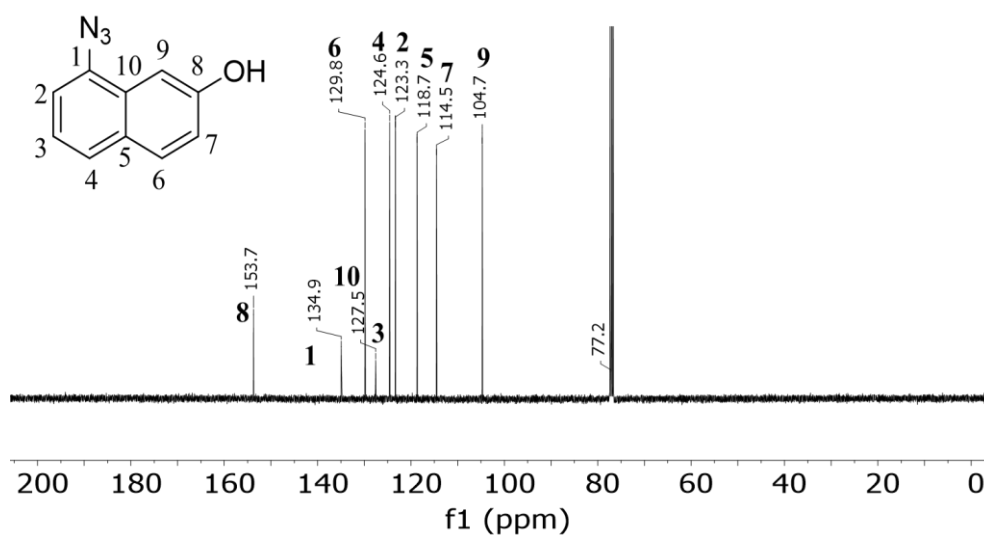

Figure A53. ^{1}H NMR spectrum of (**13**) in CDCl$_3$

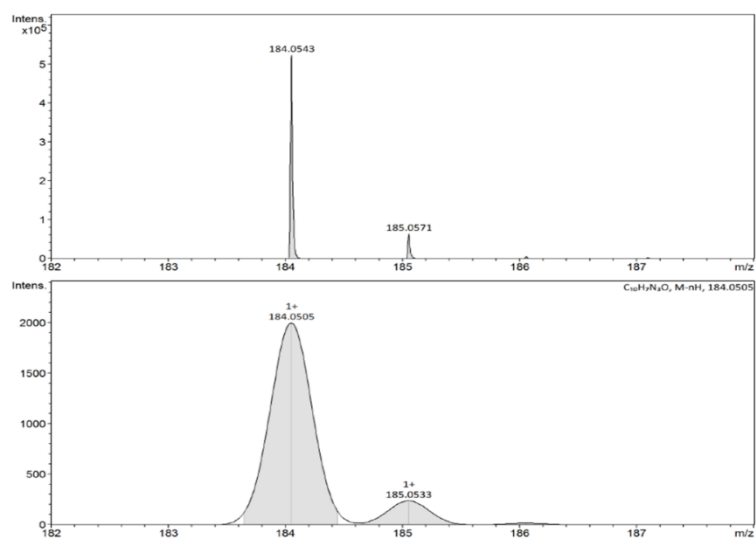**Figure A54.** ^{13}C NMR spectrum of (**13**) in CDCl$_3$.

Figure A55. ESI-ToF MS spectrum of (**13**).
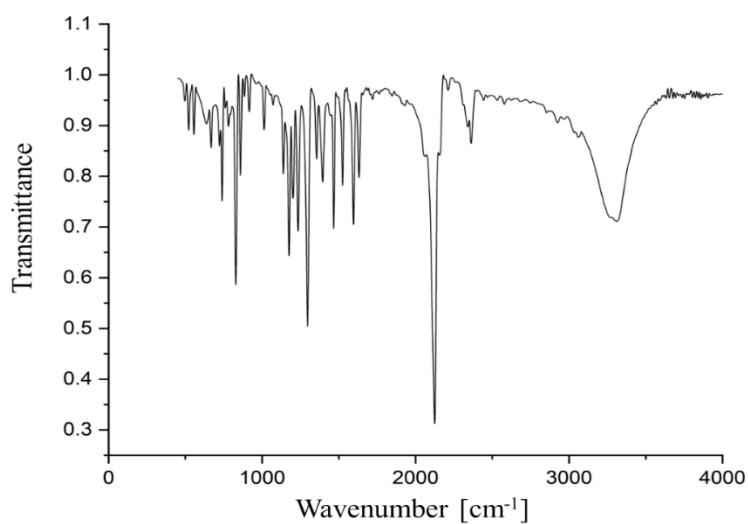

Figure A56. IR(KBr) spectrum of (**13**).

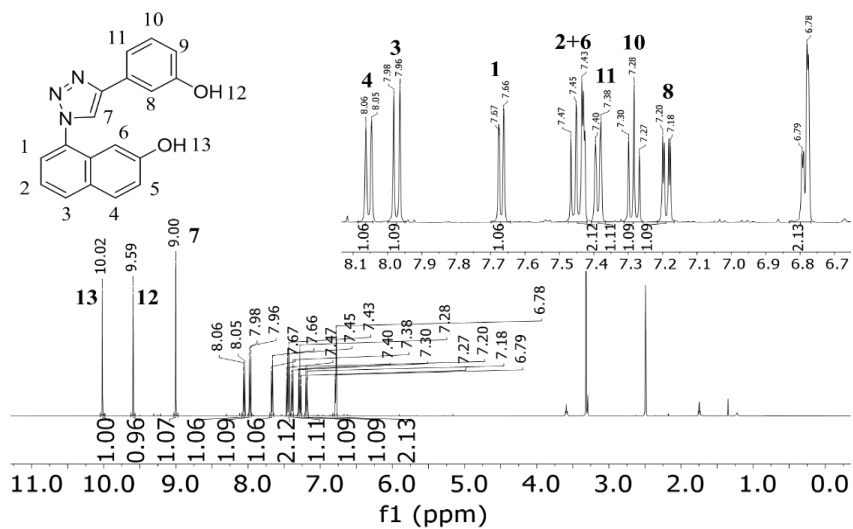### 7.3.2 Synthesis of 8-(4-(3-hydroxyphenyl)-1,2,3-triazol-1-yl)naphthalen-2-ol (15)

Figure A57. ¹H NMR spectrum of (**15**) in DMSO-d_6.

Figure A58. ^{13}C NMR spectrum of (**15**) in DMSO-d_6.

Figure A59. ESI-ToF MS spectrum of (**15**).

Figure A60. IR(KBr) spectrum of (**15**).

7.3.3 Kinetic Measurement of the Synthesis of TPU50

Table A3. GPC analysis for understanding the kinetics of O-TPU50 synthesis as per procedure of Development Stage 1 (DS1, **Chapter 5.4.2**).

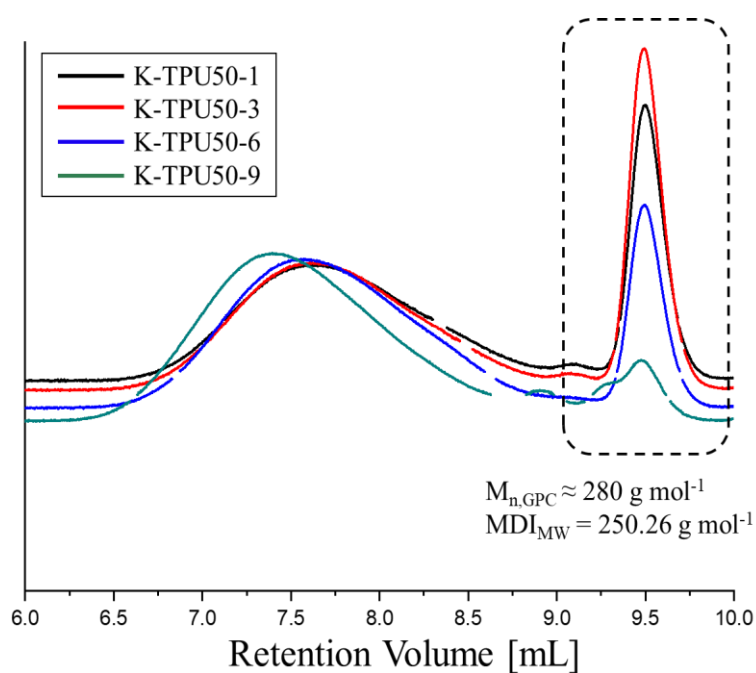| Ent	TPU Synthesis Stage	Sample Collected	M_n [g mol^{-1}]	PDI
1		K-TPU50-1	6800	1.75
2	Addition of MDI (**17**) to pTHF (**16**)	K-TPU50-2	6800	1.80
3		K-TPU50-3	6900	1.75
4		K-TPU50-4	6700	1.80
5	Addition of DBU	K-TPU50-5	6800	1.85
6		K-TPU50-6	7200	1.80
7		K-TPU50-7	7900	1.75
8	Addition of BDO (**18**)	K-TPU50-8	8900	1.70
9		K-TPU50-9	10000	1.75

Figure A61. GPC analysis of the kinetics of an O-TPU50 synthesis as per procedure of Development Stage 1 (DS1, **Chapter 5.4.2**).

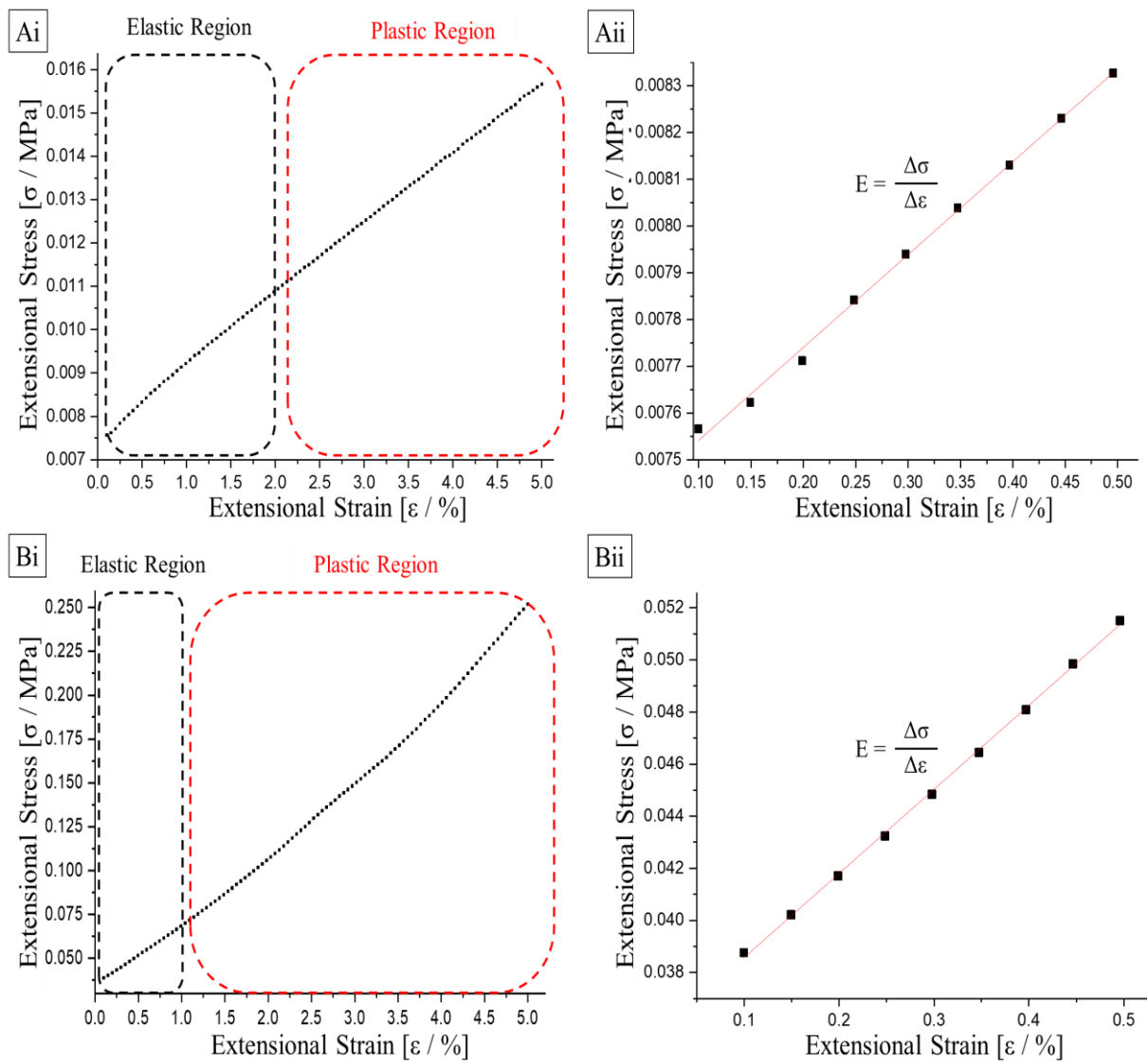## 7.3.4 Mechanical Properties of TPU30 and 70

Figure A62. The experiment was conducted with extensional rotational rheology with TPU30 or 70 foil fixed with the Universal Extensional Fixture (UXF). The hence obtained extensional stress vs. extensional strain graphs for **A**) TPU30 and **B**) TPU70 provided information about **i**) the classification of the linear elastic and plastic region which is then used to **ii**) determine the Young's modulus, calculated by using the slope of the linear regression in the low strain range from 0.01 % to 0.50 %.

7.3.5   Shape-Memory Effects of TPU50

Table A4. The calculated shape memory and recovery efficiency is based on the values obtained from **Figure 48D** and the **Equation 5.5** and **5.6**. The measurements here and graph (see **Figure 48D**) were generated from an average of two different measurements to ensure higher accuracy.

Cycle No.	Shape Memory Efficiency [%]	Recovery Efficiency [%]
1	-	-
2	94	81
3	95	~100
4	95	~100
5	94	99
6	94	~100
7	95	98
8	96	~100
9	92	86
10	92	90
11	90	98
12	93	~100
13	91	97
14[a]	99	~100
15[a]	90	55
16	92	~100
17	91	~100
18	91	~100
19	93	~100
20	91	90

[a]The entries 14 and 15 were excluded while reporting on both the efficiencies as the sample had slipped from the UXF and needed to be clamped back in the right position which was corrected from Cycle 16.

7.3.6 Quantification of Fluorogenic "Click" Reaction During Mechanochemical Activation in Stretching Experiments 2, 3 and 4.
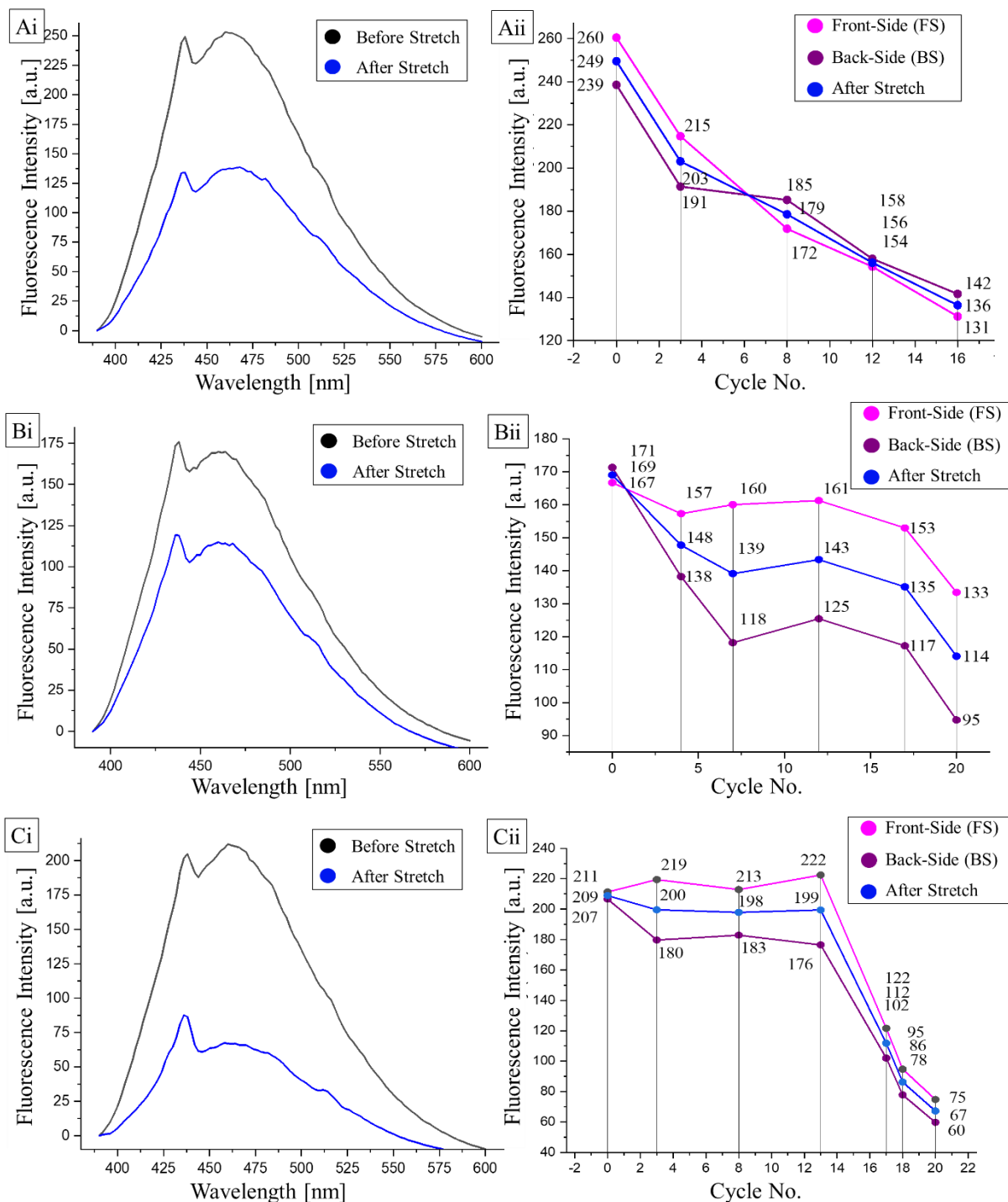

Figure A63. The oscillating tensile rheology of **A)** EXP2, **B)** EXP3 and **C)** EXP4 resulted in quantifiable fluorescence intensities, achieved with λ_{ex} = 377 nm and at λ_{em} = 458 nm. The colours correspond to the colours indicated in stretching terms indicated in **Figure 50**. These are displayed in the form of a **i)** fluorescence spectrum before and after the stretching experiment and **ii)** graph displaying the decrease in fluorescence intensities on both the sides.
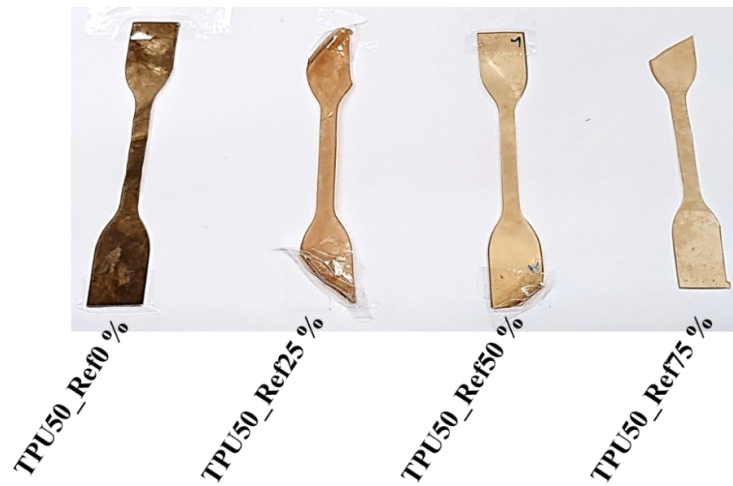
Figure A64. The samples used for calibration of TPU50 fluorogenic system as per **Chapter 5.4.10.1** showed deterioration by ageing as the samples turned brown over the months despite storage in ideal conditions.
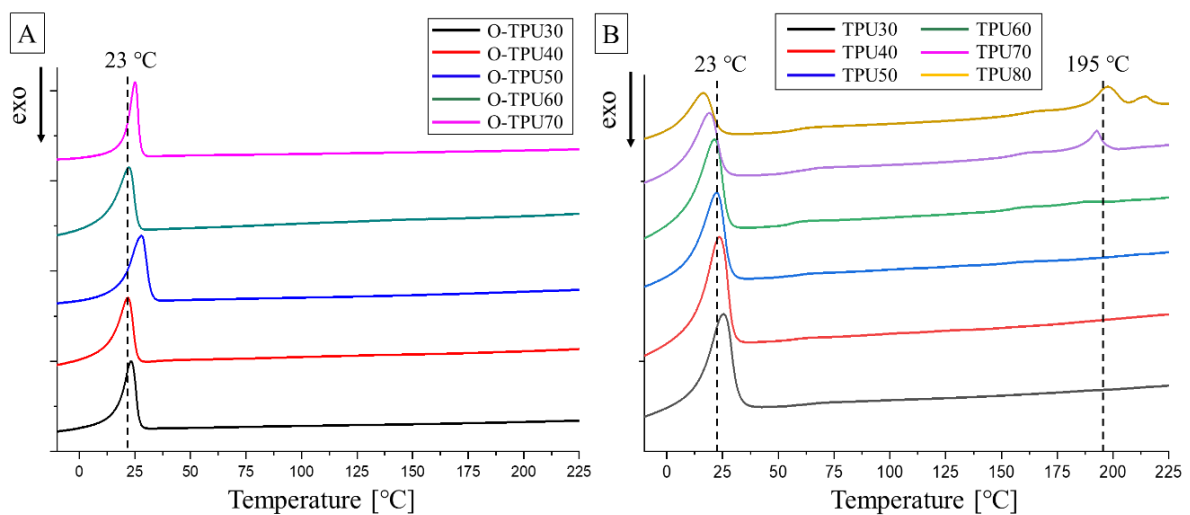
7.3.7 DSC Measurements of TPU

Figure A65. DSC measurements conducted on thermoplastic polyurethane (TPU) foils from **A)** Development Stage 1 and **B)** Development Stage 2.
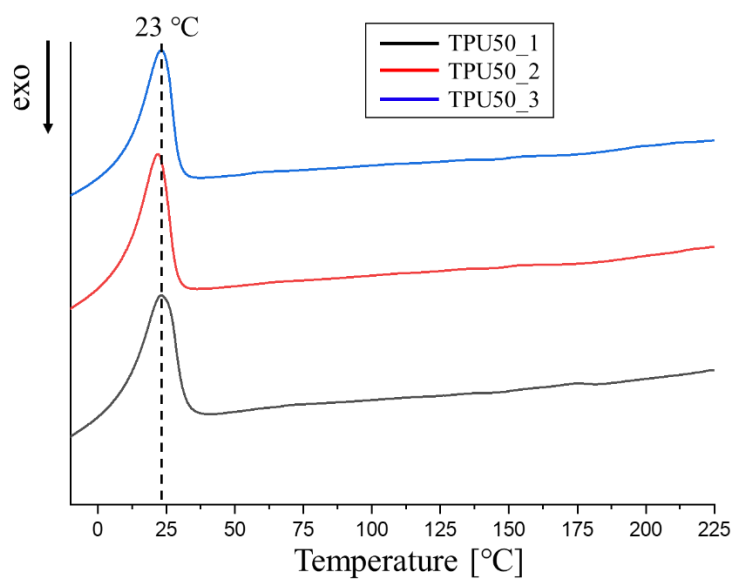
Figure A66. DSC measurements conducted on thermoplastic polyurethane (TPU) foils embedded with NHC-MOF3 as per procedure of Development Stage 3 to synthesize **A**) TPU50_1, **B**) TPU50_2 and **C**) TPU50_3.

8 CURRICULUM VITAE

Familienstand:	Ledig
Staatsangehörigkeit:	Indien

09/2023 - heute	**Polymerchemiker/Projektentwickler**
	Institut für Kunststofftechnologie & -recycling e.V.

12/2017 – 12/2022	**Wissenschaftlicher Mitarbeiter**
	Martin-Luther-Universität Halle-Wittenberg, Halle (Saale)
	Abteilung: Makromolekulare Chemie

10/2015 – 11/2017	**Masterstudium in Polymer Materials Science**
	Martin-Luther-Universität Halle-Wittenberg, Halle (Saale)
	Thesis-Thema: Development of Optical Self-Healing PMMA-Systems
	➢ Abschluss: Master of Science (1,8)

08/2011 – 07/2015	**B. Tech. in Fibres and Textile Processing Technology**
	Institute of Chemical Technology (ICT)
	Thesis-Thema: Using Natural Substances to Obtain Flame Retardancy on Cotton
	➢ Abschluss: Bachelor of Technology (1,8)

Halle (Saale), den 07.03.2024

_____

Kshitij S. Shinde

9   PUBLICATIONS

1. "*Cyclopropanation of poly(isoprene) using NHC-Cu(I) catalysts: Introducing carboxylates*"

Shinde, K. S., Michael, P., Rössle, M., Thiele, S., Binder*, W. H, *J Polym Sci*. **2020**; 58: 2864–2874.

DOI: https://doi.org/10.1002/pol.20200404

(Published under a Creative Commons license, CC BY 4.0)

2. "*A Mechanochemically Active Metal-Organic Framework (MOF) Based on Cu-Bis-NHC-Linkers: Synthesis and Mechano-Catalytic Activation*"

Shinde, K. S., Michael, P., Fuhrmann, D., Binder*, W. H., *Macromol. Chem. Phys.* **2023**, 224, 2200207

DOI: https://doi.org/10.1002/macp.202200207

(Published under a Creative Commons license, CC BY-NC-ND 4.0)

3. "*Mechanochemical Activation of a Metal–Organic Framework Embedded within a Thermoplastic Polyurethane Matrix: Probing Fluorogenic Stress-Sensing*"

Shinde, K. S., Michael, P., Binder*, W. H., *Macromol. Chem. Phys.* **2023**, 2300297

DOI: https://doi.org/10.1002/macp.202300297

(Published under a Creative Commons license, CC BY-NC 4.0)

Halle (Saale), den 07.03.2024

10 EIGENSTÄNDIGKEITSERKLÄRUNG

Hiermit erkläre ich an Eides statt, dass ich die vorliegende Arbeit selbstständig und ohne fremde Hilfe verfasst habe. Andere als die angegebenen Quellen und Hilfsmittel wurden nicht benutzt und die den benutzten Werken wörtlich oder inhaltlich entnommenen Stellen wurden als solche kenntlich gemacht.

Außerdem erkläre ich, dass ich die vorliegende Dissertation an keiner anderen wissenschaftlichen Einrichtung zur Erlangung eines akademischen Grades eingereicht zu haben.

Halle (Saale), den 07.03.2024 _____

Kshitij S. Shinde